



Swansea University
Prifysgol Abertawe



Swansea University E-Theses

Luminescent materials for biomedical and technological applications.

Hughes, Victoria A

How to cite:

Hughes, Victoria A (2008) *Luminescent materials for biomedical and technological applications..* thesis, Swansea University.

<http://cronfa.swan.ac.uk/Record/cronfa43025>

Use policy:

This item is brought to you by Swansea University. Any person downloading material is agreeing to abide by the terms of the repository licence: copies of full text items may be used or reproduced in any format or medium, without prior permission for personal research or study, educational or non-commercial purposes only. The copyright for any work remains with the original author unless otherwise specified. The full-text must not be sold in any format or medium without the formal permission of the copyright holder. Permission for multiple reproductions should be obtained from the original author.

Authors are personally responsible for adhering to copyright and publisher restrictions when uploading content to the repository.

Please link to the metadata record in the Swansea University repository, Cronfa (link given in the citation reference above.)

<http://www.swansea.ac.uk/library/researchsupport/ris-support/>

Luminescent materials for biomedical and technological applications

by

Victoria A. Hughes

*A thesis submitted in fulfilment of the requirements for the degree
of Doctor of Philosophy in the University of Wales Swansea*

Sept 2008

ProQuest Number: 10821415

All rights reserved

INFORMATION TO ALL USERS

The quality of this reproduction is dependent upon the quality of the copy submitted.

In the unlikely event that the author did not send a complete manuscript and there are missing pages, these will be noted. Also, if material had to be removed, a note will indicate the deletion.



ProQuest 10821415

Published by ProQuest LLC (2018). Copyright of the Dissertation is held by the Author.

All rights reserved.

This work is protected against unauthorized copying under Title 17, United States Code
Microform Edition © ProQuest LLC.

ProQuest LLC.
789 East Eisenhower Parkway
P.O. Box 1346
Ann Arbor, MI 48106 – 1346

Declaration

Declaration

This work has not previously been accepted in substance for any degree and is not being concurrently submitted in candidature for any degree.

.....
(Signature of candidate)
.....**7. March 2009**.....
(Date)

Statement 1

This thesis is the result of my own investigations, except where otherwise stated. Other sources are acknowledged by footnotes giving explicit references. A bibliography is appended.

.....
(Signature of candidate)
.....**7. March 2009**.....
(Date)

Statement 2

I hereby give consent for my thesis, if accepted, to be available for photocopying and for inter-library loan, and for the title and summary to be made available to outside organisations.

.....
(Signature of candidate)
.....**7. March 2009**.....
(Date)



Acknowledgements

During the course of this study I have worked and socialised with a wide range of people who have all helped to make my time in Swansea such a fantatastic experience.

My thanks go my supervisor Dr Peter Douglas whose patience, enthusiasm, expertise and perceptive advice have guided me through this project. Without his encouragement and support I would not have benefited from the many opportunities I was fortunate to have.

I would like to thank all members of the photochemistry research group past and present for their friendship and assistance. Hans, Jeremie, Steve, Rachel and Matthew, you have all entertained me in one way or another over the last few years, and have supplied numerous cups of tea, chocolate and a steady supply of diet coke. International travel was high on the agenda for all member of the group, and the group 'research' trip to Portugal, it was an experience that will stay with me for ever and was made so memorable by travelling with such an amazing group of friends. I would also like to thank the numerous friends from the Chemistry department, past, present and honoree, for many an amusing hour spent in the tearoom, JC's and Reflex in particular Ange, Ruth, Brendan, Jo, Rhysie and Gareth.

I thank Stan, John Tregembo, John Lewis and Ian Matthews for their help and the smooth running of the Chemistry department. I would also like to thank Dr. Shareen Doak, from Swansea Medical school who patiently tutored me in the standard protocols and techniques associated with cell culture and microscopy. Many thanks should also go to Prof. Chris Geddes at the University of Baltimore for the phase modulation measurements described in chapter 3. Additional thanks go to Dr Mike Garley for advice on all things computer-related.

I would like to thank EPSRC National Mass Spectrometry Service Centre in Swansea for supplying the mass spectrometry service.

Finally, I would like to thank all my family expecially my mam and Gareth for their love, support and continual encouragement.

Contents

Acknowledgements	3
Contents	4
Abbreviations	9
Abstract.....	12
Chapter 1 Introduction.....	14
1.1 Luminescent Materials.....	15
1.2 Photochemistry.....	15
1.2.1 Absorption.....	15
1.2.2 Deactivation of excited states.....	16
1.2.3 Radiative decay mechanism	16
1.2.3.1 Fluorescence	16
1.2.3.2 Phosphorescence	16
1.2.4 Non-radiative decay mechanism.....	17
1.2.4.1 Internal conversion and vibrational relaxation	17
1.2.4.2 Intersystem crossing.....	17
1.2.5 Selection rules for optical transitions.....	17
1.2.5.1 Spin selection rule: ($\Delta S = 0$).....	17
1.2.5.2 Laporte selection rule:	17
1.2.6 Quantum yields and Lifetime	20
1.2.7 Quenching	21
1.2.7.1 Oxygen Quenching.....	21
1.2.7.2 Stern-Volmer analysis	21
1.2.8 Perception of colour and colour representation.....	22
1.3 Near infrared luminescent materials for biological labelling.....	25
1.3.1 Background	25
1.3.2 Dyes for the Near Infra Red (NIR)	27
1.3.3 Organic fluorophores	27
1.3.3.1 Xanthene dyes.....	27
1.3.3.2 Phenoxazine dyes.....	28
1.3.3.3 Carbocyanine and merocyanine dyes.....	30
1.3.3.4 Squarylium dyes.....	30
1.3.3.5 Other NIR probes	31
1.4 Luminescent optical sensors	32
1.4.1 Oxygen sensors.....	32
1.4.2 Dissolved oxygen.....	33
1.4.2 Halothane sensors	33
1.4.3 Sulphur dioxide.....	33
1.4.4 Halide	34
1.4.5 Humidity.....	34
1.4.6 Oxygen sensors as transducers	34
1.4.6.2 Hydrogen peroxide	34
1.4.6.3 Glucose	35
1.4.6.4 Biosensors.....	35
1.4.7 pH and carbon dioxide sensors.....	37
1.5 Materials for optical sensors	38

1.5.1 Sol gel.....	38
1.5.2 Polymers and membranes.....	39
1.5.3 Hydrogels	39
1.6 Innovations in optical sensing	40
1.6.1 Innovations in sensing materials.....	40
1.6.1.1 Quantum dots.....	40
1.6.1.2 Molecular imprinting (MIP).....	41
1.6.1.3 Organic conducting polymers (OCP).....	41
1.6.1.4 Nanoparticles	41
1.6.1.5 Probes encapsulated by biologically localised embedding (PEBBLES) .	42
1.6.1.5.1 Polyacrylamide (PAA) hydrogel.....	42
1.6.1.5.2 Sol gel silica/organic hybrid	43
1.6.1.5.3 Decyl methacrylate hydrophobic liquid polymer.....	43
1.6.2 Multianalyte sensors	43
1.6.3 Colorimetric sensors	45
1.7 Thesis overview.....	47
1.8 References	48
Chapter 2 Experimental and instrumental	60
2.1 Materials.....	61
2.2. General method of preparation of polymer films for optical sensing.....	63
2.2.1 Lumophore solutions.....	64
2.3 Thin film optical sensor preparation.....	64
2.3.1 Type 1 - Solution based sensors	64
2.3.2 Type 2 - Incorporating PEBBLEs into thin film sensors	64
2.3.4 Type 3 -Dual lumophore PEBBLE based optical oxygen sensors	64
2.3.5 Plasticisation of the film.....	66
2.4 Synthesis and preparation of PEBBLE sensing elements.....	66
2.4.1 Organically modified silica (ORMOSIL) nanospheres [5]	66
2.5 Imaging of the nanospheres.....	66
2.5.1 SEM.....	66
2.6 Instrumental.....	67
2.6.1 Cell set up for gaseous oxygen sensing.....	67
2.6.2 Cell set up for dissolved oxygen and pH sensing	67
2.6.3 Gas mixing.....	69
2.6.4 Calibration of the gas blender.....	69
2.7 Instrumental.....	70
2.7.1 UV/VIS absorption measurements	70
2.7.2 Variable temperature measurements.....	70
2.7.3 Steady-state luminescence measurements.....	72
2.7.4 Time-resolved nanosecond laser studies	72
2.7.5 Circular dichroism	72
2.8 Data analysis.....	73
2.8.1 The integrated emission intensity for a decay trace.....	73
2.8.2 Curve fitting.....	73
2.9 Photophysical characterisation	73
2.9.1 Quantum yield determination	73
2.9.2 Radiative rate constant	73
2.9.3 pH study	74
2.9.4 Photostability	74

2.9.5 Temperature dependence of dye protein binding	74
2.10 Cell studies	74
2.10.1 Cell culture and cell viability.....	74
2.10.2 Cell imaging.....	75
2.11 NMR and mass spectrometry	76
<u>2.12 References</u>	<u>77</u>
Chapter 3 A study of the interaction between a squarylium dye and protein by optical methods	78
3.1 Introduction.....	79
3.2 Types of binding.....	79
3.2.1 Covalent labelling	79
3.2.2 Non-covalent labeling	82
3.3 Dyes for the Near Infra Red (NIR).....	82
3.3.1 Cyanine based dyes.....	83
3.3.2 Polymethine cyanine dyes	84
3.3.3 Squarylium cyanine dyes.....	86
3.4 The interaction of squarylium dyes and serum albumin.....	86
3.5 Aims of this chapter.....	89
3.6 Materials and methods	90
3.6.1 Synthesis of sulfobutylsquaraine carboxylate.....	90
3.6.2 Synthesis of intermediate 2	90
3.6.3 Synthesis of SQ-1	90
3.7 Spectroscopic characterization.....	93
3.7. 1 Spectroscopic characterisation.....	93
3.7.2 Binding with BSA (fraction V).....	93
3.7.3 Circular dichroism	99
3.7.4 Photochemical stability	99
3.8 Cell culture and imaging	109
3.8.1 Cell imaging	109
3.8.2 Cell viability	109
3.9 Conclusions	112
3.10 References	114
3.10 References	114
Chapter 4 Investigating factors affecting kinetic heterogeneity of lifetimes and oxygen quenching of PtOEP and PdOEP in thin film sensors.....	119
4.1.1 Introduction	119
4.1.2 Stern-Volmer analysis.....	119
4.3.1 Movement of gases through the polymer	122
4.3.2 Materials for immobilisation	122
4.3.3 Plasticization of polymers	125
4.1.4 Modelling heterogeneity	125
4.1.4.1 Discrete models.....	125
4.1.4.2 Continuous distributions.....	126
4.1.4.3 Empirical	126
4.1.5 Sensitivity	127
4.1.6 Dissolved oxygen sensing	127
4.1.7 Aims of the work described in this chapter.....	129

4.2 Steady-state and kinetic studies of Pt and Pd OEP in ethyl cellulose films	131
4.2.1 Results and discussion	131
4.2.2.1 PdOEP in unplasticised films	131
4.2.2.2 PtOEP in unplasticised films	131
4.2.2.3 Free fit analysis	132
4.2.2.4 Double exponential analysis	132
4.2.2.5 Fixed rate analysis	137
4.2.2.6 Stern-Volmer analysis	143
4.2.3 Steady-state and kinetic studies of Pt and PdOEP in ethyl cellulose plasticised films	148
4.2.3.1 Effect of plasticisation.....	148
4.2.3.2 Time resolved analysis	151
4.2.3.3 Stern Volmer analysis	151
4.2.3.4 Heterogeneity.....	151
4.2.3 Steady-state and kinetic studies of PtOEP in hydrogel films.....	157
4.2.3.1 Time resolved emission data	157
4.2.3.2 Free fitting single exponential analysis.....	157
4.2.3.4 Free fit double exponential analysis.....	157
4.2.3.5 Fixed rate analysis.....	164
4.2.3.6 Oxygen quenching - integrated emission intensity.....	164
4.2.3.7 Calibration and heterogeneity.....	164
4.2.3.8 Dissolved oxygen sensing	164
4.3 Discussion And Conclusion.....	174
4.4 References	176

Chapter 5 Optical thin film sensors based on luminescent nanoparticles in a biologically compatible hydrogel.....	179
5.1 Introduction	180
5.2 Oxygen sensing	180
5.3 Optical pH sensing.....	182
5.4 Innovations in optical thin film sensors.....	183
5.4.1 Micro and nano particle optical sensors.....	183
5.5 Aims of this chapter.....	186
5.5.1 Oxygen sensing material.....	186
5.5.2 pH sensing material.....	186
5.6 Results and discussion	190
5.6.1 Time resolved studies-PtOEP ormosil PEBBLES	190
5.6.1.1 Effect of concentration	190
5.6.1.1.1 Single lumophore sensor-type 2 sensors	190
5.6.1.2 Effect of PEBBLE size.....	191
5.6.1.3 Dual lumophore sensor.....	199
5.6.1.3.1 Type 2 sensors.....	199
5.6.1.3.2 Type 3 and type 4 sensor	200
5.6.2 Response characteristics of ormosil nanoparticles in hydrogel.....	206
5.6.2.1 Single lumophore sensor	206
5.6.2.1.1 Effect of concentration	206
5.6.2.1.2 Effect of PEBBLE size	206
5.6.2.2 Dual lumophore type 2 sensor	206
5.6.2.2.1 Type 2 Thin film sensors for gaseous and dissolved oxygen sensing.....	206
5.6.2.2.2 Ratiometric sensing	207

5.6.2.3 Type 4 dual lumophore sensors	217
5.6.2.3.1 Colorimetric thin film oxygen sensors	217
5.6.3 Optical pH sensing	219
5.6.3.1 Choice of material	219
5.6.3.2 Optical Response.....	219
5.6.3.3 Ratiometric pH sensor	224
5.6.4 Multi-analyte sensors	225
5.6.5 Conclusions	232
5.6.6 References	232
 Chapter 6 Conclusions.....	 239
6.1 Conclusions	240
6.1.1 A squarylium dye as non-covalent protein probes	240
6.1.2 Understanding the kinetic heterogeneity of PtOEP based sensing materials	240
6.1.3 Nanomaterials for optical sensing	241
6.2 Final remarks	242

Abbreviations

Å - Angstrom

A - Acceptor ion

Acac - acetylacetonate

Bpy - 2,2'-bipyridyl

BSA- Bovine serum albumin

CBQCA- (3-(4-carboxybenzoyl)quinoline-2-carboxaldehyde

CCD - Charge-coupled device

CD - Circular dichroism

CE- Capillary electrophoresis

CIE - Commission Internationale de l'Éclairage

CRT- Cathode ray tube

D - Donor ion

DAPI-4',6-diamidino-2-phenylindole

DL-PSP - Dual-lumophore pressure-sensitive paint

DLR- Dual lifetime referencing

Do_2 - Diffusion constant usually given in units of $cm^2 s^{-1}$

ϵ - Molar extinction coefficient in $dm^3 cm^{-1} mol^{-1}$

EC -Ethyl cellulose

FW - Formula weight

Γ = Radiative decay rate

HOMO - Highest occupied molecular orbital

HPTS-8-hydroxypyrene-1,3,6-trisulfonic acid trisodium salt

HS - High-spin

HSA-Human serum albumin

I - Intensity of light, when accompanied by a subscript 0 means in the absence of analyte

IC - Internal conversion

ICG- Indocyanine green

ISC - Intersystem crossing

IR - Infrared

J -Total angular momentum quantum number

k_0 - Intrinsic decay rate constant in s^{-1}
 k_{DA} - Donor-acceptor energy transfer rate constant in s^{-1}
 k_{IC} - Internal conversion rate constant in s^{-1}
 k_{ISC} - Intersystem crossing rate constant in s^{-1}
 k_{nat} - Natural decay rate constant in s^{-1}
 k_{nr} - Non-radiative decay rate constant in s^{-1}
 k_{obs} - Observed decay rate constant in s^{-1}
 k_p - Phosphorescence decay rate constant in s^{-1}
 k_q - Quenching rate constant in s^{-1}
 k_r - Radiative decay rate constant in s^{-1}
 k_{SV} - Stern-Volmer constant in $Torr^{-1}$
 k_{SQ} - Self-quenching rate constant in $dm^3 mol^{-1} s^{-1}$
 l - Angular momentum quantum number
 L – Lumophore
 LOD- Limit of detection
 LIF –Laser induced fluorescence
 $L(\lambda)$ - Relative photon output at wavelength, λ
 LUMO - Lowest unoccupied molecular orbital
 MAP - Modified atmosphere packaging
 MIP-Molecular imprinted polymer
 MTS-3-(4,5-dimethylthiazol-2-yl)-5-(3-carboxymethoxyphenyl)-2-(4-sulfophenyl)-
 2H-tetrazolium,
 MW - Molecular weight
 N_A - Avogadro's number
 NIR- Near infrared red
 NMR - Nuclear magnetic resonance
 OCP-Organic conducting polymer
 OEP - Ocataethyl porphyrin
 OEPK - Octaethyl porphyrin ketone
 OLED - Organic light-emitting diode
 OPA- *o*-Phthalaldehyde
 PAA-Polyacylamide
 PAH - Polyaromatic hydrocarbon
 PBS- Phosphate buffered saline

PEBBLEs- Probes encapsulated by biologically localised embedding

Phen - 1, 10-phenanthroline

P_{O_2} - Oxygen permeability in $\text{cm}^2\text{Pa}^{-1}\text{s}^{-1}$

p_{O_2} - Partial pressure of oxygen in Torr

PSP - Pressure-sensitive paint

PS - Polystyrene

PVC - Polyvinyl chloride

Φ_{em} - Emission quantum yield

Φ_p - Phosphorescence quantum yield

RLS- Rapid lifetime determination

RT - Room-temperature

s- Spin quantum number (where S represents the total spin state)

S_n - Singlet state

$S(\lambda)$ - Sensitivity of the detector at wavelength, λ

SEM -Scanning electron microscopy

S_{O_2} - Solubility constant usually given in $\text{cm}^3\text{cm}^{-3}\text{Pa}^{-1}$

STP - Standard temperature and pressure (298 K, 1 Atmosphere)

s - Standard deviation

SPQ- 6-methoxy-N-(3-sulfopropyl)quinolinium

SPA -3,6-bis(dimethylamino)acridine

t – Time

TRITC-Texas red isothiocyanate

Abstract

Squarylium dyes are an attractive group of fluorophores for protein labelling and quantification. The synthesis and photochemical characterisation of a cheap, easily synthesised (one-pot), symmetrical squarylium dye, **SQ-1**, for non-covalent labelling of proteins, is described. **SQ-1** meets the key criteria for a useable near infrared (NIR) probe including: absorption and emission maxima in the red spectral region, excellent water solubility, and high chemical and photo stability. The noncovalent labelling of proteins is an attractive option as it is a fast method which requires minimal sample handling. **SQ-1** binds non-covalently to bovine serum albumin (BSA) with $K = 2.8 (\pm 0.5) \times 10^5$ (at pH 7.2, 0.1 mol dm⁻³ phosphate buffer, I = 0.14), and shows a 4 fold increase in the quantum yield when bound in this way. The absorption and emission characteristics of **SQ-1** make it compatible with commonly used excitation sources such as red diode and He-Ne lasers, and avalanche photodiodes detectors. Storage under nitrogen or as frozen solution allows use of working stocks of **SQ-1** over a period of weeks or more without the risk of significant degradation. Cell imaging and viability studies show **SQ-1** to have low cytotoxicity and excellent imaging characteristics.

The kinetic heterogeneity observed for PtOEP polymer thin films sensor films under nitrogen has been shown to be due to a monomer:dimer equilibrium for which the kinetic data can be analysed in terms of two exponentials with $k_1 = 0.0527 \times 10^6 \text{ s}^{-1}$ (dimer), $k_2 = 0.0101 \times 10^6 \text{ s}^{-1}$ (monomer). The dimerisation constant (K_D) = 790 (± 20) mol⁻¹ dm³ in ethyl cellulose and 990 (± 50) mol⁻¹ dm³ in a polyurethane hydrogel. At low concentrations PtOEP gives linear Stern-Volmer plots, while calibration at all concentrations is possible using the Freundlich isotherm. In comparison to an unplasticised film with the same concentration of PtOEP the addition of a plasticiser causes an increase in the kinetic heterogeneity for the decay of PtOEP in the absence of oxygen. Using the monomer/dimer model this can be understood if the plasticiser shifts the equilibrium towards the dimer. The PtOEP/hydrogel sensing system has been evaluated as a dissolved oxygen sensor. The kinetic heterogeneity of the sensor is the same whether wet or dry. The sensitivity and Stern-Volmer quenching constants of the unplasticised hydrogel thin film sensor are

comparable for the wet and dry sensor. The advantageous properties of the hydrogels such as biocompatibility and low protein absorption make this sensing system ideal for further studies.

Ormosil probes encapsulated by biologically localised embedding (PEBBLEs) and self assembled sensing materials are shown to be convenient ways of encapsulating luminescent dyes before immobilization in a thin film sensor. The optical properties and response are unaltered by such a process. The development of ratiometric sensors for both oxygen and pH are described. The sensors are prepared using combinations of analyte sensitive and insensitive nanoparticles and self assembled sensing material immobilised in a biocompatible polymer. Using these materials, it is possible to use a combinatorial approach to designing colorimetric sensors for oxygen sensing and multi analyte sensors for oxygen and pH.

Chapter 1

Introduction

1. Luminescent Materials

Luminescent materials are encountered in a wide range of technological and biomedical applications, including fluorescent lighting, cathode ray tubes (CRTs), electroluminescent displays, X-ray detectors and physical and biomedical sensors. Luminescent materials absorb energy from an external source, such as high-energy photons, electrons, or chemical reactions, and re-emit the energy as electromagnetic radiation. The emitted radiation is usually in the visible and ultraviolet (UV) spectral region although infrared (IR) luminescence may also be emitted from some systems and this is gaining considerable attention in the field of biomedical science.

The aim of the work present here was to develop and evaluate novel and known luminescent systems in three different sensing technologies and applications namely: 1) near infrared probes for non-covalent labelling of biomolecules; 2) optical thin film sensors for oxygen; and 3) nanomaterials for optical analyte sensing. Although the requirements for each application are different, they all need lumophores with excellent chemical and photochemical properties which show high sensitivity to the analyte of choice within the sensing application.

To help place this work in context, this introductory chapter first of all gives a brief overview of the relevant photochemistry. This is followed by an introduction to luminescent materials for protein quantification. Then there is a section on optical sensors and current innovations in the field. The chapter ends with a brief overview of the work presented in the thesis.

1.2 Photochemistry

1.2.1 Absorption

Upon the absorption of light by a lumophore, electrons may be promoted from their normal ground state configuration to higher, previously unoccupied energy levels, resulting in the formation of high energy, short-lived excited states. The energy of the absorbed photon of light corresponds to the energy difference between the excited and ground states. In molecules, an electron is promoted from the highest occupied

molecular orbital (HOMO) to the lowest unoccupied molecular orbital (LUMO). The absorption process occurs very rapidly (10^{-15} s) allowing no time for significant displacement of the nuclei; each atom has nearly the same position and momentum before and after an electron transition (Franck Condon principle). The excited state then decays back to the ground state, losing energy in non-radiative processes and, in the case of lumophores, in the emission of luminescence. Since some of the excitation energy is converted to vibrational and rotational energy in the excited state, the emitted luminescence is of lower energy than the original excitation light.

1.2.2 Deactivation of excited states

A molecule containing excess electronic or vibrational energy may undergo a number of relaxation processes to return to the ground state, excess energy may be lost via radiative decay, characterised by emission of a photon of light i.e. luminescence. Excess energy may also be lost via radiationless energy transfer between vibronic levels in the same or lower energy states. Figure 1.1, the Jablonski diagram, represent the possible decay pathways from the singlet and triplet state. [1]

1.2.3 Radiative decay mechanism

1.2.3.1 Fluorescence

An allowed radiative transition between states of the same multiplicity, usually a singlet-singlet transition. The amount of energy emitted in this process corresponds to the energy difference between $S_1(0)$ and a particular vibrational level of S_0 . Because this is an allowed transition fluorescence usually occurs on the picosecond to nanosecond timescale.

1.2.3.2 Phosphorescence

A forbidden transition between states of differing multiplicity, usually a triplet-singlet transition. In the case of phosphorescence, the interconversion from a singlet to triplet state is not allowed by spin selection rules, and therefore does not occur readily, and generally takes place on a longer timescale than fluorescence, usually in the microsecond to second time range.

1.2.4 Non-radiative decay mechanism

1.2.4.1 Internal conversion and vibrational relaxation

Radiationless energy transfer between vibronic states of the same multiplicity i.e., when an excited molecule in the S₂ state deactivates to the S₁ state. In this process, the excess energy is dissipated in the form of heat.

1.2.4.2 Intersystem crossing

Radiationless energy transfer between vibronic states of differing multiplicity.

1.2.5 Selection rules for optical transitions

The excitation and relaxation of electronic energy states are governed by two selection rules which indicate the feasibility of a transition from one state to another. These selection rules arise due to the requirement that angular momentum must be conserved during a transition and that a photon has one unit of angular momentum.

1.2.5.1 Spin selection rule: ($\Delta S = 0$)

All radiative and non-radiative transitions are strictly forbidden between states of different multiplicity in the zero order approximation, which assumes that there is no interaction between states, i.e. they are “pure”.

1.2.5.2 Laporte selection rule:

For complexes with a centre of inversion, the only allowed transitions are those between states of different parity (i.e. wavefunctions with different symmetry). Therefore $u \rightarrow g$ and $g \rightarrow u$ transitions are allowed but $u \rightarrow u$ and $g \rightarrow g$ transitions are forbidden. Thus, the $d-d$ and $f-f$ transitions observed in transition metal and lanthanide complexes respectively are formally Laporte forbidden.

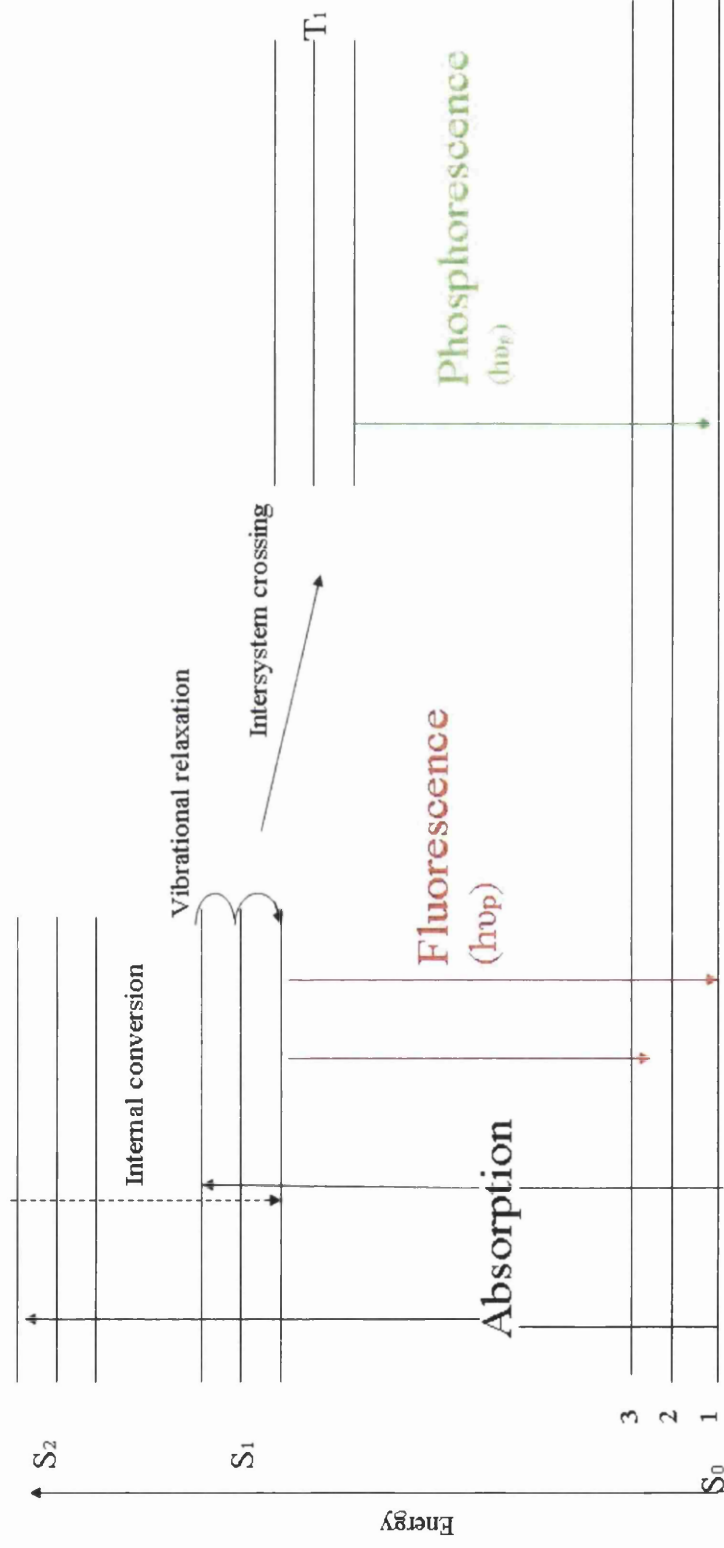


Figure 1.1. The Jablonski diagram.

1.2.5.3 Breakdown of the selection rules

Selection rules may be broken when mechanisms for coupling momenta occur or there are external perturbations. The following mechanisms have been identified as causing the failure of selection rules governing optical transitions:

- direct electronic coupling of T_1 with S_N ;
- indirect electronic coupling of T_1 with S_N via an intermediate triplet;
- elimination of a centre of symmetry via an asymmetrical vibration.

An electron orbiting the nucleus generates both spin and orbital magnetic moments. The interaction between spin and orbital magnetic moments is known as spin-orbit coupling. Spin-orbit coupling provides a magnetic “torque” capable of flipping the electron spin magnetic moment, and, can also provide a means of conserving total momentum by coupling a “spin-flip” with a compensating orbital jump. Thus, changes in spin momentum may be balanced by a change in orbital momentum; consequently the total angular momentum of the system is conserved. A second, weaker interaction between the magnetic moments of neighbouring electrons may also occur (spin-spin coupling), however in practice spin-orbit coupling dominates the breakdown of the spin-selection rule. Spin-orbit coupling mixes singlet and triplet states so that transitions become allowed to an extent which depends on the magnitude of the spin-orbit coupling constant. The strength of the coupling depends on the relative orientations of the spin and orbital magnetic moments and the nuclear charge on the atoms involved. The greater the nuclear charge, the greater the current generated by the electron orbital angular momentum, and thus the stronger the magnetic field. Since the spin magnetic moment interacts with this orbital magnetic field, it follows that the greater the nuclear charge, the stronger the spin-orbit interaction. Consequently, the degree of spin-orbit coupling increases dramatically with atomic number. For first row elements, such as C, N or O, the magnitude of spin-orbit coupling is smaller than the energy of vibrational couplings ($\sim 4\text{-}20 \text{ kJ mol}^{-1}$). [4] However, with increasing atomic number the magnitude of spin-orbit coupling begins to approach the value of electronic energy gaps ($\sim 80\text{-}125 \text{ kJ mol}^{-1}$) and strong electronic interactions such as spin inversion can occur on a timescale comparable to that of electronic motion. The heavy atom effect is a manifestation of this phenomenon, whereby the rate of a spin forbidden process is enhanced to an extent

where it becomes partially allowed, due to the presence of an atom of high atomic number, which is either part of, or peripheral to, the excited molecule.

1.2.6 Quantum yields and Lifetime

Fluorescence lifetime and quantum yield are key characteristics for a fluorophore.

The quantum yield is the number of emitted photon relative to the number of absorbed photons. The processes governed by the emissive rate of the fluorophore, Γ and its non radiative decay to S_0 (k_r). The fraction of fluorophores which decay through emission and hence the quantum yield is given by

$$Q = \frac{\Gamma}{\Gamma + k_r} \quad (1.1)$$

The lifetime determines the time available for the fluorophore to interact with or diffuse in its environment, and is defined as the average time the molecule spends in the excited state prior to return to the ground state.

$$\tau = \frac{1}{\Gamma + k_{nr}} \quad (1.2)$$

The lifetime of the fluorophore in the absence of non-radiative processes is called the natural lifetime

$$\tau_n = \frac{1}{\Gamma} \quad (1.3)$$

In principle the natural lifetime of a fluorophore can be calculated from the absorption spectra, extinction co-efficient and emission spectra of the fluorophore, the radiative rate constant can be calculated using the Strickler-Berg relationship. [3]

The natural lifetime can be calculated from the measured lifetime and quantum yield.

$$\tau_n = \frac{\tau}{Q} \quad (1.4)$$

1.2.7 Quenching

The deactivation of an excited state lumophore (L^*) to the ground state by another molecule, is known as *quenching*. [4]

1.2.7.1 Oxygen Quenching

Oxygen quenching is diffusion-limited and results in *dynamic quenching* of the excited state. When a quencher (e.g. O_2) and the excited state interact, energy is transferred from the excited state to the quencher. This results in the deactivation of the lumophore to the ground state and excitation of the quencher.



The lifetime of the luminescence is thus decreased by the presence of oxygen and the quenched luminescence lifetime, τ , is given by:

$$\tau = \frac{1}{(k_r + k_{nr} + k_q [O_2])} \quad (1.6)$$

$\tau =$ where k_q is the quenching rate constant, k_r is the radiative rate constant, and k_{nr} represents the combined rate constant for non-radiative deactivation pathways (i.e. k_{isc} and k_{ic}), where ISC is intersystem crossing and IC is internal conversion.

1.2.7.2 Stern-Volmer analysis

In general the results of quenching studies are discussed in terms of Stern-Volmer analysis of emission data. For a homogeneous system with lumophore, L , which decays naturally by a first order process, k_n , and which is dynamically quenched by oxygen, with a rate constant k_q , the rate of decay of the excited state of the lumophore, L^* , is given by:

$$-d[L^*]/dt = (k_n + k_q[O_2])[L^*] \quad (1.7)$$

For a homogeneous system, the decay of luminescence is expected to decay exponentially and there should be a linear relationship between the quenching efficiency, i.e. I_0/I or τ/τ_0 , and $[O_2]$. Given by

$$I_0/I = 1 + \tau_0 k_q [O_2] \quad (1.8)$$

Where I_0 is the emission intensity in the absence of oxygen, I is the emission intensity in the presence of oxygen, τ_0 is the lifetime in the absence of oxygen, k_q the bimolecular rate constant for oxygen quenching and $[O_2]$ is the concentration of oxygen. The equivalent kinetic equation sees I_0/I replace with τ_0/τ where τ_{is} the lifetime in the presence of oxygen at concentration $[O_2]$.

Although fluid solution studies usually yield linear Stern-Volmer plots, a characteristic of polymer encapsulated lumophores is a Stern-Volmer plot with downward curvature. This leads to problems with calibration and the usefulness of the sensors. A second common feature of oxygen quenching for almost all polymer/lumophore combinations is a non-exponential emission decay in the presence of oxygen. [5-16]

Since ground state oxygen is a triplet, quenching of a lumophore triplet state by oxygen is known as triplet-triplet annihilation. Spin statistics show that only 1 out of 9 possible triplet-triplet spin combinations results in the formation of singlet products and the rate constant for energy transfer quenching by oxygen of triplet states in fluid solution, is usually *ca.* 1/9th that for quenching of singlet states.

1.2.8 Perception of colour and colour representation

For the applications of interest to this work, the lumophore emission colour is extremely important. Since colour is a subjective phenomenon, the description of colour differences can be quite challenging. The CIE (Commission Internationale de l'Éclairage) system of colorimetry provides a numerical description of colour, known as x,y colour coordinates, that is based on the sensitivity of the human eye to light across the visible spectral region. [17-18]

Colour perception in humans is initiated by the absorption of light by three different spectral classes of cone cells present in the retina. Each class exhibits a different but overlapping spectral sensitivity, designated as λ_x , λ_y and λ_z , with maximum values at ca. 419, 531 and 558 nm respectively. The sum of the differing sensitivities is called the *photonic response* and displays a maximum value at 555 nm.

Colorimetry and the trichromatic perception of colour are based on Grassmans' laws. [17-18]

(i) Any colour may be matched by a linear combination of three other primary colours, provided that none of these may be matched by a combination of the other two.

(ii) A mixture of any two colours can be matched by linearly adding together the mixtures of any three other colours that individually match the two source colours.

(iii) Colour matching persists at all luminances.

1.2.8.2 CIE system of colorimetry

In practice, experiments on the additive mixture of light prove that there are no three colours which when mixed additionally can duplicate all spectral colours. Whilst the mixture may exhibit the required spectral hue, it generally fails to duplicate the required saturation for that colour. The only approach to obtain a perfect match is the addition of a "negative" colour, to desaturate the spectral hue. To overcome this problem in 1931 the CIE defined a system based on colour coordinates to characterise the colour properties of light. The primary colours (X , Y and Z) in this system are theoretically defined super-saturated colours, which lie outside the bounds of the spectral locus and as a consequence they eliminate the use of negative colours. An example of a CIE chromaticity diagram is shown in figure 1.2. [17-18]

In order to standardise this system, the CIE defined a secondary standard observer based on the differing sensitivity of the three classes of human cone cells. Consequently any colour, C , of wavelength, λ may be expressed as:

$$C_\lambda = \bar{x}_\lambda X + \bar{y}_\lambda Y + \bar{z}_\lambda Z \quad (1.9)$$

where X, Y, Z are the system primaries (known as tristimulus values) and $\bar{x}_\lambda, \bar{y}_\lambda$ and \bar{z}_λ are the colour matching functions as determined at a given wavelength from figure 1.6. Since the colour matching functions are non-negative over visible wavelengths, any colour may be matched by three positive values.

The $\bar{x}_\lambda, \bar{y}_\lambda$ and \bar{z}_λ terms may be used as weighting functions to determine the X, Y and Z tristimulus values that characterise the emission colour of luminescence data across the visible spectrum according to

$$\left\{ \begin{array}{l} X = \sum_{\lambda=380}^{700} \bar{x}_\lambda \cdot E_\lambda(\Delta\lambda) \\ Y = \sum_{\lambda=380}^{700} \bar{y}_\lambda \cdot E_\lambda(\Delta\lambda) \\ Z = \sum_{\lambda=380}^{700} \bar{z}_\lambda \cdot E_\lambda(\Delta\lambda) \end{array} \right. \quad (1.10)$$

The x and y chromaticity coordinates are typically plotted in a two-dimensional grid known as the (x,y)-chromaticity diagram (figure 1.2). The curve is made of the pure colours from the blue to the red, covering the entire visible spectrum (380-770 nm) and is known as the *spectral locus*. The centre of the diagram is taken as the *white point*, whose coordinates are designated as (0.33, 0.33).

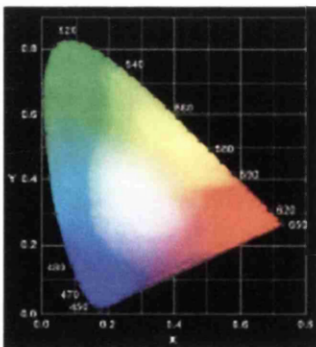


Figure 1.2 The CIE (x,y)-chromaticity diagram.. [17,18]

1.3 Near infrared luminescent materials for biological labelling

1.3.1 Background

Optical probes for labelling of biomolecules are widely used in science and clinical analysis. [19-25] The development of novel methods and new techniques for protein determination is extremely important in a number of areas including chemical and biochemical analysis, biotechnology and immunodiagnostics.[25-26] The quantification of proteins is important in clinical medicine and analytical biochemistry. [27]

There are several colorimetric methods for the determination of protein involving the binding of dyes to proteins including the biuret reaction [28] and the Lowry assay. [29] The Lowry assays are based on reduction of Cu^{2+} to Cu^{1+} by amides. The assays require the preparation of several reagent solutions, which must be carefully measured and mixed during the assay. This is followed by lengthy, precisely timed incubations at closely controlled, elevated temperatures, and then immediate absorbance measurements of the unstable solutions. Both assays can be affected by other substances frequently present in biochemical solutions, including detergents, lipids, buffers and reducing agents.[29] In 1976, Bradford [30] introduced the Coomassie brilliant blue method, a colorimetric protein assay, based on an absorbance shift in the dye Coomassie when the previously red coomassie reagent changes and stabilizes into coomassie blue by the binding of protein. This method is characterized by high sensitivity and short reaction time. The Bradford assay is faster, involves fewer mixing steps, does not require heating, and gives a more stable colorimetric response than the assays described above. Like the other assays, however, its response is prone to influence from non protein sources, particularly detergents, and becomes progressively more nonlinear at the high end of its useful protein concentration range. However, there is a slight nonlinearity in the response pattern because of an overlap in the spectrum of the bound and unbound dyes. [30]

Luminescence techniques have attracted particular attention. Sensitive spectrofluorometric methods also have been developed for the determination of protein in solution, such as the NanoOrange protein quantitation assay,[31] CBQCA protein quantitation assay,[32] fluorescamine method and OPA method. [33]

The use of intrinsic amino acid absorption and fluorescence can be used as a simple and non-invasive method for determining protein concentrations. Amino acids, tryptophan, tyrosine and phenyl alanine absorb at 280, 276 and 257 nm respectively. However, proteins have, by their very nature, poor UV absorption, and this method always suffers interference from accompanying substances and matrices which show absorption in the ultra-violet region. [34]

Most protein assays are run in the visible region and have serious background interferences from coexisting biomolecules. The fundamental barriers to the use of optical techniques for protein determination and imaging in vitro and in vivo are high light scattering, autofluorescence, and high absorption by endogenous particles of the skin and tissue. Hemoglobin (Hb), myoglobin, melanin and other heme proteins absorb visible light significantly in certain tissues. [35-36] Use of red and near-infrared light is the most basic step towards improved imaging. [35] Moving to near-infrared wavelengths confers other advantages for imaging mammalian tissues: less background fluorescence is excited, since autofluorescence in tissues (mainly due to pyridine nucleotides, folates, and flavins) is mostly excited by near ultraviolet and blue light; and less autofluorescence interferes, since fluorescence from most mammalian tissues peaks in the yellow and is very low beyond 650 nm. Rayleigh and Raman scattering are also reduced at higher wavelengths. For both processes the scattering intensity depends on $1/\lambda^4$ and operating at high wavelength improves the signal to scattering ratio. In addition sample decomposition is generally reduced when compared to lower wavelength excitation because of the lower photon energy.

Limitations on extending optical imaging even further toward the infrared are set by water absorption; not only are excitation and emission wavelengths attenuated, but significant heating of tissue is induced. The high concentration of water in tissues assures that its absorbency dwarfs contributions by other tissue components. If imaging at millimeter to centimeter depths is to be done with minimal signal attenuation and sample heating, the most favourable windows are below 950 nm and in the small window of reduced absorbency between ~1000-1100 nm. Of course, for imaging at shallow depths, more absorption is tolerable and 1300nm wavelengths have been used for both optical coherence tomography [36] and confocal scanning reflectance microscopy. [37] A balance is needed between reduced scattering and increased water absorption as wavelength moves beyond 950nm: because scattering

dominates in some tissues, high absorbency by water and other tissue components may be tolerated in order to get improved light output and better resolution. [38-39]

1.3.2 Dyes for the Near Infra Red (NIR)

The use of, dyes which emit in the near infrared region (600-1000 nm) is a rapidly developing area of research. [40-42] The photophysical properties of near infrared dyes have resulted in their use in a variety of applications including: photodynamic therapy, silver halide sensitizers, laser diodes and optical data storage. Recently NIR dyes have been found to have considerable applicability in protein based assays. In comparison to the ultraviolet and visible regions, NIR fluorescence has several advantages.

Since NIR wavelengths can effectively penetrate through skin and overlaying tissue There is the possibility of developing non-invasive clinical diagnostics, such as blood glucose monitoring. [43] Other materials such as plastics, glass, cloth and turbid water, paint and some building material are also transparent in the NIR regions. This suggests that NIR dyes may be useful in a wider variety of applications than the biomedical uses discussed here. [44] Experimentally excitation in the NIR can be accomplished by using cheap, stable and compact diode lasers and sensitive and stable NIR avalanche photodiode detectors are now readily available at relatively low cost. [45-46]

1.3.3 Organic fluorophores

1.3.3.1 Xanthene dyes

Fluorescein is an example of a classical xanthene dye. [47] Its absorption and emission wavelengths correspond closely to that of protein bound bilirubin. [48] Texas red and derivatives are shifted to longer wavelengths, with rhodamine 800 fitting most of the criteria for a NIR dye including excitation bands at 635nm, which is suitable for diode lasers. However protein interactions with rhodamine 800 result in only small fluorescence enhancements and give a blue shifts in the emission, making it unsuitable as a fluorescent protein probe. [49]

1.3.3.2 Phenoxazine dyes

Cresyl violet and Nile red [50-51] have both been identified as potential protein labels and probes. Nile red finding application as a polarity sensitive probe in protein misfolding and amyloid fibril studies. [52] Oxazine 750, [53] has an excitation wavelength well suited to 660-670 nm diode laser and is used in methods for the identification and characterization of reticulocytes in whole blood. [54]

Table 1.1. Properties of some commonly used semiconductor emitters. DL represents diode laser and LED represent light emitting diode. [55]

<i>Peak emission</i>	<i>Emitter type/nm</i>	<i>SC material</i>
515	DL	ZnCdSe
555	LED	
555-605	LED	GaP
590-630	LED	AlGaInP
630-690	DL and LED	AlGaInP
660-889	DL and LED	AlGaAs
940	DL	GaAs
980	DL	InGaAs
1300-1550	DL	InGaAsP

1.3.3.3 Carbocyanine and merocyanine dyes

There are numerous examples of carbocyanine dyes and their derivative in the literature. They have, for example, been employed extensively as: spectral sensitizers for silver halide photography and other inorganic large band-gap semiconductor, [56] recording materials in optical disks, [57] lasering materials, [58] light harvesters in model systems for photosynthesis, [59] photorefractive materials, antitumor agents [60] and as probes for biological systems. [61-71] The propensity of carbocyanines to photooxidise makes them useful in photographic film. [72] Cyanine dyes have widespread use as laser dyes due to their availability, high extinction coefficient, adequate quantum yields and small Stokes shifts. Cyanine dyes exhibit an increased fluorescence in non polar solvents due their propensity to aggregate in polar media. The most promising class of cyanine dyes for protein labelling are the covalent derivatives designed by Waggoner et al. and Research Organics. [73] The reactive fluorophores have emission peaks at 550nm, 650nm and 750nm for CY3, CY5 and CY7 respectively, with isothiocyanate and N-hydroxysuccinimide groups for covalent attachment to proteins. The extensive conjugation in the dye molecule increases the chemical and photochemical instability which can result in photobleaching and shortened shelf-life. This instability may be reduced by appropriate dye design such as incorporating the polymethine chain into a cyclic structure. Indocyanine green (ICG) is a cyanine dye that is currently approved for use in vivo as a probe of liver function and blood volume determination. [74-75]

1.3.3.4 Squarylium dyes

Squarylium cyanine dyes offer improved photostability over simpler cyanine type dyes. [76] also the squarate residue shifts the absorption and emission maxima to longer wavelengths.

Much like the analogous polymethine cyanine dyes, Squarylium dyes have attracted attention mainly because of their potential applications as photoconductor photoreceptors, [77] and in photodynamic therapy, [78] optical recording media, [79] nonlinear optics, [80] and organic solar cells. [81]

Examples of both symmetrical and asymmetrical squarylium dyes are known in the literature. A study by Terpetschnig suggests that symmetrical squarylium dyes have better photostability. [83-85] They show a strong non-covalent binding to proteins

with a concomitant bathochromic shift and increase in fluorescence intensity. Oswald and co-workers determined protein concentration using fluorescence spectroscopy. [86] The group compared the fluorescent properties of squaraine carbocyanine dye Sq635-b-NHS-ester with the commonly used noncovalent protein label Cy5. Quantum yield values for Cy5 were reported to decrease considerably in the presence of protein while Sq635-b-NHS-ester which exhibits a low quantum yield in water ($\phi = 0.15$) gave a much high quantum yields ($\phi = 0.6-0.7$) when bound to protein. The molar absorptivities for Cy5 and Sq635-b-NHS-ester were reported to be 250000 and 140000 L mol⁻¹ cm⁻¹ respectively. Due to the high extinction coefficient and quantum yield of the squaraine dye, detection limits in whole blood were twice as low as Cy5. Several example of squarylium probes for use in capillary electrophoresis are known due to their non covalent binding abilities, as discussed in chapter 3.

Squarylium dyes have also found uses in the area of studying protein–lipid complexes which is important for understanding molecular self assembly and the role of membranes and lipids in physiological and pathological processes. [87] Volkova et al. have recently shown the potential use of squarylium dyes for distinguishing between native and fibrillar proteins associated with neurodegenerative diseases such as Parkinsons and Alzheimers disease. [88]

Due to the ease of synthesis of squarylium dyes, [90-91] several groups have designed squarylium optical ion sensors. [91,92] NIR dyes for optical sensing of ions afford the advantages of having absorption and emission spectrally removed from that of biological material making them particularly well suited for intracellular sensing and imaging.

1.3.3.5 Other NIR probes

Both metallated and non metallated phthalocyanines and naphthalocyanines emit in the NIR and show exception stability. Substitution of the macrocycle improves the solubility of the dyes, with sulfonated phthalocyanines being water soluble. Transition metal polypyridyl complexes containing osmium emit from charge transfer bands at longer wavelengths that the ruthenium derivatives, which have gained so much attention due their favourable properties in solar energy and immunoassay research. Molecular probes/Invitrogen have produced a series of Bidipy derivatives that show considerable promise as protein labels, the longest wavelength derivatives emitting at just below 700 nm. [94]

1.4 Luminescent optical sensors

A chemical sensor is a device capable of providing continuous real-time chemical information about a sample of interest. [95] Optical sensors represent a group of chemical sensors in which electromagnetic radiation is used to generate the analytical signal in a transduction element. These sensors can be based on absorption, reflectance, luminescence and fluorescence, covering all regions of the spectra.

Luminescence based optical sensor are abundant in the literature. Emission parameters that can be measured include: intensity, decay time, anisotropy, quenching efficiency, and luminescence energy transfer. [96-98, 126, 100]

It is the ability of optical materials to give a rapid real time responses to a diverse range of analytes, with unmatched sensitivity, together with compatibility with other sensing technologies such fibre optics [99] and LED excitation, [100] which makes optical sensing technologies so exciting.

1.4.1 Oxygen sensors

Polyaromatic hydrocarbons (PAHs) were the first lumophores to be extensively used in the development of luminescent thin film oxygen sensors. PAHs are efficiently quenched at *ca.* 400 Torr oxygen [101-108], but their short natural lifetimes (10-100 ns) mean they are less suitable for low pressure sensing applications. Transition metal complexes, such as ruthenium diimines were first identified as being susceptible to oxygen quenching in solution in 1977. Demas and co-workers later showed that thin film oxygen sensors could be prepared by incorporating these complexes into silicone films. [101,103]

Transition metal complexes exhibit relatively long natural lifetimes (*ca.* 0.6 to 5 μ s) Good molar absorptivity and photo- and thermal stability, reasonably high quantum yields of luminescence, and often absorb and emit in the visible.[101-108] Attention has focused primarily on ruthenium polypyridyl complexes such as $[\text{Ru}(\text{dpp})_3]^{2+}$ $[\text{Ru}(\text{bpy})_3]^{2+}$ and $[\text{Ru}(\text{phen})_3]^{2+}$. Mills et al introduced the idea of ion pairing with a hydrophobic anion such as tetraphenyl borate or dodecyl sulphate to improve polymer compatibility. [105]

The use of metalloporphyrins have dominated the development of more sensitive optical oxygen sensors. Platinum and palladium porphyrins remain the most

commonly used lumophores as they have high quantum yields (ca. 0.4-0.9 and 0.1-0.2 respectively), exhibit long lifetimes, are compatible with hydrophobic polymers, and have excitation and emission wavelengths in the visible. [110-119] Modification of the porphyrin ring by the addition of alkyl or ketone groups produces lumophores of different natural lifetime and oxygen sensitivity. Pt and Pd octaethylporphyrins (PtOEP, PdOEP) remain the most widely used lumophores for oxygen sensor applications, but other derivatives such as PtTFPP [120] and PtOEPK [121] are receiving increasing attention due to their enhanced photostability.

1.4.1.2 Dissolved oxygen

Although there has been much work on gas phase oxygen sensors there is little literature on the use of metalloporphyrins as optical sensors for dissolved oxygen. [122-126] One group reports the design of dissolved oxygen sensor based on PtOEP in a fluorinated polymer but this gave a very non-linear response. [122] Other examples of dissolved oxygen sensors include the use of erythrosin B encapsulated in a sol-gel [123] and in a sol-gel/fluoropolymer combination. [124] However, the response of these sensors also show considerable deviation from linearity.

1.4.2 Halothane sensors

Halothane (2-bromo-2-chloro-1,1,1-trifluoroethane) is an inhalation narcotic frequently used in anesthesia and effectively quenches the decacyclene fluorescence. The fluorescence of decacyclene is quenched by molecular oxygen and aryl and alkyl halides. The cross sensitivity of decacyclene has led to the development of sensors incorporating a second oxygen sensitive reagent to monitor the oxygen interference. [127]

1.4.3 Sulphur dioxide

Sulphur dioxide monitoring in air and in combustion gases is important in industry and environmental science. [128] Polycyclic aromatic hydrocarbons are effectively quenched by sulphur dioxide, and example of lumophores used in SO₂ sensors include fluoroanthene, benzo(b)fluoroanthene and pyrene. Wolfbeis et al. [127] have designed a fibre optic SO₂ sensor by dissolving benzo(b)fluoroanthene in a silicone polymer. Additional lumophores are required due to the cross sensitivity of the lumophore to

olefins and alkyl bromides, the sensors was found to have a response time less than 60 s and a useful analytical range of 0-6% detection range in air.

1.4.4 Halide

The sensing of halides is important for environmental analysis particularly in ground and waste water. [129] Quinolinium (6-methoxy-N-(3-sulfopropyl) quinolinium SPQ) and acridium (3,6-bis(dimethylamino)acridine SPA) compounds are dynamically quenched by halide ions. Sensors have been prepared by covalently attaching these lumophores to a glass surface. These sensors having a sensitivity in the mMol range for chloride (10mM), iodide (0.4mM) and bromide (0.15mM) and a response time of 40 s in a flow-through cell. [130-131]

1.4.5 Humidity

The design of humidity sensors based on silica gel absorbed perylene dyes has been described. [132-133]

1.4.6.1 Oxygen sensors as transducers

Many chemical and biochemical reactions produce or consume oxygen which can lead to a change in emission of an oxygen sensitive lumophore. A catalyst for a particular reaction involving oxygen production or release can also be immobilised in the sensor, and if the catalyst is biologically active, such as an enzyme, a simple biosensor can be constructed.

1.4.6.2 Hydrogen peroxide

Sensors based on the dynamic quenching of ruthenium-(II)-tris(bipyridyl) by oxygen produced by decomposition of hydrogen peroxide have been reported. [134-136]

The decomposition of hydrogen peroxide by the enzyme catalyse, or silver powder, yields water and oxygen,

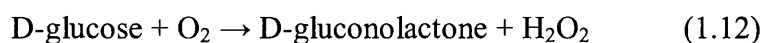


and the concentration of oxygen can then be related to the hydrogen peroxide concentration. Wolfbeis et al. [134] described a fibre optical hydrogen peroxide sensor based on co-immobilisation of catalase and an oxygen sensitive dye immobilised on silica gel embedded in a silicone polymer, A second sensor based on

the use of silver powder applied as a second layer showed improved long term storage stability.[136]

1.4.6.3 Glucose

Optical glucose sensors have been the subject of much research due to its importance in biomedicine and biotechnology. [137-139] If a sensor incorporates the enzyme glucose oxidase, which mediate the air oxidation of glucose according to equation 1.12, then the consumption of molecular oxygen can be used to obtain the concentration of glucose.



Glucose oxidase is commercially available, inexpensive and extremely stable. Such sensors have been designed using glucose oxidase covalently attached to a nylon membrane which was fixed on an oxygen sensitive layer consisting of solubilised decacyclene dissolved in silicone. Improved sensitivity was achieved by replacing the nylon membrane with a glutaraldehyde-crosslinked enzyme layer. Differing sensing schemes based on sol-gel technology have been described. [203,206]

1.4.6.4 Biosensors

In theory, the sensing scheme for glucose is applicable to all enzymes that consume molecular oxygen during their enzymatic reaction. [140] A small number of oxidases and oxygenases have been designed and tested. The main problem with the sensor design is the long term stability of enzyme. Table 3.2 lists the biosensors that have been designed in this way.

Table 1.2 Optical sensors based on oxygen optodes as the transducers. [141-142]

<i>Substrate</i>	<i>Enzyme</i>
L-Lactate	L-Lactate monooxygenase
L-Lactate	L-Lactate oxidase
Cholesterol	Cholesterol oxidase
Ascorbic acid	Ascorbic acid oxidase
L-glutamate	L-glutamate oxidase
Hypoxanthine	Xanthine oxidase
Ethanol	alcohol oxidase
Tyrosine	Tyrosine oxidase
Phenol	Phenol oxidase
Catechol	Catechol oxidase
Urea	Urea oxidase

1.4.7 pH and carbon dioxide sensors

Biochemical processes frequently involve protonation and deprotonation of biomolecules, leading to changes in pH. A number of important biological phenomena including: calcium regulation, chemotaxis, neuronal activity, cell growth and division, are highly dependent on pH. Optical sensors for pH based on changes in absorbance, [143] intensity [144] and lifetime [145-146] are known.

Fluorescent pH probes have been used in studies relating to cancer, cell proliferation and endocytosis. [147-150] It is well established that the pH of interstitial fluid in malignant tumours tends to be higher than normal tissue. The pH dependent change in the fluorescence properties of 5,6 carboxyfluorescein and its low cytotoxicity makes it an ideal candidate for intracellular pH sensing. [151-152] Conjugation of fluorescein isothiocyanate (FITC) to proteins and sugars sees the retention of the pH sensing properties, making them potential candidates for FITC labelled antibodies for site specific intracellular pH sensing. [153-154] One of the key problems associated with the UV/vis absorbing and emitting dyes is poor visualisation in biological media such as tissues and blood. The sensitivity is low because endogenous chromophores also either absorb or emit in this range. However, new NIR fluorescent pH sensors based on cyanine dyes absorb between 600-700 nm with emission between 600 to 800nm have been reported with pK_a values in the physiological range. [155]

Characteristics for an ideal biomedical optical thin film pH sensor should include the following.

- pK_a in the physiological range
- Easily immobilised in a suitable polymer
- Excitation wavelength compatible with inexpensive plastic fibre optics
- Non toxic
- Rapid response
- Reversible response

One of the inherent drawbacks of early pH sensors was the leaching of dyes from the sensor. Early attempts saw phenol red and neutral red immobilised on activated diacetylcellulose. [156] The stability of the linkage groups is a very important factor,

ester linkages and acidamide linkages are not stable in very acid or alkaline conditions. An attempt to covalently immobilise phenol red in microspheres, produced a sensor with limited useable lifetime due to the hydrolysis of the acidimide linkage. Activation of phenol red with formaldehyde to produce hydroxyl methyl groups reacted with polyvinyl alcohol (PVA) to produce a thin film sensor with good spectral and stability characteristics. [157]

Optical sensors for the determination of carbon dioxide play an important role in several environmental, industrial and biological processes. Here, detection limit and insensitivity to humidity are often the most important sensor parameters. [158] Typically, optical CO₂ sensors are based upon the immobilisation of a pH sensitive indicator. [159]

Carbon dioxide and acidic gas sensors can be classified as wet (liquid phase) or dry. The wet or liquid phase carbon dioxide sensors use a pH sensitive dye in an aqueous medium containing sodium carbonate immobilised in a gas permeable, ion impermeable membrane. [160] The basic principle are simple and similar to those of the Severingus carbon dioxide electrode. A disadvantage of the wet sensor is sensitivity to the water pressure or osmotic pressure of the system, which if significantly different to that of the sensor can leading to either hydration or dehydration of the sensor and the need for recalibration. Dry sensors circumvent the need for the sodium bicarbonate layer by the incorporation of phase transport agents (PTA's) such as tetraoctyl ammonium hydroxide which, when mixed with a pH sensitive hydrophilic indicator dye, form ion pairs that can be dissolved in non-aqueous hydrophobic solvents. [109]

1.5 Materials for optical sensors

1.5.1 Sol gel

Sol gel technology offers an alternative to conventional glass production, enabling the final product to have high homogeneity and purity. The excellent optical properties and ease of preparation has seen the design of a number of sol gel, and more recently organically modified sol gel (ormosils), based sensors. [161-162]

The basic sol gel process can be represented by the following equation (1.11)



Sol gel characteristics, such as porosity, surface area, and refractive index, are determined by factors such as: type of precursor, pH, nature and concentration of catalyst, H₂O: Si molar ratio, co-solvents, temperature and drying time. [162] Sol gel based sensors can be either hydrophilic or hydrophobic in nature.

1.5.2 Polymers and membranes

Commonly used polymer in optical sensors may be divided into:

- (i) silicone polymers e.g. poly(dimethylsiloxane). [163-164]
- (ii) organic polymers e.g. polystyrene, [165] poly(vinylchloride) and poly(methylmethacrylate). [166]
- (iii) fluoropolymers e.g. poly(2,2,2-trifluoroethylmethacrylate). [167]
- (iv) cellulose derivative polymers e.g. ethyl cellulose and cellulose acetate butyrate. [168, 169]

The properties of the sensor film will strongly depend on the properties of the polymer matrix, and in particular, its permeability to gases, P . Table 3.3 summarises the oxygen mobility parameters of some common polymers (oxygen diffusion (D), permeability (P) and solubility (S) constants). [170] There has been considerable interest in new and innovative supports for oxygen sensing material. Ruthenium and porphyrin based lumophore have been adsorbed onto mesoporous silica and thin layer silica and alumina chromatography plates. [171-173] Gaseous and dissolved oxygen sensors have also been produced using organically modified silicates, class II xerogels, as supports. [174-175]

1.5.3 Hydrogels

Hydrogel polymers have gained much attention for use in biomedicine. [176-179] Typical example of hydrogels include: cellulose, dextrans, polyacrylamides and polyurethanes. Polyurethane hydrogels have recently been used in a variety of sensing applications and in commercial instrumentation, and sensors for water soluble analytes such as urea, glucose and hydrogen peroxide have been described. Those

most useful hydrogels for optical sensors are expected to be insoluble in, but highly permeable to, water and aqueous samples including serums. In many cases these properties can be controlled by their monomer composition. [178] Several examples of micro and nanoparticles immobilised in hydrogel polymers for optical pH, oxygen and temperature have been described. [194-196]

1.6 Innovations in optical sensing

1.6.1 Innovations in sensing materials

1.6.1.1 Quantum dots

Quantum dots (Q-dots) are considered as semiconducting materials that are neither small molecules nor bulk solids. Typically they are sulphides or selenides of cadmium. [180-184] The Q-dots have diameters ranging from 3-30nm and are highly fluorescent non bleaching fluorophores with narrow symmetric emission spectra ranging from the UV to NIR spectral range. The colour can be tuned by changing the size and material as shown in table 1.4

Table 1.4 Materials used to make quantum dots and their characteristic emission wavelengths. [181-184]

<i>Material</i>	<i>Emission wavelengths</i>
CdS	Uv blue emission
CdSe	Visible
CdTe	Near and far IR

The largest potential use of Q-dots is in biosensing where surface modification with both hydrophobic and hydrophilic materials enables sensing in both lipid and aqueous environments respectively. The surface can also be used for conjugation to proteins, oligonucleotide, biotin and avidin. Yet surface charge, limited excitation wavelengths aggregation and nonspecific binding limit their usefulness.

1.6.1.2 Molecular imprinting (MIP)

Polymeric networks can be used to create materials with cavities of specific shape and size for a specific analyte template. [188-192] They can be prepared from hydrophobic or hydrophilic polymers including crosslinked polyacryamides and polyacrylates. Optical and mass-sensitive devices are suitable for trace analyses down to the ppb range. Imprinted polymers can be combined with pre-organized supramolecular hollows, which lead to further improvements in selectivity and sensitivity. Use of a colorimetric or chromametric dye has for amine has successfully been designed. [188] The MIPs have been termed plastic antibodies and may offer an alternative to current immunosensors and may even be capable of mimicking antibodies and biomolecular receptors. [192]

1.6.1.3 Organic conducting polymers (OCP)

OCPs are obtained by chemical or electrochemical polymerisation of organic monomers such as anilines, pyrroles or thiophenes. The fluorescence of the materials is not particularly selective and spectral changes can be induced by pH, and acid gases such as HCl, SO₂ and ammonia. Coating the OCP with a polymer also allows the material to sense these gases in aqueous environments. The response to pH changes is often slowly reversible or non reversible. OCP have also been designed to be responsive to hydrogen peroxide and ozone. OCPs can be functionalised with boronic acid side groups for the detection of saccharides. [190, 193]

1.6.1.4 Nanoparticles

In one of the earliest paper on the use of nanoparticles in optical sensing zeolite γ -nanocrystals were used as cavities for lumophores. The fluorescent oxygen sensitive probe ruthenium-2,2',bipyridyl was prepared inside the zeolite from which its size inhibited its escape, producing a sensor with effective oxygen quenching properties and long term stability. [197] The use of permeation-selective microbeads also enabled simultaneous sensing of pH and O₂ using carboxyfluorescein in amino-modified polyacrylamide or poly(hydroxyethyl methacrylate) microparticles as the pH indicator along with ruthenium-tris-diphenylphenanthroline²⁺ in organo silica microspheres within a hydrogel matrix for oxygen detection. [179] The advantages of using lifetime-based and ratiometric evaluation methods were also impressively

demonstrated recently, where a scheme combined of time-domain DLR and RLD (rapid lifetime determination) was employed, along with comparable indicator chemistry, for high-resolution dual imaging of pH and pO₂ in marine sediments. [198] The method uses a platinum porphyrin luminophore in polystyrene as the oxygen-sensitive layer, and a lipophilic ion pair of 8-hydroxypyrene-1,3,6-trisulfonic acid trisodium salt (HPTS) within ethyl cellulose (EC) microbeads which were dispersed along with reference beads containing an iridium(III)-coumarin luminophore within a gas impermeable poly(acrylonitrile-co-acrylic acid), all placed in a layer of silicone. [199] Changes in colour and brightness can be readily visualized. The readout of the signal for oxygen is based on the reduction of luminescence lifetime, while that of carbon dioxide is based on frequency-domain dual lifetime referencing (fd-DLR). The dual sensor served to monitor the growth of an oxygen-consuming and CO₂-producing *Pseudomonas putida* bacterial culture.

1.6.1.5 Probes encapsulated by biologically localised embedding (PEBBLES)

Small sensors are crucial for precise intracellular/subcellular analyte detection. [200-210] Small sensor size provides many advantages including greater chemical imaging resolution and acuity, lower detection limits and faster response.[201] The smallest sensor have been microelectrodes and submicrometer fibre based optodes, the dimensions and shape of both are not compatible with cell dimensions and volumes. In particular the penetration volume is usually more than 1% of the total cell volume, and this large penetration volume induces severe biological perturbation and endangers cell viability.

PEBBLE sensors are an outgrowth of fluorescent microspheres and beads. The PEBBLE composition including the matrix, the fluorophores and other components can be optimised for a particular task. The science of nanooptode production relies on advances in nanoscale production using emulsion and dispersion fabrication techniques. There are three main classes of PEBBLES, the method of production involves simple wet chemistry methods, that once optimised provide a simple and reliable method of production. [203]

1.6.1.5.1 Polyacrylamide (PAA) hydrogel

The production of acrylamide PEBBLES is based on the nanoemulsion technique studies by Daubres. [203] Control over particle size and shape is achieved by adjusting the surfactant to water ratios in the emulsion. A typical procedure involves a

hydrophilic dye of choice. Several examples of PAA nanospheres are known in the literature for pH, oxygen, or calcium, sensing. [204-205]

1.6.1.5.2 Sol gel silica/organic hybrid

Sol gel glass has also been used as the matrix for the fabrication of PEBBLEs because of the superior properties over organic polymers. Sol gel glass is a porous, high purity optically transparent and homogenous material, making it ideal for spectroscopy. The preparation of sol gel glasses involves soft chemical conditions including low temperatures and mild pH, allowing the use of organic dyes and biomolecules. The properties of the sol gel can be tailored and controlled by varying the processing conditions and the concentrations or type of reactants used. Real time measurement of dissolved oxygen inside living cells by organically modified silicate nanosensors has been performed. [206-208]

1.6.1.5.3 Decyl methacrylate hydrophobic liquid polymer

The use of fluorescent indicator molecules has proven valuable in the study of intracellular analytes, however many ions exist for which no fluorescent indicator is sufficiently selective or even available. The decyl methacrylate hydrophobic liquid polymer offers an alternative class of tandem optical sensors. [209-210]

1.6.2 Multianalyte sensors

Multispot sensors have been described for a variety of analytes. The first multi sensor for O₂, CO₂ and pH was constructed of sensor spots placed in close proximity. [211]

A multisensor for halide determination utilizes SPQ and SPA which are not specific to a halide and are increasingly effectively quenched by chloride, bromide and iodide respectively. [129-130] To compensate for cross sensitivity multisport sensors consisting of lumophores with differing sensitivities has been employed. Dual sensors compensating for oxygen include those for glucose where an oxygen sensor is used to compensate for the variable supply of oxygen to glucose oxidase and for halothane where the indicator lumophore is sensitive to both halothane and oxygen. Other multi sensors include those for penicillin and pH, where the pH sensor compensates for the pH dependent signal causes by the penicillinase. [205]

The use of multiple sensors are becoming increasingly popular in biotechnology and biomedicine. An optical sensor for oxygen and pH for a high through put bioreactor

has been demonstrated. Optical density, O₂ and glucose has been monitored using a multiple sensor in a microprocessor.[212] Osmetech have produced a disposable kit for the determination of pH, O₂, CO₂, Na⁺, K⁺ Ca²⁺ hematocrit and glucose. [213]

In a recent review Nagl highlights the need for a true dual or multi analyte sensor and suggests that there are several limitations with the current sensors designs. [214] It is suggested that for a true multiple sensor cross sensitivity should be avoided. In the case of a dual layer sensor cross leaching of the components may occur, including the indicators and plasticisers. For multiple sensors generation of singlet oxygen in oxygen sensors can lead to an increased photodecomposition and signal drifts compared to single sensors. The author suggests the use of micro and nanoparticles to overcome these problems.

There has been much research centred around the use of a second sensing element in optical oxygen sensors where, because of the inherent temperature dependency of oxygen sensors, much work has centred around simultaneous sensing of oxygen and temperature. [215] Pressure-sensitive paint (PSP) is a luminescent oxygen-sensitive film, which, when combined with CCD-based luminescence imaging methods, is used for the measurement of surface-air pressure distributions on aerodynamic models in wind tunnels. However, these paints are susceptible to systematic measurement errors due to changes in the excitation intensity, the distribution of surface illumination and model motion during measurement. These variables maybe corrected for by the use of dual-lumophore PSP (DL-PSP), which contains one lumophore that is quenched by oxygen and a second reference lumophore that corrects for excitation variations and luminescence intensity changes.[216-217] Recently, Schanze and co-workers, [218] reported a multi-lumophore PSP containing three lumophores: (i) an oxygen and temperature sensitive dye (PtTFPP); (ii) a temperature sensitive dye ([Ru(phen)₃]Cl₂) encapsulated in oxygen-impermeable polyacrylonitrile (PAN) nanoparticles; and (iii) an intensity reference dye (rhodamine 110). PAN has a very low gas permeability and has been the material of choice for optical temperature sensing as there is no cross sensitivity with oxygen. [216, 218]

Oxygen and pH are of fundamental importance in medicine and biotechnology. Both parameters are needed to control the quality of drinking water, the freshness of food

and optimum conditions for cell activity in bioreactors. Knowing pH and oxygen concentration is also essential in clinical analysis of samples such as blood and other physiological liquids. The determination of both parameters is also important in marine research and sea water analysis.

Examples of dual sensors for O₂ and pH are known in the literature but these employ two sensors operated in parallel. The space limitations and sample volumes available makes the use of such sensors difficult. Hence the design of a simple and small sensor for both analytes, with excitation at a single wavelength would be a very powerful tool in biomedicine and biotechnology. A fibre optic system composed of indicator loaded microbeads has been described based on dual lifetime referencing, with 5,6-carboxyfluorescein microspheres and ruthenium phenanthroline nanoparticles as sensing elements. [179] Although there is little cross sensitivity the response of the Ru oxygen sensing material shows deviations from linearity which can lead to problems with calibration. It is worth noting that the temperature cross sensitivity of RuPhen was not considered.

1.6.3 Colorimetric sensors

Whilst Stern-Volmer analysis is a useful tool for the quantitative measurement of oxygen, an understanding of sophisticated instrumentation is needed for accurate determination. An alternative approach is the design of colorimetric sensors. [219] Colorimetric absorption based sensors are well known, but still need a detection unit. A red-green traffic light response, detectable by the human eyes has been reported for sensor films based on immobilising a red emitting oxygen sensitive lumophore (PtOEP) and a green emitting oxygen insensitive lumophore (cyclo metallated platinum complexes of N^CN-coordinating ligand 1,3-di-(2-pyridyl)benzene) in an ethyl cellulose thin film sensor. Key to the development of the optical sensors is the simplification of instrumentation. Many sensors are designed with lumophores that are compatible with common simple LED excitation systems. PtOEP is one such lumophore, and a simple, reliable colorimetric sensors based on using a green LED and PtOEP/EC sensing material has recently been described. [219-220] Colorimetric analysis of biomolecules is also possible using absorption based methods. [221] Gold nanoparticle aggregates with interparticle distance greater than particle diameter appear red, but as the separation distance is decreased to less than the average particle

diameter the colour becomes blue shifted. Such a method has been used to detect femtomolar quantities of oligonucleotide.

1.7 Thesis overview

In this work several novel and known luminescent systems will be investigated for use in different technological applications namely:

- 1: near infrared probes for non-covalent labelling of biomolecules;
- 2: metallo octaethylporphyrins in optical thin film sensors, and;
- 3: nanomaterials for optical analyte sensing.

Particular attention has been paid to designing materials with useable characteristics applicable to biomedicine and biotechnology.

Chapter 2 describes the experimental techniques used during the course of this study. Chapter 3 describes the synthesis, chemical and photochemical characterisation of a squarylium dye together with an evaluation of its use as a probe in biomedical systems. Chapters 4 and 5 are related to the design of optical thin film sensors. Chapter 4 focuses on understanding the unquenched kinetic heterogeneity of PtOEP in thin film sensors. A polyurethane hydrogel is also evaluated as a biocompatible polymer for optical sensing. Chapter 5 describes the preparation and use of lumophore doped nanoparticles, and lumophore doped self assembled materials, in the design of ratiometric oxygen, pH, and oxygen and pH optical sensors. The potential use of nanoparticles to prepare a colorimetric oxygen sensor is also discussed. Chapter 6 provides a brief summary and discussion of the results obtained during this work, together with some suggestions for further studies.

1.8 References

- 1 J.R. Lakowicz, Principles of Fluorescence Spectroscopy. 3rd ed.; Springer Science: New York, 2006.
- 2 D.A. Skoog, D.M. West, Fundamentals of Analytical Chemistry. 8th ed.; Brooks/Cole-Thomson Learning: Belmont, 2004.
- 3 S.J. Strickler and R.A. Berg, *J. Chem. Phys.*, 37, (1962), 814-22.
- 4 P. M. Gewehr and D. T. Delpy, *Med. Biol. Eng. Comput.*, 31, (1996), 2-6.
- 5 H.N. McMurray, P. Douglas, C. Busa and M.S. Garley, *J. Photochem. Photobiol. A: Chem.*, 80 (1994), 283-288.
- 6 I. Klimant and O.S. Wolfbeis, *Anal. Chem.*, 67, (1995), 3160-3166.
- 7 P. Hartmann, M.J.P. Leiner and M.E. Lippitsch, *Sens. Actuators B.*, 29, (1995), 251-257.
- 8 E.R. Carraway, J.N. Demas, B.A. DeGraff and J.R. Bacon, *Anal. Chem.*, 63. (1991), 337-342.
- 9 E.R. Carraway, J.N. Demas and B.A. DeGraff, *Langmuir*, 7, (1991), 2991-2998.
- 10 A. Mills and A. Lepre, *Anal. Chem.*, 69, (1997), 4653-4659.
- 11 S. Lee and I. Okura, *Spectrochim. Acta. A.*, 54, (1998), 91-100.
- 12 P.M. Gewehr and D.T. Delpy, *Med. Biol. Eng. Comput.*, 32, (1994), 659-664.
- 13 P.M. Gewehr and D.T. Delpy, *Med. Biol. Eng. Comput.*, 31, (1993), 11-21.
- 14 S. Lee and I. Okura, *Analyst*, 122, (1997), 81-84.
- 15 J. Kavandi, J. Callis, M. Gouterman, G. Khalil, D. Wright, E. Green, D. Burns and B. McLachlan, *Rev. Sci. Instrum.*, 61, (1990), 3340-3347.
- 16 Y. Amao, K. Asai and I. Okura, *J. Porphyrins Phthalocyanines*, 4, (2000), 292-299.
- 17 D. B. Judd and G. Wyszecki, 'Color in Business, Science and Industry', Wiley,
- 18 R. W. G. Hunt, 'Measuring Colour', Ellis Horwood, 1991.
- 19 G. Patonay, J. Salon, J. Sowell and L. Streckowski, *Molecules*, 9, (2004), 40-49.
- 20 S. A. Soper, Q. L. Mattingly, *J. Am. Chem. Soc.*, 116, (1994), 3744-3752.
- 21 C. Sun, J. Yang, L. Li, X. Wu, Y. Liu and S. Liu, *Journal of Chromatography B*, 803, (2004), 173-190.

- 22 M.L. Sánchez-Martínez, M.P. Aguilar-Caballo and A. Gómez-Hens, *Analytica Chimica Acta*, 523, (2004), 35-41.
- 23 B. Sendra, S. Panadero, S. Eremin and A. Gómez-Hens, *Talanta*, 47, (1998), 153-160.
- 24 F.-Y. Wu, F.-Y. Xie, Y.-M. Wu and J.-I. Hong, *Spectrochimica Acta Part A: Molecular and Biomolecular Spectroscopy*, 70, (2008), 1127-1133.
- 25 H.J. Gruber, C.D. Hahn, G. Kada, C.K. Riener, G.S. Harms, W. Ahrer, T.G. Dax and H.-G. Knaus, *Bioconjugate Chem.*, 11, (2000) 696-704.
- 26 E. Rusinova, V. Tretyachenko-Ladokhina, O.E. Vele, D.F. Seneor and J.B. Alexander Ross, *Anal. Biochem.*, 308, (2002) 18-25.
- 27 H. Zheng, Y.X. Mao, D.H. Li and C.Q. Zhu, *Analytical Biochemistry*, 318, (2003), 86-90.
- 28 J.G. Wang. In: Linchuang Shenghua Jianyan, Human Science and Technology Press, Changsha (1996), p. 489
- 29 O.H.Lowry, N.J. Rosebrough, A.L.Farr, R.J. Randall, *J Biol. Chem.*, 193, (1951), 265–275.
- 30 M.M. Bradford, *Anal. Biochem.*, 72, (1976), 248–254.
- 31 J.P. Liu, Y.Z. Hsieh, D. Wiesler and M. Novotny, *Anal. Chem.*, 63, (1991), 408–412.
- 32 R.P. Haugland, in: Handbook of Fluorescent Probes and Research Chemicals, sixth ed., Molecular Probes, pp. 180–182.
- 33 A. Lorenzen and S.W. Kenndy, *Anal. Biochem.*, 214, (1993), 346–348.
- 34 A.Demchenko, Ultraviolet spectroscopy of proteins, (1981),Springer-Verlag, New York
- 35 S. Wan, R.R. Anderson and J.A Parrish, *J. Photochem. Photobiol.*, 34, (1981), 493-500.
- 36 J.Sandby-Moller, T. Poulsen and H.C.Wulf, *J. Photochem. Photobiol.*, 77, (2003), 616-620.
- 37 Y. Pan, D.L.Farkas, *Proc. SPIE.*, 93 ,(1997), 2983-2990.
- 38 Y. T. Lim, S Kim, A Nakayama, N. E Stott, M. G Bawendi and J.V. Frangioni, *J.Mol. Imaging*, 2, (2003), 50-55.
- 39 C.P. Parungo, S.Ohnishi, A.M De Grand, R.G Laurence, E.G.Soltesz, Y.L Colson, P.M Kang, T.Mihaljevic, L.H. Cohn and J.V. Frangioni, *Ann Surg Oncol.*, 12, (2004) 1085-92.

- 40 A. Gómez-Hens and M.P. Aguilar-Caballo, *TrAC Trends in Analytical Chemistry*, 23, (2004), 127-136.
- 41 F. Song, X. Peng, E. Lu, R. Zhang, X. Chen and B. Song, *J. Photochem and Photobiol A: Chem.*, 168, (2004), 53-57.
- 42 J. Arden-Jacob, J. Frantzeskos, N.U. Kemnitzer, A. Zilles and K.H. Drexhage, *Spectrochimica Acta Part A: Molecular and Biomolecular Spectroscopy*, 57, (2001), 2271-2283.
- 43 X.-D. Wang, T.-Y. Zhou, X. Chen, K.-Y. Wong and X.-R. Wang, *Sensors and Actuators B: Chemical*, 129, (2008), 866-87.
- 44 E. Shives, Y. Xu, and H. Jiang, *Optics express*, 20, (2002), 1557-1562.
- 45 B. Oswald, M.Gruber,M. Böhmer, F. Lehmann, M. Probst, O.S. Wolfbeis, *Photochemistry and Photobiology*, 74, (2001), 237 – 245.
- 46 B. Oswald, L. Patsenker, J. Duschl, H. Szmazinski, O.S. Wolfbeis and E. Terpetschnig, *Bioconjugate Chem.*, 10, (1999), 925-931.
- 47 H. Maeda, N. Ishida, H. Kawauchi And K. Tuzimura, *J. Biochem.*, 65,(1969), 777-783.
- 48 B.T Doumas, T.W Wu and B. Jendrzejcak, *Clinical Chemistry*, 33, (1987), 769-774.
- 49 N. Nizomov1 , Z. F. Ismailov, É. N. Kurtaliev, Sh. N. Nizamov, G. Khodzhaev and L. D. Patsenker, *Journal of Applied Spectroscopy*, 73, (2006), 432-436.
- 50 R. Kiesslich and M.F. Neurath, *Digestive and Liver Disease*, 38,(2006), 301-302.
- 51 T. E. Edmonds, J. N. Miller, N. J. Seare, *J. Fluorescence*, 3, (1993) 129-131.
- 52 B. Demeulea, R. Gurnya, T. Arvinte, *International Journal of Pharmaceutics*, 329, (2007) , 37-45.
- 53 T. Kanela and T. Imasaka. *Anal. Chem.*, 67, (1995), 829-834
- 54 "S S.Ben-David, D.Colella, G. M.Cupo, A. Fischer, G.Ornstein, US Patent 5360739.
- 55 O.Wolfbeis, in *Fluorescence, spectroscopy, imaging and probes*, Springer, Berlin, 2002.
- 56 N. Gadjev, T. Deligeorgiev, I. Kanev, M. Tasseva and R. Sabnis, *Dyes and Pigments*, 24, (1994), 93-98.

- 57 R.Kietzmann, A. Ehret, M. Spitler and F. Willig, *J. Am. Chem.Soc.*, 115, (1993), 1930-1935
- 58 J.X. Meng, K.F. Li, J. Yuan, L.L. Zhang, W.K. Wong and K.W. Cheah. *Chem. Phys. Lett.*, 332, (2000), 312-317.
- 59 A.J.G. Mank, H. Lingeman and C.V. Gooijer. *Trends Anal. Chem.*, 11, (1992), 210-215 .
- 60 T. Deligeorgiev, N. Gadjev and A. Lugade, *Dyes and Pigments*, 19, (1992), 215-222.
- 61 T. Deligeorgiev, A. Vasilev and K.-H. Drexhage, *Dyes and Pigments*, 67, (2005), 21-26.
- 62 T.G. Deligeorgiev, N.I. Gadjev, K.-H. Drexhage and R.W. Sabnis, *Dyes and Pigments*, 29, (1995), 315-322.
- 63 T.G. Deligeorgiev, N.I. Gadjev, A.A. Vasilev, V.A. Maximova, I.I. Timcheva, H.E. Katerinopoulos and G.K. Tsikalas, *Dyes and Pigments*, 75, (2007), 466-473.
- 64 T.G. Deligeorgiev, D.A. Zaneva, H.E. Katerinopoulos and V.N. Kolev, *Dyes and Pigments*, 41, (1999), 49-54.
- 65 M.A. Haidekker and E.A. Theodorakis, *Org. Biomol. Chem.*, 5, (2007), 1669 - 1678.
- 66 J. Sowell, R. Parihar and G. Patonay, *Journal of Chromatography B: Biomedical Sciences and Applications*, 752, (2001), 1-8.
- 67 Sturmer, D. P. In Kirk-Othmer Encyclopedia of Chemical Technology, 3rd ed.; Interscience: New York, 1979; p 393.
- 68 B. Oswald, F. Lehmann, L. Simon, E. Terpetschnig and O.S. Wolfbeis, *Anal. Biochem.*, 280, (2000), 272-277.
- 69 R.B. Mujumdar, L.A. Ernst, S.R. Mujumdar, C.J. Lewis and A.S. Waggoner, *Bioconjugate Chem.*, 4, (1993), 105-111.
- 70 S.R. Mujumdar, R.B. Mujumdar, C.M. Grant and A.S. Waggoner, *Bioconjugate Chem.*, 7, (1996), 356-362.
- 71 J.H. Flanagan, S.H. Khan, S. Menchen, S.A. Soper and R.P. Hammer, *Bioconjugate Chem.*, 8, (1997), 751-756.
- 72 W. West, P.B. Gilman. In *The Theory of the Photographic Process*; James, T. J., Ed.; Macmillan: New York, 1977; p 277.

- 73 R. B Mujumdar, L.A.Ernst, S.R. Mujumdar, C. Lewis, and A.S.Waggoner, *Bioconjugate Chem.*, 4, (1993), 105-111
- 74 A. Chopdar, A.M. Turk and D.W. Hill. *Trans. Ophthal. Soc.*, 98, (1978), 142-146.
- 75 T. Higashijima, T. Fuchigami, T. Imasaka and N. Ishibashi. *Anal. Chem.*, 64 (1992), 711-718
- 76 W. West, P.B. Gilman. In *The Theory of the Photographic Process*; James, T. J., Ed.; Macmillan: New York, 1977; p 277.
- 77 D. Keil, H. Hartmann and T. Moschny, *Dyes and Pigments*, 17. (1991), 19–27.
- 78 D. Ramaiah, I. Eckert, K.T. Arun, L. Weidenfeller and B. Epe, *Photochem. Photobiol.*, 79, (2004), 99–104.
- 79 K.Y. Law and F.C. Bailey, *J. Imag. Sci.*, 31 (1987), 172–175.
- 80 Polaroid Corporation, US Patent 5795981.
- 81 V.Y. Merritt and H.J. Hovel, *Appl. Phys. Lett.*, 29, (1976), 414–416.
- 82 P. Zuo, C. Li, Y. Wu, X. Ai, Xue-Song Wang, B.Zhang, J. Zhang *Journal of Photochem. Photobiol. A: Chem.*, 183, (2006), 138-145.
- 83 E. Terpetsching, H. Szmecinski and J.R. Lakowicz, *Analytica Chimica Acta.*, 282, (1993), 633-641.
- 84 E. Terpetschnig and J.R. Lakowicz, *Dyes and Pigments*, 21, (1993), 227-234.
- 85 E. Terpetschnig, H. Szmecinski, A. Ozinskas and J.R. Lakowicz, *Anal.Biochem.*, 217, (1994). 197-204.
- 86 B.Oswald, L. Patsenker, J. Duschl, H. Szmecinski, O.S Wolfbeis, E.Terpetschnig, *Bioconjug. Chem.*, 10, (1999), 925-931.
- 87 V. M. Ioffe, G. P. Gorbenko, T.Deligeorgiev, N. Gadjev, A. Vasilev *Biophysical Chemistry*, 128, (2007), 75-86.
- 88 K.D. Volkova, V.B. Kovalska, A.O. Balanda, R.J. Vermeij, V. Subramaniam, Yu. L. Slominskii and S.M. Yarmoluk, *Journal of Biochemical and Biophysical Methods*, 70, (2007), 727-733.
- 89 L. Tarazi, N. Narayanan, J. Sowell, G. Patonay, L. Streckowski, *Spectrochimica Acta Part A: Molecular and Biomolecular Spectroscopy*, 58, (2002), 257-264.
- 90 S.Kim, S. Han, S. Park, S. Lee, S. Lee, K. Koh, S. Kang, *Dyes and Pigments*, 41, (1999), 221-226.
- 91 S. Yagi, H. Nakazumi, *Functional Dyes*, (2006), 215-255

- 92 A. Chopdar, A.M. Turk and D.W. Hill. *Trans. Ophthalm. Soc.* 98 (1978), 142-146.
- 93 T. Higashijima, T. Fuchigami, T. Imasaka and N. Ishibashi. *Anal. Chem.*, 64, (1992), 711-718.
- 94 M. Olofsson, S Kalinin, J Zdunek, M Oliveberg and LB-Å Johansson, *Phys. Chem. Chem. Phys.*, 8, (2006), 3130-3140.
- 95 O. S. Wolfbeis, *Anal. Chem.*, 80, (2008), 4269–4283.
- 96 Y. Kostov, Z. Gryczynski and G. Rao, *Anal. Chem.*, 74, (2002), 2167-2171.
- 97 M. Valledor, J.C. Campo, I. Sánchez-Barragán, J.C. Viera, J.M. Costa-Fernández and A. Sanz-Medel, *Sens and Actuators B*, 117, (2006), 266-273.
- 98 W. Trettnak, C. Kolle, F. Reininger, C. Dolezal and P. O'Leary, *Sens and Actuators B: Chemical Proceedings of the Sixth International Meeting on Chemical Sensors*, 36, (1996), 506-512.
- 99 O.S. Wolfbeis, L.J. Weis, M.J.P. Leiner and W.E. Ziegler, *Anal. Chem.*, 60, (1988), 2028-2030.
- 100 G. O'Keeffe, B.D. MacCraith, A.K. McEvoy, C.M. McDonagh and J.F. McGilp, *Sens and Actuators B: Chemical Proceedings of the 2nd European Conference on Optical Chemical Sensors and Biosensors*, 29, (1995), 226-230.
- 101 E. R. Carraway, J. N. Demas, B. A. DeGraff, and J. R. Bacon, *Anal. Chem.*, 59, (1991), 332
- 102 I. Klimant and O. S. Wolfbeis, *Anal. Chem.* 1995, 67, 3160
- 103 J. R. Bacon and J. N. Demas, *Anal. Chem.* 1987, 59, 2780.
- 104 J. N. Demas and B. A. DeGraff, *Anal. Chem.* 1991, 63, 829A.
- 105 A. Mills and M. Thomas, *Analyst*, 1997, 122, 63.
- 106 J. F. Fernández-Sánchez, R. Cannas, S. Spichiger, R. Steiger, and U. E. Spichiger-Keller, *Anal. Chim. Acta*, 2006, 566, 271.
- 107 R. Q. Albuquerque, Z. Popovic, L. De Cola, and G. Calzaferri, *Chem. Phys. Chem.*, 2006, 7, 1050.
- 108 B.-H. Han, I. Manners, and M. A. Winnik, *Anal. Chem.*, 2005, 77, 8074
- 109 H. N. McMurray, P. Douglas, M. S. Busa, and M. S. Garley, *J. Photochem. Photobiol. A*, 1994, 80, 283-285
- 110 P. Douglas and K. Eaton, *Sens. Actuators B*, 82 (2002), 48–53.
- 111 P.M. Gewehr and D.T. Delpy, *Med. Biol. Eng. Comput.*, 32 (1994), 659–664.

- 112 Y.Kostov, G.Rao, *Sens Actuators B*, 90 (2003), 139-142.
- 113 M. Valledor, J.C. Campo, F.J. Ferrero, J.C. Viera, M. Gonzalez, C. Blanco, J.M. Costa, I. Sanchez and A. Sanz-Medel, *Instrumentation and Measurement Technology Conference, 2005. IMTC 2005. Proceedings of the IEEE*, 2, (2005),1172-1176.
- 114 S. Lee and I. Okura, *Spectrochim. Acta A*, 54 (1998), 91-100.
- 115 S. Lee and I. Okura, *Analyst*, 122 (1997), 81-84
- 116 D.B. Papkovsky, *Sens. Actuators B*, 11 (1993), 293-300.
- 117 V.Hughes and P.Douglas, *J.Fluorescence*, 16 (2006), 403-409.
- 118 M. Gouterman, 'The Porphyrins', ed. D. Dolphin, Academic Press, 1978.
- 119 K. Kalyanasundaram, 'Photochemistry of polypyridine and porphyrin complexes', Academic Press, 1992.
- 120 S.-K. Lee and I. Okura, *Anal. Commun.*,68,(1997), 2615-2619.
- 121 D. B. Papkovsky, G. V. Ponomarev, W. Trettnak, and P. O'Leary, *Anal. Chem.*,54, (1995), 91-99.
- 122 R.N. Gillanders, M.C. Tedford, P.J. Crilly and R.T. Bailey, *Analytica Chimica Acta*, 545, (2005), 189-194.
- 123 R.N. Gillanders, M.C. Tedford, P.J. Crilly and R.T. Bailey, *Journal of Photochemistry and Photobiology A: Chemistry*, 162, (2004), 531-535.
- 124 R.N. Gillanders, M.C. Tedford, P.J. Crilly and R.T. Bailey, *Journal of Photochemistry and Photobiology A: Chemistry*, 163, (2004), 193-199.
- 125 L. Guo, Q. Ni, J. Li, L. Zhang, X. Lin, Z. Xie and G. Chen, *Talanta*, 74, (2008) 1032-1037.
- 126 C. McDonagh, C. Kolle, A.K. McEvoy, D.L. Dowling, A.A. Cafolla, S.J. Cullen and B.D. MacCraith, *Sens.Actuators B*, 74, (2001), 124-130.
- 127 O. S. Wolfbeis, H. E. Posch and H. W. Kroneis, *Anal. Chem.*, 1985, 57, 2556-2561.
- 128 T. M. A. Razeq, M.I J. Miller, S. S. M. Hassan, M. A. Arnold, *Talanta*, 50, (1999), 491-498.
- 129 E. Urbano, H. Offenbacher and O. S. Wolfbeis, *Anal. Chem.*, 56, (1984). 427-429.
- 130 C. Zhu, F. V. Bright and G. M. Hieftje, *Appl. Spectrosc.*, 44, (1990), 59-63.
- 131 Ch. Huber, T. Werner, Ch. Krause and O. S. Wolfbeis, *Microchim. Acta*, 142, (2003), 245-253.

- 132 A.Vijayan, M. Fuke, R. Hawaldar, M. Kulkarni, D. Amalnerkar, R.C. Aiyer, *Sens. and Actuator. B*, 129, (2008), 106-112.
- 133 N. Carmona, E. Herrero, J. Llopis, M.A. Villegas *Sens Actuators B*,126, (2007), 455-460.
- 134 H. E. Posch, O. S. Wolfbeis, *Mikrochim. Acta*, 1, (1989), 41-49.
- 135 K.-S. Tseng, L.-C. Chen and K.-C. Ho, *Sens. Actuators B: Chemical Proceedings of the Tenth International Meeting on Chemical Sensors*, 108, (2005), 738-745.
- 136 A.K. Poulsen, A.M. Scharff-Poulsen and L.F. Olsen, *Anal. Biochemistry*, 366, (2007), 29-36.
- 137 Z. Rosenzweig and R. Kopelman, *Sens. Actuators B: Chemical Proceedings of the Sixth International Meeting on Chemical Sensors*, 36, (1996), 475-483.
- 138 A. Pasic, H. Koehler, I. Klimant and L. Schaupp, *Sens. Actuators B*, 122, (2007), 60-68.
- 139 O.S. Wolfbeis, I. Oehme, N. Papkovskaya and I. Klimant, *Biosensors and Bioelectronics*, 15, (2000), 69-76.
- 140 M.C. Moreno-Bondi, O.S. Wolfbeis, M.J.P. Leiner and B.P.H. Schaffar, *Anal. Chem.*, 62, (1990), 2377-2380.
- 141 W. Trettnak, Chapter 7, Fluorescence spectroscopy, Springer Verlag, 1992
- 142 W. Trettnak, O. S. Wolfbeis, *Analytica Chimica Acta*, 221, (1989), 195-203.
- 143 U.-W. Grummt, A. Pron, M. Zagorska and S. Lefrant, *Analytica Chimica Acta*, 357, (1997), 253-259.
- 144 S.W. Bishnoi, C.J. Rozell, C.S. Levin, M.K. Gheith, B.R. Johnson, D.H. Johnson and N.J. Halas, *Nano Letters*, 6, (2006), 1687-1692.
- 145 L.Y. Ma, H.Y. Wang, H. Xie and L.X. Xu, *Spectrochimica Acta Part A: Molecular and Biomolecular Spectroscopy*, 60, (2004), 1865-1872.
- 146 L. Tolosa, Y. Kostov, P. Harms and G. Rao, *Biotechnol. Bioeng.* 80, (2002), 594-597.
- 147 X.D. Ge, Y. Kostov and G. Rao, *Biotechnol. Bioeng.*, 89, (2005), 329-334.
- 148 O.S. Wolfbeis, Fiber-optic chemical sensors and biosensors, *Anal. Chem.*, 72 (2000), 81R-89R.
- 149 B. Weidgans, C. Krause, I. Klimant and O.S. Wolfbeis, *Analyst*, 129, (2004), 645-650.

- 150 J.W. Parker, O. Laksin, C. Yu, M.L. Lau, S. Klima, R. Fisher, I. Scott and B.W. Atwater, *Anal. Chem.*, 65, (1993), 2329-2334
- 151 M.L. Wahl, P.M. Pooler, P. Brand, D.B. Leeper, *J. Cell. Physiol.*, 183, (2000), 373-380.
- 152 X.X. He, Y. Wang, K.M. Wang, J.F. Peng, F. Liu and W.H. Tan, *Science in China Series B-Chemistry*, 50, (2007), 258-265.
- 153 W.H. Chan, A.W.M. Lee, Y.S. Lam and K.M. Wang, *Analytica Chimica Acta*, 351, (1997), 197-203.
- 154 G. Harsanyi, *Sensors for measuring chemical quantities in biology*, in *Sensors in Biomedical Applications*, 2000, CRC Press
- 155 Y. Xu, Y. Liu and X. Qian, *Journal of Photochemistry and Photobiology A: Chemistry*, 190, (2007), 1-8.
- 156 Y. Kostov, S. Tzonkov, L. Yotova and M. Krysteva, *Analytica Chimica Acta*, 280, (1993), 15-19.
- 157 G. Serra, A. Schirone and R. Boniforti, *Analytica Chimica Acta*, 232, (1990), 337-344.
- 158 Y. Amao, T. Komori and H. Nishide, *Reactive and Functional Polymers*, 63, (2005), 35-41.
- 159 N. Nakamura and Y. Amao, *Sens. Actuators B*, 92, (2003), 98-101.
- 160 C.-S. Chu and Y.-L. Lo, *Sens. Actuators B*, 129, (2008), 120-125.
- 161 M. García-Heras, C. Gil, N. Carmona, J. Faber, K. Kromka and M.A. Villegas, *Analytica Chimica Acta Papers Presented at the Analytical Forum*, 540 (2005), 147-152.
- 162 X. Li, F. Ruan and K. Wong, *Analyst*, 118, (1993), 289-292.
- 163 O. S. Wolfbeis, 'Fibre Optic Chemical Sensors and Biosensors', CRC Press, 2001. New York.
- 164 D.B. Papkovsky, G.V. Ponomarev, W. Trettnak and P. O'Leary, *Anal. Chem.* 67, (1995), 4112-4117.
- 165 Y. Amao, T. Miyashita and I. Okura, *Anal. Chim. Acta.*, 421, (2000), 167-174.
- 166 A. Mills and A. Lepre, *Anal. Chem.*, 69, (1997), 4653-4659.
- 167 K. Eaton and P. Douglas, *Sens. Actuators B*, 82, (2002), 94-104.
- 168 P. Douglas and K. Eaton, *Sens. Actuators B*, 82, (2002), 200-208.
- 169 S. Pauly, 'Polymer handbook', Wiley, 1989.
- 170 W.R. Vieth, *Diffusion in and through polymers*, (1991), Hanser.

- 171 B.-H. Han, I. Manners and M.A. Winnik, *Chem. Mater.*, 17, (2005), 3160-3171.
- 172 W.H. Chan, A.W.M. Lee, Y.S. Lam and K.M. Wang, *Analytica Chimica Acta*, 351, (1997), 197-203.
- 173 T Zeng, R Claus, F Zhang, W Du and K L Cooper, *Smart Mater. Struct.*, 10, (2001), 780–785.
- 174 Z. Tao, E. C. Tehan, Y. Tang, and F. V. Bright, *Anal. Chem.*, 78,(2006), 1939-1954.
- 175 Y. Tang, E. C. Tehan, Z. Tao, and F. V. Bright, *Anal. Chem.*, 75,(2003), 2407-2415.
- 176 O.S.Wolfbeis, *J.Mater.Chem.*, 15,(2005), 2657-2669.
- 177 M.L.Davies, S.M.Murphy, C.J.Hamilton, B.J.Tighe, *Biomaterials*, 13, (1992), 991-999.
- 178 G.T. John, I. Klimant, C. Wittmann and E. Heinzle, *Biotechnol. Bioeng.*, 81 (2003), 829–836.
- 179 G.S. Vasylevsk, S.M. Borisov, C. Krause and O.S. Wolfbeis, *Chem. Mater.*, 18, (2006), 4609-4616.
- 180 P.A.S. Jorge, C. Maule, A.J. Silva, R. Benrashid, J.L. Santos and F. Farahi, *Analytica Chimica Acta*, 606, (2008), 223-229.
- 181 L. Basabe-Desmonts, D.N. Reinhoudt and M. Crego-Calama, *Chem. Soc. Rev.*, 36, (2007), 993-1017.
- 182 P.A.S. Jorge, C. Maule, A.J. Silva, R. Benrashid, J.L. Santos and F. Farahi, *Analytica Chimica Acta*, 606, (2008), 223-229.
- 183 J.M. Costa-Fernández, R. Pereiro and A. Sanz-Medel, *TrAC Trends in Analytical Chemistry*, 25, (2006), 207-218.
- 184 G. Liebsch, I. Klimant, C. Krause and O. S. Wolfbeis, *Anal. Chem.*, 73, (2001), 4354–4363.
- 185 S. M. Borisov, C. Krause, S. Arain and O. S. Wolfbeis, *Adv. Mater.*, 18, (2006), 1511–1516.
- 186 R. J. Woods, S. Scypinski, L. J. C. Love and H. A. Ashworth, *Anal. Chem.*, 56, (1984), 1395–1400
- 187 U. Lange, N.V. Roznyatovskaya and V.M. Mirsky, *Analytica Chimica Acta*, 614, (2008), 1-26.

- 188 A. Gräfe, K. Haupt and G.J. Mohr, *Analytica Chimica Acta*, 565, (2006), 42-47.
- 189 B. Wandelt, A. Mielniczak, P. Turkewitsch and S. Wysocki, *Journal of Luminescence, Proceedings of the 2002 International Conference on Luminescence and Optical spectroscopy of Condensed Matter*, 102-103, (2003), 774-781.
- 190 D. W. Hatchett and M. Josowicz, *Chem. Rev.*, 108, (2008), 746-769
- 191 F.L. Dickert and O. Hayden, *TrAC Trends in Analytical Chemistry*, 18, (1999), 192-199.
- 192 K. Yano and I. Karube, *TrAC Trends in Analytical Chemistry*, 18, (1999), 199-204.
- 193 U. Lange, N.V. Roznyatovskaya and V.M. Mirsky, *Analytica Chimica Acta*, 614, (2008), 1-26,
- 194 O. S. Wolfbeis, M. Schaeferling and A. Duerkop, *Microchim. Acta*, 143, (2003), 143, 221-230.
- 195 M. Schaeferling, M. Wu, J. Enderlein, H. Bauer and O. S. Wolfbeis, *Appl. Spectrosc.*, 57, (2003), 1386-1394.
- 196 G. Liebsch, I. Klimant, B. Frank, G. Holst and O. S. Wolfbeis, *Appl. Spectrosc.*, 54, (2000), 548-560.
- 197 B. Meier, T. Werner, I. Klimant and O. S. Wolfbeis, *Sens. Actuators, B*, 29, (1995), 240-245.
- 198 G. Liebsch, I. Klimant, C. Krause and O. S. Wolfbeis, *Anal. Chem.*, 73, (2001), 4354-4363.
- 199 R. J. Woods, S. Scypinski, L. J. C. Love and H. A. Ashworth, *Anal. Chem.*, 56, (1984), 1395-1400
- 200 E. Monson, M. Brasuel, M. A. Philbert and R. Kopelman, *Biomedical Photonics Handbook*. T. Vo-Dinh, editor. CRC Press, Boca Raton, FL (2003)
- 201 S. Dourado and R. Kopelman, *Spie (Int. Soc. Opt. Eng.) Proc* 2836, 2 (1996).
- 202 J.P Sumner, J.W Aylott, E. Monson and R Kopelman, *Analyst*, 127, (2002), 11-16.
- 203 C. Daubresse, C. Granfils, R. Jerome, and P. Teyssie, *Journal of Colloid and Interface Science*, 168, (1994), 222-230.
- 204 H. A. Clark, S. L. R. Barker, R. Kopelman, M. Hoyer, and M. A. Philbert, *Sens. Actuators B*, 51, (1998), 12-20.

- 205 H. A. Clark, M. Hoyer, M. A. Philbert, and R. Kopelman, *Anal.Chem.* 71, (1999), 4831-4840.
- 206 D. R. Uhlmann, G. Teowee, and J. Boulton, *Journal of Sol-Gel Science and Technology*, 8, (1997), 1083-1090.
- 207 H. Xu, J. W. Aylott, R. Kopelman, T. J. Miller, and M. A. Philbert, *Anal. Chem.*, 73, (2001), 4124-4130.
- 208 Y.E. Koo Y. Cao , R.Kopelman , S.M.Koo, M. Brasuel M, M.A.Philbert,*Anal Chem.*, 76, (2004), 2498-2505
- 209 M.G. Brasuel, T.J. Miller, R. Kopelman and M.A. Philbert, *Analyst*, 128, (2003),1262-1267
- 210 Y. Cao, Y.-E. Koo and R. Kopelman, *Analyst*, 129, (2004).745-750.
- 211 B. G. Healey and D. R. Walt, *Anal. Chem.*, 67, (1995), 4471–4476.
- 212 A. Zanzotta, N. Svita, P. Boccazzi, P. Lessard, A. J. Sinskey and K. F. Jensen, *Biotechnol. Bioeng.*, 87, (2006), 244–254.
- 213 <http://www.osmetech.com>, 2007.
- 214 S.Nagi, O.Wolfbeis, *Analyst*, 2007, 132, 507-511.
- 215 J. Hradil, C. Davis, K. Mongey, C. McDonagh and B. D. MacCraith, *Meas. Sci. Technol.*, 2002, 13, 1552–1557.
- 216 M. E. Köse, A. Omar, C. A. Virgin, B. F. Carroll and K. S. Schanze, *Langmuir*, 21, (2005), 9110–9120.
- 217 G. E. Khalil, C. Costin, J. Crafton, G. Jones, S. Grenoble, M. Gouterman, J. B.Callis, and L. R. Dalton, *Sens. Actuators B*, 97, (2004), 13-19.
- 218 J. M. Kürner, I. Klimant, C. Krause, H. Preu, W. Kunz and O. S. Wolfbeis, *Bioconjugate Chem.*, 12,(2001), 883–889.
- 219 R.Evans, P. Douglas, J.Williams, D. Rochester, *J.Fluorescence*, 16, (2006), 201-206.
- 220 R.Evans, P. Douglas, *Anal. Chem.*, 78, (2006), 5645-5652.
- 221 S.Ricketts, P.Douglas, *Sens and actuators*, b. 2008 in press

Chapter 2

Experimental and instrumental

2.1 Materials

All materials used were the highest grade available

Chemical	Supplier
0.1M phosphate buffer, pH 7.5	Aldrich
1,2 dichlorobenzene	Aldrich
1,4 squaric acid	Aldrich
10% ammonium persulfate solution	Aldrich
Acetic acid glacial	Fisher Scientific, UK
Acetone	Fischer
Acrylamide	Aldrich
Air	BOC
Ammonium hydroxide	Aldrich
Bovine serum albumin (BSA) (Fraction V)	Aldrich
Brij 30	Aldrich
Butane sultone	Aldrich
Butanol	Aldrich
Cell proliferation assay kit, CellTiter 96®	
Aqueous one solution	Promega, US
Cellulose acetate butyrate	Aldrich
Dichloromethane	Fischer
Diphenylphenanthroline	Aldrich
Ethanol	Fischer
Ethyl cellulose (ethoxy content 46%)	Aldrich
Glacial acetic acid	Fischer
HBSS/Ca/Mg	Gibco, UK
Hexane	Aldrich
HNO ₃	Aldrich
Horse serum	Gibco, UK
Hydrazinobenzoic acid	Aldrich
Hygromycin-B	Sigma, UK
Isopropylmethylketone	Aldrich
L-Glutamine (100x strength)	Gibco, UK
MCL-5 human lymphoblastoid cell line	Gentest Corporation, USA
Methanol	Fisher Scientific, UK
Methyl trimethoxy silane (MTMS)	Aldrich
N,N,N,N tetramethylthyldiamine	Aldrich
NaCl	Aldrich
NaOH	Aldrich

Nitrogen(Oxygen free)	BOC
N,N methyl bis(acrylamide)	Aldrich
Oxygen	BOC
Palladium octaethyl porphyrin	Aldrich
Phenyl trimethoxy silane (PTMS)	Aldrich
Phosphate buffered saline (PBS)	Aldrich
Platinum octaethyl porphyrin	Frontier Scientific, UK
Polystyrene	Aldrich
Polyvinylchloride	Aldrich
RPMI-1640 growth medium	Gibco, UK
Sodium acetate	Aldrich
Sodium dioctyl sulfosuccinate	Aldrich
Tetrahydrofuran	Fischer
Toluene	Fisher Scientific, UK
Tributyl phosphate	BDH Fischer
Trypan Blue (0.4% in toluene)	Sigma, UK

2.2. General method of preparation of polymer films for optical sensing

The structure of the thin film optical sensors used in the work described in this thesis can be generalised as transparent sensing membranes in which are dissolved, or encapsulated, lumophores. These films were prepared by spin coating onto a glass support. Each film was prepared 3 time and the average results shown in this work.

The exact composition of the films, and the lumophores used, will be discussed in detail in the relevant chapters.

Polymer solutions were prepared by dissolving the polymers in an appropriate solvent. i.e. for ethyl cellulose a 5:1 w/v in 9:1 v:v toluene/ethanol solution was used; and for the polyurethane hydrogel 9:1 w/w in 9.1 w:w ethanol/water was used.

2.2.1 Lumophore solutions

Table 2.1 below gives details of the solvents used for the different lumophores, together with the application the lumophore was used for.

Table 2.1 Lumophores solutions used in this work

<i>Lumophore</i>	<i>Solvent</i>	<i>Application</i>
PtOEP	THF	O ₂
PdOEP	THF	O ₂
(5)-6- carboxyfluorescein	THF	pH
Rhodamine 6G	THF	O ₂ reference
Coumarin 110	THF	O ₂ reference
Coumarin 153	THF	O ₂ reference
Tetraphenylporphyrin	Ethanol	pH reference

2.3 Thin film optical sensor preparation

For the purposes of this study it is appropriate to classify the sensors as shown in figure 2.1. Typical film thickness were ca. 7 and 10 μm for spin speeds of 3600 and 750 revolutions per minute (r.p.m) respectively.[6]

2.3.1 Type 1 - Solution based sensors

Solution based oxygen sensors were prepared by adding 2 ml of the lumophore solution to 5 g of the polymer solution. Thin films were prepared by spin coating this solution onto glass slides using a spin speed of 3600 rpm. For colorimetric sensors a second layer was spin coated onto the first layer once it was dry.[6]

2.3.2 Type 2 - Incorporating PEBBLES into thin film sensors

Single lumophore PEBBLE based optical oxygen sensors were prepared by mixing 500 mg of polymer solution and 50 mg of analyte sensitive PEBBLES. The PEBBLE/polymer solution was then sonicated for 30 minutes. Thin films were prepared by spin coating this solution onto glass slides using a spin speed 750 rpm.

2.3.4 Type 3 -Dual lumophore PEBBLE based optical oxygen sensors

Layer 1 is a solution based analyte insensitive layer prepared by adding 2 ml of the lumophore solution to 5 g of the polymer solution and spin coating onto a glass slide. Once this was dry a second layer of PEBBLE based optical oxygen sensors (prepared by mixing 500 mg of polymer solution and 50 mg of analyte sensitive PEBBLES) was spin coated onto layer 1.

2.3.4 Type 4 - Dual lumophore PEBBLE based optical oxygen sensors

Dual lumophore PEBBLE based optical oxygen sensors were prepared by mixing 750 mg of polymer solution and 50 mg of analyte sensitive PEBBLES and 25 mg of analyte insensitive PEBBLES and sonicating for 30 minutes Thin films were prepared by spin coating this solution onto glass slides using a spin speed of 750 rpm.

All films were dried in a desiccator in the dark for 24 hours before use.

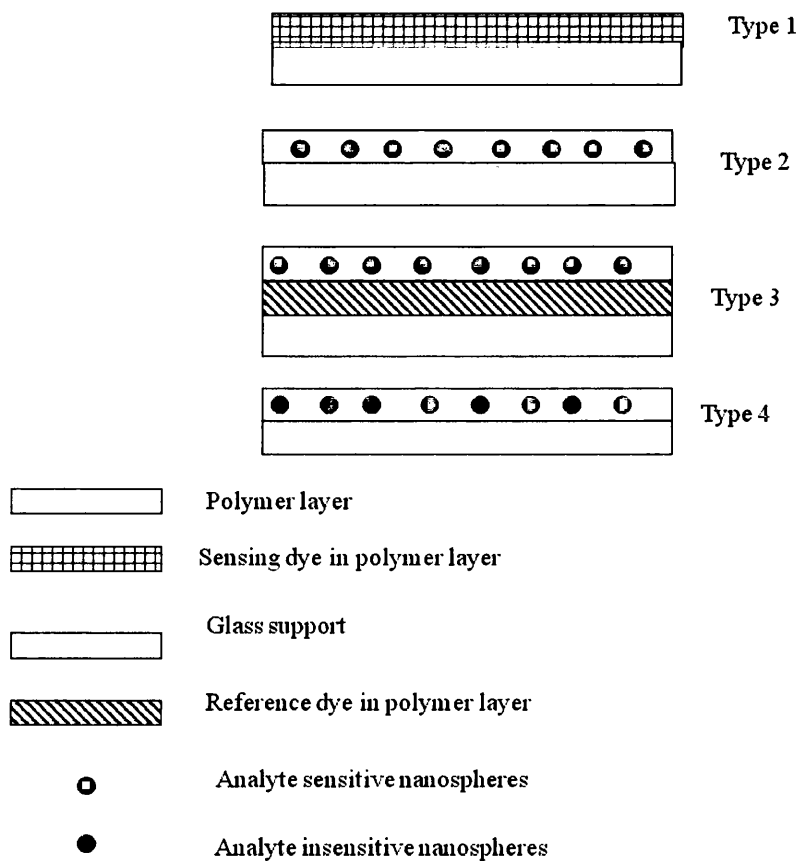


Figure 2.1 Classification of sensors used in this study

2.3.5 Plasticisation of the film

When required, a plasticiser i.e. either tributyl phosphate (TBP), dimethyl phthalate (DMP) or triethyl phosphate (TEP) was used. [5,6] Plasticiser concentrations are given in parts per hundred resin, (pphr), where resin is the ethyl cellulose polymer.

2.4 Synthesis and preparation of PEBBLE sensing elements

2.4.1 Organically modified silica (ORMOSIL) nanospheres [5]

In this work PEBBLES was prepared by mixing 31 ml of deionised water with 38 μ l of HNO₃, stirring at 60 °C, and then adding to this a 0.1 ml sample of PTMS and then stirring the solution at full speed. The time for reaction was dependent on the size of particles desired. 6 ml of ammonium hydroxide was added and the mixture was stirred for a further 2 hours in order for condensation of the silane. The sensing dyes were then added in an appropriate solvent as described in table 2.1. Following this 0.2 ml of MTMS was added and mixed for a further 60 minutes. The resulting PEBBLES were then filtered using suction filtration through a nylon membrane (pore size 0.2 μ m). The PEBBLES were washed three times with water, then re-suspended in a water/ethanol 1:2 v/v mix and further sonicated for 5 minutes. The PEBBLES were then filtered through a 0.02 μ m Whatman filter membrane and allowed to dry in a desiccator.

2.5 Imaging of the nanospheres

2.5.1 SEM

Dry PEBBLES were lightly scattered onto carbon pads and characterized using a Philips XL30CP scanning electron microscope.

2.6 Instrumental

2.6.1 Cell set up for gaseous oxygen sensing

All measurements were taken at 22-25 °C. The films were held in a 1 cm quartz curvette, the lid of which carried two needles suspended on either side of the film within the cell. This allows the gas stream of known composition into the cell and thus onto the film as illustrated by figure 2.2. Purging was carried out for 15 minutes before each measurement to allow equilibration between the gas stream and the film.

2.6.2 Cell set up for dissolved oxygen and pH sensing

All measurements were taken at 22-25 °C.

A 1 cm x 1 cm 'cup' with a quartz window and two rubber rings was used to trap the sensor film and give a sealed flow cell in which a stream of water of known oxygen concentration flows over the sensor film. For pH studies aqueous buffer solutions were pumped through the cell and over the sensor film.

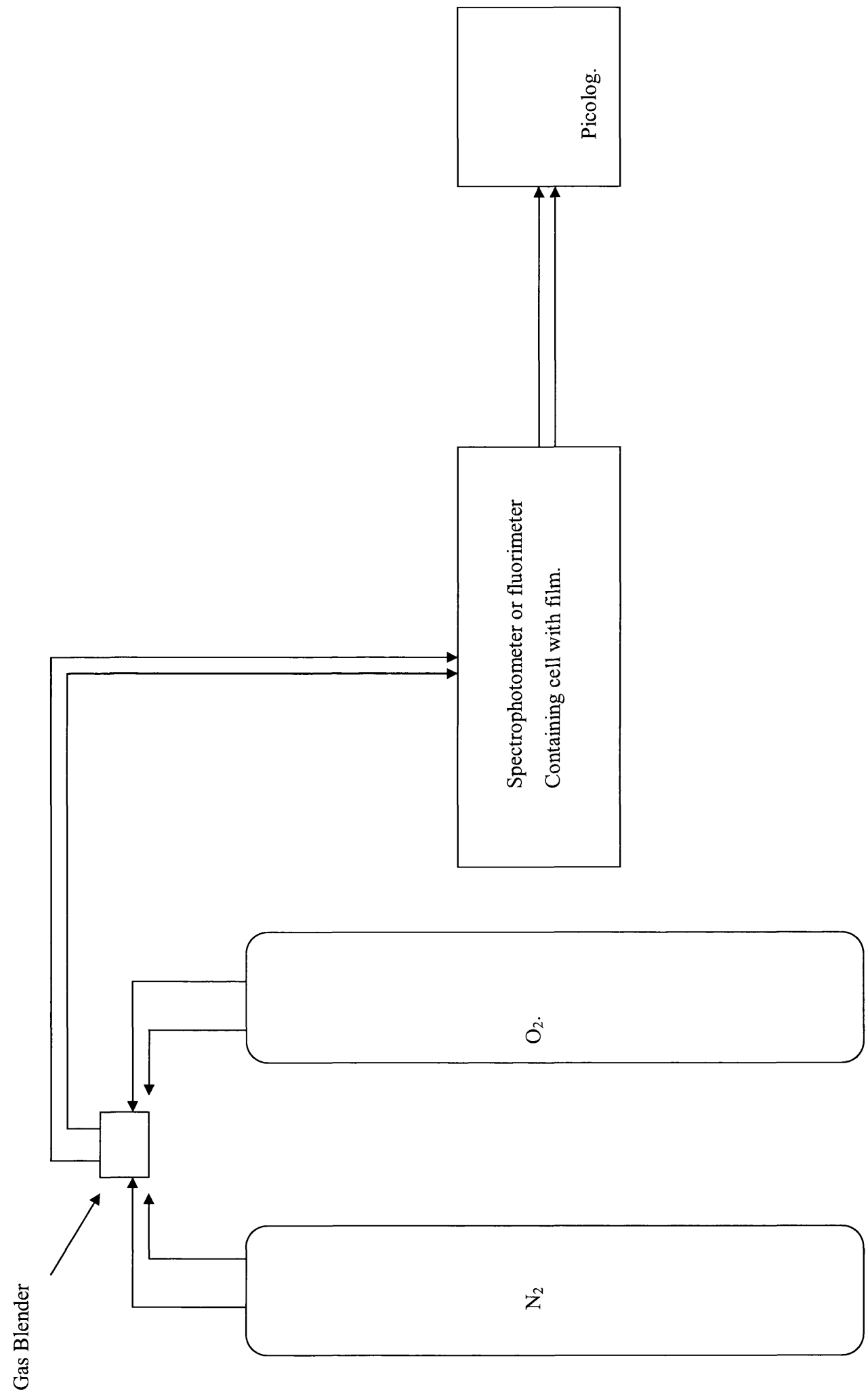


Figure 2.2 Experimental set up for oxygen and pH sensing

2.6.3 Gas mixing

Gas mixtures from 0-100 % air and 0-100 % oxygen were generated using a gas blender (model no. 852 V1-B, Signal Instruments Co, UK) with nitrogen as the diluent gas. The manufacturer's calibration graph, showing the relationship between the dial reading on the gas blender and the % oxygen produced, is given in fig. 2.3. [2] In order to minimise sample evaporation and avoid change in concentration when working with solutions, long neck quartz cells were used and the gases were first bubbled through solvent. The samples were purged for 15 minutes to allow equilibrium between the gas and solution to be reached before each reading was taken.

2.6.4 Calibration of the gas blender

Stern-Volmer analysis on the oxygen quenching of an aqueous solution of ruthenium(II) tris(2,2'- bipyridyl)dichloride $[\text{Ru}(\text{bpy})_3]\text{Cl}_2$ ($1 \times 10^{-5} \text{ mol dm}^{-3}$) was used as the calibration standard. Gases were bubbled through distilled water and the sample purged for 15 minutes to allow equilibrium between the gas and solution to be reached before each reading was taken.

Correction of the manufacturer's values for the true gas concentration were needed as the gas blender is calibrated by the manufacturer using one gas stream containing a trace of propane in air, with pure air as the diluent. When blending gases with different specific gravities, it is necessary to employ a correction factor to obtain the "true" gas mixture. The true instrument setting required to obtain the required percentage of oxygen is obtained from equation 2.1,

$$P_n = \frac{R_n}{100C_n} \sum_{n=1}^{S+1} R_n C_n \quad (2.1)$$

where R_n is the required %O₂; C_n is the manufacturers correction factor for each gas present, including the diluent stream ($C_n = 0.961$ and 1.032 for O₂ and N₂ respectively), S is the number of gas streams (in this case $S = 1$ as O₂ is the only gas to be blended), $S+1$ takes into account the N₂ diluent stream; and finally P_n is the percentage to be set to obtain the required %O₂. Once calculated, P_n is interpolated from the manufacturer's calibration sheets to obtain the required instrument setting.

2.7 Instrumental

2.7.1 UV/VIS absorption measurements

All absorption spectra were recorded using 10 mm quartz absorption cells and a Hewlett-Packard diode array spectrometer.

2.7.2 Variable temperature measurements

Variable temperature luminescence measurements were carried out using a fluorimeter equipped with Tecam circulator c100 variable temperature water pump. The temperature in the reaction vessel was recorded using a Hewlett-Packard 2802A thermometer and HP34740A display unit measuring the temperature in an identical cell in the same heating block. The thermometer was calibrated against different temperature water samples and a mercury thermometer.

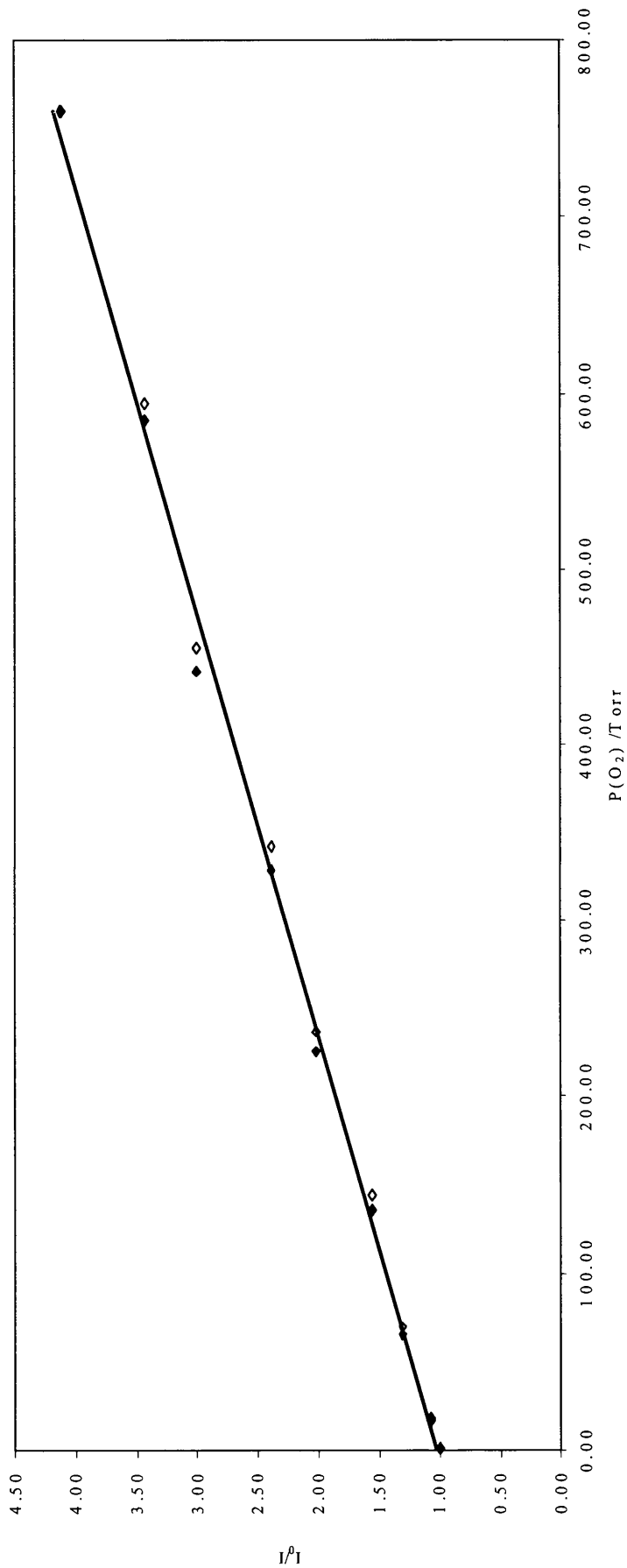


Figure 2.3 Stern-Volmer plot for the oxygen quenching of $[Ru(bpy)_3]Cl_2$ ($1.2 \times 10^{-5} \text{ mol dm}^{-3}$) in aqueous solution, where \blacktriangle represent the manufacturer's pO_2 and Δ are corrected pO_2 values for an O_2/N_2 gas blend. The straight line represents the linear regression fit to the corrected pO_2 values.

2.7.3 Steady-state luminescence measurements

Room temperature and low temperature 77 K luminescent measurements were carried out using an MPF-44E Perkin-Elmer connected to an analog to digital converter (Pico Technology Ltd., Cambridgeshire, UK).

2.7.4 Time-resolved nanosecond laser studies

These were made using a Nd/YAG Spectron laser with an Applied Photophysics laser kinetic spectrometer. The frequency doubled pulse (532 nm) was used. For all work except that with PdOEP/EC, 18.6 mm emission slits were used and the average trace from 32 shots of laser excitation was collected on an Gould OS4072 8 bit digital storage oscilloscope and transferred to a PC for analysis. For studies with PdOEP/EC advantage was taken of the longer lifetime available and the 12 bit data collection available with the Picoscope™ analog to digital converter (Pico Technology Ltd., Cambridgeshire, UK) was used. In this case 32 scans were averaged and, to improve signal to noise still further, slit widths of 32 nm were used.

2.7.5 Circular dichroism

Far UV CD spectra were measured using a Jasco J-815 CD spectrometer, (Tokyo Japan) using a 1 mm pathlength quartz cell. The CD results are expressed in terms of mean residue ellipticity (MRE) in $\text{deg cm}^2 \text{d mol}^{-1}$ and calculated according to equation 2.2.

$$\text{MRE} = \frac{\text{Observed CD signal}}{C_p \cdot n \cdot l} \quad (2.2)$$

Where C_p is the molar concentration of protein, n is the number of amino acid residues and l is the pathlength. The α -helical contents of the dye can be calculated from equation 2.3, using 4000 and 33000 the MRE of β -sheet and random coil structures respectively at 208nm

$$\% \alpha - helix = \left(\frac{-MRE_{208} - 4000}{33000 - 4000} \right) \cdot 100 \quad (2.3)$$

2.8 Data analysis

2.8.1 The integrated emission intensity for a decay trace

The area under an emission decay plot gives the total integrated emission intensity.

2.8.2 Curve fitting

Curve fitting to pH response curves was carried out using Origin lab 6.

Time resolved emission decay traces were analysed using the curve fitting programme Table curve 2D™ (Jandel Scientific Software Inc.) an example of an experimentally obtained decay trace and Table curve fits to both a single and double exponential are shown in figure 2.4. The goodness of fit was evaluated by examination of the residuals of the fit from the curve fitting program.

2.9 Photophysical characterisation

2.9.1 Quantum yield determination

The emission quantum yield was obtained by reference to an ethanolic solution of tetra phenyl porphyrin (quantum yield of fluorescence, Φ_f , of 0.11 [1]) made up to have the same absorption at the excitation wavelengths (590 nm and 590nm for TPP and SQ-1 respectively) using equation 2.4.

$$\Phi_x = \Phi_y \frac{F_x}{F_y} \cdot \frac{\eta_x}{\eta_y} \frac{I_{TPP}}{I_{SQ-1}} \quad (2.4)$$

Where Φ_x is the quantum yield of SQ-1, Φ_y is the quantum yield of the TPP standard, F is $\int I(\lambda) d\lambda$ and η is the refractive index of solutions X and Y respectively. [1]

2.9.2 Radiative rate constant

The radiative rate constant, k_{rad} , was calculated from the Strickler Berg Equation 2.5. [3]

$$k_{rad} = 2.88 \times 10^{-9} \cdot n^2 \cdot \nu_{\bar{n}}^3 \int \epsilon \cdot d \cdot \ln \nu_{abs} \quad (2.5)$$

where n is the refractive index of the medium, $\nu_{\bar{n}}$ is the mean reciprocal emission wavelength, and $\int \epsilon \cdot d \cdot \ln \nu_{abs}$ is calculated from the integral of a plot of extinction co-efficient against the natural logarithm of the frequency of the absorption band.

The observed rate constant for the deactivation of the singlet state k_{fl} , was then calculated using k_{rad} and Φ_f as follows

$$k_{fl} = \left(\frac{k_{rad}}{\Phi_f} \right) \quad (2.6)$$

2.9.3 pH study

The effect of pH on fluorescence was measured by addition of successive 20 μ l aliquots of HCl to a 200 ml 1.3×10^{-5} mol dm⁻³ solution of **SQ-1** in 0.01 M NaOH, with pH measured using a calibrated Jenway 3305 pH meter.

2.9.4 Photostability

Photostability was measured by following the decrease in fluorescence intensity as a function of irradiation time using a Jobin-Yvon JY3 fluorimeter with irradiation at 360 nm (10 nm slits) and detection at 570 nm (4 nm slits). The radiant excitation flux was obtained using ferrioxalate actinometry. [1]

2.9.5 Temperature dependence of dye protein binding

Thermodynamic analysis of protein binding was carried out using a fluorimeter equipped with Tecam circulator c100 variable temperature water pump. Known concentrations of BSA and dye were premixed in a glass vial and left for 30 minutes at 4 °C before use. The sample was then transferred to a 1cm quartz cell. and allowed to equilibrate to the temperature of the heating block. The temperature in the quartz cell was determined by use of a digital thermometer in an identical sample in the heating block and the emission spectrum recorded at various temperatures.

2.10 Cell studies

These were carried out in the Medical School Swansea University. I would like to thank Dr.S. H. Doak for allowing me access to the equipment used in these cell studies, and also for her assistance in carrying out this work.

2.10.1 Cell culture and cell viability

The Chinese hamster lung fibroblast cell line V79 was maintained in Dulbecco's modified Eagle's medium supplemented with 10% foetal bovine serum (Gibco, Invitrogen, Paisley, UK). Cells were incubated at 37 °C in a 5% CO₂/air atmosphere and sub-cultured when confluent by detaching the cells from the flask with 0.25% trypsin in Hanks solution.

For fluorescent staining purposes, cell preparations on slides were required. Sterile glass slides were each seeded with ca. 1×10^5 V79 cells, placed in square Petri dishes containing growth media and allowed to grow for 24 h. The slides were then rinsed with PBS, fixed in 4% paraformaldehyde for 30 min at ambient temperature and stored at $-20\text{ }^\circ\text{C}$ until needed.

Slides to be stained were rinsed with 0.05% Tween-20/PBS, then 50 μl **SQ-1** (0.1 mg/ml) was applied and the slides incubated in a humidified chamber at $37\text{ }^\circ\text{C}$ for 24 h. Following hybridisation, slides were washed in 0.05% Tween-20/PBS for three 5 min cycles. They were then allowed to air dry before the nuclei were counterstained by mounting the samples in 4, 6-diamidino-2-phenylindole (DAPI).

2.10.2 Cell imaging

Slides for cell culture were viewed under an Olympus BX50 fluorescence microscope using a UplanF1 100x/1.3 oil objective. Fluorescence responses were detected with single- and multiple-band pass filter sets. Standard fluorescein isothiocyanate (FITC) and texas red isothiocyanate (TRITC) filter sets (maximum transmission at 480 nm and 570 nm respectively) were used for excitation and emission filters for **SQ-1** imaging, while a UV filter (maximum transmission at 360 nm) was required for the DAPI counterstain. Images were captured with a cooled CCD camera and analysed with the MacProbe version 4.1 software (Applied Imaging, Newcastle Upon Tyne, UK).

The MCL-5 cell line is a human lymphoblastoid cell line that constitutively expressing a relatively high level of native CYP1A1, four other human cytochromes namely CYP1A2, CYP2A6, CYP3A4 and CYP2E1 as well as microsomal epoxide hydrolase carried as cDNAs in plasmids. It is a metabolically competent cell line and maintained using the methods described by Crespi *et al.* [4].

MCL-5 cells were grown in RPMI 1640 supplemented with 9% horse serum and 1% L-glutamine. At each passage hygromycin B in 0.035 M acetic acid was added to a final concentration of 200 $\mu\text{g/ml}$. At least two sets of experiments were conducted with the same stock of **SQ-1** dye. For each experiment, two 25 cm^3 tissue culture flasks were used for each dose.

Prior to treatment, the cell cultures were seeded into several 25 cm^3 tissue culture flasks to achieve a final concentration of 1.5×10^5 cells per ml in 10 ml growth medium. The cells were then gassed with 5% CO_2 in air and incubated at $37\text{ }^\circ\text{C}$ for 20 hours (i.e. one cell cycle).

After one cell cycle, 10 ml of cell cultures were treated with increasing doses of **SQ-1**. The cells were then incubated for one further cell cycle under the same condition as above. The cell suspensions were dispensed into centrifuge tubes and centrifuged at 1500 rpm for 8 minutes. The supernatants were discarded and the cell pellets were used according to the need of the viability assays performed. Both the trypan-blue exclusion assay and the MTS (CellTiter) assay were performed as described by the manufacturer.

2.11 NMR and mass spectrometry

¹H nmr spectra were recorded on a Bruker AC 400 MHz spectrometer using tetramethyl silane as an internal standard.

Mass spectra were recorded at the EPSRC mass spectrometry centre at the University of Wales Swansea using low resolution EI/CI techniques on a VG analytical Quattro II triple quadrupole mass spectrometer.

2.12 Phase modulation lifetime measurements

Phase modulation plots were obtained at the Institute of Fluorescence, Univeristy of Balimore.

References

- [1] S.L.Murov, I.Carmichael, G.L.Hug, Handbook of photochemistry, 2nd ed, Marcel Dekker inc, New York, 1993.
- [2] J. R. Lakowicz, Principles of Fluorescence Spectroscopy, 2nd ed., Kluwer Academic/ Plenum Press, New York, 1999.
- [3] S. J. Strickler , R A Berg. *J. Chem. Phys.*, 37, (1962),814-22.
- [4] C.C.Crespi, F.J.Gonzalez, D.T.Steinle, T.R.Turner, H.V.Gebourn, B.W.Penman
R.Langerbach, *Chem, Res, Toxicol.*, 4, (1991) 566-572
- [5] S. Pauly, in: Brandrup, Immergut, Grulke (Eds.), Polymer Handbook, fourth ed., Wiley, 1999, pp. VI/543–VI/569.
- [6] A. Mills, *Platinum Met. Rev.*, 41 (1997), 115–12.
- [7] Y.L. Koo, Y Cao, R Kopelman, S.M. Koo, M. Brasuel and M.A. Philbert, 76, (2004) *Anal. Chem.*, 2498-2505.
- [6] R.C.Evans, Thesis, The University of Wales, Swansea

Chapter 3

A study of the interaction between a squarylium dye and protein by optical methods

3.1 Introduction

The measurement of fluorescence has become an invaluable tool in environmental analysis, and medical, industrial and biological research. [1-4] In particular the development of novel methods and new fluorescence dyes [5-8] has become very important in a number of areas such as chemical and biochemical analysis, immunotechnology, biotechnology and the pharmaceutical industry. [1-15]

Protein quantification is very important in clinical analysis, pathology, immunology and biochemistry. Conventional methods include: the Biuret method, the Lowry method, the Bradford method and the bromocresol method, all of which suffer from limited sensitivity and dynamic range, and low detection range.[1] Some involve difficult sample preparation. Other relatively new methods have included: mass spectrometric detection, which needs expensive instrumentation and sample preparation, [54] Rayleigh light scattering, [55] chemiluminescence [56]; and electrochemical methods, [57] which can be complicated by protein adsorption at the electrode surface even at very low protein concentrations. [1, 16] Fluorescence spectroscopy can also be used. This offers extremely high sensitivity, which makes it possible to detect even single molecules, and fluorescence spectroscopy can be easily combined with many separation techniques including capillary electrophoresis and HPLC. [11, 17-20]

Although proteins can possess intrinsic fluorophores such as phenyl alanine, tyrosine and tryptophan, leading to blue green emission, the quantum yield of these intrinsic fluorophores is too low to detect low concentrations of proteins. [21] There are two common ways to determine the concentration of proteins using fluorescent dyes, covalent [22-26] and non-covalent labelling. [10, 26-32]

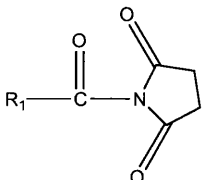
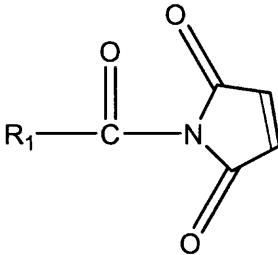
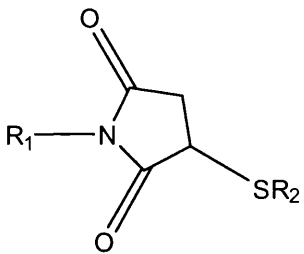
3.2 Types of binding

3.2.1 Covalent labelling

Many dyes containing reactive groups for specific biological applications are known in the literature. Reactive groups on the protein include primary amines and side chain functional groups. [1, 6-10, 58] Fluorescent dyes can be designed to include reactive groups for amines, thiols phenols and carboxylic acid. [1] Hydrazide and amine groups can be used for carboxylic acid side chain substitutions [58] Table 3.1 summarises the reactive groups that

can incorporated into fluorescent dyes and the groups with which they react on the protein to form the covalent bond. [22-26,35,58]

Table 3.1 Summary of potential reactive pathways of labelling groups for covalent labelling of amino or sulfhydryl groups in proteins.

Reactive dyes moiety	Protein reactive moiety	Resulting covalent derivative
Isothiocyanate $R^1-N=C=S$	R^2NH_2	Thiourea $R^1-NH-C=S(NH)-R^2$
Succinimidyl ester 	R^2NH_2	Carboxamide $R^1-C(O)NHR^2$
Sulfonyl chloride R^2-SO_2-Cl	R^2NH_2	Sulfonamide $R^2-SO_2-NHR^2$
Alkyl halide $R-CH_2-X$	R^2SH	Thioether $R^1-CH_2-SR^2$
Maleimide 	R^2SH	Thioether 

3.2.2 Non-covalent labeling

Non-covalent interactions play a critical role in many biological receptor ligands processes such as enzyme-substrate, antibody-antigen and drug receptor interactions. [6] Non-covalent interactions of hydrophobic interaction such as ANS can also provide information on protein conformation. [33] Changes in the spectral properties of fluorescent rotor molecules can give information on the microenvironment of a protein. [34]

The advantage of non-covalent labelling compared to covalent labelling is the removal of time consuming derivatisation reactions. Covalent derivatisation requires rigorous control of the pH in order to maintain satisfactory labelling efficiency. High pH is needed to deprotonate amine groups for successful labelling are this may not be compatible with biological samples. [6,36] The process is complicated by analyte molecules having differing numbers of dye molecules attached to them, leading to band broadening. [58] To complicate the method further, purification to separate unbound dye molecules is also commonly required. [6,58] The non-covalent linkages can involve ionic, electrostatic, hydrophobic and hydrogen bonding interactions. [6] Although not as stable as covalent linkages, the increased rate of bond formation, favourable physiological pH and a lack of purification steps make non-covalent interactions favourable for protein based assays. When used in conjunction with capillary electrophoresis-laser induced fluorescence (CE-LIF) increased the limit of detection By using CE-LIF, the LOD was increased to twice that of UV detection measurements. [17-19]

3.3 Dyes for the Near Infra Red (NIR)

Luminescent dyes in the near infrared region (600-1000 nm) is a rapidly developing area [1,4, 7-9,40-47]. The photophysical properties of near infrared dyes have resulted in their use in a variety of applications including: photodynamic therapy, silver halide sensitizers, laser diodes and optical data storage. Recently NIR dyes have been found to have considerable applicability in protein based assays. In comparison to the ultraviolet and visible regions, NIR fluorescence has several advantages.

1. The absorption and fluorescence of biological material generally decrease with increasing wavelength. Therefore there is generally a lower level of background interference, since few naturally occurring molecules undergo electronic transitions in this low energy region of the electromagnetic spectrum. [48]

2. NIR wavelengths can effectively penetrate through skin and over laying tissue. This raises the possibility of development of non-invasive clinical diagnostics, such as blood glucose monitoring. [59] Other materials such as plastics, glass, cloth and turbid water, paint and some building material are also transparent in the NIR regions. This suggests that NIR dyes may be useful in a wider variety of applications than the biomedical uses discussed here. [59, 60]
3. Raleigh and Raman scattering are reduced at higher wavelengths. For both processes the scattering intensity depends on $1/\lambda^4$ and operating at high wavelength improves the signal to scattering ratio.
4. Sample decomposition is generally reduced when compared to lower wavelength excitation because of the lower photon energy.
5. Excitation in the NIR can be accomplished by using cheap, stable and compact diode lasers and sensitive and stable NIR avalanche photodiode detectors are now readily available at relatively low. [22,49]

Much recent research in the area of NIR dyes has focused on the design of functionalised dyes with favourable chemical and photophysical properties for bimolecular probes. Generally the molecules designed for this region have extensive conjugation to generate electronic transitions in the NIR region.

Key properties include: high quantum yields, narrow absorption and emission bands, large Stokes shifts, good chemical and photochemical stability, low susceptibility to quenching, good biocompatibility and low toxicity. Until recently the only NIR probe approved by FDA was indocyanine green (ICG) due to the toxicity of other dyes. [38,39]

3.3.1 Cyanine based dyes

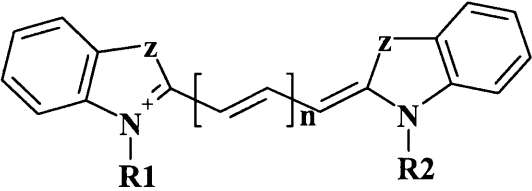
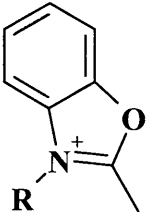
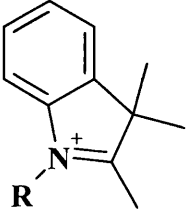
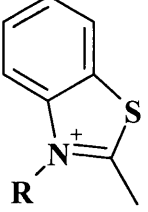
In terms of absorption and emission properties, cyanine dyes are an attractive class of compound,[1,24,25] with their absorption and emission maxima between 600-800 nm and molar absorptivities above $10^5 \text{ mol}^{-1} \text{ dm}^3 \text{ cm}^{-1}$. However they generally suffer from limited water solubility and poor photostability. [24,50] Many examples of cyanine dyes are known in the literature differing in the structure of the nitrogenous bases and/or the alkyl chain

joining them. The ease of structural manipulation makes cyanines and their derivatives ideal starting points for the designs of biomolecular probes, since both their chemical and photochemical properties can be uniquely tailored for specific applications.

3.3.2 Polymethine cyanine dyes

Polymethine dyes are characterised by a methene chain, which is a conjugate system that can be fine tuned for the desirable absorption and emission properties. The absorbance maxima of cyanine dyes increases as the polymethine chain increase, and typically for each CH-CH group added there is an increase of 100 nm in λ_{\max} . However increasing the conjugation, makes the dyes less stable and prone to photobleaching, as well as generally lowering both absorptivity and quantum yield. It also often causes an increase in dye aggregation. Several groups have worked on designing and synthesising analogues of cyanine dyes to overcome these limitation of long chain polymethine dyes. [7-9, 26-32] Figure 3.1a compares the structures of the different classes of cyanine dyes. Table 3.2 collects absorption and emission data on selected carbocyanine dyes.

Table 3.2. Absorption and emission properties of a series of carbocyanine dyes as a function of increasing polymethine chain length. [62]

Heterocyclic base	Carbon chain length #	λ absorption max/nm	λ emission max/nm
			
	1	490	515
	2	585	620
	3	680	740
	1	550	590
	2	650	690
	3	750	790
	1	560	590
	2	660	690
	3	765	810

Carbon chain length refers to the number of double bonds in the polymethine chain

3.3.3 Squarylium cyanine dyes

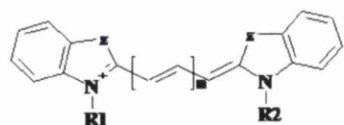
Squarylium cyanine dyes are now attracting attention as promising biological probes. [7-10] With high extinction coefficients, high protein binding constants ($1-3 \times 10^5 \text{ dm}^3 \text{ mol}^{-1}$) and high chemical and photostability improved by incorporation of a ring system. [52] A further advantage of these classes of dyes is the relatively ease of synthesis. The squaraine dyes are 1,3 bis-substituted products obtained by the reaction of squaric acid with electron donor groups, particularly indolenium units. Example of both symmetrical and asymmetric squarylium dyes are known in the literature. [6-9] We were particularly interested in symmetrical squarylium dyes due to the potential for 'one pot' synthesis.

3.4 The interaction of squarylium dyes and serum albumin

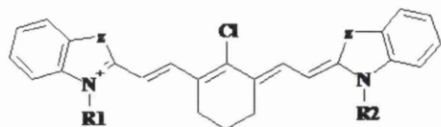
Serum albumin is one of the most abundant carrier proteins responsible for transport and disposition of both endogenous and exogenous ligands in the body, and thus has been studied for numerous clinical and medical applications. [6, 53, 61] Drug interactions with albumin influences drug toxicity, activity, excretion and metabolism. [53] The high structural homology between human serum albumin (HSA) and bovine serum albumin (BSA) has seen BSA used in numerous studies. [61] BSA is a single peptide chain with 583 residues and consists of three domains. Each domain contains two sub domains, and has a high content of charges residues, glycine and lysine and has a strong affinity for anionic and cationic ligands including metal ions Figure 3.1b. The domains are stabilised by various inter-domain forces including hydrophobic interactions, salt bridge interactions and helical extensions. Techniques that have been used to study ligand albumin interactions include equilibrium dialysis, circular dichroism, affinity capillary electrophoresis and laser induced fluorescence capillary electrophoresis. Non-covalent labelling of proteins has been exploited to facilitate protein determination by capillary electrophoresis and fluorescence titration where it offers an increased sensitivity compared to absorbance detection and a simpler and faster labelling protocol compared to conventional covalent labelling. [6]

Several examples of squarylium dyes as protein probes are now known in the literature, Terpetschnig et al. [7] showed that the interaction of squarylium dyes with BSA resulted in an enhancement of fluorescence and increased lifetime of the dye, such that the lifetime became sufficiently long to allow the use of simple phase modulation lifetime instrumentation. [7,8] When covalently attached to proteins, amine reactive squarylium dyes showed an increase in fluorescence intensity and enhanced lifetimes as compared to aqueous

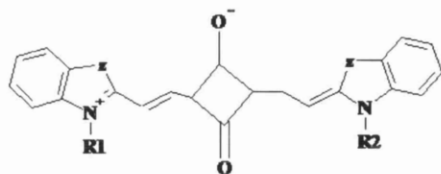
solution; this is thought to be the result of the shielding effect of the protein. Lakowicz et al. [7,8] found that the symmetry of the dye had little effect on the solvatochromic properties of a series of squarylium dyes, whereas, of the 10 squarylium dyes studied by Terpetschnig et al. [7-9] the symmetrical indolenine based squarylium displayed the highest fluorescence intensity increase upon binding to proteins and these are suggested as the most suitable group for biomedical applications.



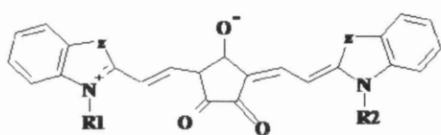
(3.1a)



(3.1b)

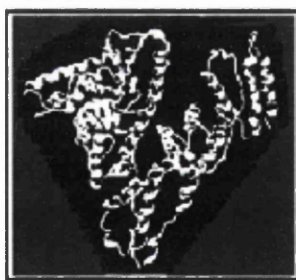


(3.1c)



(3.1d)

N form



~ pH 5 - pH 8

Figure 3.1. a General structures of indolium substituted (a) indolenine heptamethine cyanine dye and indolium substituted (b) tricarboyanine, (c) squarylium, and (d) croconium heptamethine cyanine dyes. **3b:** 3 dimensional structure of the secondary structure of BSA at pH 5-7.

3.5 Aims of this chapter

Squarylium dyes are a class of red absorbing and emitting fluorescent dyes that show exceptional photochemical properties. Here we describe the synthesis a squarylium dye, **SQ-1**, via a cheap and easy synthetic pathway.

Compared to polymethine cyanine dyes photostability increased by introduction of a the squarylium group. Introduction of sulfobutyl groups are thought to reduce aggregation and improve aqueous solubility. To fully understand the chemical and photochemical properties of the dye, characterization of the excitation wavelength, photostability, pH and temperature dependence of emission will be investigated.

A common property of squarylium dyes is a change in fluorescence when bound to proteins, a kinetic and thermodynamic investigation of **SQ-1** to BSA will also be investigated.

Cell imaging and viability studies will also be evaluated with the view to using squarylium dyes for fixed and live cell imaging

3.6 Materials and methods

3.6.1 Synthesis of sulfobutylsquaraine carboxylate

(SQ-1) was synthesised from squaric acid and 5-carboxy substituted-1-sulfonatopropyl, 2,3,3-triethylindolenine by modification of the established literature procedures of Terpetschnig et al. [5] The synthetic pathway is shown in figure 3.3.

The synthesis of the intermediate **1** (5-carboxyl-2,3,3-trimethyl,3H, indolenine) has already been given. [5] (Yield 56%; NMR (D₂O) δ 1.4(s 6H), 2.4(s 3H), 7.5 (d), 8.0(s), 8.1(d); m/z 204.09 ([M+H]⁺ (EI/CI)).

3.6.2 Synthesis of intermediate 2

5-Carboxyl -1-sulfobutyl-2,3,3 Trimethyl 3H-indolenine: [3, 5]

1.36 g of intermediate **1** (6.6 mmol) and 4.35 g of 1,4-butanedisulfone (9.92 mmol) were suspended in 20 ml of 1,2-dichlorobenzene and heated at 180 °C for 5 hours. The mixture was cooled to room temperature and the precipitate was filtered and collected. The resulting red solid, intermediate **2**, was washed with acetone and then used without further purification. (Yield 56%; NMR (DMSO) δ 1.5(s 6H), 1.72 (m 2H), 1.94 (m 2H), 2.5 (t) 2.8 (s 3H), 4.5 (m 2H), 8.1(s 2H), 8.3(s 1H); m/z 339 ([M+H]⁺ (EI/CI)).

3.6.3 Synthesis of SQ-1

0.634 g of intermediate **2** (1.85 mmol) and 0.0567 g of squaric acid (0.49 mmol) were heated under reflux with a Dean-Stark trap for 7 hours in a 1:1 v/v mixture of toluene and butanol, (in this method water produced in the condensation is removed as an azeotrope *via* the Dean-Stark trap). The solution turned blue after 3 hours of heating, and heating and stirring was continued for a further 4 hours. The solution was then cooled to room temperature and excess solvents removed using a rotary evaporator. The solid residue was titrated with diethyl-ether, filtered and collected. After drying in a dessicator the crude solid was purified using reverse phase preparative TLC using water:methanol (2:1) as eluent. A small sample was purified using high performance liquid chromatography (HPLC) on an Apex ec C8 5 μ column (Reverse phase), (Jones chromatography) attached to a Milton Roy variable wavelength detector HPLC using 60% acetonitrile:water with a detection wavelength of 363 nm. NMR (MeOD) δ 1.55 (s 12H), 1.72 (m 2H), 1.92 (m 2H), 2.88 (m 2H), 4.1(M, 4H), 5.9 (s 2H), 6.8 (m, 4H), 7.1 (m, 4H), 7.2(m, 4H) : m/z 761 ([M+H]⁺ (EI/CI))

For all experiments a stock solution of **SQ-1** in PBS was prepared to a concentration of $2 \times 10^{-4} \text{ mol dm}^{-3}$ and this was stored in the dark at $4 \text{ }^{\circ}\text{C}$ when not in use. Solutions were prepared by dilution of this stock solution as and when needed, and left at room temperature in the dark for 1 hour prior to use.

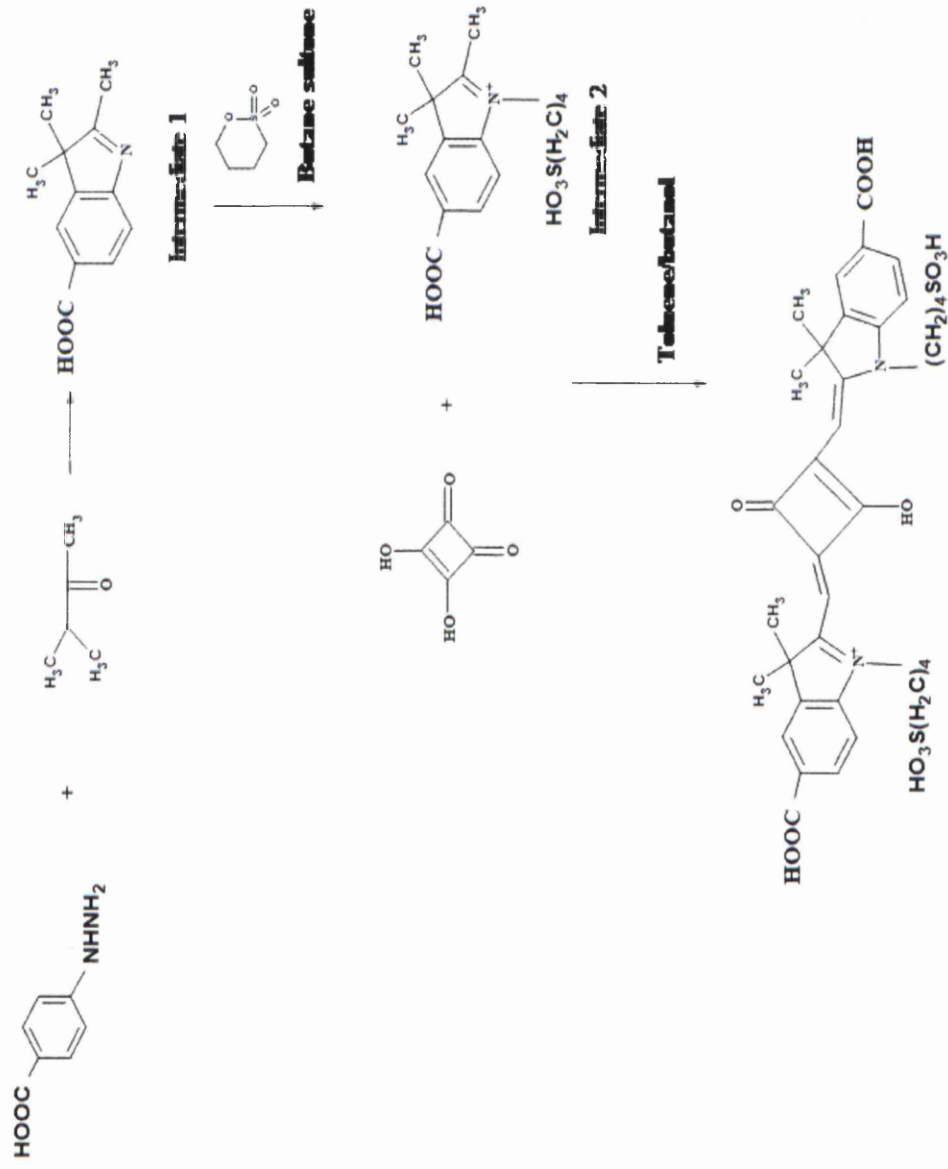


Figure 3. 2: Synthetic pathway to the bis- functional butyl-sulfonate squaraine carboxylate - **SQ-1**.

3.7 Spectroscopic characterization

3.7.1 Spectroscopic characterisation

Figure 3.3 gives absorption and emission spectra for **SQ-1** in room temperature PBS. The insert shows a Beers' law plot of absorbance against concentration. The good linearity indicates no detectable aggregation over this concentration range, which we attribute to the presence of alkyl sulfonate groups on the indolenium moiety. The molar extinction coefficient for **SQ-1** of $1.0 (\pm 0.05) \times 10^5 \text{ mol}^{-1} \text{ dm}^3 \text{ cm}^{-1}$ is comparable to that of other squarylium dyes. [1,14,16] Absorption and emission spectra show a Stokes' shift of 10 nm, and the room temperature emission quantum yield (Φ) is 0.08 (8%). The quantum yield is comparable to that of other unbound squarylium dyes in PBS. [16] The absorption spectrum of **SQ-1** overlap with common laser and LED excitation sources as shown in figure 3.4.

When frozen at 77 K in a low temperature water/glycerol (1:1 v/v) glass the emission quantum yield is increased ca. three fold to ≈ 0.24 with little change in emission spectrum, (Fig 3.5.). There is little change in either emission intensity or emission spectrum across the pH range 4-9 as shown in figure 3.6. Estimation of the excited-state lifetime using the Strickler-Berg equation [19] gives a radiative lifetime of 1.46×10^{-9} s which, when combined with the quantum yields, suggests lifetimes of 1.8×10^{-9} s at room temperature and 6.1×10^{-9} s at 77 K.

3.7.2 Binding with BSA (fraction V)

In the presence of BSA, **SQ-1** shows a bathochromic shift in emission maximum of ca. 11 nm, and a significant enhancement of fluorescence intensity (Fig. 4), but no change in absorption spectrum. The increase in quantum yield can be rationalised by a decrease in the rate of internal conversion upon binding, since internal conversion has been shown to be a major pathway in polymethine dyes due to the non-planar structure of the molecule arising from the 'loose' polymethine chain linking the two heterocyclic bases. [62] Decreasing or restricting the molecule to a planar confirmation can dramatically reduced the rate of internal conversion. [22] Lifetime studies show a bound lifetime of 2.4 ns ($\chi^2 = 1.3$) in the presence of BSA ($[\text{SQ-1}] = 5 \times 10^{-5} \text{ mol dm}^{-3}$ and $[\text{BSA}] = 7.5 \times 10^{-5} \text{ mol dm}^{-3}$ Figure. 3.7. This is consistent with that estimated from the Strickler-Berg equation which, with a quantum yield of 0.32 gives an estimated lifetime of 2.3 ns, and is in good agreement with values for other squarylium dyes bound to BSA. [5]

The binding constant for **SQ-1** and BSA was determined by fluorimetric titration of **SQ-1** with BSA. Using the simplest analysis, i.e. only one protein binding site accessible for binding with **SQ-1**, (insert Fig. 3.7) gives a binding constant, K , of $2.8 (\pm 0.5) \times 10^5$ (at pH 7.2, 298 K, 0.1 mol dm^{-3} phosphate buffer, $I = 0.14$) which is comparable with K for similar squarylium and methine cyanine dyes (typically $0.2\text{-}2 \times 10^6$). [4] A large hydrophobic cavity is present in the subdomain II of BSA and this is the probable target for **SQ-1** binding. [20]

The emission spectrum of **SQ-1** in PBS does not change with ionic strength in the range 0.14-1.85, however, when **SQ-1** is in the presence of BSA addition of NaCl causes a reduction in intensity and a blue shift in emission maximum consistent with a decrease in the binding constant with increasing ionic strength (Fig. 3.8). This suggests that the binding of **SQ-1** to BSA is dominated by electrostatic interactions.

The temperature dependence of binding is shown in figure 3.9. A thermodynamic analysis reveals a linear van't Hoff plot at temperatures between 288 and 320 K (insert Fig. 3.9). K decreases with temperature and analysis of the linear van't Hoff plot gives a negative enthalpy term and a positive entropy term again indicating that electrostatic forces are predominant in the binding. [25] Table 3.3 summarises the photochemical properties of **SQ-1** along with thermodynamic data for binding to BSA.

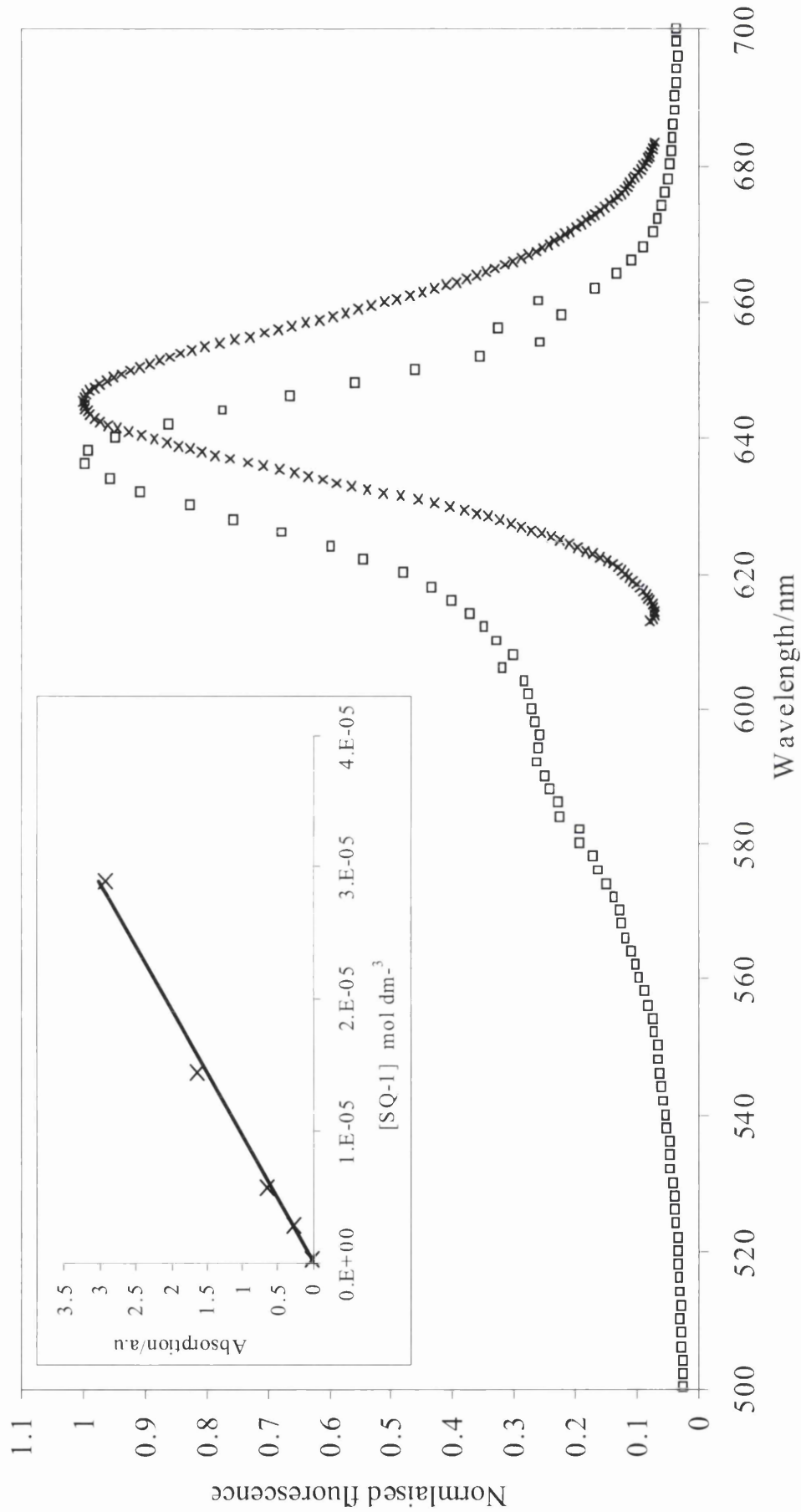


Figure 3.3: Normalised absorption (\square) and emission spectrum (\times) of **SQ-1** in PBS, $\lambda_{\text{exc}} = 590$ nm. Insert: Beer-Lambert plot for **SQ-1** in PBS. $\epsilon = 1 (\pm 0.05) \times 10^5 \text{ mol}^{-1} \text{ dm}^3 \text{ cm}^{-1}$.

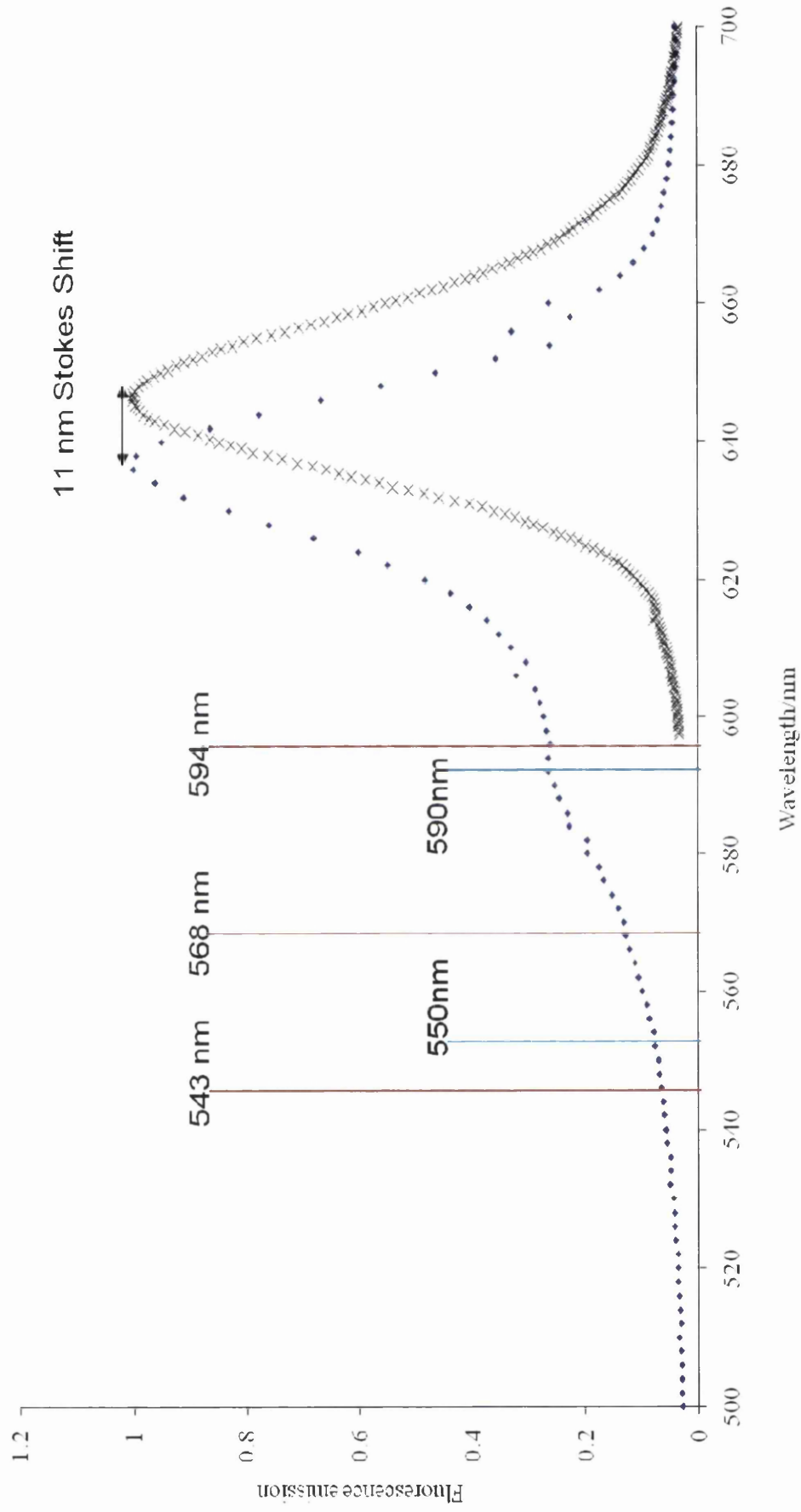


Figure 3.4. Normalised absorption and emission spectra annotated with lines to indicate common laser (543nm= He-Ne laser, 569nm = Ar-Kr and 594= He-Ne)) and LED (550nm= Al arsenide LED AND 590nm = gallium arsenide LED) excitation wavelengths.

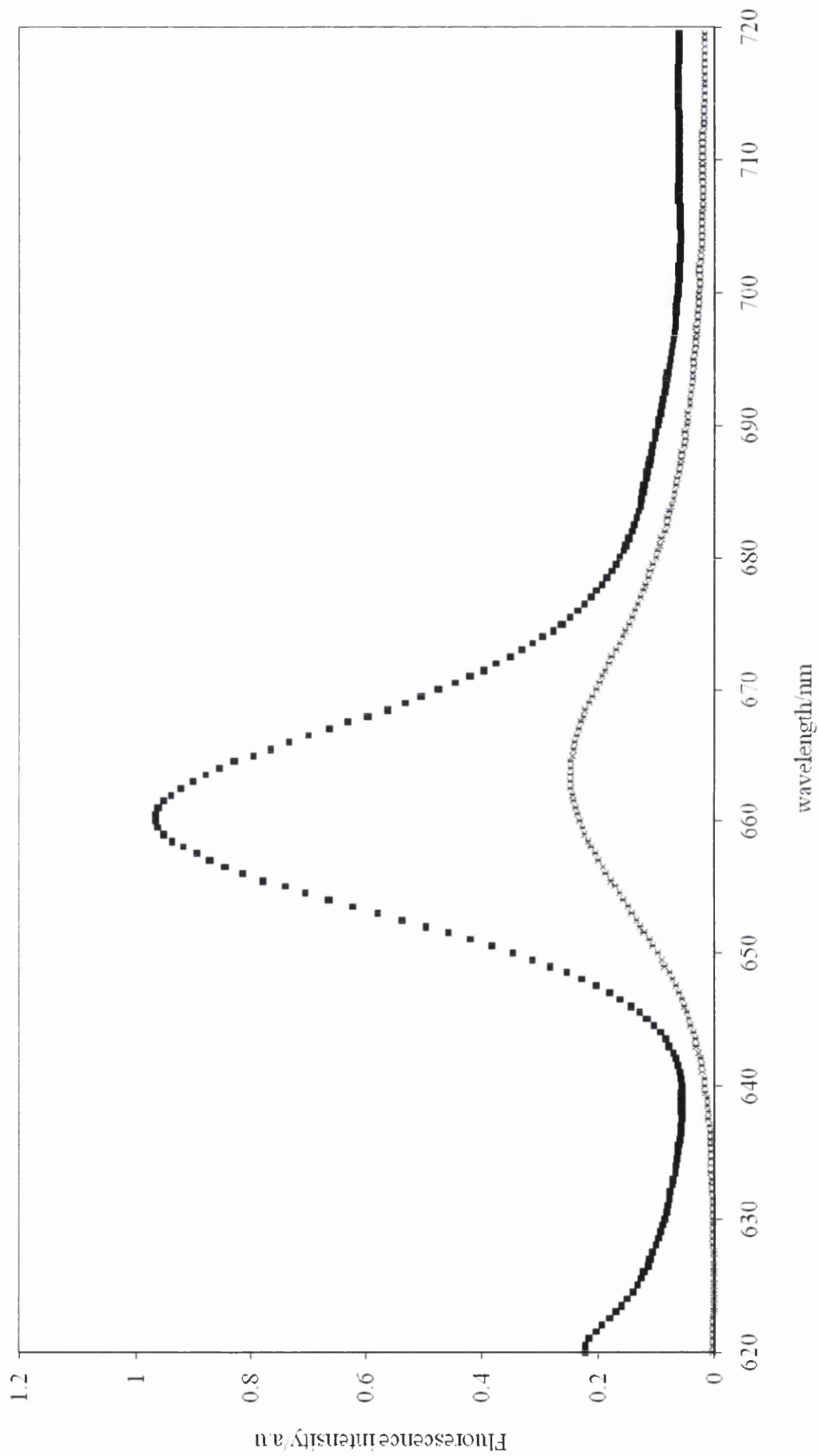


Figure 3.5. Low temperature emission spectra of SQ-1 in water/glycerol glass (1:1 v/v). ■ = 77 K * = room temperature..

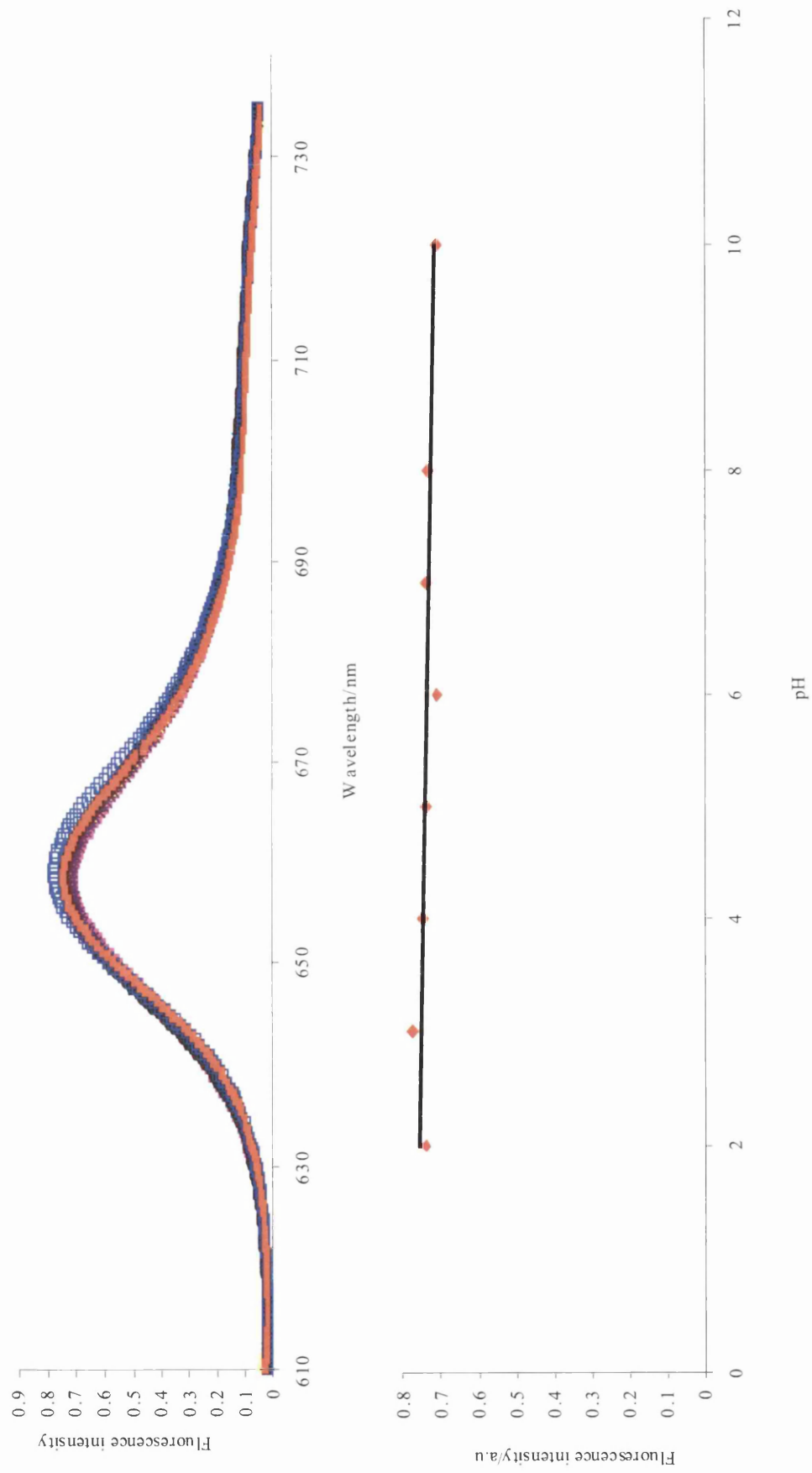


Figure 3.6. Change in fluorescence intensity of SQ-1 as a function of pH. $Y = 0.77(\pm 0.16) - 0.05 (\pm 0.02)\text{pH}$.

3.7.3 Circular dichroism

CD is a sensitive technique to monitor conformational changes in a protein upon interaction with a ligand. The CD spectra of BSA in the absence and presence of increasing concentration of dye is shown in figure 3.10. The CD spectra of BSA exhibited two negative bands in the UV region at 209 and 222nm characteristic of an α -helical protein. The CD results are expressed in terms of mean residue ellipticity (MRE) in $\text{deg cm}^2 \text{ mol}^{-1}$ and calculated according to equation 3.1

$$\text{MRE} = \frac{\text{Observed CD signal}}{C_p \cdot n \cdot l} \quad (3.1)$$

Where C_p is the molar concentration of protein, n is the number of amino acid residues and l is the pathlength. The α -helical contents of free and dye bound BSA can be calculated from equation 3.2

$$\alpha - \text{helix}\% = \left(\frac{-\text{MRE}_{208} - 4000}{33000 - 4000} \right) \cdot 100 \quad (3.2)$$

Where MRE_{208} is the observed MRE at 208nm, 4000 is the MRE of the β -form and random coil conformation and 33000 is the MRE of pure α -helix. From equation 3.2 the quantitative analysis of the α -helix in the secondary structure of BSA can be obtained. Upon increasing concentration of **SQ-1** there is a loss of the α -helical structure from 74% in the free BSA to 54% in the **SQ-1**-BSA [**SQ-1**] = $0.6 \times 10^{-4} \text{ mol dm}^{-3}$. This suggests that the binding of increasing amounts of **SQ-1** to BSA interrupts the hydrogen bonding networks that make up the polypeptide chain.

3.7.4 Photochemical stability

Stock solutions of $1 \times 10^{-6} \text{ mol dm}^{-3}$ **SQ-1** in aqueous PBS were exposed to different environments as follows. One was purged with N_2 for 15 minutes, sealed, and kept in the dark (A); one similarly purged and sealed but left in ambient room light (B); one open to air kept in the dark (C), and one open to air and left in ambient room light (D); and finally one frozen and kept in the dark at -5°C (E) Emission spectra were obtained periodically over 200 hours for all samples (the frozen sample was warmed to room temperature before measurement and then refrozen after measurement, other samples were re-purged as

necessary before re-storage). There was no change in emission spectrum or intensity for A and B but for samples in air-equilibrated water there is significant loss of emission intensity (Fig. 3.12). This suggests degradation is oxidative but not light driven. Storage under nitrogen or as frozen solution allows use of working stocks of **SQ-1** over a period of a week or more without the risk of significant degradation.

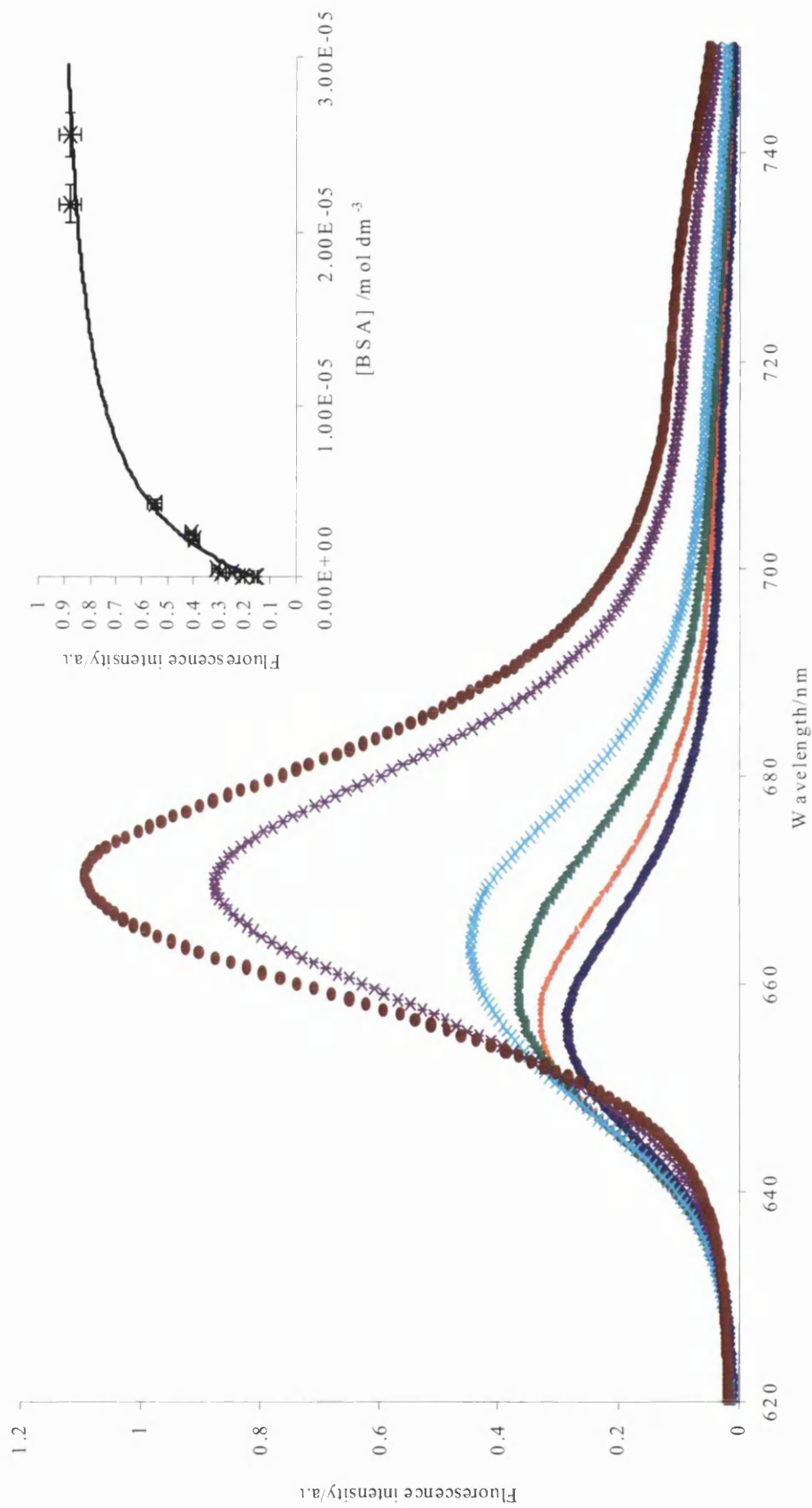


Figure 3.7. Increase in fluorescence intensity as a function of increasing [BSA] with constant [SQ-1] ($1.45 \times 10^{-6} \text{ mol dm}^{-3}$). $\bullet = 2.55 \times 10^{-4}$, $\ast = 2.55 \times 10^{-5}$, $+ = 2.55 \times 10^{-6}$, $\square = 2.55 \times 10^{-7}$, $\blacksquare = 2.55 \times 10^{-8}$ and $\ast = 0 \text{ mol dm}^{-3}$ BSA.

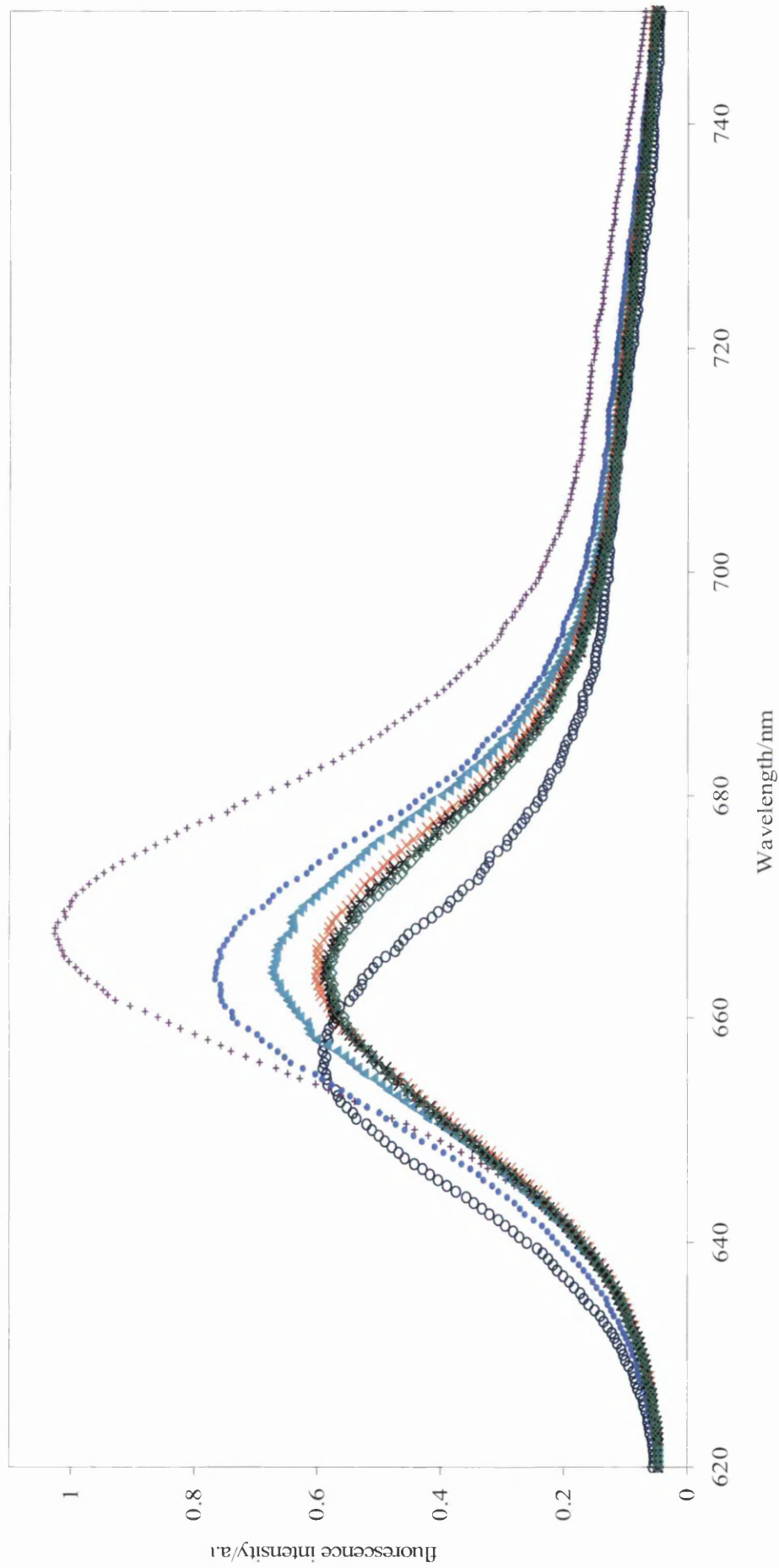


Figure 3.8. Effect of ionic strength on the fluorescence emission of **SQ-1** ($1.45 \times 10^{-6} \text{ mol dm}^{-3}$) in the presence of $[\text{BSA}] = 2.55 \times 10^{-5}$, Where I is as follows: + = 0.1397; ● = 0.3537; ▲ = 0.557; □ = 0.7817; x = 0.9957; * = 1.4237; ◇ = 1.8517.

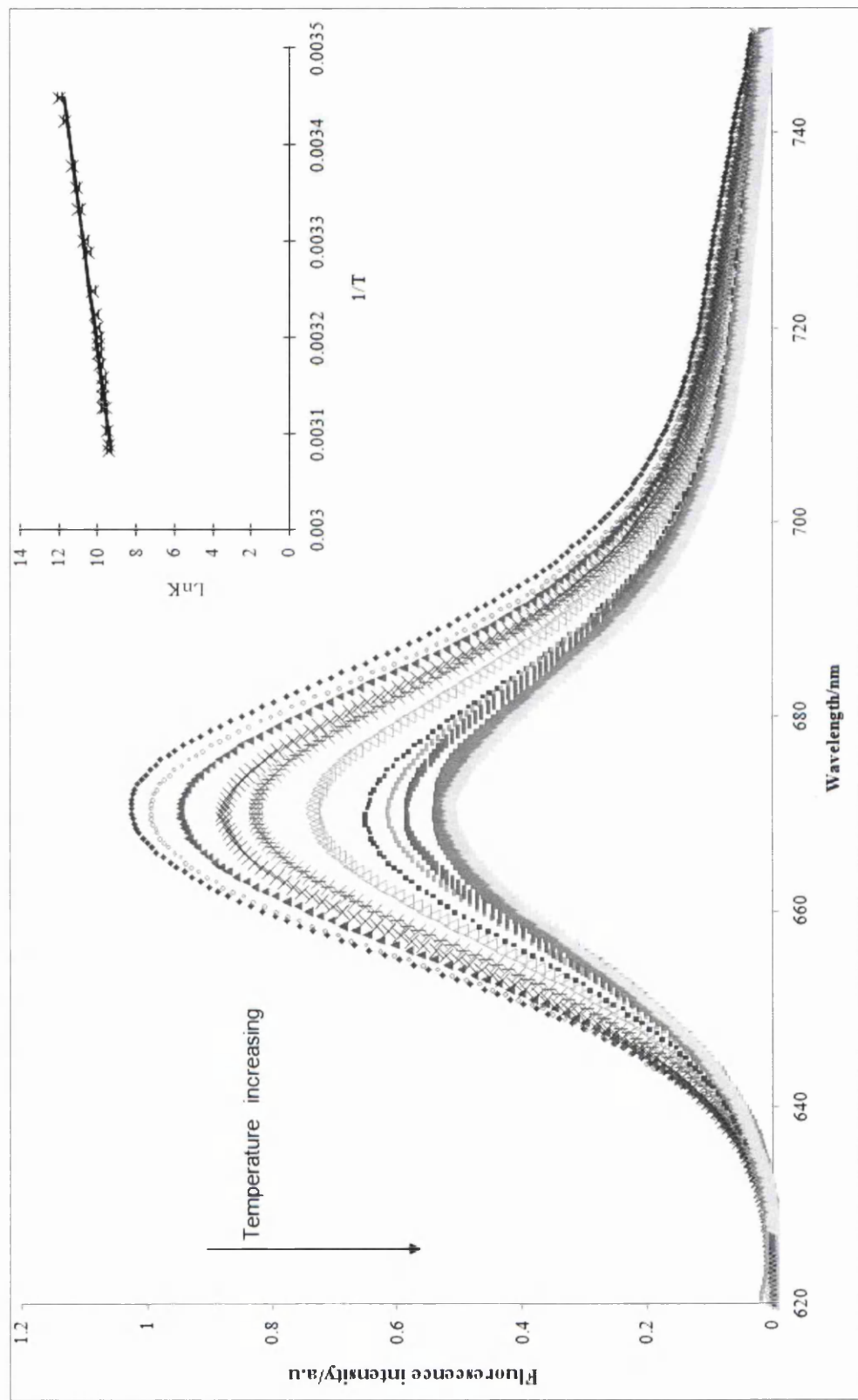


Figure 3.9. Effect of temperature on the binding of **SQ-1** to BSA. **[SQ-1]** (1.45×10^{-6} mol dm^{-3}) **[BSA]** ($=2.55 \times 10^{-5}$). Spectra for temperature range 288-320 K. Inset is the corresponding van't Hoff plot for the data.

Table 3.3. Comparison of the photochemical properties of **SQ-1** non-covalently bound to BSA. **[SQ-1]** 5×10^{-5} mol dm⁻³. **[BSA]** $= 7.5 \times 10^{-5}$ mol dm⁻³.

		Lifetime (ns)	
	Quantum yield (%)	Phase modulation	Steady state Estimate
SQ-1	8.0	0.8 [#]	0.83
SQ-1 and BSA	24.0	2.4	2.2

[#] Determined from ratio of steady state quantum yields.

*determined from steady state data and Strickler Berg relationship[19]

Table 3.4. Thermodynamic properties for the non-covalent binding of SQ-1 to BSA [SQ-1] ($1.45 \times 10^{-6} \text{ mol dm}^{-3}$) and [BSA] ($=2.55 \times 10^{-5}$)

Tempertaure/K	Binding constant $K \times 10^{-5} \text{ M}^{-1}$	ΔG kJ mol^{-1}	$T\Delta H$ kJ mol^{-1}	ΔS J mol^{-1}
288	18.6	-8.13		
298	2.8	-8.21		
303	1.85	-8.25	-5.67	85.42
308	1.23	-8.30		

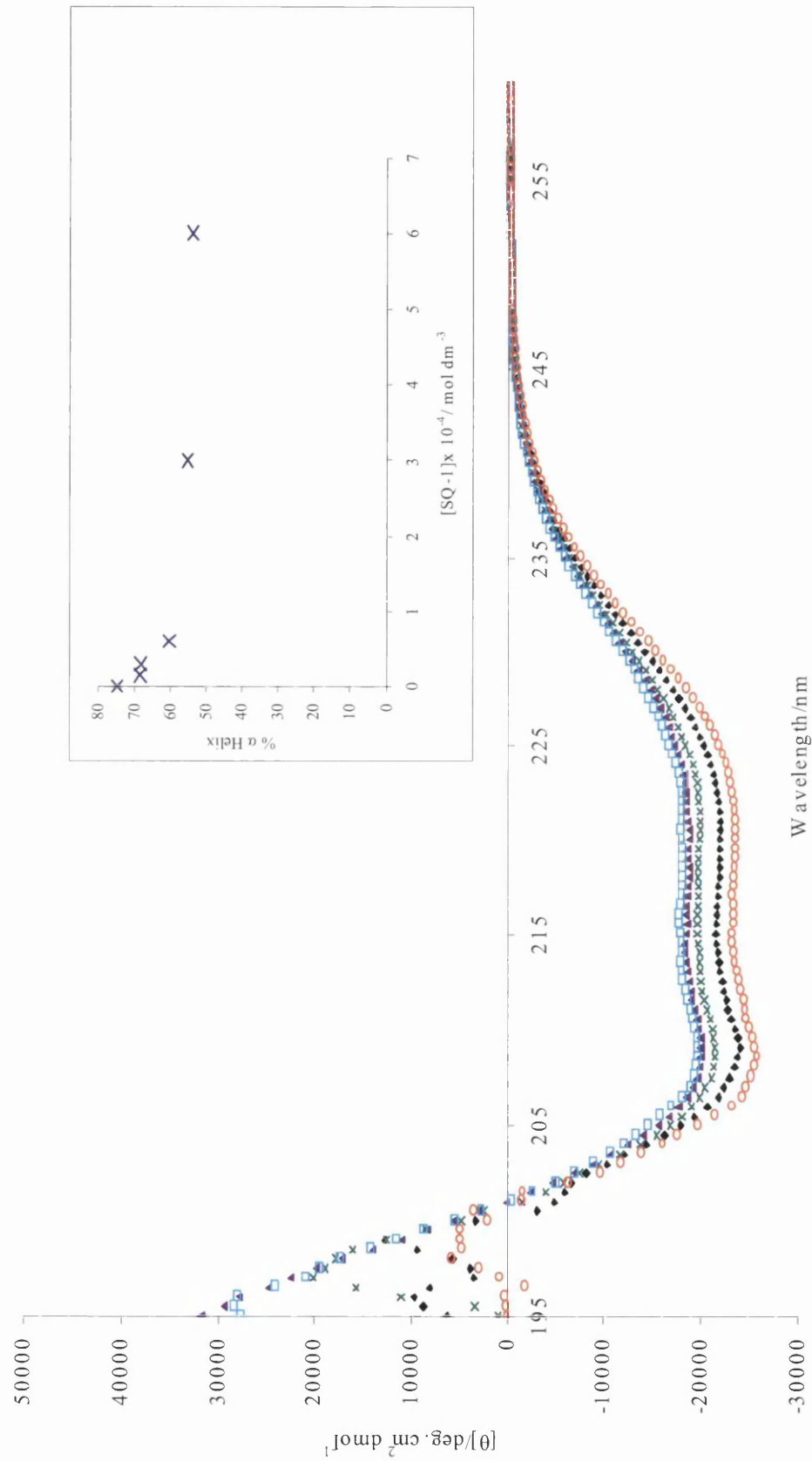


Figure 3.10. Circular dichroism spectra of BSA and BSA in the presence of increasing [SQ-1]. Where the $[SQ-1] \times 10^{-4} \text{ mol}^{-1} \text{ dm}^3$ is: $\circ=0$, $\diamond=0.3$, $\times=0.6$, $\blacktriangle=3$, $\square=6$. Insert shows the change in percentage of α -helical conformation as a function of increasing concentration **SQ-1**.

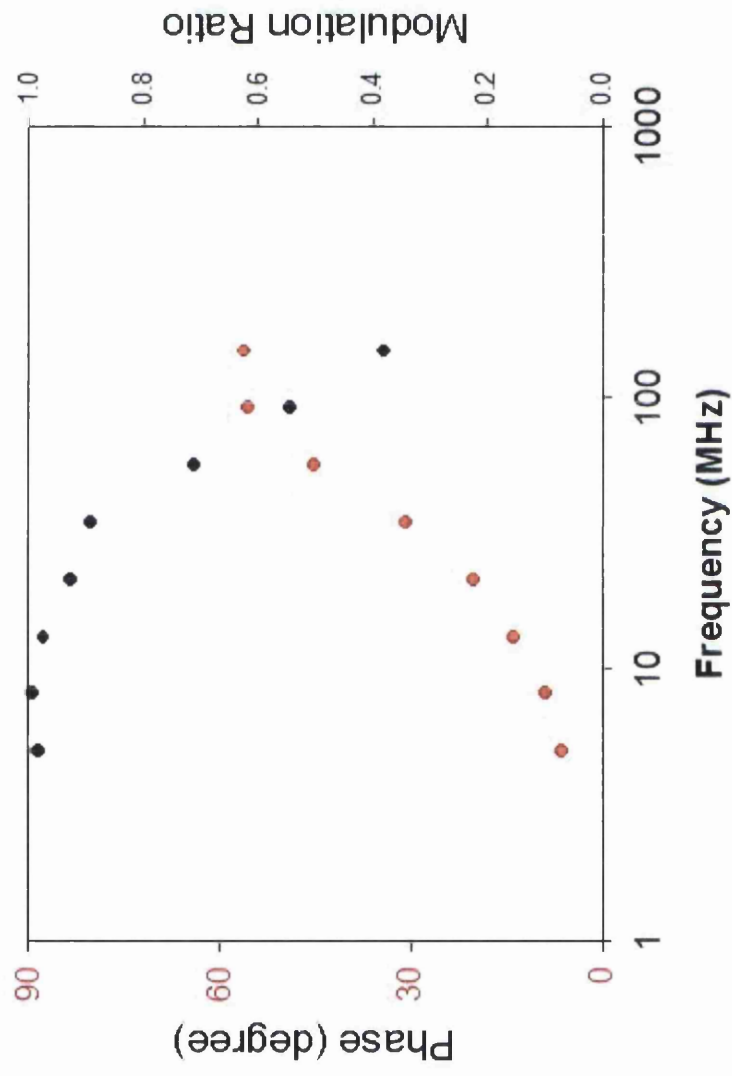


Figure 5.11 Phase modulation lifetime plots for covalent binding of SQ-1 to BSA [SQ-1] ($1.45 \times 10^{-6} \text{ mol dm}^{-3}$) and [BSA] (2.55×10^{-5}). This work was carried out by Prof. C. Geddes, University of Baltimore.

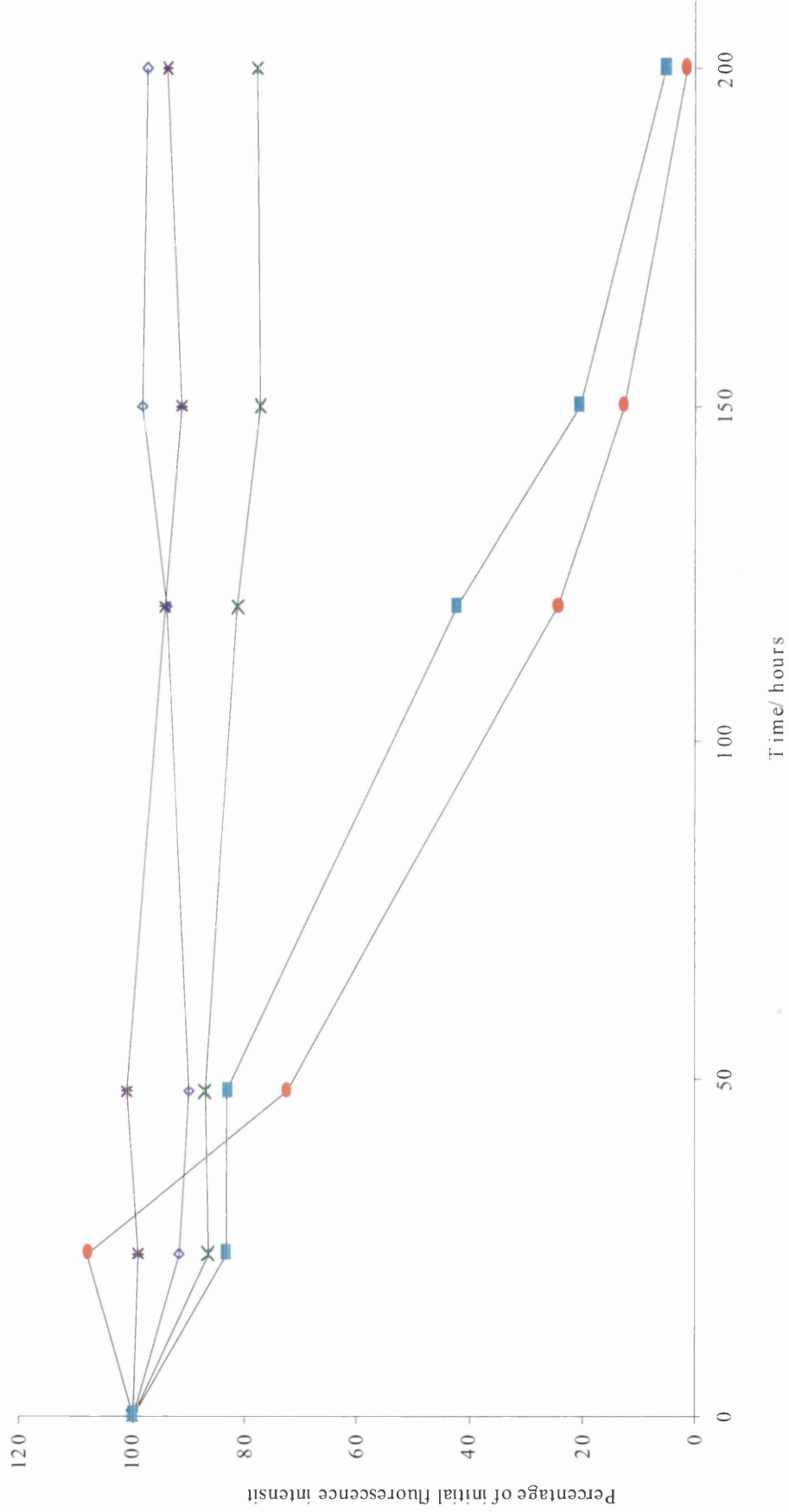


Figure 3.12: Degradation studies of SQ-1 in PBS under different conditions. X= A- purged and sealed but left in ambient room light; * = B - open to air kept in the dark; □ = C-open to air in ambient lighting; ● = D - left in ambient room light, ◇=E - frozen at -5 °C and kept in the dark

The quantum yield of degradation in PBS, for excitation with 590 nm light, was measured to be 4.2×10^{-5} by reference to the ferrioxalate actinometer [17]. This low value indicates a dye which is very stable to excitation into the visible absorption band. In D_2O the quantum yield of degradation is increased to 3.7×10^{-4} ; an observation which is consistent with a singlet oxygen photodegradation route, as found previously for other squarylium dyes. [23]

3.8 Cell culture and imaging

3.8.1 Cell imaging

As can be seen in Figure 3.13 **SQ-1** is capable of binding to the cell membrane proteins resulting in a strong fluorescence over the entire cell with negligible background fluorescence.

SQ-1 is compatible with common microscopic excitation sources and band pass filters, producing a strong image and good resolution. The excellent photostability of the dye allows an increased time for observation and image capture. The water solubility and possibility of covalent labelling of amine groups, suggest that highly fluorescent bioconjugates could be produced with potential applications in immunoassays and *in vivo* studies, without the need for organic solvents or complex labelling reactions.

3.8.2 Cell viability

Two different cell viability assays were carried out using dye concentrations in the range $0.004 - 6 \times 10^{-4} \text{ mol dm}^{-3}$. At the concentration range studied there was no significant increase in cell death for metabolically competent cells used in this study. As seen in Fig. 3.14, cell viability remains largely invariable with dose, and even at the top dose of $6 \times 10^{-4} \text{ mol dm}^{-3}$ it remains at 94%. The results of the cell viability tests and the clear, high resolution microscopic images suggest that at the concentrations studied **SQ-1** could be used to image live cells without significant cell death.

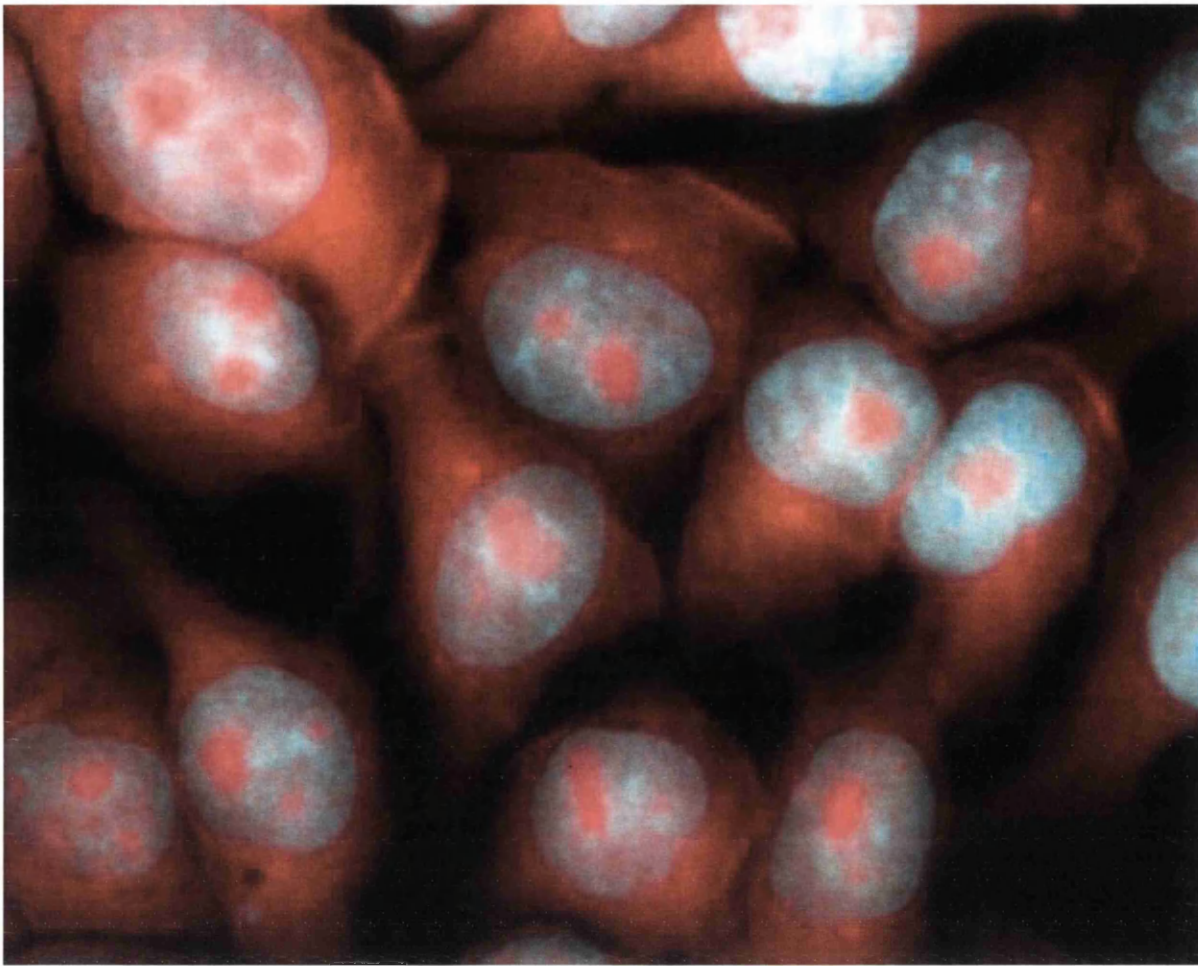


Figure 3.13: V79 cells fixed using 90% paraformaldehyde, stained using SQ-1, counterstained with DAPI. Red emission from SQ-1 bound to membrane proteins and blue emission from DAPI bound to nuclear DNA.

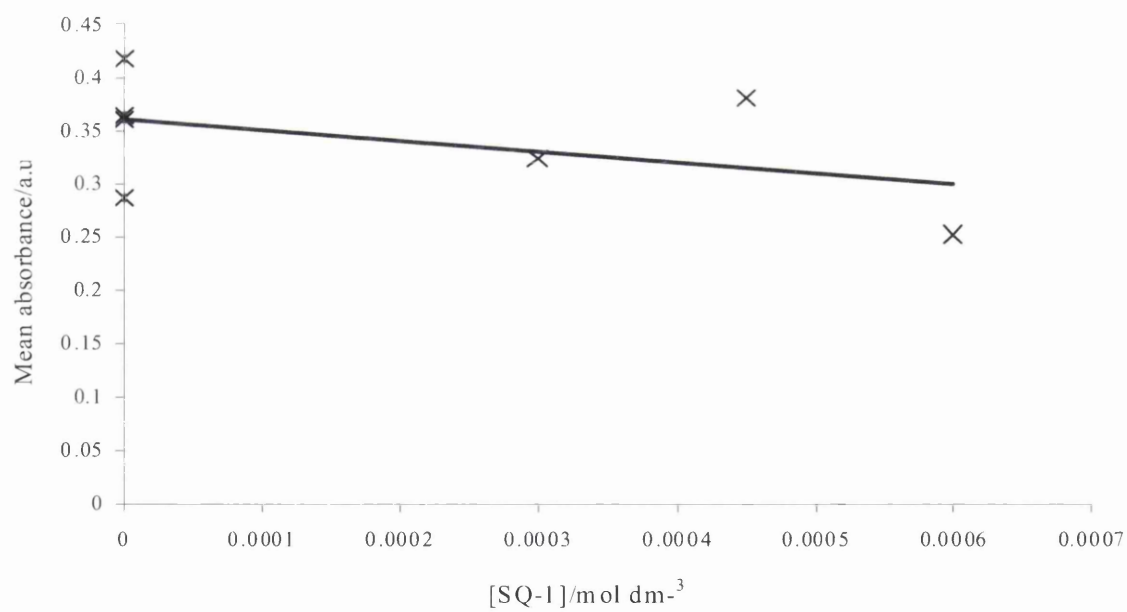
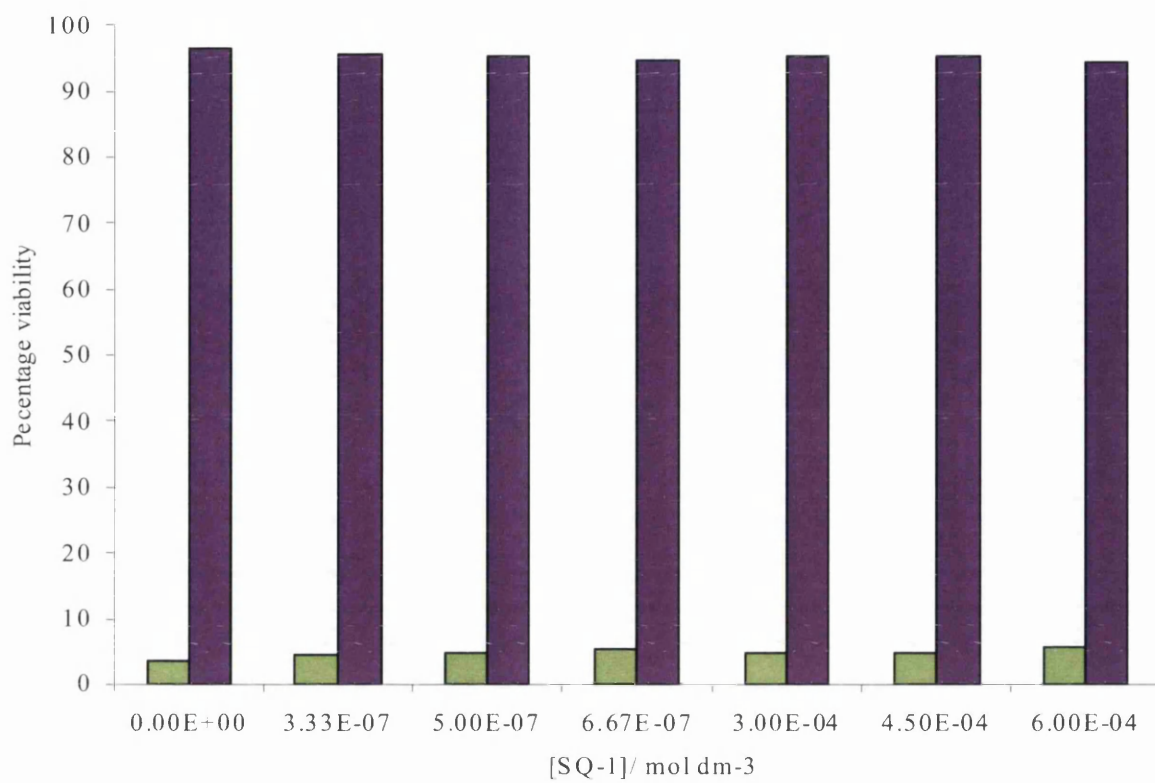


Figure 3.14: **a.** Effect of SQ-1 on cell viability using Trypan-blue exclusion assay. Solid column: % of cell which are viable; open column: % cells which are non-viable Standard error = 0.6. **b.** Effect of SQ-1 on cell viability as demonstrated by the MTS assay.

3.9 Conclusions

The synthesis and photochemical characterisation of a cheap, easily synthesised (one-pot) symmetrical squarylium dye, **SQ-1**, for non-covalent labelling of proteins, has been described. **SQ-1** meets the key criteria for a useable NIR probe including: absorption and emission maxima in the red spectral region, excellent water solubility, and high chemical and photostability. The noncovalent labelling of proteins is an attractive option as it is a fast method which requires minimal sample handling.

Key photochemical characteristics of **SQ-1** are: $\epsilon(\lambda_{\max}) = 1.0 (\pm 0.05) \times 10^5 \text{ mol}^{-1} \text{ dm}^3 \text{ cm}^{-1}$; $\Phi_{\text{RT solution}} = 0.08$; $\Phi_{77 \text{ K}} \approx 0.24$; solution fluorescence anisotropy = 0.22 (± 0.02); a quantum yield of photodegradation in PBS of only 4.2×10^{-5} ($\lambda_{\text{ex}} = 360 \text{ nm}$ with a singlet oxygen route suggested for photodegradation; and little variation in emission properties with either ionic strength or pH over the range pH 4-10. **SQ-1** binds non-covalently to BSA with $K = 2.8 (\pm 0.5) \times 10^5$ (at pH 7.2, 0.1 mol dm^{-3} phosphate buffer, $I = 0.14$), and shows a 4 fold increase in the quantum yield when bound in this way. This is in contrast to a number of currently commercially available dyes, e.g. CY5, where the decrease in quantum yield when bound to proteins [24] can cause a decrease in the overall sensitivity in immunoassays. Phase modulation measurements give a bound lifetime of 2.4 ns sufficiently long for practical measurement in a clinical environment. K decreases with temperature and analysis of the linear van't Hoff plot gives a negative enthalpy term and the positive entropy term indicating that electrostatic forces are predominant in the binding. [25]

The absorption and emission characteristics of **SQ-1** make it compatible with commonly used excitation sources such as red diode and He-Ne lasers, and avalanche photodiodes detectors.[13] Storage under nitrogen or as frozen solution allows use of working stocks of **SQ-1** over a period of weeks or more without the risk of significant degradation. The carboxylic acid functionality offers the possibility of conversion to the amine reactive N-hydroxysuccinimide ester for covalent labelling of fluorescent markers to drugs, DNA and antibodies.

Cell imaging and viability studies show **SQ-1** to have low cytotoxicity and excellent imaging characteristics.

Due to the favourable chemical and photochemical characteristics **SQ-1** will be particularly useful for fluorescence based biomedical applications such as immunoassays.

3.10 References

- [1] C. Sun, J. Yang, L. Li, X. Wu, Y. Liu and S. Liu, *Journal Chromatography B*, 803, (2004), 173-190.
- [2] F. Wang, W.B. Tan, Y. Zhang, X.P. Fan and M.Q. Wang, *Nanotechnology*, 17, (2006), R1-R13.
- [3] J.V. Frangioni, *Current opinions in chemical biology*, 7, (2003), 626-634.
- [4] J. Arden-Jacob, J. Frantzeskos, N.U. Kemnitzer, A. Zilles and K.H. Drexhage, *Spectrochimica Acta Part A: Molecular and Biomolecular Spectroscopy*, 57, (2001), 2271-2283.
- [5] T. Fukushima, Noriko Usui, Tomofumi Santa and K. Imai, *Journal of Pharmaceutical and Biomedical Analysis*, 30, (2003), 1655-1687.
- [6] G. Patonay, J. Salon, J. Sowell and L. Strekowski, *Molecules* 9, (2004), 40-49.
- [7] E. Terpetsching, H. Szmecinski and J.R. Lakowicz, *Analytica Chimica Acta*, 282, (1993), 633-641.
- [8] E. Terpetschnig and J.R. Lakowicz, *Dyes and Pigments*, 21, (1993), 227-234.
- [9] E. Terpetschnig, H. Szmecinski, A. Ozinskas and J.R. Lakowicz, *Analytical Biochemistry*, 217, (1994), 197-204.
- [10] K.D. Volkova, V.B. Kovalska, A.L. Tatarets, L.D. Patsenker, D.V. Kryvorotenko and S.M. Yarmoluk, *Dyes and Pigments*, 72, (2007), 285-292.
- [11] F. Welder, B. Paul, H. Nakazumi, S. Yagi and C.L. Colyer, *Journal of Chromatography B. Derivatization of Large Biomolecules*, 793, (2003), 93-105.
- [12] W. Yan and C.L. Colyer, *Journal of Chromatography A.*, 1135, (2006), 115-121.
- [13] L.D. Lavis and R.T. Raines, *ACS Chem. Biol.* 3, (2008), 142-155.
- [14] M. Gumbleton and D.J. Stephens, *Advanced Drug Delivery Reviews Advances in Fluorescence Imaging: Opportunities for Pharmaceutical Science*, 57, (2005), 5-15.
- [15] H.R. Petty, *Microsc Res Tech* 70, (2007), 687-709.
- [16] M.D Vestergaard, K. Kerman and E. Tamiya, *Sensors*, 7, (2007), 3442-3458.
- [17] P.R. Banks, *Trends Anal. Chem.*, 17, (1998), 612-617.
- [18] D.L. Gallaher and M.R. Johnson, *Analyst*, 124, (1999), 1541-1546.
- [19] S. Nagaraj, S.V. Rahavendran and H.T. Karnes, *Journal of Pharmaceutical and Biomedical Analysis*, 18, (1998), 411-420.

- [20] A.J.G. Mank, H. Lingeman and C. Gooijer, *TrAC Trends in Analytical Chemistry*, 15, (1996), 1-11.
- [21] M.R. Eftink. in (Lakowicz, J.R., ed.) *Topics in Fluorescence Spectroscopy Volume 6: Protein Fluorescence*, Springer US 2002.
- [22] B. Oswald, F. Lehmann, L. Simon, E. Terpetschnig and O.S. Wolfbeis, *Analytical Biochemistry*, 280, (2000), 272-277.
- [23] B. Oswald, L. Patsenker, J. Duschl, H. Szmecinski, O.S. Wolfbeis and E. Terpetschnig, *Bioconjugate Chem.*, 10, (1999), 925-931.
- [24] R.B. Mujumdar, L.A. Ernst, S.R. Mujumdar, C.J. Lewis and A.S. Waggoner, *Bioconjugate Chem.*, 4, (1993), 105-111.
- [25] S.R. Mujumdar, R.B. Mujumdar, C.M. Grant and A.S. Waggoner, *Bioconjugate Chem.* 7, (1996), 356-362.
- [26] J.H. Flanagan, S.H. Khan, S. Menchen, S.A. Soper and R.P. Hammer, *Bioconjugate Chem.* 8, (1997), 751-756.
- [27] N. Gadjev, T. Deligeorgiev, I. Kanev, M. Tasseva and R. Sabnis, *Dyes and Pigments* 24, (1994), 93-98.
- [28] T. Deligeorgiev, N. Gadjev and A. Lugade, *Dyes and Pigments* 19, (1992), 215-222.
- [29] T. Deligeorgiev, A. Vasilev and K.-H. Drexhage, *Dyes and Pigments* 67, (2005), 21-26.
- [30] T.G. Deligeorgiev, N.I. Gadjev, K.-H. Drexhage and R.W. Sabnis, *Dyes and Pigments* 29, (1995), 315-322.
- [31] T.G. Deligeorgiev, N.I. Gadjev, A.A. Vasilev, V.A. Maximova, I.I. Timcheva, H.E. Katerinopoulos and G.K. Tsikalas, *Dyes and Pigments*, 75, (2007), 466-473.
- [32] T.G. Deligeorgiev, D.A. Zaneva, H.E. Katerinopoulos and V.N. Kolev, *Dyes and Pigments*, 41, (1999), 49-54.
- [33] O.K. Gasymov and B.J. Glasgow, *Biochimica et Biophysica Acta (BBA) - Proteins & Proteomics*, 1774, (2007), 403-411.
- [34] M.A. Haidekker and E.A. Theodorakis, *Org. Biomol. Chem.*, 5, (2007), 1669 - 1678.
- [35] J. Sowell, R. Parihar and G. Patonay, *Journal of Chromatography B: Biomedical Sciences and Applications*, 752, (2001), 1-8.

- [36] J. Sowell, K.A. Agnew-Heard, J. Christian Mason, C. Mama, L. Strekowski and G. Patonay, *Journal of Chromatography B: Biomedical Sciences and Applications*, 755, (2001), 91-99.
- [37] A.A. Ishchenko, *Kvantovaya Elektronika*, 21, (1994), 513-534.
- [38] E.M.C. McCorquodale, C. L., *Electrophoresis*, 22, (2001), 2403-2408.
- [39] E.D. Moody, P.J. Viskari and C.L. Colyer, *Journal of Chromatography, B: Biomedical Sciences and Applications*, 729, (1999), 55-64.
- [40] M.I. Daneshvar, J.M. Peralta, G.A. Casay, N. Narayanan, L. Evans, G. Patonay and L. Strekowski, *Journal of Immunological Methods*, 226, (1999), 119-128.
- [41] A Gómez-Hens, and M. P Aguilar-Caballo, *TrAC Trends in Analytical Chemistry*, 23, (2004), 127-136
- [42] C. Chen, X. Qi and B. Zhou, *Journal of Photochemistry and Photobiology A: Chemistry*, 109, (1997), 155-158.
- [43] A.S. Tatikolov and G. Ponterini, *Journal of Photochemistry and Photobiology A: Chemistry*, 117, (1998), 35-41.
- [44] A.S. Tatikolov, L.A. Shvedova, N.A. Derevyanko, A.A. Ishchenko and V.A. Kuzmin, *Chemical Physics Letters*, 190, (1992), 291-297.
- [45] A.L. Tatarets, I.A. Fedyunyaeva, E. Terpetschnig and L.D. Patsenker, *Dyes and Pigments*, 64, (2005), 125-134.
- [46] A.L. Tatarets, I.A. Fedyunyayeva, T.S. Dyubko, Y.A. Povrozin, A.O. Doroshenko, E.A. Terpetschnig and L.D. Patsenker, *Analytica Chimica Acta*, 570, (2006), 214-223.
- [47] L. Tarazi, N. Narayanan and G. Patonay, *Microchemical Journal*, 64, (2000), 247-256.
- [48] K. Nielsen, J.P. Lu Z, S. JJ, S. K and M. J., *Photochem Photobiol.*, 80, (2004), 450-455.
- [49] R.B. Thompson. in (J.R.Lakowicz, ed.) *Topics in fluorescence spectroscopy*, Plenum press, NY and London .
- [50] N.Kuramoto, *JSDC.*, 106, (1990), 181-186.
- [51] S.H. Kim, S.K. Han, S.H. Park, S.M. Lee, S.M. Lee, K.N. Koh and S.W. Kang, *Dyes and Pigments*, 41, (1999), 221-226.
- [52] S.H. Kim and S.H. Hwang, *Dyes and Pigments*, 35 (1997), 111-121.
- [53] P.J. Sadler and J.H. Viles, *Inorg. Chem.*, 35, (1996), 4490-4496.

- [54] J. Hardouin, *Mass Spectrom. Rev.*, 26, (2007), 672-682.
- [55] J Yguerabide, E E Yguerabide, *J Cell Biochem.*, 37, (2001), 71-81.
- [56] O.I. Vesterberg, *J. Biochem, Biophys Methods*, 30, (1995), 301-314.
- [57] A. Schwarz, O. Bagel, H. Girault, *Electroanalysis*,. 12, (2000), 811-815
- [58] D. B Craig, N.J Dovichi, *Anal. Chem.*, 70, (1998), 2493-2494.
- [59] L. Tolosa, H. Szmecinski, G, Rao, G. and J.R. Lakowicz, J.R. *Anal. Biochemistry*, 250, (1997), 102-108.
- [60] O. O. Abugo, P. Herman, and J. R. Lakowicz, *J. Biomed. Opt.*, 6, (2001), 359-365.
- [61] T.J. Peters TJ. All about albumin: biochemistry, genetics and medical applications. San Diego (CA): Academic Press; 1996.
- [62] G.Patonay and M.D.Antoine, *Anal. Chem.*, 63, (1993), 321-327.

Chapter 4

Investigating factors affecting kinetic heterogeneity of lifetimes and oxygen quenching of PtOEP and PdOEP in thin film sensors

4.1 Introduction

4.1.1 Introduction

Chemical sensor research is one of the most fruitful, exciting and interdisciplinary areas of analytical chemistry. Sensor for molecular oxygen, which it is one of the most important gases in our environment and a key metabolite in aerobic systems, are particularly important since the measurement of oxygen is a key parameter in many areas of technology and research. Oxygen measurement finds widespread application in biotechnology, industry, marine science and biomedicine. It is often essential to control the gaseous flow, and solution concentration of oxygen in many aspects of engineering and biomedicine. [1-9]

Much attention has centred around the use of polymer encapsulated oxygen-quenched lumophores as optical oxygen sensors. For these sensors there is an $[O_2]$ dependent reduction in luminescence intensity as a consequence of oxygen quenching of the emitting state. [5,10-24] As discussed in chapter 1 the use of transition metal porphyrins for oxygen sensing has become increasingly popular. [16-29] Platinum and palladium porphyrins remain the most commonly used metalloporphyrin lumophores as they have: high quantum yields of emission, long excited-state lifetimes, (0.1-0.2 and 0.4-0.9 ms respectively, [17,19,20,25,29,30]), are compatible with hydrophobic polymers, and have excitation and emission wavelengths in the visible region of the spectrum. [10-16] Modification of the porphyrin ring by the addition of alkyl or ketone groups produces lumophores of different natural lifetimes and oxygen sensitivities. Pt and Pd octaethylporphyrins (PtOEP, PdOEP) (Figure 1) remain the most widely used lumophores [25,26, 30-32] but other derivatives such as PtTFPP, [32-34] and PtOEPK [23], are receiving increasing attention due to their enhanced photostability.

4.1.2 Stern-Volmer analysis

In general the results of such studies are discussed in terms of Stern-Volmer analysis of emission data. For a homogeneous system with lumophore, L, which decays

naturally by a first order process with rate constant, k_{uq} , and which is dynamically quenched by oxygen, with a rate constant k_q , the rate of decay of the excited state of the lumophore, L^* , is given by:

$$-d[L^*]/dt = (k_{uq} + k_q[O_2])[L^*] \quad (4.1)$$

For a homogeneous system, luminescence is expected to decay exponentially and there should be a linear relationship between the quenching efficiency, i.e. I_0/I or τ/τ_0 , and $[O_2]$. Given by

$$I_0/I = 1 + \tau_0 k_q [O_2] \quad (4.2)$$

Where I_0 is the emission intensity in the absence of oxygen, I is the emission intensity in the presence of oxygen, τ_0 is the lifetime in the absence of oxygen, k_q the bimolecular rate constant for oxygen quenching and $[O_2]$ is the concentration of oxygen. The equivalent kinetic equation sees I_0/I replaced with τ_0/τ where τ_0 and τ are the lifetimes in the absence and presence of oxygen at concentration $[O_2]$ respectively.

Although fluid solution studies usually yield linear Stern-Volmer plots, a common characteristic of oxygen quenching of polymer encapsulated lumophores is a Stern-Volmer plot with downward curvature. A second common feature of oxygen quenching for almost all polymer/lumophore combinations is a non-exponential emission decay in the presence of oxygen and a non-linear relationship between I_0/I or τ/τ_0 and pO_2 . [10-28] Such behaviour is usually discussed in terms of heterogeneity in which the lumophore is considered to occupy a distribution of sites.

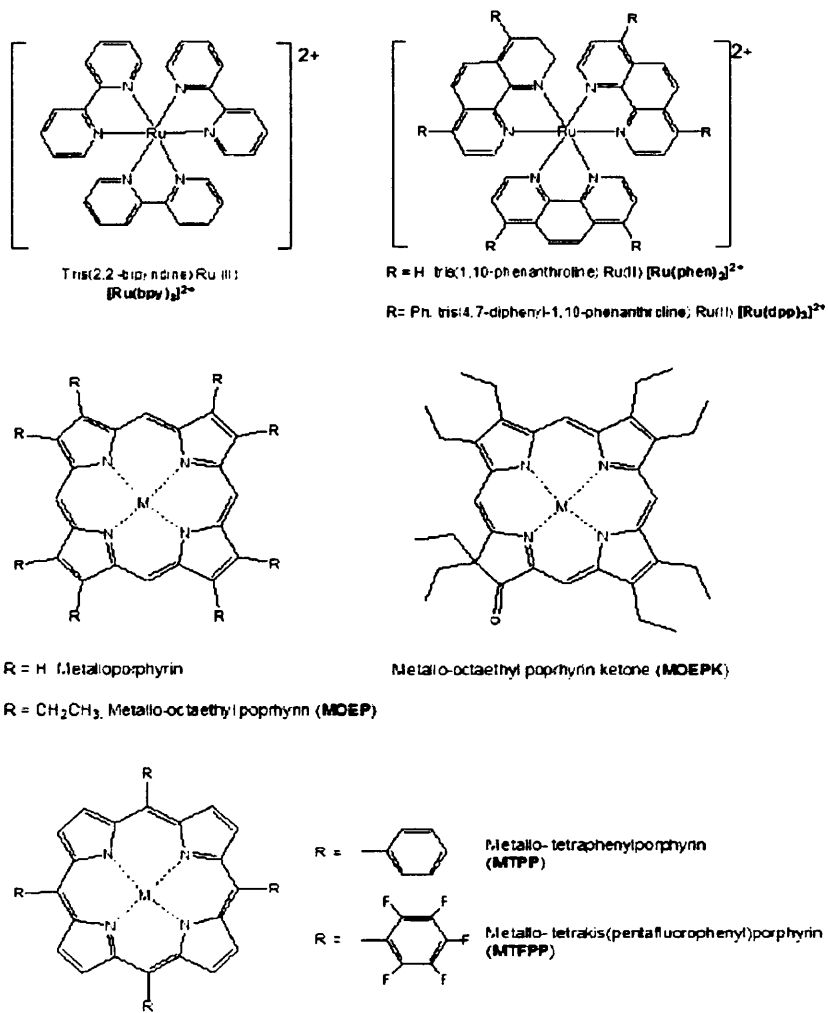


Figure 4.1 structure of lumophores discussed in this chapter.

4.1.3 Polymers

The work in this chapter deals with polymer encapsulated lumophores and a brief introduction to the relevant properties of the polymers used will be given here.

4.3.1 Movement of gases through the polymer

The matrix used to encapsulate and support the lumophore must be permeable to the analyte. With respect to oxygen the permeation through polymers is thought to involve several stages: (i) sorption of the gas onto the entering face of the polymer, (ii) dissolution of the gas in the polymer (iii) diffusion through the polymer (iv) desorption from the other face. [37]

The oxygen permeability P_{O_2} is given by:

$$P_{O_2} = S_{O_2} D_{O_2} \quad (4.3)$$

Where S_{O_2} and D_{O_2} are the solubility and diffusion constants for oxygen respectively. The magnitude of D_{O_2} is related to the packing of polymer chains; the looser the packing, the faster and easier the diffusion process. In turn, this is related to the polymer crystallinity. In a polymer there can be regions of high crystallinity (low disorder) where the D_{O_2} and S_{O_2} will be low, and regions of low crystallinity (high disorder) where D_{O_2} and S_{O_2} will be high. A polymer film can therefore be considered heterogeneous with a distribution in both S_{O_2} and D_{O_2} . Polymer crystallinity may be decreased by the addition of a plasticiser such as a phthalate or phosphate, to produce a more oxygen permeable film. [16. 38-40]

4.3.2 Materials for immobilisation

Many different lumophore/polymer combinations are known in the literature, example of support matrices include ion-exchange resins, silicones [12], polymers [24,44,45] and sol gels. [42,43] Thin film sensors which use an encapsulated lumophore in a single polymer film offer advantages in terms of ease of fabrication, stability, speed of response and polymer-plasticiser tuneability. Commonly used polymers in optical oxygen sensors may be divided into:

(i) silicone polymers e.g. poly(dimethylsiloxane). [46,47]

(ii) organic polymers e.g. polystyrene [35], poly(vinylchloride) and poly(methylmethacrylate). [45];

(iii) fluoropolymers e.g. poly(2,2,2-trifluoroethylmethacrylate). [45]

(iv) cellulose derivatives e.g. ethyl cellulose and cellulose acetate butyrate. [16, 26]

The properties of the sensor film will strongly depend on the properties of the polymer matrix, and in particular, its permeability to oxygen. Table 4.1 summarises the relevant properties of some common polymers.

Hydrogel polymers have gained much attention recently. Hydrogels polymers are water swollen polymers exhibiting a range of permeability and selectivity characteristics which may be controlled by their monomer composition. [48] Hydrogels form a large and highly variable class of polymers. [41, 48-50] Those for use in optical sensors for solutions need to be insoluble in water but also highly permeable to water and aqueous samples including serums. Typical examples of hydrogels include cellulose, dextrans, polyacrylamides and polyurethanes. [49-50] Polyurethane hydrogels have recently been used in a variety of sensing applications and in commercial instrumentation because the polymer is highly biocompatible and has a high water uptake.

Table 4.1 The oxygen permeability of commonly used polymers. [58]

POLYMER	OXYGEN PERMEABILITY x 10¹³/ cm² s⁻¹ Pa⁻¹	OXYGEN DIFFUSION x10⁶/cm² s⁻¹
Poly(vinyl alcohol)	0.00665	-
Poly(vinyl chloride)	0.34	0.012
Poly(vinyl acetate)	0.36	0.056
Polystyrene	1.9	-
Polyethylene	2.2	0.46
Ethyl cellulose	11.0	0.639
Cellulose acetate butyrate	3.56	

4.3.3 Plasticization of polymers

Plasticization alters many properties of a polymer including oxygen diffusion and solubility. Plasticizers are typically small molecules such as phthalates and phosphates that can decrease the attractive forces between polymer chains and increase polymer flexibility. The more open the plasticized polymer structure, the greater gas permeability compared to that of an unplasticized polymer. Prior to 1968 very little had been published on the diffusion of gases through plasticized polymers even though their use was widespread. The early 1990's saw the use of plasticizers in CO₂ sensor preparation to improve sensor response. In 1997 Mills et al. found that increasing the plasticizer concentration improved both sensitivity and speed of response of optical oxygen sensor. [16,38,39,51]

Plasticiser and polymer need to be compatible, i.e. have a similar solubility parameter, δ , for the polymer to improve the response characteristics. A low difference between the solubility parameter of polymer and plasticizer indicates high compatibility.

4.1.4 Modelling heterogeneity

The curvature of Stern-Volmer plots can arise in several ways and analysis of both the lifetime and intensity of emission can give useful information about the cause of non-linearity. [25-26] In order to understand or model these deviations from linearity the lumophore is usually considered to occupy a distribution of sites differing in one or more relevant property ie $S0_2$, DO_2 or τ_0 . Modelling the luminescence decay kinetics has been the subject of much work and discrete [14,52] continuous [53-55] and semi-empirical models [14,15] have all been used.

4.1.4.1 Discrete models

Discrete models assume that there are two or more sites differing in a relevant property. One approach, the dual site model, assumes that the lumophore can exist in two sites. Some debate still stands over whether only one or both sites is quenchable, but they have differing characteristic quenching constants. [15,16,39,52] The multisite model takes this one step further and assumes that the lumophore can occupy a number of different sites. A second model is based on the non-linear gas solubility model

which arises from the lumophore having different solubility co-efficient in different regions of the polymer. [46]

4.14.2 Continuous distributions

Continuous distributions of essentially arbitrary form such as Gaussian [53,56] or log Gaussian [53,55,56] are often used when data can take values across a continuous range, although generally the continuous distributions discussed here are modelled using a large number of discrete sites.

4.1.4.3 Empirical

Empirical methods used for the modelling of heterogeneity within these films include the Langmuir isotherm adapted from adsorption studies of heterogeneous systems [15] and the Freundlich isotherm [59] which is usually used in adsorption studies when deviation from the Langmuir isotherm occur due to non-uniform surfaces, interactions between molecules, and/or multilayer adsorption.

4.1.4.4 Isotherms

The Langmuir isotherm is used to describe uniform adsorption of a gas onto energetically equivalent sites of a solid material.

$$\frac{[O_2]_{ads}}{[O_2]_{max}} = \frac{(K_{ads}pO_2)}{1 + K_{ads}pO_2} \quad (4.4)$$

Where $[O_2]_{ads}$ is the concentration of the surface adsorbed oxygen, $[O_2]_{max}$ is the maximum concentration of oxygen that can be adsorbed and K_{ads} is the equilibrium constant for adsorption.

The Freundlich isotherm described systems where some regions are energetically more favourable for gas adsorption, i.e, there is a distribution of adsorption sites.

$$\frac{[O_2]_{ads}}{[O_2]_{max}} = apO_2^{\frac{1}{n}} \quad (4.5)$$

Here a and n are considered to be empirical constants with no immediate physical significance. [14]

Since the heterogeneity observed with the thin film sensors is thought to be due to a distribution of some property, it seems reasonable to first consider the use of a simple Freundlich isotherm when attempting to understand and model Stern Volmer plots. Studies of the response characteristic of PtOEP and PdOEP in a variety of polymers of differing sensitivities have shown that the sensor response can be modelled well using a power law identical to the Freundlich isotherm [25].

$$\frac{I_0}{I} - 1 = \alpha(pO_2)^\beta \quad (4.6)$$

This can be used to give simple and precise calibration data. α is the Stern-Volmer constant between 0 and 1, and β gives a measure of the deviation from the linearity of the Stern-Volmer plot and hence an indication of film heterogeneity. Table 4.2 shows the unquenched lifetime, sensitivities and average values of α and β from the analysis of both emission decay and steady-state data for a range of lumophores and polymers. [25,26] β varies very little from sensor to sensor and has an average value of 0.90 ± 0.03 , this suggests that the nature of heterogeneity within the films is general and not strongly dependent upon lumophore or polymer.

4.1.5 Sensitivity

It has proved convenient to express the sensitivity of the sensing system as the reciprocal of the partial pressure that lead to quenching of 50% of the initial luminescence ($1/S_{50}$). The sensitivity for a linear Stern-Volmer relationship is equal to the Stern-Volmer constant. There is a linear relationship between the oxygen permeability and sensitivity of PtOEP polymer films. Examination of the sensitivity of differing polymer systems and the effect of humidity is known in the literature and may be a useful parameter in designing sensors for specific applications such as dissolved oxygen sensing. [25,26]

4.1.6 Dissolved oxygen sensing

As discussed in chapter 1 determination of dissolved oxygen is extremely important in a variety of technological and bio medicinal industries. To date, the Clark type oxygen

electrode is the most commonly used sensors for oxygen determination for many years. Unfortunately, electrodes of this type possess the disadvantages of: oxygen consumption during the measuring of oxygen, the need for continual stirring, long measurement times, and electrode “poisoning”.

Metalloporphyrins immobilized in polymer matrices have been widely investigated as gas phase oxygen sensor yet there is little literature on the use of metalloporphyrins as optical sensors for dissolved oxygen. One group reports the design of dissolved oxygen sensor based on PtOEP in a fluorinated polymer but the sensor response showed significant deviations from linearity [59-60] And while fluorinated organic polymers possess many of the desirable properties for use as an oxygen sensor matrix they are not readily soluble in common solvents Other examples of dissolved oxygen sensors include the use of erythrosin B encapsulated in a sol-gel [60] and in a sol-gel/fluoropolymer combination. [62] However the responses of these sensors also show considerable deviation from linearity, and this can lead to problems with calibration. Hydrogel polymers are a group of potential polymers for the design of dissolved oxygen sensors. They have excellent mechanical properties, excellent stability across a range of pH and excellent water uptake. Furthermore the low adhesion of proteins to the hydrogel increases the biocompatibility.

Humidity has been shown to effect the sensor response and sensitivity, but little is known on the effect of water on the heterogeneity or sensitivity of POEP in hydrogel polymers.

4.1.7 Aims of the work described in this chapter

Although porphyrin thin film sensors have received much attention as optical oxygen sensors, many factors affecting the response characteristics of the sensor are still not fully understood. Understanding kinetic heterogeneity is an important step in understanding response characteristics, and in this chapter results from two studies of kinetic heterogeneity in thin film polymer sensors are described and discussed. The first study examines oxygen quenching of Pt and Pd OEP in ethyl cellulose films with gas phase sensors in mind, while in the second study they are incorporated into a polyurethane hydrogel for application as solution phase sensors.

Table 4.2 Unquenched lifetime, sensitivities and α and β values for Pd and Pt porphyrins in different polymers (from [26])

Sensor	τ_0	1/S ₅₀	Average values	
			A(Torr ⁻¹)	B
PtOEP/Ethyl cellulose(EC)	0.081	0.196	0.238	0.86
PdOEP/EC	1.41	3.475	2.94	0.91
PtOEP/Cellulose acetate buterate (CAB)	0.1	0.081	0.104	0.91
PdOEP/CAB	1.45	1.27	1.185	0.92
PtOEP/Polyvinyl chloride(PVC)	0.09	0.0061	0.010	0.91
PdOEP/PVC	1.34	0.081	0.098	0.94

4.2 Steady-state and kinetic studies of Pt and Pd OEP in ethyl cellulose films

4.2.1 Results and discussion

The non-linearity of Stern-Volmer plots from steady state and kinetic studies of oxygen quenching of Pt and Pd OEP in ethyl cellulose films can be modelled well using the Freundlich isotherm. Heterogeneity of the oxygen quenching reaction kinetics has been linked to a distribution in S_{O_2} and/or D_{O_2} . In the presence oxygen luminescence decay curves give poor fits to single and double exponential analysis and this has previously been assigned to heterogeneity in k_q within the films. Better fits to a double exponential fit are seen in the absence of oxygen, and initial studies suggested the goodness of fit to a single exponential is improved at lower porphyrin concentrations.

4.2.1.1 PdOEP in unplasticised films

As expected from previous work [25,26,36] in the presence of oxygen the time resolved emission decay curves of polymer encapsulated PdOEP are poor fits to single and double exponentials, figure 4.2 illustrates the time resolved oxygen quenched decays of PdOEP/EC along with the fits to single and double exponentials and corresponding residuals as both the high and low PdOEP concentration used here ($1.2\text{-}22 \times 10^{-5} \text{ mol dm}^{-3}$). However, the unquenched time resolved emission decay curves for PdOEP/EC films show good fits to single exponentials across the concentration range studied, and there is no variation in lifetime with concentration.

4.2.1.2 PtOEP in unplasticised films

The unquenched time resolved emission decay curves for PtOEP in EC thin films of increasing concentration are shown in figure 4.3. Unlike PdOEP these show a decrease in lifetime with increasing concentration.

4.2.1.3 Free fit analysis

In the presence of N₂ time resolved emission decay curves of the polymer encapsulated PtOEP at low concentration ($1.56 \times 10^{-5} \text{ mol dm}^{-3}$) are good fits to single exponential of the type $y = A + \alpha e^{-kt}$ where A is a small background correction term, α the amplitude and k the rate constant. As the concentration of PtOEP increases the single exponential fits become very poor. Figure 4.4 shows the results of free fitting the decay curve for the lowest and highest PtOEP concentration ($1.1 \times 10^{-5} \text{ mol dm}^{-3}$ and $49.9 \times 10^{-5} \text{ mol dm}^{-3}$) to a single exponential decay and the corresponding residuals for each concentration.

The good single exponential fit to the low concentration film experimental data gives $k = 0.0101 \times 10^6 \text{ s}^{-1}$.

4.2.1.4 Double exponential analysis

As the concentration increases a single exponential fit is inadequate to describe the experimental data. A double exponential of the type $y = A + \alpha_1 e^{-k_1 t} + \alpha_2 e^{-k_2 t}$ can be used to describe the data and figure 4.5 shows the single and double exponential fits and corresponding residuals for the time resolved emission decay for $[\text{PtOEP}] = (1.24 \times 10^{-5} \text{ mol dm}^{-3})$ and highest ($49.6 \times 10^{-5} \text{ mol dm}^{-3}$)

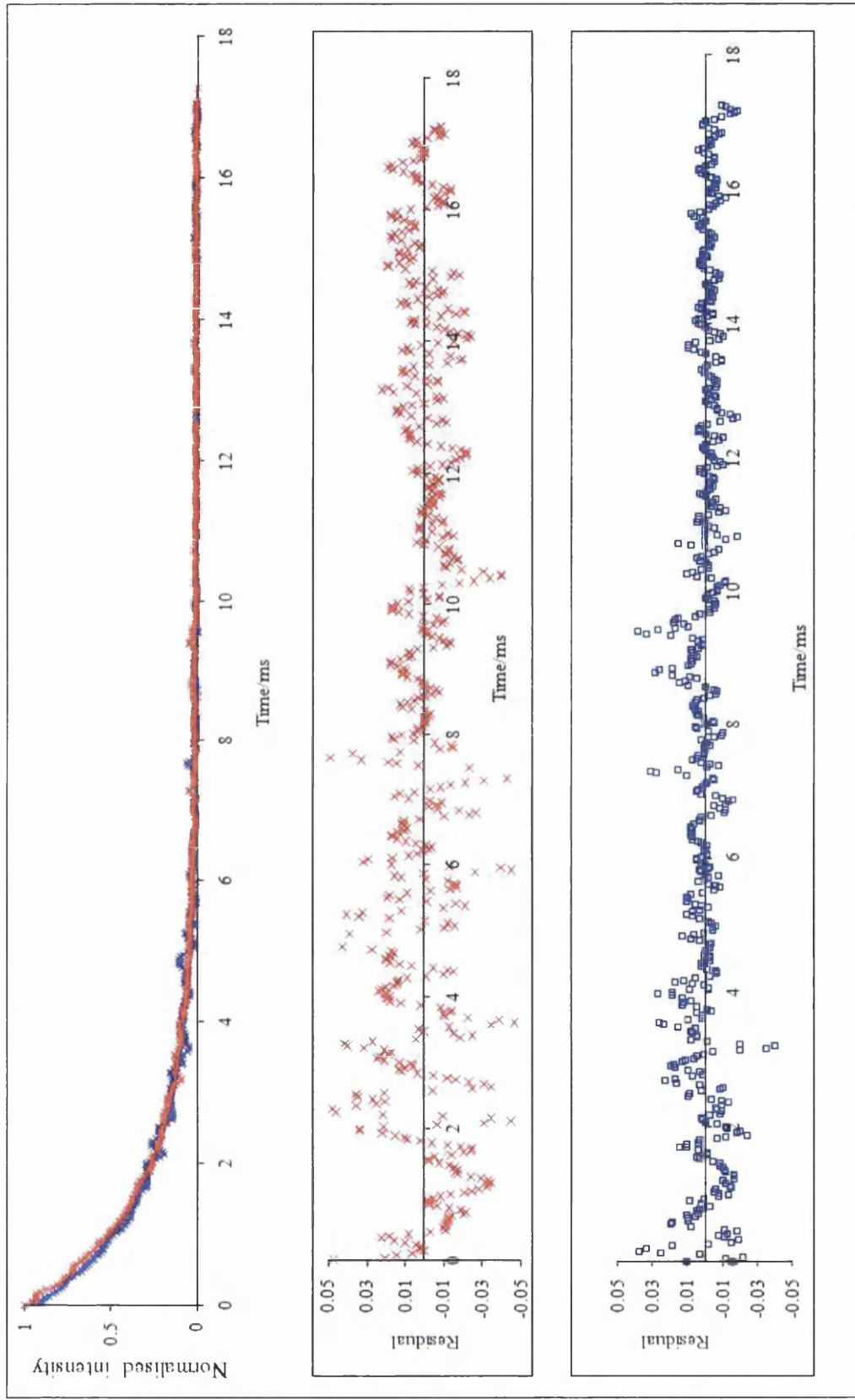


Figure 4.2. Unquenched time resolved emission of PdOEP/EC at two different porphyrin concentrations: Red - $[\text{PdOEP}] = 1.2 \times 10^{-5} \text{ mol dm}^{-3}$
 Blue - $[\text{PdOEP}] = 50 \times 10^{-5} \text{ mol dm}^{-3}$ with the residuals for a single exponential fit to the data.

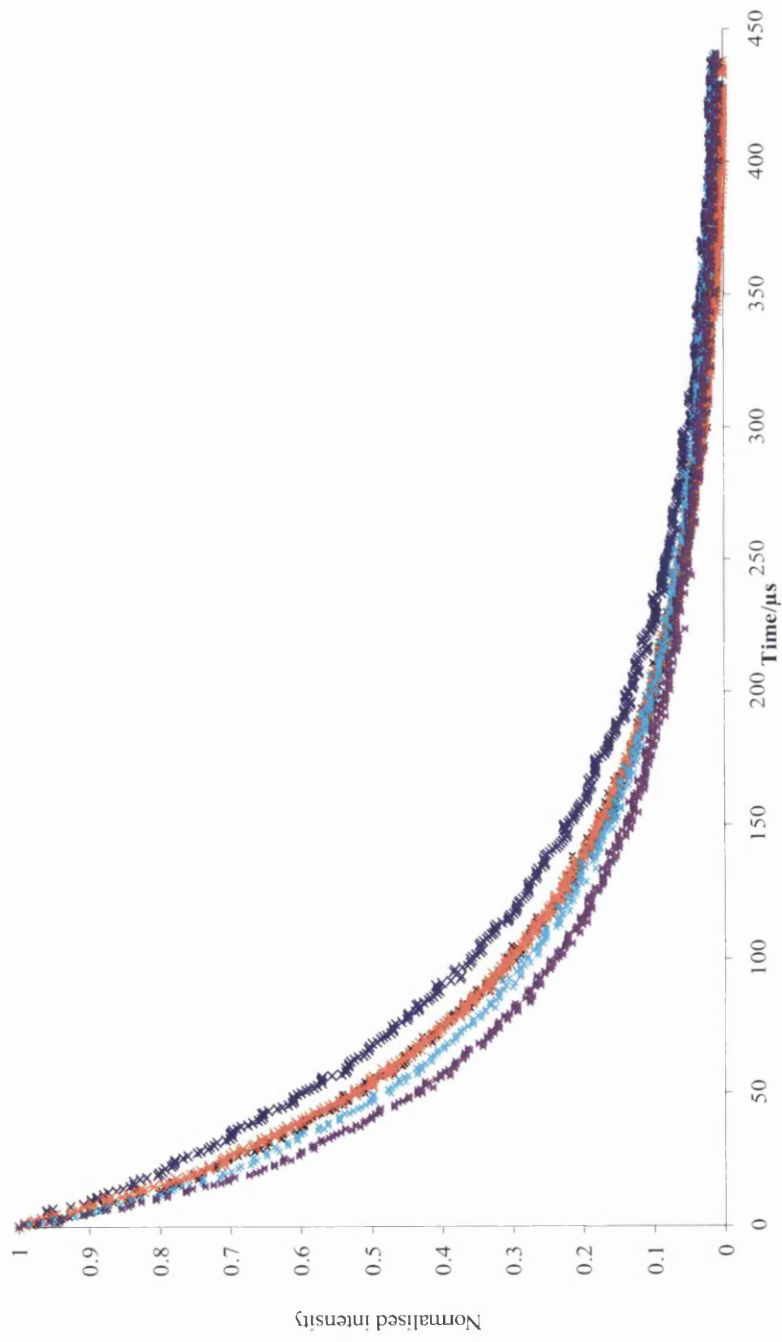


Figure 4.3. Unquenched time resolved emission decay for varying concentrations of PtOEP in PtOEP/EC thin film sensors [PtOEP] = 1.24×10^{-5} mol dm⁻³.

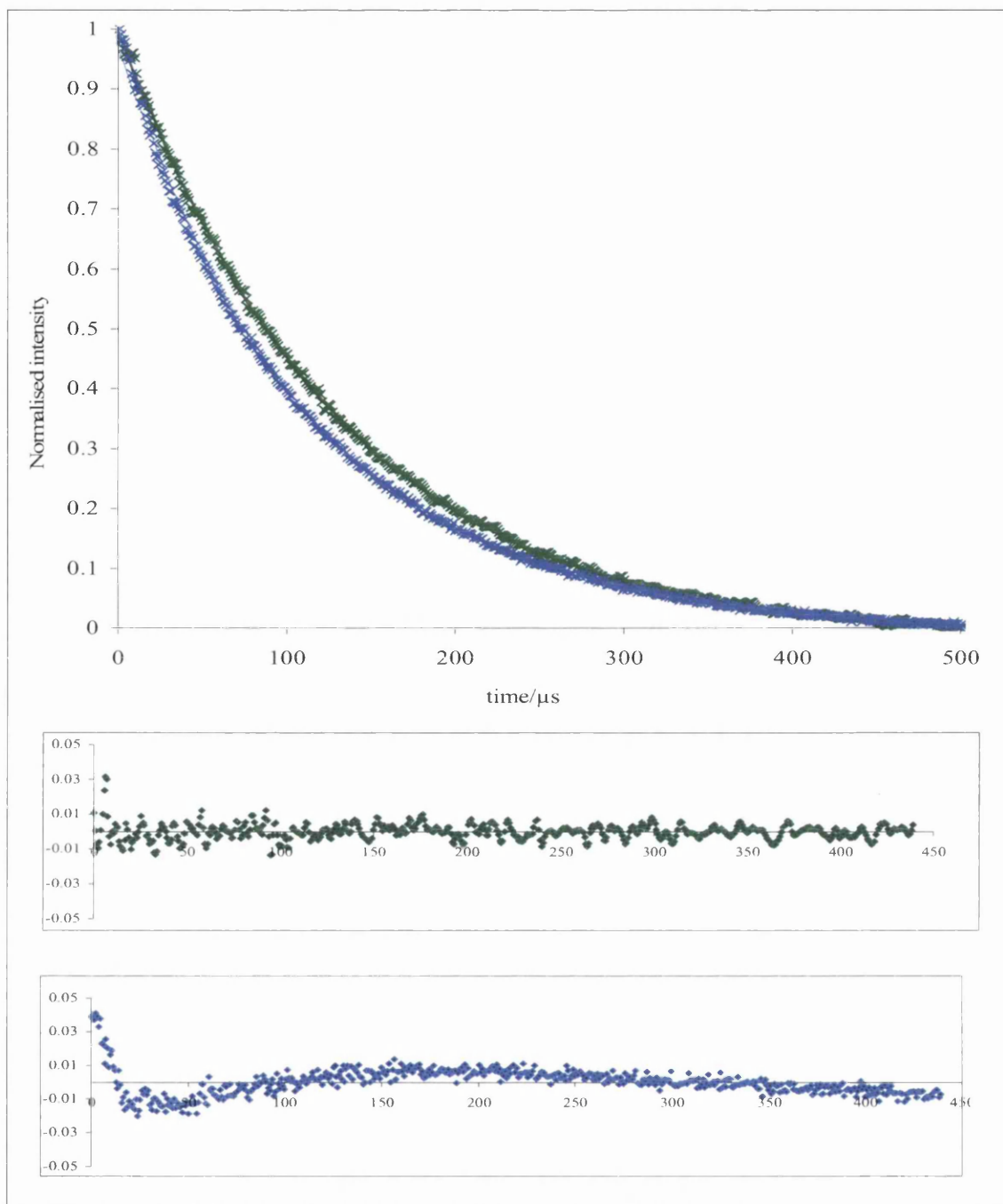


Figure 4.4. Emission decay curves for lowest ($1.24 \times 10^{-5} \text{ mol dm}^{-3}$) (Green) and highest ($49.6 \times 10^{-5} \text{ mol dm}^{-3}$) (Blue) concentration of PtOEP in PtOEP/EC films under N_2 . Curve fit to single exponential fit of the form $y = A + \alpha_1 e^{-k_1 t}$ shown as solid lines. **B** and **C** give residuals.

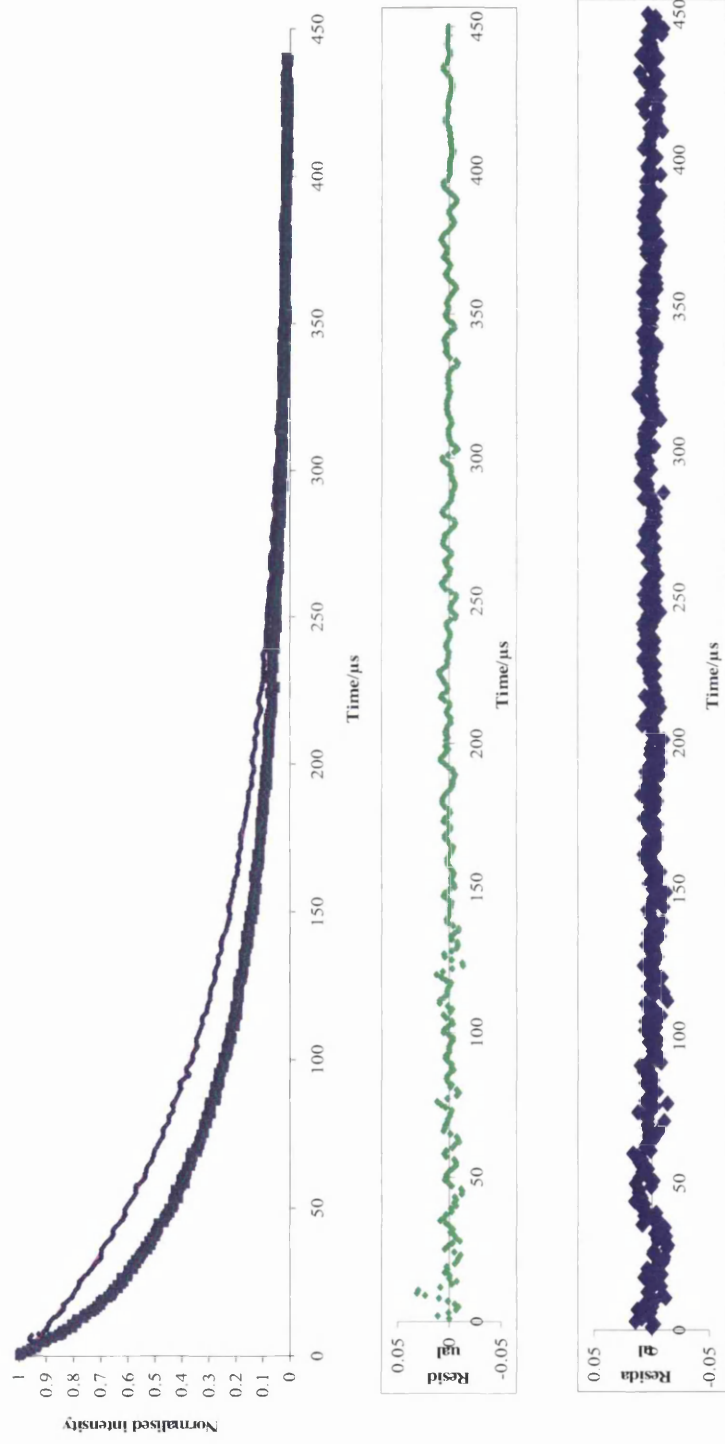


Figure 4.5 Emission decay curves for lowest ($1.24 \times 10^{-5} \text{ mol dm}^{-3}$) and highest ($49.6 \times 10^{-5} \text{ mol dm}^{-3}$) concentration of PtOEP in PtOEP/EC films under N_2 . Curve fit to double exponential fit of the form $Y = A + \alpha_1 e^{-k_1 t} + \alpha_2 e^{-k_2 t}$ where k_1 and k_2 equal $0.0527 \times 10^{-6} \text{ s}^{-1}$ and $0.0101 \times 10^{-6} \text{ s}^{-1}$ respectively. shown as solid lines. **B** and **C** give residuals

At high concentration the double exponential decay can be analysed as two components with k_1 ca. $0.010 \times 10^6 \text{ s}^{-1}$ and k_2 ca. $0.05 \times 10^6 \text{ s}^{-1}$.

4.2.2.5 Fixed rate analysis

One sensible interpretation of the data is that there are two distinct species with different lifetimes present in the sample, e.g. a monomer and an aggregate. With this in mind a double exponential fixed rate analysis where α_1 and α_2 are allowed to vary freely but k_1 and k_2 are fixed at 0.0527 and 0.0101 respectively was fitted to the experimental data. This gives a good fit to the decay curves for all concentrations and Table 3.3 shows the concentration dependence of the amplitudes of two species and the contribution of these species to the overall decay. The contribution of the “slow” species can be seen to decrease as the concentration increases with a corresponding increase in the contribution from the “fast” component.

$$Y = A + \alpha_1 e^{-0.0527x} + \alpha_2 e^{-0.0101x} \quad (4.7)$$

Table 4.3 Amplitudes of the rate constants and contributions from a double exponential analysis [$Y = A + \alpha_1 e^{-k_1 t} + \alpha_2 e^{-k_2 t}$] of time resolved emission from PtOEP/EC film at 0 torr.

[porphyrin]/ $10^{-5} \text{ mol dm}^{-3}$	α_1		α_2		k_1		k_2	
	fast	slow	fast	slow	fast	slow	fast	slow
1.24	0.355	0.640	0.014	0.009	0.014	0.009	0.014	0.009
3.10	0.260	0.791	0.012	0.009	0.012	0.009	0.012	0.009
6.20	0.198	0.803	0.026	0.011	0.026	0.011	0.026	0.011
12.4	0.221	0.781	0.030	0.011	0.030	0.011	0.030	0.011
24.8	0.318	0.690	0.035	0.012	0.035	0.012	0.035	0.012
49.6	0.313	0.684	0.047	0.013	0.047	0.013	0.047	0.013

Table 4.4 Amplitudes of the fixed rate constants from a double exponential analysis [(Y = A + $\alpha_1 e^{-0.0527x} + \alpha_2 e^{-0.0101x}$) of time resolved emission from PtOEP/EC film at 0 Torr oxygen

[porphyrin]/ $10^{-5} \text{ mol dm}^{-3}$	Percentage contribution	
	k_1 (Fast)	k_2 (Slow)
1.24	1.1	98.9
3.10	2.2	97.8
6.20	11.2	88.8
12.4	13.8	86.2
24.8	23.8	76.2
49.6	34.0	66.0

To express the dimerisation constant K_D in terms of contributions of the fast (dimer α_1) and slow (monomer α_2) from the fixed fit data (Table 4.4)



Then the dimerisation constant $K_D = \frac{[D]}{[M]^2}$ (4.9)

Assume that the laser pulse is exciting both the monomer and dimer equally the extinction co-efficient (ϵ) of dimer = 2ϵ of monomer therefore the total concentration of porphyrin is equal to $(2[D]+[M])$

We show that

$$K([M]+2[D]) = \frac{\alpha_1}{2(\alpha_2)^2} \quad (4.10)$$

If $\alpha_1 = \frac{2[D]}{(2[D]+[M])}$ (4.11)

And $\alpha_2 = \frac{[M]}{(2[D]+[M])}$ (4.12)

Substituting equations 4.11 and 4.12 into 4.10

$$\frac{\alpha_1}{2(\alpha_2)^2} = \frac{\frac{2[D]}{(2[D]+[M])}}{2[M]^2}}{(2[D]+[M])^2} \quad (4.13)$$

Cancel throughout

$$\frac{\alpha_1}{2(\alpha_2)^2} = \frac{[D]}{[M]^2} ([M] + 2[D]) \quad (4.14)$$

Substitute $\frac{[D]}{[M]^2}$ for K_D gives equation 4.10

If there is an equilibrium of the form $2M=D$, then a plot of $\alpha_1/2(\alpha_2)^2$ against PtOEP concentration, where α_1 corresponds to the dimer component and α_2 corresponds to the monomer, will be linear with slope = K_D . The result of such an analysis is shown in Figure 4.6; it shows good linearity from which a value of K_D of $790 (\pm 20) \text{ mol}^{-1} \text{ dm}^3$ is obtained. The linearity of the plot suggests that the interpretation of the two species present in the PtOEP thin film sensors as a monomer and an aggregate is reasonable. This has important implications in sensor design since it can be used to determine the maximum concentration of PtOEP that can be used before significant deviation from linearity of Stern-Volmer plots arise.

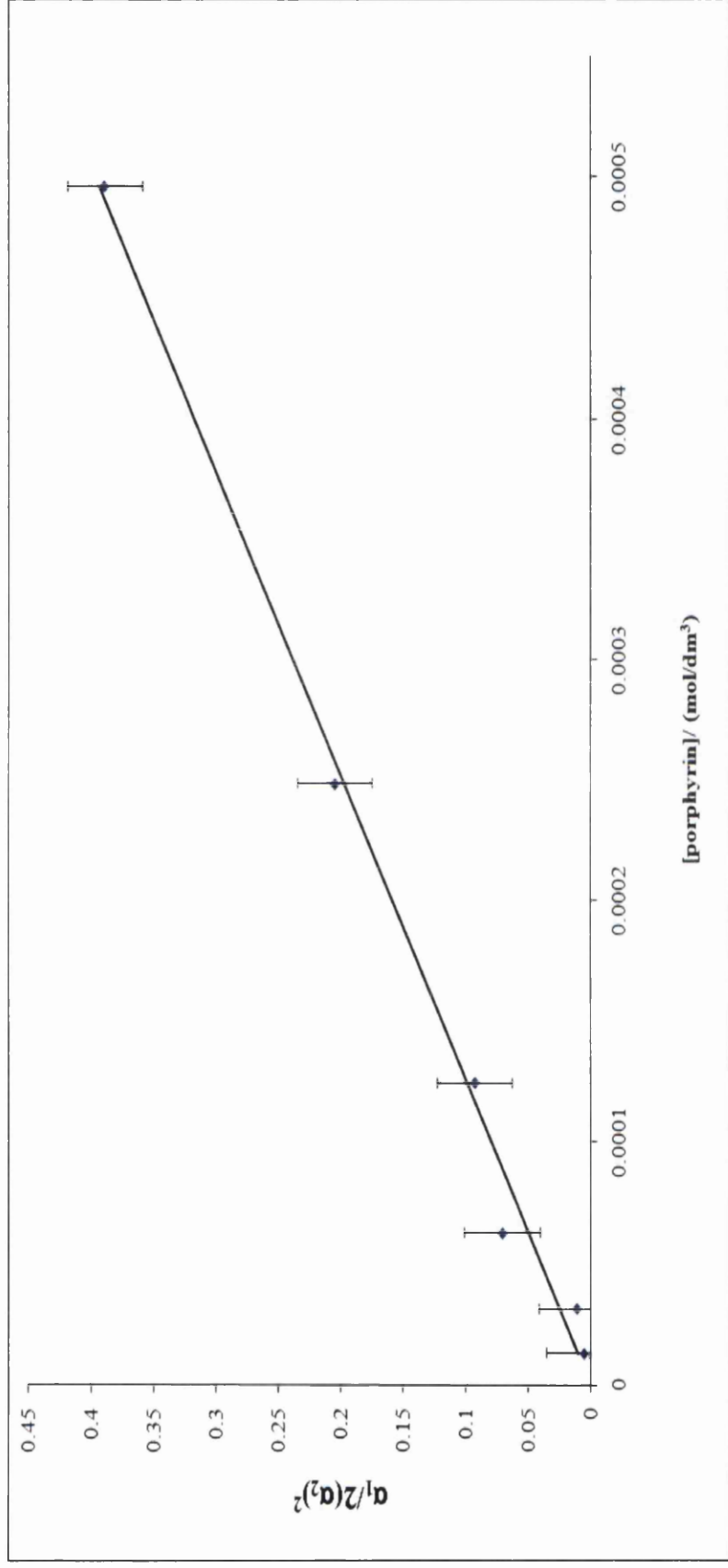


Figure 4.6. A plot of $\alpha_1/2(\alpha_2)^2$ against [PtOEP] where α_1 is the amplitude of the slow species representing a monomer and α_2 is the amplitude of the fast species representing a dimer. Solid line is the line of best fit with gradient = $K_D = 790 \pm 20 \text{ mol}^{-1} \text{ dm}^{-3}$. Errors calculated from linear regression analysis.

4.2.2.6 Stern-Volmer analysis

Stern-Volmer data, from the integrated emission decay following laser excitation, for all concentrations of porphyrin in the ethyl cellulose films were obtained as described in section 4.2.1. The logarithmic Freundlich equation provides a simple and reliable method of calibration for PtOEP/polymer films using either steady state or time resolved emission data, [25,26]. As described in section 4.1.4.4 a simple form of the equation can be used to model luminescence data, where:

$$\frac{I_0}{I} - 1 = \alpha(pO_2)^\beta \quad (4.15)$$

$$\text{Ln} \left(\left(\frac{I_0}{I} \right) - 1 \right) = \text{Ln} \alpha + \beta \text{Ln} O_2 \quad (4.16)$$

Figure 4.7 shows the logarithmic plots for PtOEP/EC data obtained from steady state and time resolved emission, and table 4.6 summarises α and β values. There is good agreement between the values obtained for steady state and time resolved emission (table 4.6) These data shows that both α and β show a concentration dependence. The significant decrease in β , previously assigned to changes in heterogeneity [25, 26], with increasing concentration suggests that the heterogeneity of the sensing system is increasing, it is therefore suggested that the proportion of dimer contributing to the decay can affect the heterogeneity of oxygen sensing. Variation in α with increasing concentration can be rationalised by the decrease in lifetime (calculated from experimental data and curve fitting by Jandel curve fit) with increasing concentration, and, a plot of $\text{Ln} \alpha$ vs $\beta \text{Ln}(\tau_0)$ is linear.

Table 4.5. α and β values for PtOEP/EC thin films sensors calculated using the logarithmic Freundlich isotherm as a function of PtOEP concentration.

$[\text{PtOEP}]/10^{-5}$ Mol dm^{-3}	τ_0/ms	α/Torr^{-1}	β
1.56	0.101	0.05	1.12
3.1	0.100	0.06	1.06
6.2	0.090	0.09	0.98
12.4	0.088	0.13	0.81
24.8	0.080	0.21	0.76
49.2	0.078	0.38	0.72

Table 4.6 Unquenched lifetime and α and β from evaluation of steady state and lifetime emission data of increasing oxygen concentration. Where τ_0 is determined from best fit analysis using Jandel table curve.

[PtOEP]/ 10^{-5} mol dm $^{-3}$	Steady state			Time resolved			Average value		
	τ_0	A	β	A	β	β	α	α	β
1.1	0.10	0.02	0.93	0.02	0.93	0.93	0.02	0.02	0.93
2.4	0.09	0.02	0.91	0.02	0.90	0.90	0.02	0.02	0.93
5.3	0.09	0.02	0.90	0.02	0.89	0.89	0.02	0.02	0.93
9.2	0.09	0.02	0.87	0.02	0.77	0.77	0.02	0.02	0.93
20.1	0.08	0.02	0.86	0.02	0.88	0.88	0.02	0.02	0.87
33.1	0.07	0.02	0.83	0.02	0.89	0.89	0.02	0.02	0.87
66.2	0.06	0.01	0.82	0.01	0.88	0.88	0.01	0.01	0.85

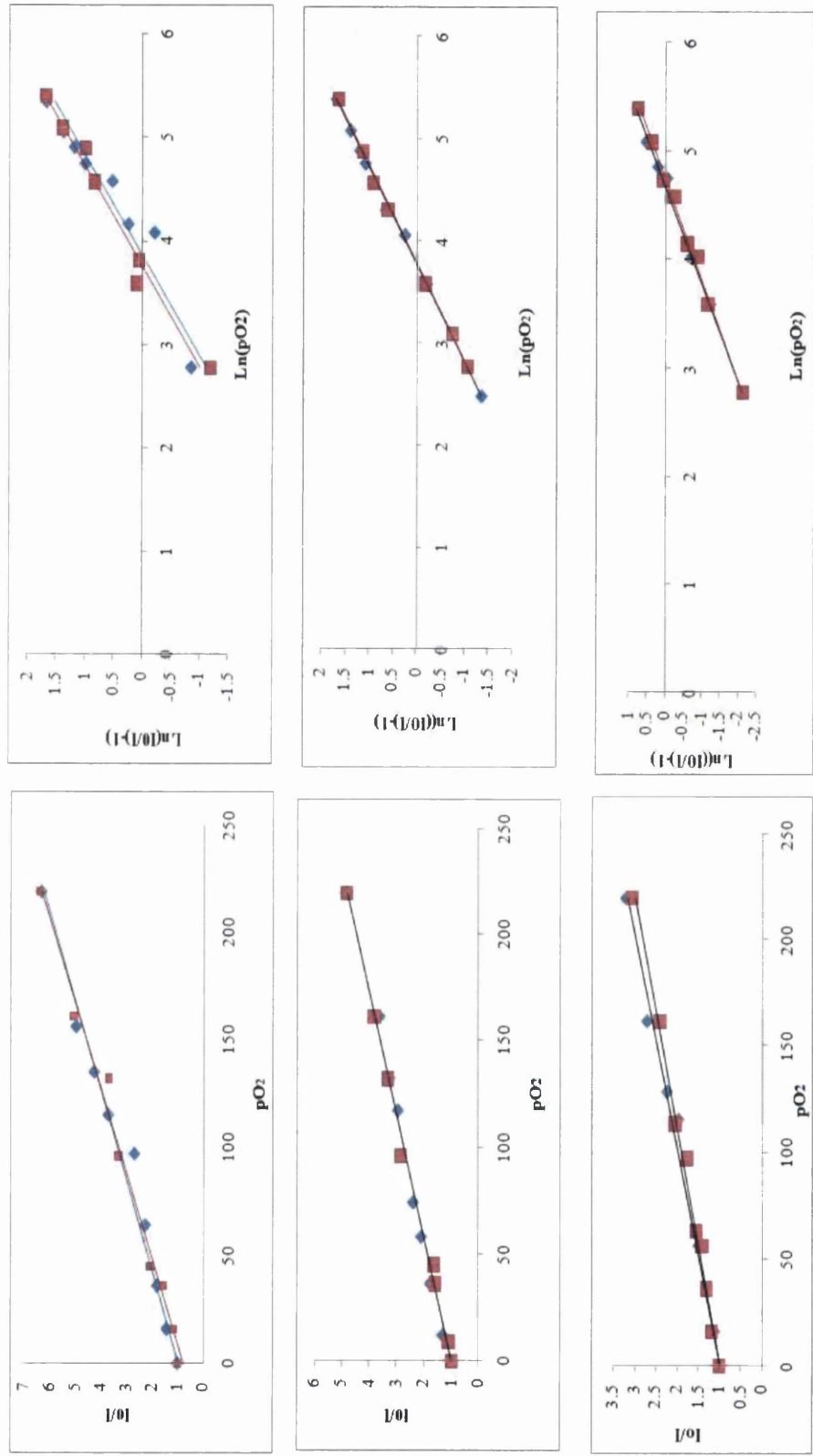


Figure 4.7. Steady state (blue) and time resolved (red) Stern-Volmer and Freundlich isotherms for PtOEP/EC thin film sensors. $A=1.56$, $B=9.2$ and $C=66.2 \times 10^{-5} \text{ mol dm}^{-3}$

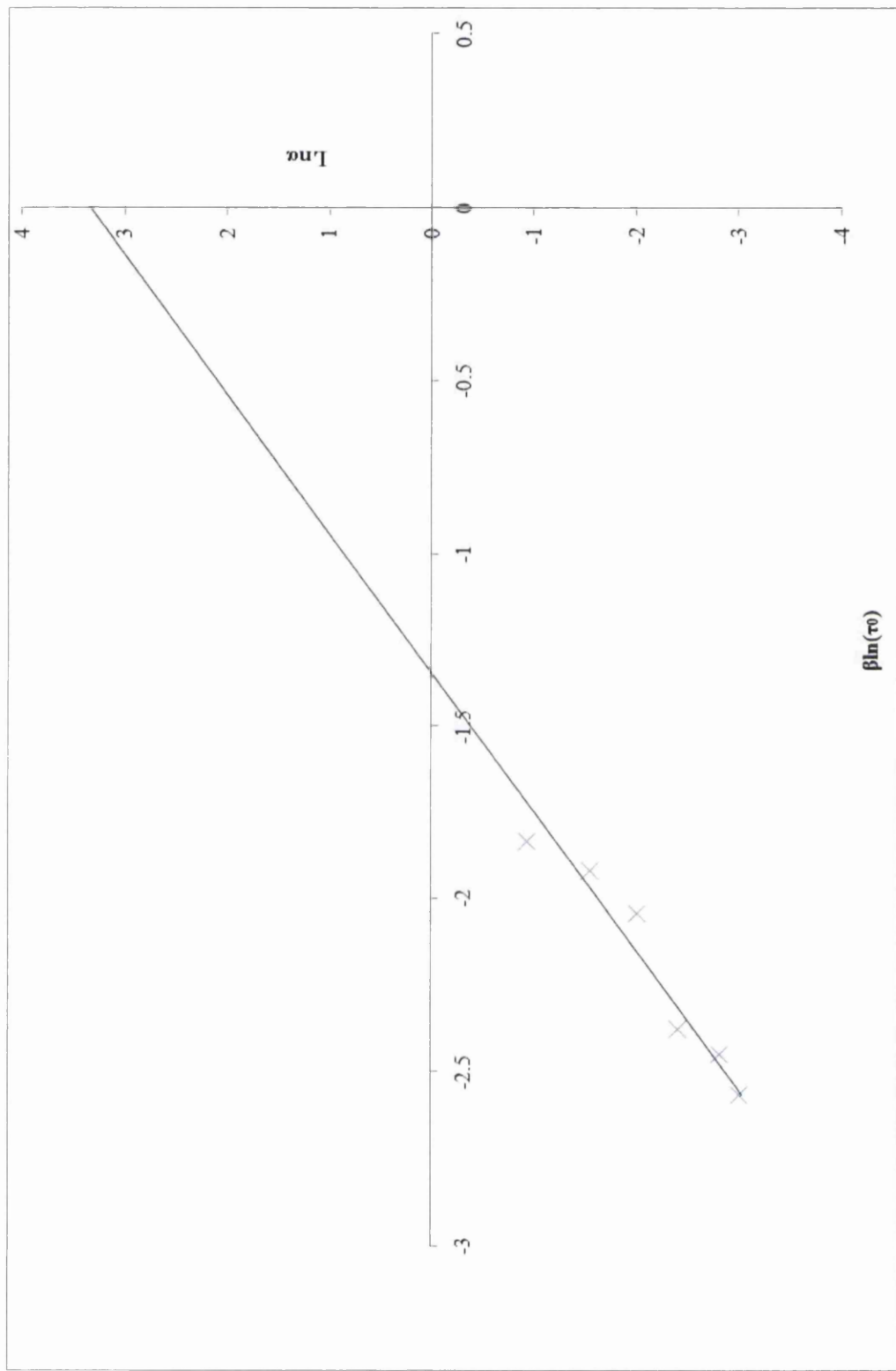


Figure 4.8 $\ln \alpha$ versus $\beta \ln(\tau_0)$ for PtOEP/EC thin film sensors of increasing concentration of PtOEP.

4.2.3 Steady-state and kinetic studies of Pt and PdOEP in ethyl cellulose plasticised films

4.2.3.1 Effect of plasticisation

Plasticisers have been widely used in thin polymer film sensors to influence sensor response [13, 38-39]. Plasticiser-polymer compatibility is determined by the relative strengths of the intermolecular forces between and within the plasticiser and polymer. Some measure of this is given by the difference in solubility parameter, δ , of plasticiser and polymer [13, 38-39]. For this study we chose plasticisers of different δ as shown in table 3.1 with δ_{EC} , δ_{TEP} , δ_{TBP} and δ_{DMP} being 21.1, 22.3, 17.5 and 19.2 (J cm^{-3})^{1/2} respectively.

Table 4.8 Amplitudes of the fixed rate constants from a double exponential analysis where k_1 and k_2 are fixed at 0.0527 and $0.0101 \times 10^6 \text{ s}^{-1}$ of unquenched time resolved emission from plasticised PtOEP/EC film.

Sensor	[Plasticisor]/ pphr	α_1 (slow)	α_2 (fast)	Total	% slow	% fast	Standard deviation
TBP	10	0.75	0.27	1.02	73.4	26.6	
TBP	20	0.74	0.29	1.04	71.8	28.2	
TBP	30	0.73	0.31	1.04	69.8	30.2	
TBP	40	0.77	0.25	1.02	75.3	24.8	
TBP	50	0.83	0.21	1.04	80.0	20.0	3.89
TEP	10	0.71	0.32	1.03	69.2	30.8	
TEP	20	0.61	0.40	1.00	60.7	39.3	
TEP	30	0.76	0.26	1.02	74.0	26.0	
TEP	40	0.68	0.35	1.03	65.7	34.3	
TEP	50	0.63	0.40	1.03	61.2	38.9	5.62
DMP	10	0.63	0.39	1.02	61.4	38.6	
DMP	20	0.65	0.36	1.01	64.3	35.7	
DMP	30	0.70	0.34	1.03	67.6	32.4	
DMP	40	0.63	0.38	1.01	62.0	38.0	
DMP	50	0.63	0.38	1.01	62.8	37.2	2.48

Table 4.9 Comparison of the Freundlich isotherm data for the highest and lowest concentration of plasticiser used.

Plasticiser	[Plasticizer)/pphr	K_{sv}	A	β
TEP	10	0.097	0.07	1.13
TEP	50	0.126	0.08	1.05
TBP	10	0.099	0.03	1.27
TBP	50	0.145	0.16	1.00
DMP	10	0.096	0.12	0.96
DMP	50	0.121	0.14	0.99

4.2.3.2 Time resolved analysis

The unquenched emission decays for PtOEP/plasticised/EC films with increasing concentration of plasticiser are shown in figure 4.9 a-c. Although there are minor differences in the decay curves increasing the concentration of plasticiser does not significantly affect the unquenched time resolved emission. A single exponential fit is inadequate for any of the data,. However, for all cases a double exponential free fit analysis of the type used for unplasticised films gives a good fit to the data, as shown in Fig.4.10 -4.12 Table 3.9 collects the kinetic parameters for each system. The rate constants for the two decay components are typically ca. $0.012 \times 10^6 \text{ s}^{-1}$ and ca. $0.055 \times 10^6 \text{ s}^{-1}$, similar to those found in unplasticised films. As found in the study of concentration effects with PtOEP in EC films a fixed rate double exponential fit with k_1 and $k_2 = 0.0527$ and $0.0101 \times 10^6 \text{ s}^{-1}$ gives a satisfactory fit for all decay curves, and table 3.11 gives the relative contributions of fast and slow components. It can be seen that the major contribution to the decay is the slow species previously assigned to the monomer. The concentration of PtOEP used in the plasticised films ($1.1 \times 10^{-5} \text{ mol dm}^{-3}$) is expected to have a high proportion of monomer in excess of 95% (table 4.4). It is therefore concluded that the relative proportions of monomer and aggregate are significantly affected by plasticiser presence independent of the concentration of plasticiser.

4.2.3.3 Stern Volmer analysis

As seen in previous studies the presence of plasticiser increases the sensitivity of the response. With increasing plasticiser concentration there is a slight increase in the downwards curvature of the Stern Volmer plots, as shown in figure 4.13.

4.2.3.4 Heterogeneity

The result show that an increase in plasticiser concentration causes an increase in sensitivity as found previously for other polymer/lumophore systems. When analysed using the Freundlich isotherm the average value for β for plasticised films is 1.1 ± 0.12 . The value is higher than that seen for unplasticised ethyl cellulose of comparative concentration (0.90 ± 0.03).

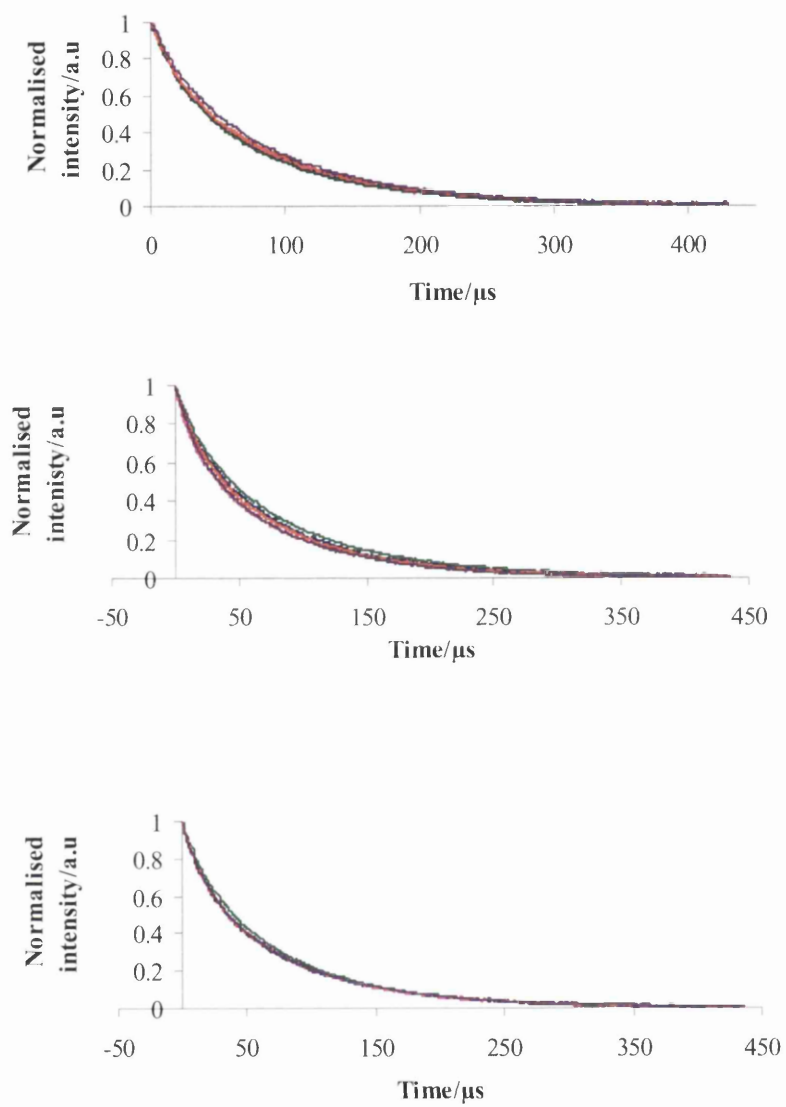


Figure 4.9. Unquenched time resolved emission for 10 – 50 pphr plasticised PtOEP/EC. A- TBP, B is DMP and c is TEP.

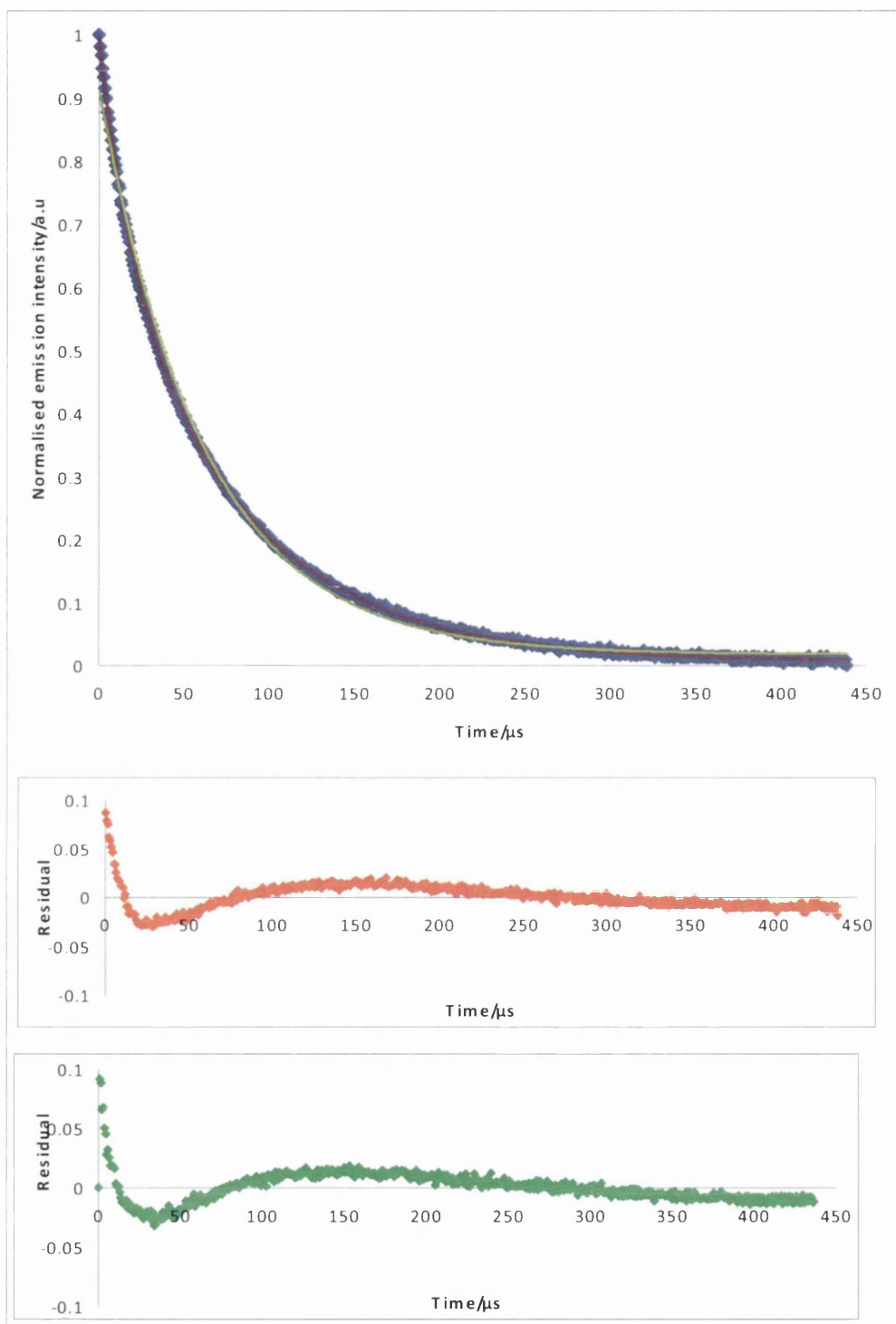


Figure 4.10. Unquenched time resolved emission of PtOEP/EC plasticised with 10pphr (red) and 50pphr (green) TBP and fits to a single exponential.

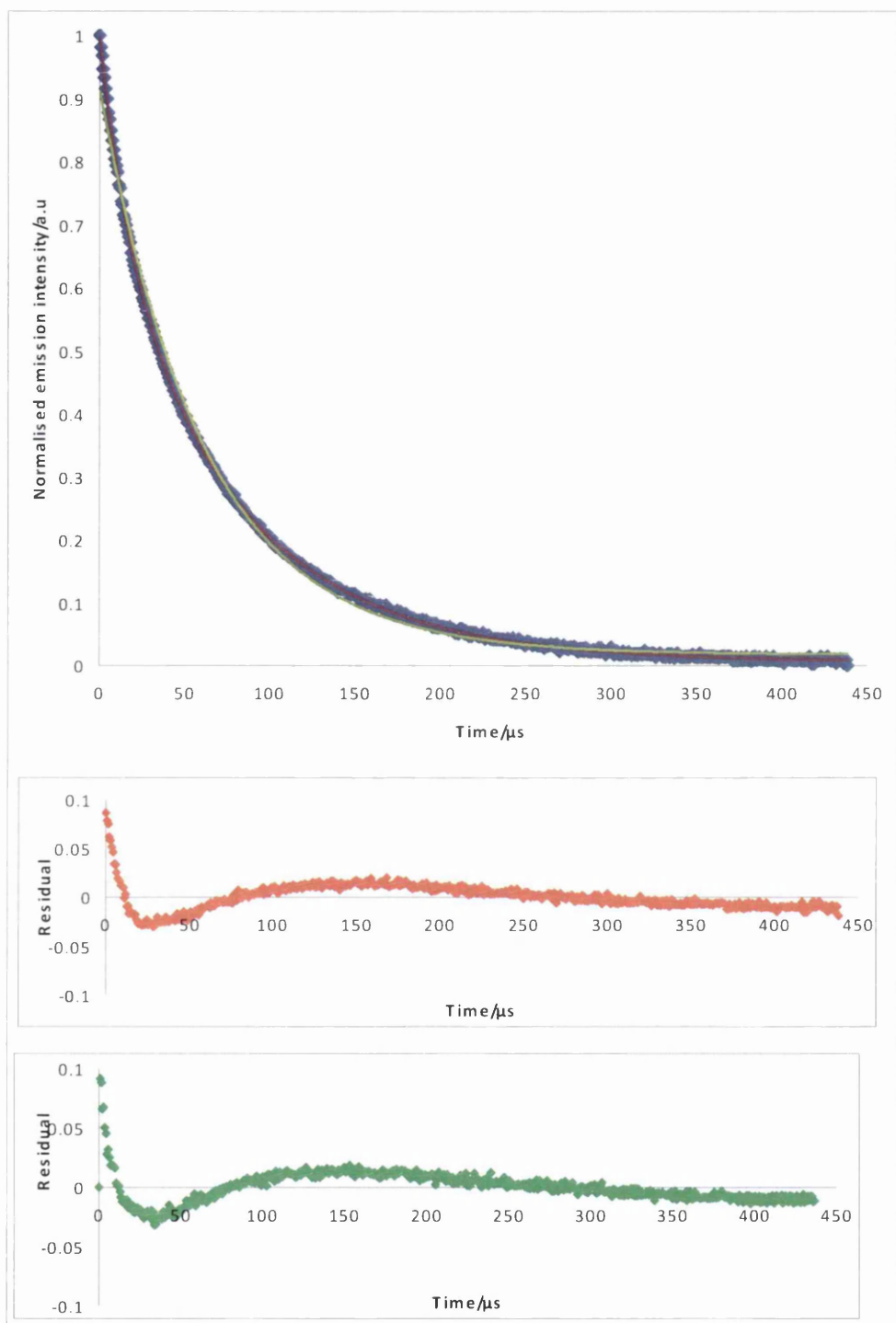


Figure 4.11. Unquenched time resolved emission of PtOEP/EC plasticised with 10pphr (red) and 50pphr (green) TEP and fits to a single exponential (blue).

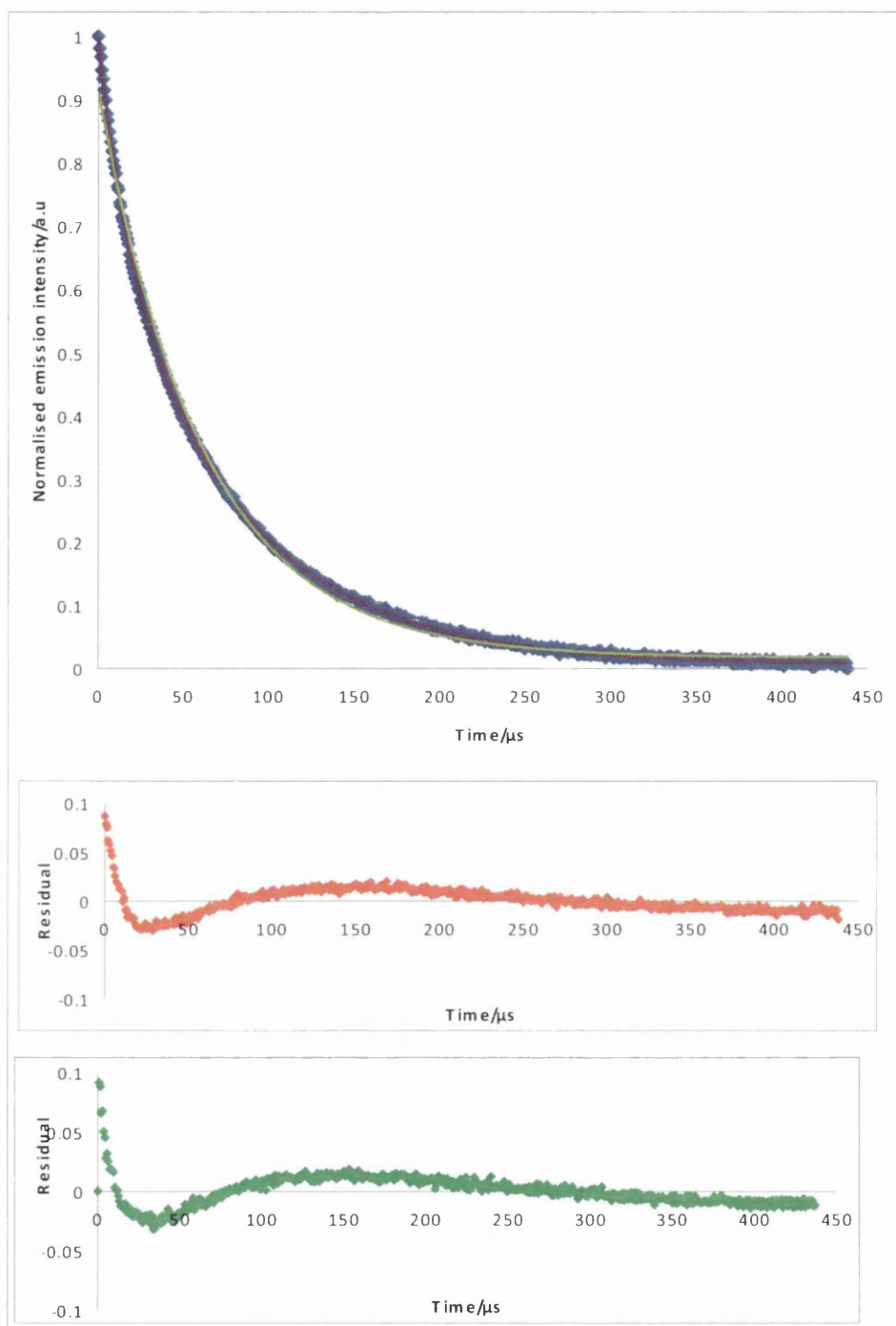


Figure 4.12. Unquenched time resolved emission of PtOEP/EC plasticised with 10pphr (red) and 50pphr (green) DMP and fits to a single exponential (blue).

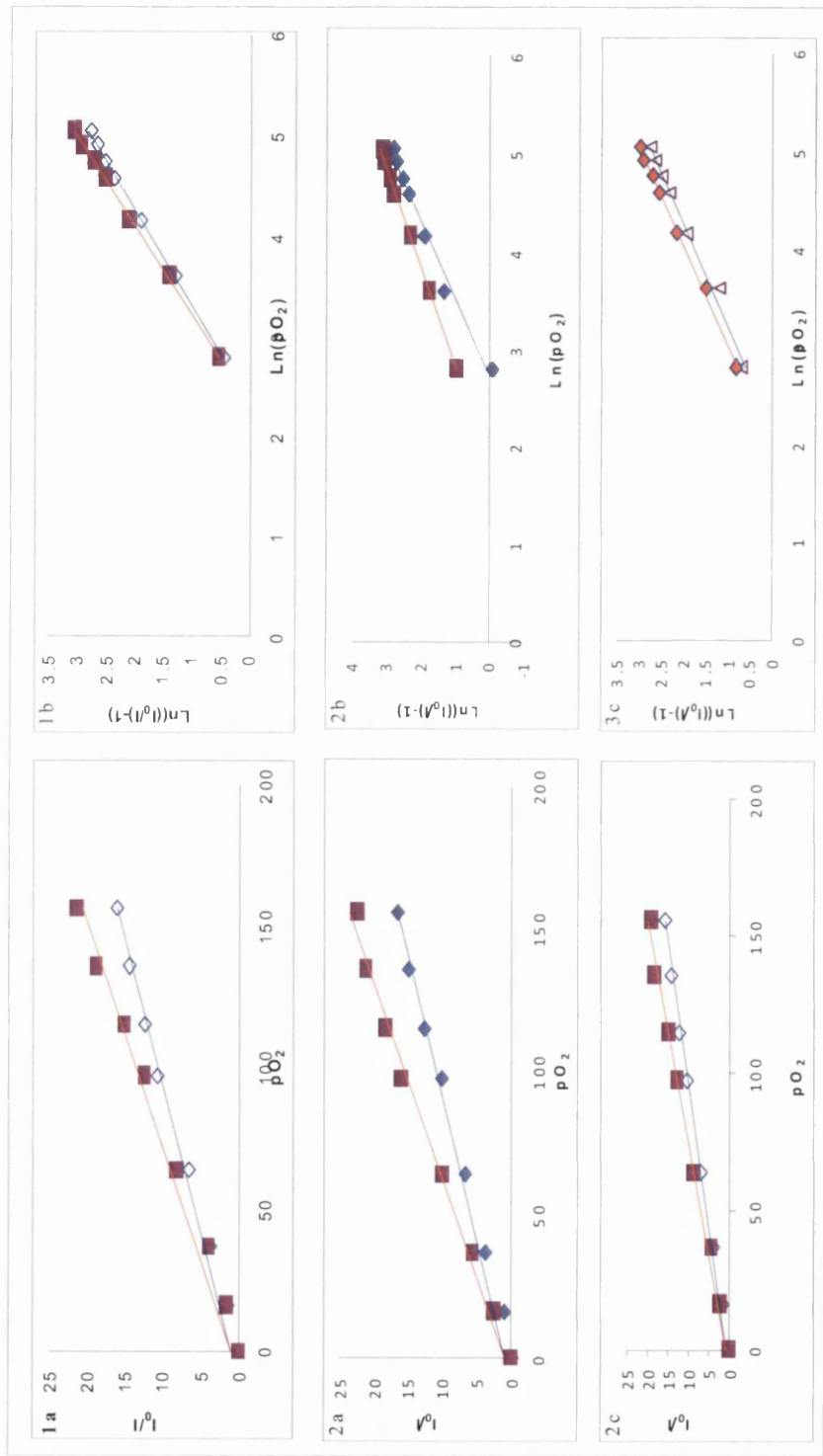


Figure 4.13. Time resolved emission Stern-Volmer, (a), and Freundlich, (b), analysis for plasticised PtOEP/EC . Red is 10pphr and blue is 50pphr A- TBP, B is TEP and c is DMP

4.2.3 Steady-state and kinetic studies of PtOEP in hydrogel films

Hydrogels form a large and highly variable class of polymers [41, 48-50]. Those used in biomedicine are insoluble in water. Polyurethane hydrogels have recently been used in a variety of sensing applications and in commercial instrumentation. A high water uptake and good biocompatibility make these potentially useful materials for thin films sensors for biomedical applications. [48-50]

4.2.3.1 Time resolved emission data

Figure 4.14 shows the time resolved emission of PtOEP/hydrogel film as a function of PtOEP concentration. As, perhaps, expected from previous work with EC films, the unquenched emission show a decrease in lifetime with increasing concentration.

4.2.3.2 Free fitting single exponential analysis

At low concentration ($1.1 \times 10^{-5} \text{ mol dm}^{-3}$) the decay curves are good fits to single exponential of the type $y = A + \alpha e^{-kt}$. Figure 1.15 shows the results of free fitting the decay curve for the lowest PtOEP concentration ($1.1 \times 10^{-5} \text{ mol dm}^{-3}$) in hydrogel to a single exponential decay and the corresponding residuals.

4.2.3.4 Free fit double exponential analysis

At a higher concentration ($[\text{PtOEP}] = 66.2 \times 10^{-5} \text{ mol dm}^{-3}$) a single exponential fit is inadequate but a double exponential free fit of the type $(Y = A + \alpha_1 e^{-k_1 t} + \alpha_2 e^{-k_2 t})$ was applied to the experimental decay data in which all α and k are allowed to vary freely, the decay curves of all concentrations can be fitted well as shown in figure 4.16. (Intermediate concentrations omitted for clarity). Table 4.10 summarises the kinetic analysis from free fitting.

The double exponential analysis of the experimental data suggests that globally the decays can be analysed as two distinct components, one fast and one slow. The slow component has a rate constant of *ca.* $0.010 \times 10^6 \text{ s}^{-1}$, which is comparable to that found at low concentration in the single exponential analysis and the fast component has *k ca.* $0.050 \times 10^6 \text{ s}^{-1}$, comparable to that found for ethyl cellulose films.

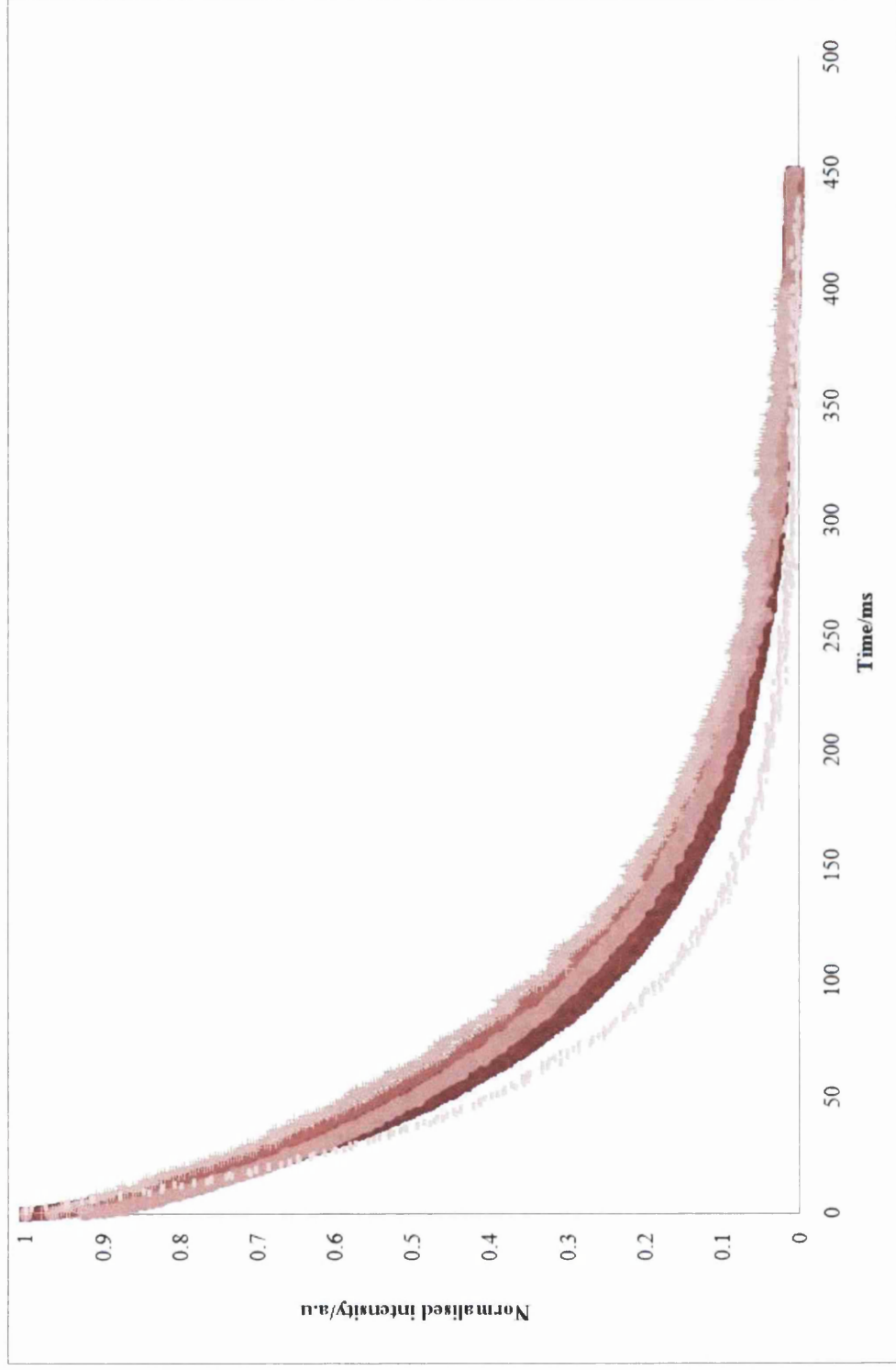


Figure 4.14. Unquenched time resolved emission decay for varying concentrations of PtOEP in PtOEP/hydrogel thin film sensors

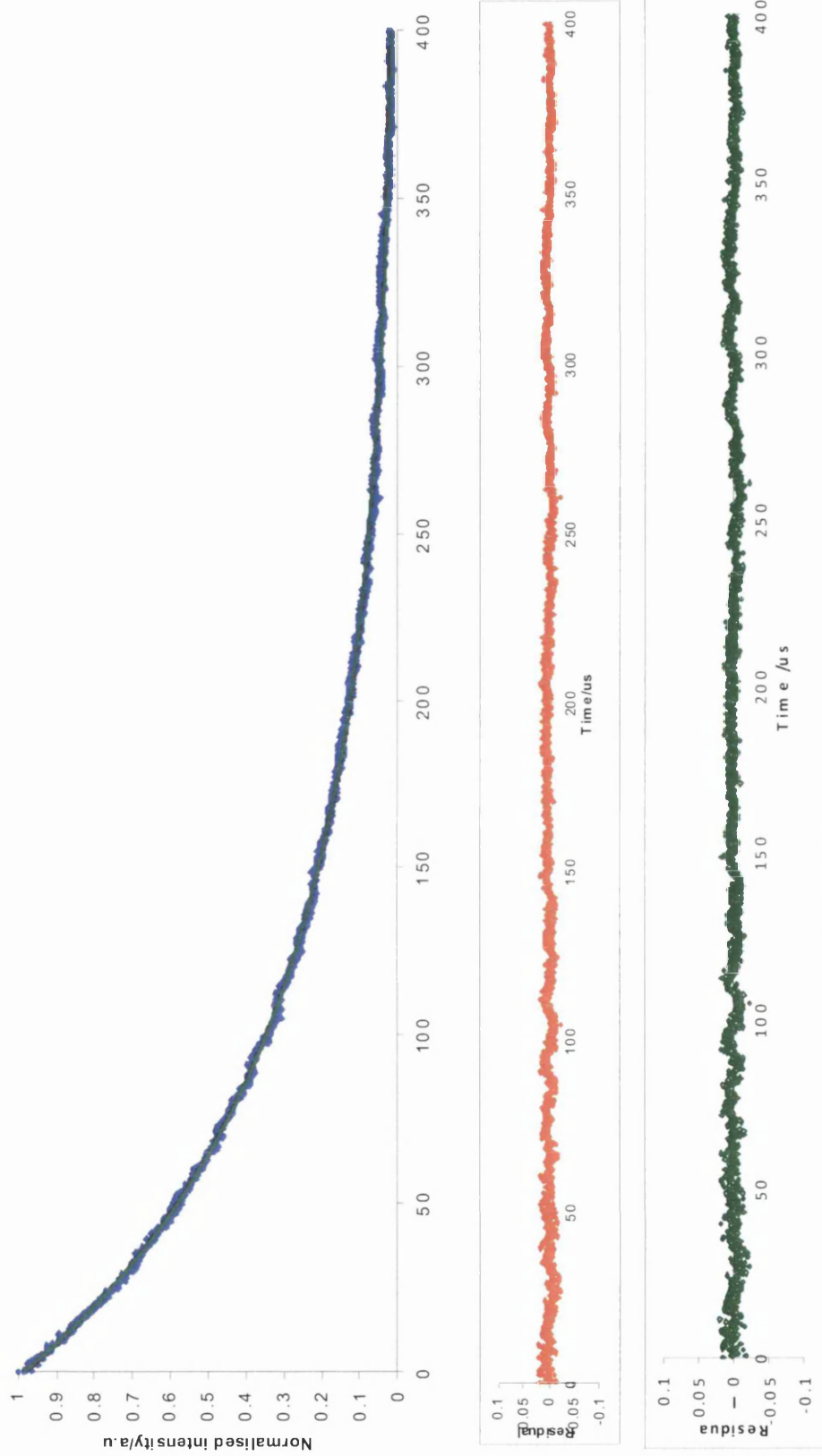


Figure 4.15. Emission decay curves for the lowest concentration of PtOEP in PtOEP/hydrogel films under N_2 . Curve fits to single and double exponential decays. **B** and **C** give residuals for single (red) and double exponential (green) curve fits.

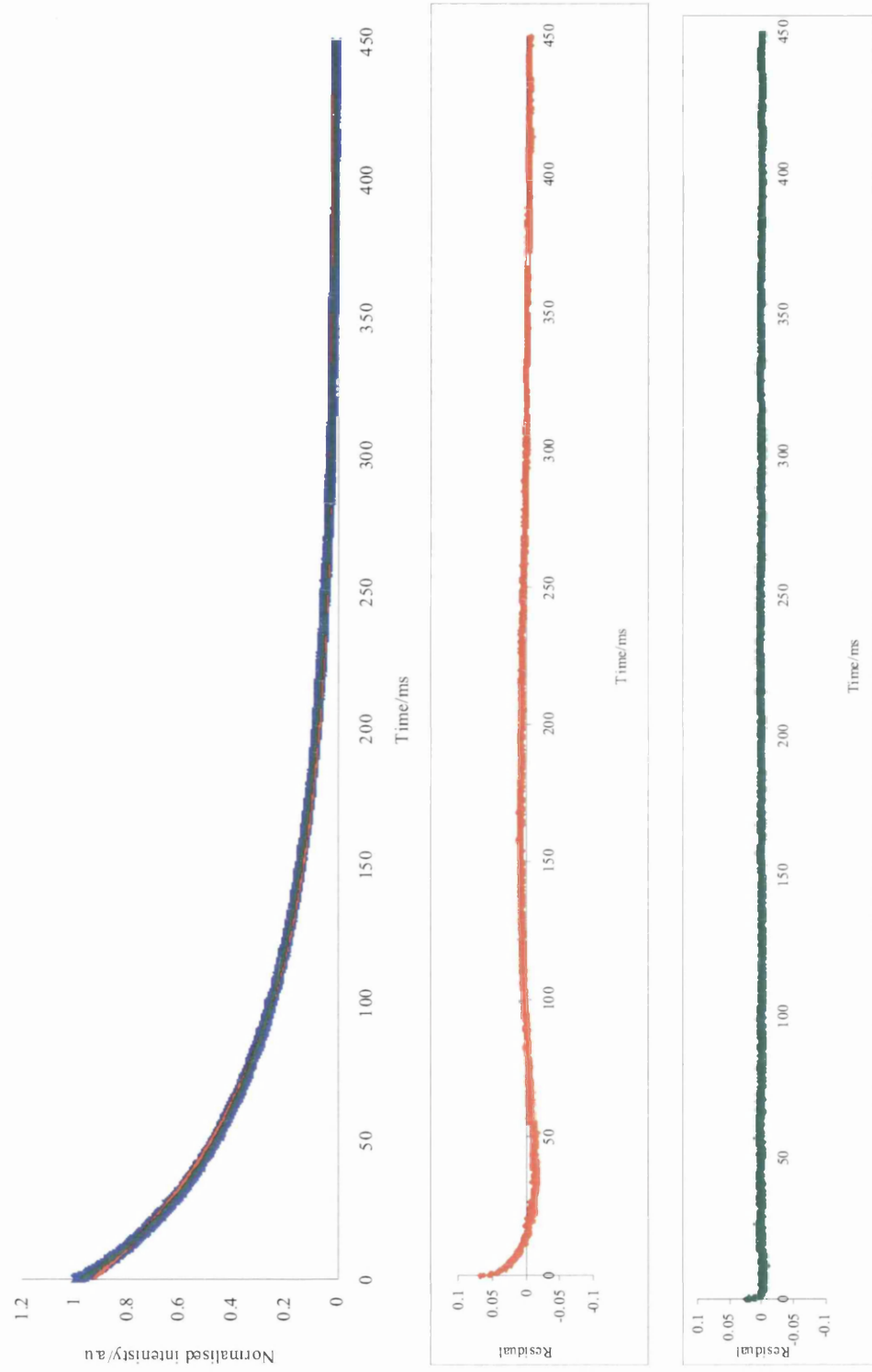


Figure 4.16 Emission decay curves for highest concentration of PtOEP in PtOEP/hydrogel films under N₂. Curve fits to single and double exponential fits. **B** and **C** give residuals for single (red) and double exponential (green) curve fits

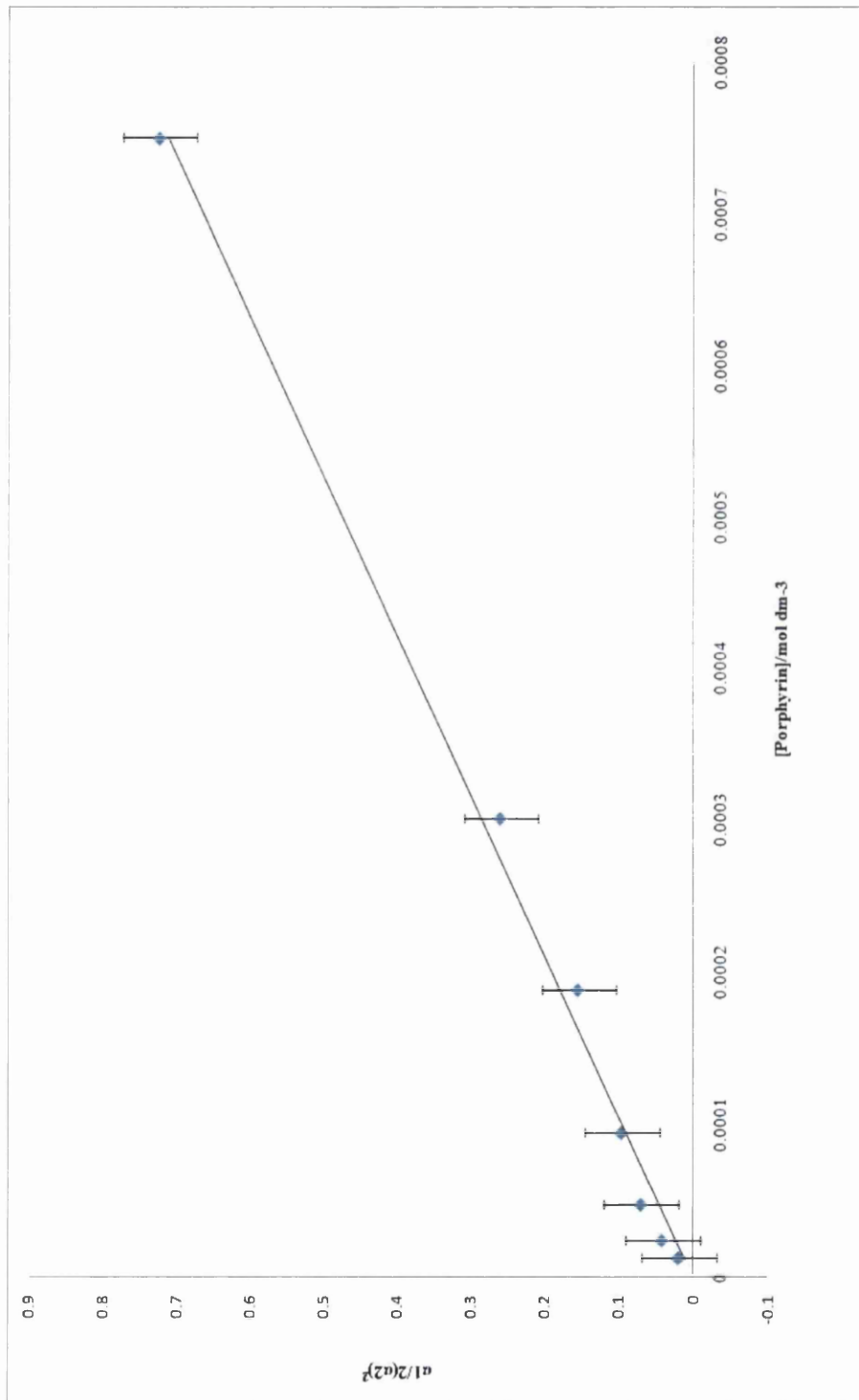


Figure 4.17. A plot of $\alpha_1/2(\alpha_2)^2$ against [PtOEP] where α_1 is the amplitude of the slow species (monomer) and α_2 is the amplitude of the fast species (dimer). Solid line is the line of best fit with gradient = $K_D = 990 \pm 20 \text{ M}^{-1}$

Table 4.10 Amplitudes and rate constants from a free fit double exponential analysis [$Y = A + \alpha_1 e^{-k_1 t} + \alpha_2 e^{-k_2 t}$] of time resolved emission from PtOEP/hydrogel film under nitrogen

	α_1	k_1	α_2	k_2
1.1	0.4097	0.0129	0.5602	0.0089
2.4	0.8019	0.0551	0.9069	0.0026
5.3	0.0802	0.0755	0.9021	0.0150
9.2	0.9087	0.0520	0.8882	0.0108
20.1	0.1203	0.0459	0.8470	0.0112
33.1	0.1674	0.0455	0.8059	0.0118
66.2	0.2315	0.1057	0.6866	0.0142

Table 4.11 Amplitudes of the two components from a fixed rate double exponential analysis [(Y = A + $\alpha_1 e^{-0.0527x}$ + $\alpha_2 e^{-0.0101x}$) where k_1 and k_2 are fixed at 0.0527 and $0.0101 \times 10^6 \text{ S}^{-1}$] for the unquenched time resolved emission of PtOEP/hydrogel films.

[PtOEP]/ $10^{-5} \text{ mol dm}^{-1}$	Percentage contribution	
	$\alpha_1 (k = 0.101 \times 10^6 \text{ s}^{-1})$	$\alpha_2 (k = 0.527 \times 10^6 \text{ s}^{-1})$
1.1	96.44	3.56
2.4	92.90	7.10
5.3	89.03	10.97
9.2	85.92	14.08
20.1	80.20	19.80
33.1	72.63	27.37
66.2	55.44	44.56

4.2.3.5 Fixed rate analysis

Table 3.13 collects kinetic data for a fixed rate analysis similar to that used for EC films with fixed rate constants of 0.010 and $0.0527 \times 10^6 \text{ s}^{-1}$. The relative amplitude of the fast species increases with increased concentration. Following the analysis used earlier for PtOEP in EC films a plot of $\alpha_1/2(\alpha_2)^2$ against [PtOEP] is shown in Figure.4.17. It shows good linearity from which a value of K_D of $990 (\pm 50) \text{ mol}^{-3}\text{dm}^3$ can be obtained.

4.2.3.6 Oxygen quenching - integrated emission intensity

Stern-Volmer analyses of the total integrated emission intensity found from the area under the decay curves in figure as a function of increasing oxygen pressure for [PtOEP= $1.1 \times 10^{-5} \text{ mol dm}^{-3}$] is shown in figure 4.18. The Stern-Volmer plot does not significantly deviate from linearity at low concentration, whereas a more significant deviation is seen as the concentration increases.

4.2.3.7 Calibration and heterogeneity

Figure 4.18 shows the logarithmic plots for analysis using the Freundlich isotherm for PtOEP/hydrogel sensors. Table 3.14 collects α and β values for both the steady state and lifetime data; the two sets of data are well with each other. The Freundlich isotherm provides an easy calibration for both gaseous PtOEP/hydrogel thin film sensors. The data also shows that both α and β show a concentration dependence. The significant decrease in β with increasing concentration suggests that the heterogeneity of the sensing system is increasing, which may be a result of increasing dimer contribution.

4.2.3.8 Dissolved oxygen sensing

At a low concentration of PtOEP the fits to a single exponential when the film is used for sensing dissolved oxygen is adequate, figure 4.19, with increasing concentration

the fit is less adequate and can be described well with a double exponential figure 4.20. A comparison of Stern Volmer plots for steady state and time resolved emission is shown in figures 21 and 22 respectively and both can be described well using the Freundlich isotherm. At a given concentration the value of β does not vary significantly for gaseous or dissolved oxygen which is further confirmation that there is no significant change in heterogeneity when the sensor is used in solution for dissolved oxygen rather than dry for gas phase sensing as summarised in table 4.12

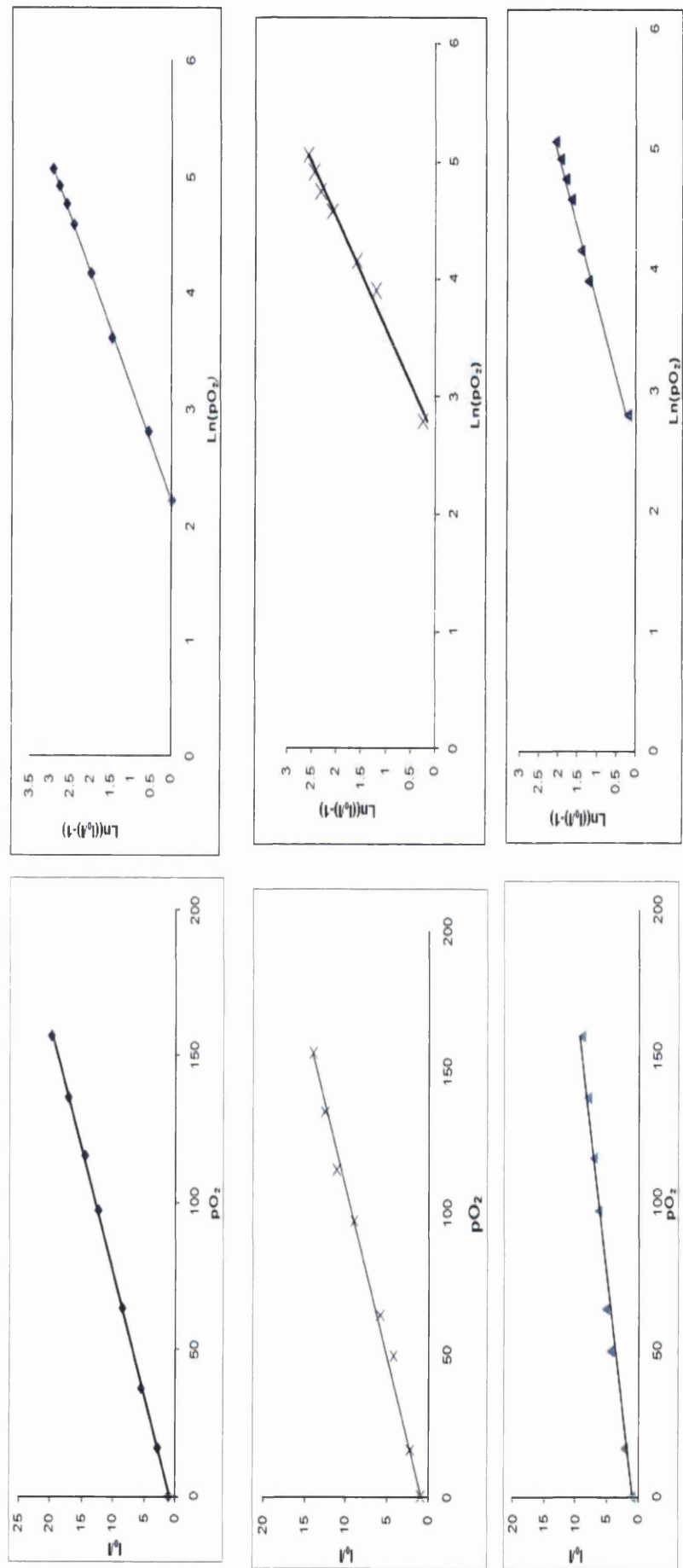


Figure 4.18. Stern-Volmer plots for PtOEP in hydrogel film at concentrations of (a) 1.1, (b) 2.4 and (c) 20.1 x 10⁻⁵ mol dm⁻³ PtOEP. Plots d-f are the corresponding logarithmic plot. Solid lines are lines of best fit for the data

Table 4.10 Amplitudes and rate constants from a free fit double exponential analysis [$Y = A + \alpha_1 e^{-k_1 t} + \alpha_2 e^{-k_2 t}$] of time resolved emission from PtOEP/hydrogel film under nitrogen.

	α_1	k_1	α_2	k_2
[PtOEP] x 10⁻⁵/ mol dm⁻¹				
1.1	0.41	0.0129	0.56	0.0089
2.4	0.80	0.0551	0.91	0.0026
5.3	0.08	0.0755	0.90	0.0150
9.2	0.91	0.0520	0.89	0.0108
20.1	0.12	0.0459	0.85	0.0112
33.1	0.17	0.0455	0.81	0.0118
66.2	0.23	0.1057	0.69	0.0142

Table 4.11 Amplitudes of the two components from a fixed rate double exponential analysis [$Y = A + \alpha_1 e^{-0.0527t} + \alpha_2 e^{-0.0101t}$] i.e. where k_1 and k_2 are fixed at 0.0527 and $0.0101 \times 10^6 \text{ s}^{-1}$] for the unquenched time resolved emission of PtOEP/hydrogel films.

[PtOEP]/ $10^{-5} \text{ mol dm}^{-3}$	Percentage contribution	
	$\alpha_1 (k = 0.101 \times 10^6 \text{ s}^{-1})$	$\alpha_2 (k = 0.527 \times 10^6 \text{ s}^{-1})$
1.1	96.4	3.6
2.4	92.9	7.1
5.3	89.0	11.0
9.2	85.9	14.1
20.1	80.2	19.8
33.1	72.6	27.4
66.2	55.4	44.6

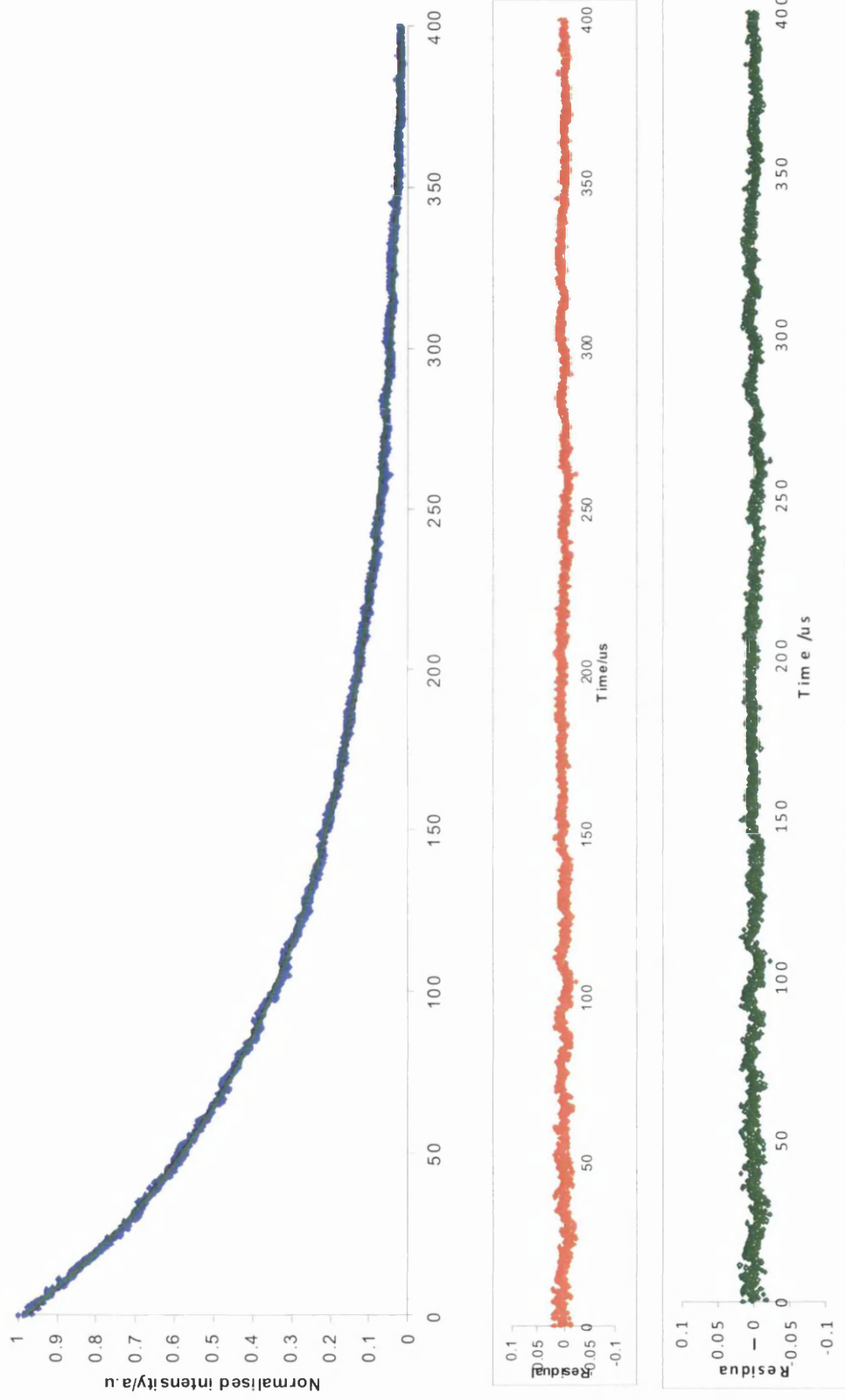


Figure 4.19. Unquenched time resolved emission for PtOEP/Hydrogel thin film sensor $[\text{PtOEP}] = 1.1 \times 10^{-5} \text{ mol dm}^{-3}$ for sensing dissolved oxygen. With fits to a single and double exponential, also shown are residuals for single (red) and double (green) exponential fits.

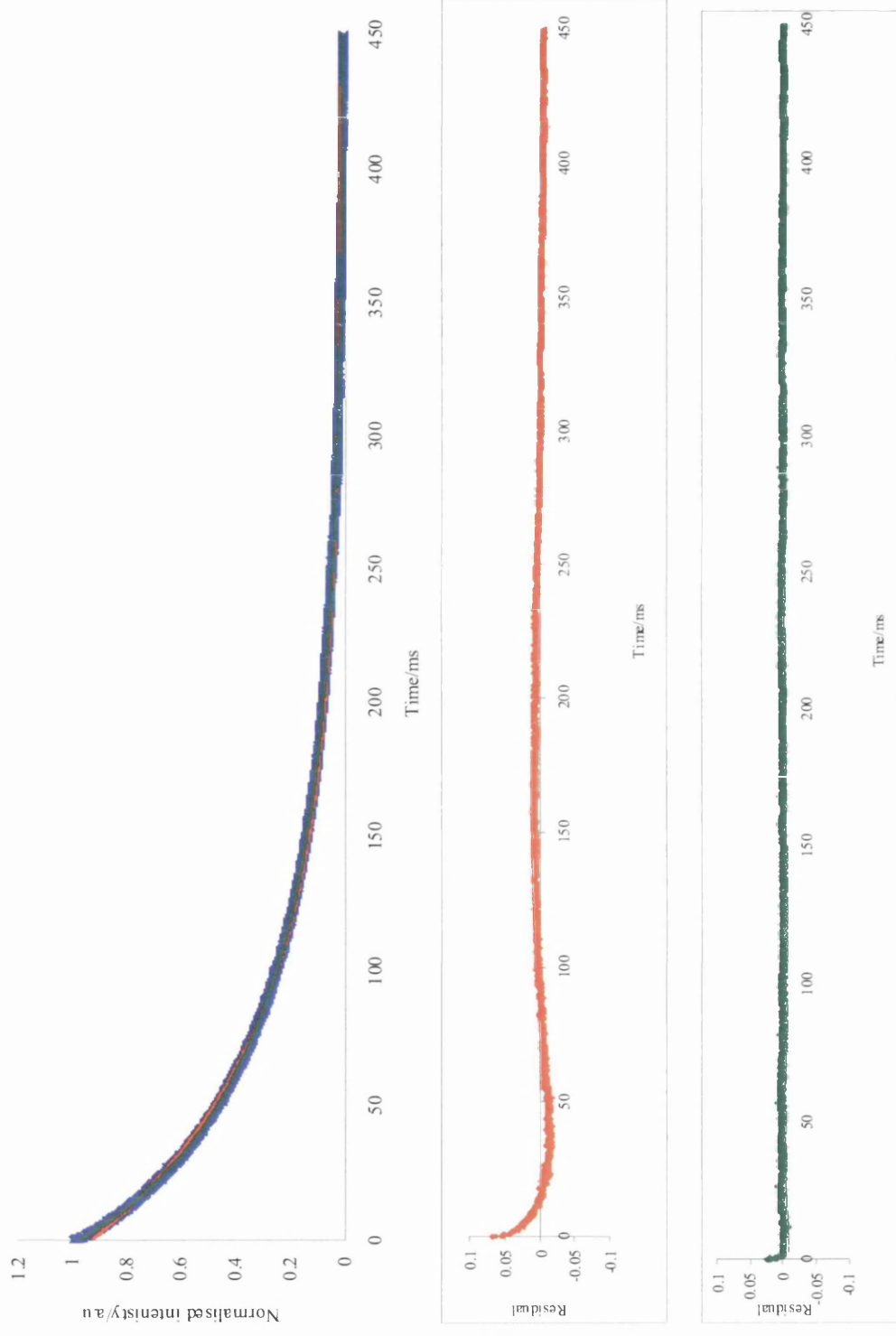


Figure 4.20. Unquenched time resolved emission for PtOEP/Hydrogel thin film sensor $[PtOEP]=6.6 \times 10^{-5} \text{ mol dm}^{-3}$ sensing dissolved oxygen. With fits to a single and double exponential, also shown residuals for single (red) and double (green) exponential fits

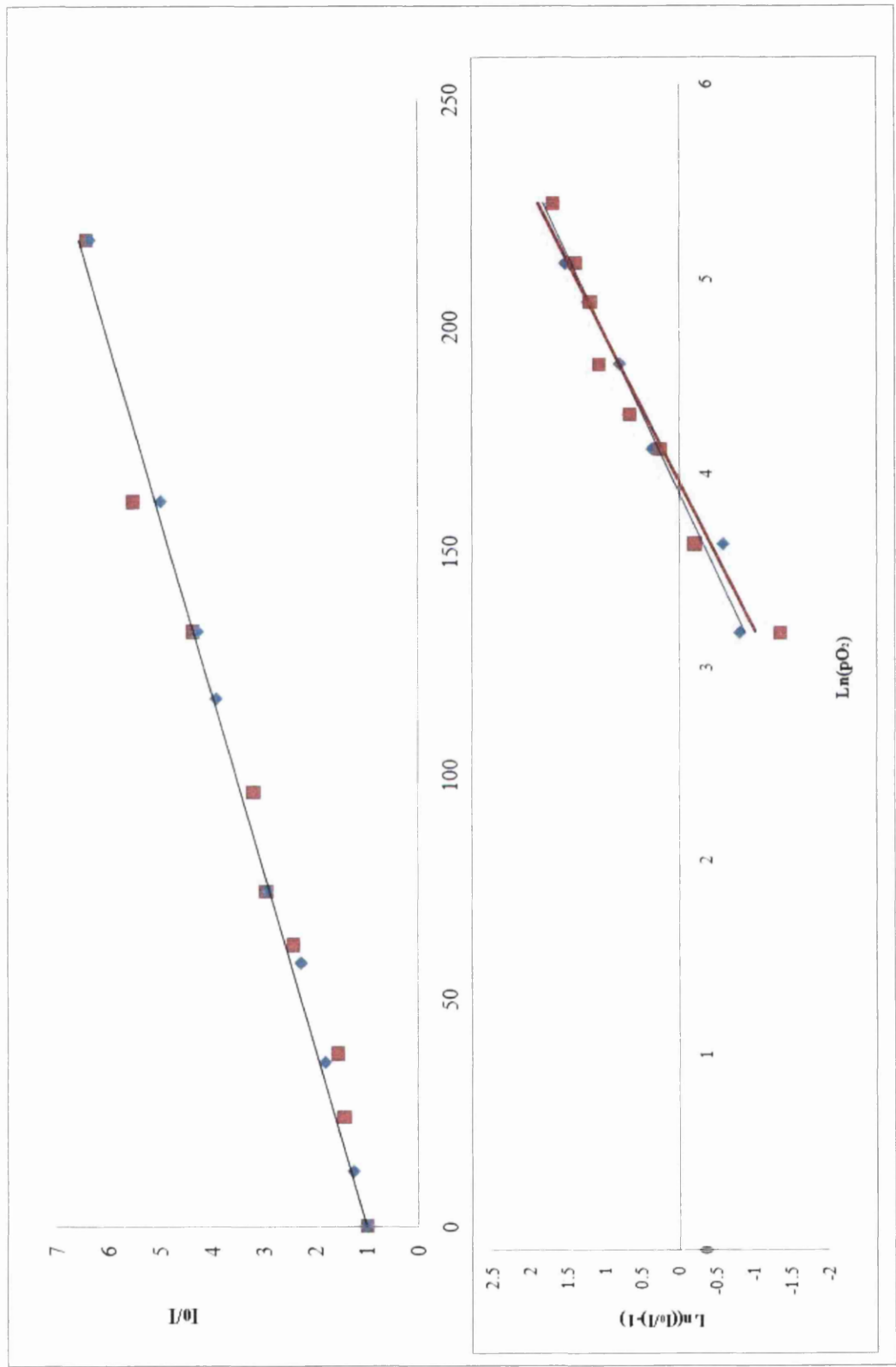


Figure 4.21. Steady state Stern-Volmer and Freundlich isotherm of PtOEP/hydrogel thin film sensor. ($[PtOEP]=1.1 \times 10^{-5} \text{ mol dm}^{-3}$). Blue = gas sensing and red = dissolved oxygen sensor.

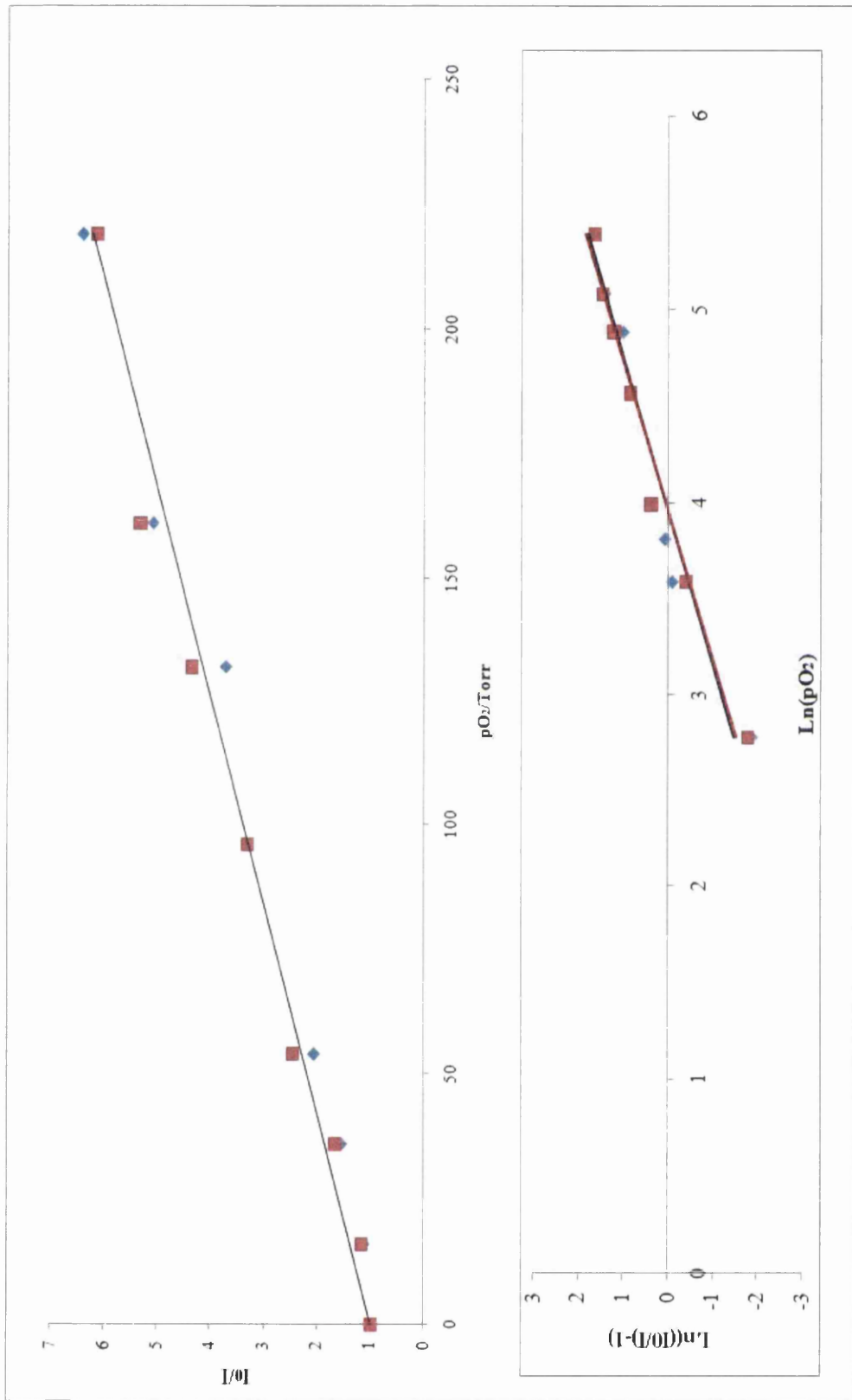


Figure 4.22. Stern Volmer and Freundlich isotherm of PtOEP/hydrogel thin film sensor using integrated area from time resolved emission decay curves. ($[PtOEP] = 1.1 \times 10^{-5} \text{ mol dm}^{-3}$). Blue = gas sensing and red = dissolved oxygen sensor.

Table 4.12. Comparison of steady state and time resolved emission data for PtOEP/hydrogel with [PtOEP] = 1.1×10^{-5} mol dm⁻³ for measurement of gaseous and dissolved oxygen concentration

	Steady state		Lifetime	
	Gas	Dissolved oxygen	Gas	Dissolved oxygen
k_{sv}	0.230	0.250	0.240	0.240
α	0.020	0.040	0.018	0.036
β	0.930	0.918	0.932	0.988

4.3 DISCUSSION AND CONCLUSION

The kinetic heterogeneity observed for PtOEP polymer thin films sensor films under nitrogen has been shown to be due to a monomer:dimer equilibrium for which the kinetic data can be analysed in terms of two exponentials with $k_1 = 0.0527 \times 10^6 \text{ s}^{-1}$ (dimer), $k_2 = 0.0101 \times 10^6 \text{ s}^{-1}$ (monomer). The dimerisation constant (K_D) = 790 (± 20) $\text{mol}^{-1} \text{ dm}^3$ for EC and 990 (± 50) $\text{mol}^{-1} \text{ dm}^3$ for polyurethane hydrogel. With low concentrations of PtOEP yielding linear Stern Volmer plots. Calibration at all concentrations is possible using the Freundlich isotherm.

In contrast, for PdOEP in PdOEP/EC films there is no detectable aggregation with good fits to single exponential curves at all concentrations studied ($1.22\text{-}22 \times 10 \text{ mol dm}^{-3}$).

The formation of Pt-Pt dimers is not surprising and can be explained in terms of metal-metal interactions forming due to the platinum in the porphyrin adopting a square planar geometry as is expected of d^8 platinum complexes. The metal-metal interactions are caused by molecular orbital symmetry interaction between the σ^* anti-bonding orbitals and the empty $P_z\sigma$ and σ^* orbitals. The result is an increase in energy of the empty orbitals and a decrease in energy of the filled orbitals generating a weak metal metal bond

The electronic ground state of Pt the $d9s1$ state is the ground state, the $d10$ configuration being 0.48 eV (11.1 kcal mol⁻¹) higher. In contrast, the ground state for Pd corresponds to a closed-shell $d10$ configuration, the open-shell $d9s1$ configuration lying 0.95 eV (i.e., 21.9 kcal mol⁻¹) above. [63-64] Some examples of $d8/d8$ Pd(II)/Pd(II) interactions, although weak due to a pseudo-closed-shell type, are also known. [64]

Unquenched laser traces for unplasticised films are good fits to single exponentials when $[\text{PtOEP}] = 1.1 \times 10^{-5} \text{ mol dm}^{-3}$. In comparison to an unplasticised film with the same concentration of PtOEP the addition of plasticiser causes an increase in the kinetic heterogeneity for the decay of PtOEP in the absence of oxygen. Using the monomer/dimer model this can be understood if the plasticiser shifts the equilibrium towards the dimer.

The PtOEP/hydrogel sensing system has been evaluated as a dissolved oxygen sensor. The kinetic heterogeneity of the sensor is unaltered when wet. The sensitivity and Stern Volmer quenching constants of the unplasticised hydrogel thin film sensor (Table 3.12) are comparable for the wet and dry sensor. The advantageous properties of the hydrogels such as biocompatibility and low protein absorption make this sensing system ideal for further studies.

References

- 1 I. Bergman , *Nature*, 218, (1968), 396.
- 2 D.B. Papkovsky, Method in optical oxygen sensing: protocols and critical analyses. In: C.K. Sen and G.L. Semenza, Editors, *Methods in Enzymology* vol. 381, Academic Press, San Diego (2004), pp. 715–735.
- 3 D.B. Papkovsky, N. Papkovskaia, A. Smyth, J.P. Kerry and V.I. Ogurtosov, *Food Control*, 17, (2000), 286-292
- 4 G.T. John, I. Klimant, C. Wittmann and E. Heinzle, *Biotechnol. Bioeng.* 81, (2003), 829–836.
- 5 H.W. Kroneis and H.J. Marsoner , *Sens. Actuators*, 4, (1983), 587–592.
- 6 J.P. Kerry and D.B. Papkovsky, *Research Advances in Food Science*, 3, (2002), 121–140.
- 7 M. Fitzgerald, D.B. Papkovsky, M.A. Smiddy, J.P. Kerry, C.K. O’Sullivan, D.B. Buckley and G.G. Guilbault, *Journal of Food Science*, 66, (2001), 105–110.
- 8 R.D. Guarino, L.E. Dike, T.A. Haq, J.A. Rowley, J.B. Pitner and M.R. Timmins, *Biotechnol. Bioeng.*, 86, (2004), 775–787.
- 9 T. C. O’Riordan, D. Buckley, V. Ogurtsov, R. O’Connor and D. B. Papkovsky, *Anal. Biochem.*, 278, 15, (2000), 221-227.
- 10 W. Xu, R. Schmidt, M. Whaley, J.N. Demas, B.A. DeGraff, E.K. Karikari and B.L. Farmer , *Anal. Chem.*, 67, (1995), 3172–3180.
- 11 H.N. McMurray, P. Douglas, C. Busa and M.S. Garley, *J. Photochem. Photobiol. A: Chem.*, 80, (1994), 283–288.
- 12 I. Klimant and O.S. Wolfbeis , *Anal. Chem.*, 67, (1995), 3160–3166.
- 13 P. Hartmann, M.J.P. Leiner and M.E. Lippitsch , *Sens. Actuators B*, 29, (1995), 251–257.
- 14 E.R. Carraway, J.N. Demas, B.A. DeGraff and J.R. Bacon , *Anal. Chem.*, 63, (1991), 337–342.
- 15 E.R. Carraway, J.N. Demas and B.A. DeGraff , *Langmuir*, 7, (1991), 2991–2998.
- 16 A. Mills and A. Lepre , *Anal. Chem.*, 69, (1997), 4653–4659.
- 17 S. Lee and I. Okura, *Spectrochim. Acta A*, 54, (1998), 91–100.
- 18 P.M. Gewehr and D.T. Delpy, *Med. Biol. Eng. Comput.*, 32, (1994), 659–664.

- 19 P.M. Gewehr and D.T. Delpy , *Med. Biol. Eng. Comput.*, 31, (1993), 11–21.
- 20 S. Lee and I. Okura , *Analyst*, 122, (1997), 81–84.
- 21 J. Kavandi, J. Callis, M. Gouterman, G. Khalil, D. Wright, E. Green, D. Burns and B. McLachlan , *Rev. Sci. Instrum.*, 61, (1990), 3340–3347.
- 22 Y. Amao, K. Asai and I. Okura , *J. Porphyrins Phthalocyanines*, 4, (2000), 292–299.
- 23 P. Hartmann and W. Trettnak , *Anal. Chem.*, 68, (1996), 2615–2620.
- 24 G. DiMarco and M. Lanza , *Sens. Actuators B*, 63, (2000), 42–48.
- 25 K. Eaton and P. Douglas , *Sens. Actuators B* ,82 (2002), 94–104.
- 26 P. Douglas and K. Eaton , *Sens. Actuators B*, 82, (2002), 200–208.
- 27 W.W. Lee, K. Wong, X. Li, Y. Leung, C. Chan and K. Chan , *J. Mater. Chem.*, 3, (1993), 1031–1035.
- 28 D.B. Papkovsky , *Sens. Actuators B*, 29, (1995), 213–218.
- 29 D.B. Papkovsky, G.V. Ponomarev, W. Trettnak and P. O’Leary , *Anal. Chem.*, 67, (1995), 4112–4117.
- 30 A. Mills , *Platinum Met. Rev.*, 41, (1997), 115–12.
- 31 B.J. Basu , *Sens. Actuator B*, 123, (2007), 568-577.
- 32 C.Chu, Y.Lo, *Sens. Actuator B*, 124, (2007), 376-382.
- 33 Y. Amao, T. Miyashita and I. Okura , *J. Fluorine Chem.*, 107, (2001), 101–106.
- 34 S.K. Lee and I. Okura , *Spectrochim. Acta A*, 54, (1998), 91-98
- 35 D.B. Papkovsky, G.V. Ponomarev, W. Trettnak and P. O’Leary , *Anal. Chem.*, 67, (1995), 4112–4117.
- 36 V.A.Hughes and P.Douglas , *J.Fluorescence*,16, (2006), 403-409.
- 37 W.R.Vieth, *Diffusion in and through polymers*, (1991), Hanser, New York 1991.
- 38 A.Mills and M. Thomas , *Analyst*, 63 (1997), 122-127.
- 39 A.Mills and F.C. Williams , *Thin Solid Films*, 306, (1997), 163–170.
- 40 A.Mills , *Sens. Actuators B*, 51, (1998), pp. 60–67.
- 41 O.S.Wolfbeis , *J.Mater.Chem.*, 15,(2005) 2657-2669.
- 42 O. Lev, M. Tsionsky, L. Rabinovich, V. Glezer, S. Sampath, I. Pankratov and J. Gun , *Anal. Chem.* 67, (1995), 22A–30A.
- 43 S.K. Lam, M.A. Chan and D. Lo , *Sens. Actuators B*. 73, (2001), 135–141.
- 44 E. Vander Donckt, B. Camerman, R. Herne and R. Vandeloise , *Sens. Actuators, B*. 32 (1996), 121–127.
- 45 Y. Amao, T. Miyashita and I. Okura , *Anal. Chim. Acta* 421, (2000), 167–174.

- 46 X. Li, F. Ruan and K. Wong, *Analyst* 118, (1993), 289–292.
- 47 O. S. Wolfbeis, 'Fibre Optic Chemical Sensors and Biosensors', CRC Press, 2001.
New York.
- 48 M.L.Davies, S.M.Murphy, C.J.Hamilton, B.J.Tighe, *Biomaterials*, 13, (1992), 991-999.
- 49 G.T. John, I. Klimant, C. Wittmann and E. Heinzle, *Biotechnol. Bioeng.*, 81, (2003), 829–836.
- 50 G.S. Vasylevsk, S.M. Borisov, C. Krause and O.S. Wolfbeis, *Chem. Mater.*, 18, (2006), 4609-4616.
- 51 F A. Nwachukwu, M G. Baron, *Sens. Actuators B*, 90, (2003), 276-285.
- 52 J.N. Demas, B.A. DeGraff and W. Xu, *Anal. Chem.* 67 (1995), 1377–1380.
- 53 J.N. Demas and B.A. DeGraff, *Sens. Actuators B*, 11, (1993), 35–41.
- 54 A.Mills , *Sens. Actuators B*, 51, (1998), 67–76.
- 55 A.Mills, *Analyst*, 124, (1999), 1309–1314.
- 56 A.Mills, *Analyst*, 124, (1999), 1301–1307.
- 57 K. Eaton, Response characteristics of thin film optical oxygen sensors, Ph.D. Thesis, University of Wales Swansea, 2002.
- 58 S. Pauly, in: Brandrup, Immergut, Grulke (Eds.), *Polymer Handbook*, fourth ed., Wiley, 1999, pp. VI/543–VI/569.
- 59 K.J. Laidler (Ed.), *Chemical Kinetics*, third ed., Harper Collins Publishers, 1987.
- 59 R.N. Gillanders, M.C. Tedford, P.J. Crilly and R.T. Bailey, *Anal. Chim. Acta*, 502, (2004), 1–6.
- 60 R.T.Bailey, F.R.Cruickshank, G.Deans, R.N.Gillanders and M.C.Tedford, *Anal. Chim. Acta.*, 487, (2003), 101-108.
- 61 S. Xiao, Y.Mo, M.F.Choi, *Meas., Sci., Technol.*, 14, (2003), 826-867.
- 62 R.N.Gillanders, M.C.Tedford, P.J.Crilly, R.T.Bailey, *J.Photochem. Photobiol. A: Chem.*, 163, (2004), 193-199.
- 63 J. Low, W.A. Goddard, *J. Am. Chem., Soc.* 108, (1986), 6115-6128.
- 64 G. Aullo'n, S. Alvarez, *J.Chem. Eur.*, 3, (1997), 655-670.

Chapter 5

***Optical thin film sensors based on
luminescent nanoparticles in a
biologically compatible hydrogel***

5.1 Introduction

Chemical sensor research is an exciting interdisciplinary area of analytical chemistry [1-7]. Sensors play an important role in technology, particularly environmental and biomedical technologies. [1-14] Molecular luminescent sensors have received an increasingly enormous attention due to their high sensitivity, ease of preparation and ability to sense more than one analyte with a given sensor [1-4]. Luminescence optical sensors are typically prepared by incorporating an analyte sensitive lumophore into an analyte permeable support matrix.[1-6] The response characteristics depend on both the lumophore used and matrix characteristics such as solubility and diffusion which in turn can often be related to matrix properties such as density, viscosity and hydrophobicity. [14-16]. The immobilization of luminescent probes within polymer and inorganic particles is of great interest in order to prepare new sensors for: viscosity, solvent polarity, metal ion detection [17], and for pH measurements in biological systems. [18]

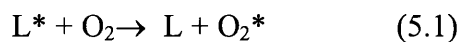
5.2 Oxygen sensing

Oxygen sensors play an important role in technology, particularly environmental and biomedical technologies where the measurement and control of gaseous and dissolved oxygen is often a key parameter. [7-13] Accurate measurements of dissolved oxygen concentrations are required in many biological studies and applications, e.g. in the study of living cells or cell components where oxygen is used as an electron acceptor at the end of the aerobic pathway of glucose oxidation. [13, 19-20] In recent years, thin film optical oxygen sensors have emerged as attractive candidates for both gaseous and dissolved oxygen detection and measurement. [20-25] In these devices, the sensor response is characterised by a change in some optical property, such as luminescence or absorbance, as a function of oxygen concentration. [7-13, 21-34]

Luminescence-based devices provided a non-destructive means of quantitative oxygen measurement and, to some extent, are tuneable with regard to oxygen sensitivity [30-35]. Some dissolved oxygen optical sensors are commercially available, for example Ocean Optics and Fluorometrix have launched optical sensors for dissolved oxygen but they are still very expensive and large, which makes them inconvenient for field use. The need for personal computers for control, and expensive software, further complicates the design and increases cost. [29] Luminescence optical oxygen sensors are typically prepared by incorporating an oxygen sensitive lumophore into an oxygen permeable support matrix. The

response characteristics depend on both the lumophore used and matrix characteristics such as oxygen solubility and diffusion. [29-33]

Luminescence optical sensing involves the quenching of luminescence from an excited-state lumophore, L^* , as a function of changing oxygen concentration



In heterogeneous systems the relationship between the degree of luminescence quenching and oxygen concentration, $[O_2]$, is described by the Stern-Volmer relation.

$$I_0/I = \tau_0/\tau = 1 + \tau_0 k_q [O_2] \quad (5.2)$$

Where k_q is the bimolecular quenching rate constant, τ_0 and I_0 are the lifetime and intensity in the absence of oxygen respectively, and τ and I are the lifetime and intensity at oxygen concentration $[O_2]$, and the Stern-Volmer constant is given by $\tau_0 k_q$. [30-34]

Luminescent oxygen sensing systems have been prepared using both intensity and lifetime based sensing. However the inherent drawbacks of intensity based measurements include fluctuations in light source intensity, photobleaching of the analyte sensitive material, drifts in the optoelectronic setup, and background fluorescence. Sensors based on lifetime measurement do not suffer from excitation source fluctuations, variations in probe concentration, or photobleaching, but require more sophisticated instrumentation and some scientific skill in their use. [35-37] An alternative approach that circumvents the problems associated with intensity-based measurements, and the expensive complex instrumentation needed for lifetime studies, is the use of ratiometric detection. This method is based on the use of an analyte sensitive lumophore and an analyte insensitive lumophore with emission at different wavelengths. Like lifetime measurements, ratiometric techniques are insensitive to the variations of the excitation light and optical path. A very interesting development is the use of lumophore doped nanoparticles containing both the sensing element and the reference element. [40-43, 46,50-54]

Phosphorescent metalloporphyrins have a number of desirable characteristics for use as luminescent oxygen probes for biological applications. [34-39] These include: relatively long wavelengths for excitation (compatible with common LED and laser sources) and emission, long excited state lifetimes, large Stokes' shifts, and high luminescence quantum yields.

Metalloporphyrins have been widely studied as the sensing element in gas phase oxygen sensors but there are few studies of their use as sensors for dissolved oxygen. [26, 51] As described in chapter 1 and 3 the use of far-red/NIR lumophores have significant advantages such as lower sample decomposition and low background fluorescence. In addition phosphorescent dyes with long decay times can overcome problems with background intrinsic fluorescence as the background signal often decays faster than the lumophore. These characteristics make metalloporphyrins ideal lumophores for biomedical oxygen sensing applications.

5.3 Optical pH sensing

Fluorescent pH sensors are used in analytical chemistry, bioanalytical chemistry, cellular biology and medicine. Much attention has been focused on the development of pH sensors due to their widespread applications in industrial and hazardous environments, biomedical diagnoses, process control and scientific research, [49-54] and the development and use of fluorescent sensors to measure pH has been widely studied. [52,55-56]

The continuous monitoring of blood pH is of high medical importance and there has been much research directed toward the development of optical sensors for continuous pH measurement within blood and for tissue pH. [49-53] The measurement of pH is of particular importance for patients who have suffered traumatic brain injury or stroke. Recent findings have shown that brain pH decreased from a normal pH of 7.4 to a pH of 6.75 during the brain insult and that a continuous monitoring system would be beneficial in the treatment of comatose neurosurgical patients. [57-60] It has also been shown that the pH of tumour cells is lower than that of healthy cells, and the use of a simple pH sensitive fluorophore can distinguish between healthy cells and tumour cells. [61]

The development of materials for incorporation into fibre optic based sensors has been at the centre of many investigations. [60] Recently, the fiber optic system) was developed to measure intraparenchymal brain pO_2 , pCO_2 , and pH. (Paratrend 7, Biomedical Sensors, Malvern, PA

The monitoring of pH in the building industry is also of vital importance. One important application is in monitoring and studying corrosion in reinforced concrete. Although it depends on the type of concrete, the pH in concrete is normally around 12.6. However,

through carbonization, which requires a relative humidity of 50% to 85%, pH can be lowered to values around 8. Carbonization does not damage concrete itself, but is highly damaging to steel reinforcement. To protect against damage the steel reinforcement has a protective layer, which only develops at pH values greater 9.5. Understanding, monitoring and detecting the carbonization process in concrete is vitally important in the building industry. By measuring both humidity and pH, most chemical corrosion processes in concrete can be detected and monitored. If these processes are detected at an early state, they can be eliminated before any serious damages may occur. [72]

Many fluorophores show a sensitivity to pH, which is apparent as either a change in emission intensity or changes in the emission or absorption spectrum. The exact response to pH is usually dependent on fluorophore environment. Immobilisation in a polymer matrix, as is commonly required for a sensor device, often has three kinds of effects on the fluorescence response: a shift in fluorophore pK_a , a change in spectral shape, and a change in the shape of the response curve. [4]

Many research groups have shown strong interest in incorporating fluorescein or its derivatives into substrates to prepare optical pH sensors. Hao et al. prepared a fluoresceinamine pH sensor at the surface of polystyrene. [62] Badini et al. impregnated fluorescein isothiocyanate (FITC) into silica sol-gel. [69] Wang et al. prepared a long lifetime sensor based on (FITC). Millar et al. reported a new technique for viewing a sample and measuring surface that employs a coherent imaging fiber [71].) Recently Chen and co-workers prepared an oligomeric pH indicator (fluorescein-formaldehyde) by an expedient one-pot method. [72]

Fluorene derivatives are also known to exhibiting high fluorescence quantum yields with excellent photostability and reversible pH dependence The good behaviour of NR as a water-soluble colorimetric pH indicator is widely known and it has been successfully used in pH sensor applications in the past and it can be immobilized in polymers to give pH sensitive films. [72-73]

5.4 Innovations in optical thin film sensors

5.4.1 Micro and nano particle optical sensors

Chapter 1 details several classes of micro and nanoparticulate materials used in sensor technologies. The incorporation of lumophores into micro and nanoparticles has several

advantages including a reduction in photobleaching and dye leaching, increase in storage stability, and control over shape, size and photochemical and chemical properties. [74-80] Key to the development of intracellular analyte sensors is the encapsulation of the lumophores within nanoparticles, and the miniaturisation of sensors systems to reduce the effects of using intracellular sensors on the cell itself. [74] Much research has centred around the miniaturisation of electrodes and fibre optics. [1] Common methods for single cell analysis include pulled optical fibres and electrodes, and chemically etched tips or tubes.

With diameters ranging from 20-500 nm PEBBLES are a submicron sized class of nanosensors. They are based on the use of a polymer matrix to encapsulate an analyte sensitive lumophore and are designed to be minimally invasive and capable of monitoring single cells in real time. PEBBLES are an excellent way of encapsulating lumophores. Several advantages of PEBBLES over naked dyes include: no interaction between the dye and cell, introduction of more than one sensing analyte, and the introduction of reference lumophores for ratiometric sensing. [74-79] PEBBLES offer similar advantages for use in thin film sensors, including: a wide variety of dyes as the limitation of polymer solvent solubility is reduced, a large PEBBLE surface area, reduction in leaching from the sensor film which allows the use of a variety of dyes that may be toxic to cells. Furthermore the ability to combine several PEBBLES in one film offer the possibility of a “lab on a chip sensor” for several parameters. [79-81] With biomedical applications in mind, a combination of oxygen and pH sensing would be ideal.

Figure 5.1 a gives a diagrammatic representation of a PEBBLE. The three main classes of PEBBLE that are commonly used have previously been discussed in chapter 1. The most interesting class of PEBBLE for use in optical oxygen thin film sensors are PEBBLES synthesized from traditional sol gel materials, e.g. oxygen permeable organically modified sol gel silica (ormosil) PEBBLES. [81-83] The synthesis of these PEBBLES utilizes the materials and techniques developed in sol gel technology. Careful choice of the starting material can produce a spherical nanosphere comprising a two layer system as shown in figure 5.1b.

It has recently been shown that adsorption of lumophores to mesoporous silica particles, or even simple thin-layer chromatography (TLC) plates, has been shown to yield oxygen sensors with a very rapid response. [85-86] Amai et al. have recently shown that lumophores sensitive to oxygen can be attached to silica and alumina in the form of TLC plates. For this they utilized the interaction between COOH on carboxyphenyl porphyrin and the silica material.[88]

The use of lumophores in thin film sensors also allows a combinatorial approach to sensor design. Nanoparticles can be prepared which are sensitive or insensitive to a particular analyte, and then several of these nanoparticles can be included within one film, reducing interaction between lumophores and reducing inner-filter effects caused by lumophores in different layers.

5.5 Aims of this chapter

We describe the preparation and characterization of a series of nanoparticles and self assembled silica sensing species for use in optical thin films sensors for oxygen and/or pH. The sensing materials are immobilised in either ormosil or a polyurethane hydrogel. The latter matrix is particularly useful for biomedical applications. The materials described here are all compatible with current fibre optic and LED systems.

5.5.1 Oxygen sensing material

Optical oxygen sensing system for both gaseous and dissolved oxygen in which luminescent nanoparticles are incorporated into a biologically compatible polyurethane hydrogel are described.

Little is known on the effect of nanoparticle immobilization on the heterogeneity of PtOEP, therefore a study has been conducted to investigate changes in PtOEP kinetic heterogeneity in single and multilophore doped ormosil PEBBLEs using time resolve emission methods.

Having examined the stability and gaining a better understanding of the PtOEP ormosil PEBBLEs, optical thin film sensors based on ratiometric sensing of gaseous and dissolved oxygen, have been developed. PtOEP is used as the oxygen sensitive lumophore with rhodamine 6G as the insensitive ratiometric reference. The results are discussed in terms of sensitivity and Stern-Volmer analysis.

A colorimetric oxygen sensor for gaseous and dissolved oxygen sensing is also described. Colorimetric sensing simplifies the sensing system for use without the need for any complicated instrumentation. . An initial study into the potential use of PEBBLEs for colorimetric sensors has been undertaken using PtOEP and coumarin 153 doped ormosil PEBBLEs. The lumophores can both be excited at 382 nm, reducing the need for complex excitation systems and making the sensor compatible with cheap LED excitation sources [90].

5.5.2 pH sensing material

Cheap reliable alternative to immobilisation technologies may help to advance the field of multiple analyte sensing. A number of pH sensors based on the pH sensitivity of 5,6-carboxyfluorescein fluorescence have been developed. A comparison has been made between

sensors prepared using polyacrylamide nanospheres and those made using a simpler method based on an alumina self assembled material.

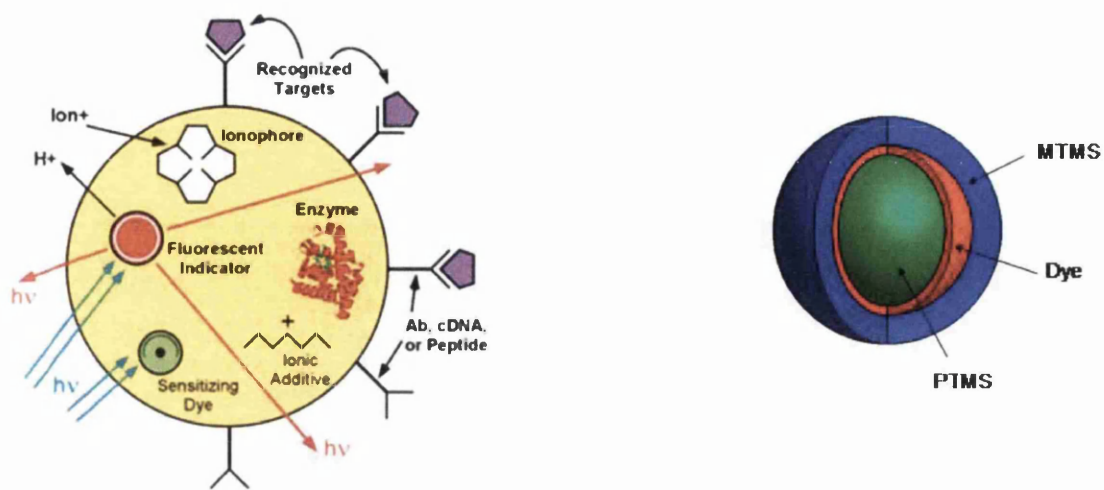
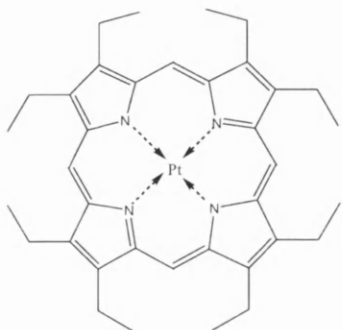
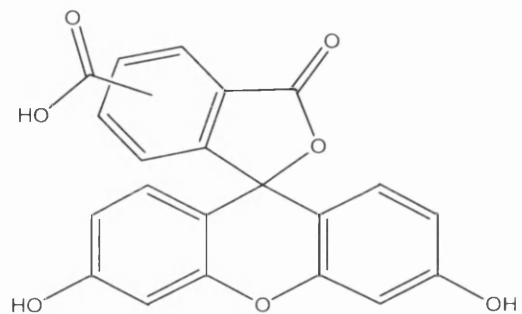


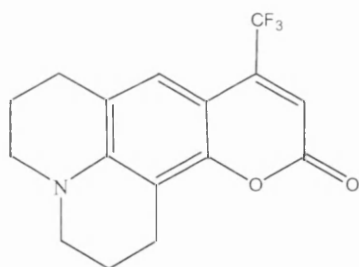
Figure 5.1 a) schematic of PEBBLE based sensors; b) schematic of the ormosil PEBBLE used in this study. [84]



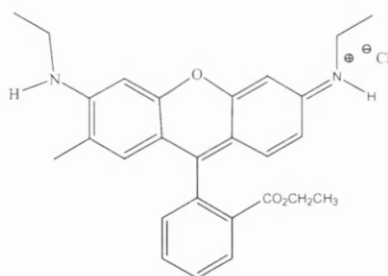
5.2a



5.2b



5.2c



5.2d

Figure 5.2 lumophores used in this study a:PtOEP, b:5,6,carboxyfluorescein, c:coumarin 153 and d: rhodamine 6g

5.6 Results and discussion

5.6.1 Time resolved studies-PtOEP ormosil PEBBLES

Chapter 2 details the types of sensors described in this work. We have previously shown that the emission decay of PtOEP in type 1 thin organic film sensors under nitrogen can be well described using a double exponential fit, where the two emission lifetimes are due to either monomeric or dimeric PtOEP [45]. All unquenched emission decay curves for type 1 thin films sensors prepared using either an ethyl cellulose or polymer matrix can be fitted using a double exponential with fixed rate constants as shown in equation 5.3 .

$$Y = A + \alpha_1 e^{-0.0527x} + \alpha_2 e^{-0.0101x} \quad (5.3)$$

There is considerable interest in the use of micro and nanoparticles for use as individual sensing elements for both intracellular sensing and, more general, thin film sensors. Understanding the effect of encapsulation on the lumophores kinetic heterogeneity is important in the design of sensors using these materials.

5.6.2 Effect of concentration

5.6.2.1 Single lumophore sensor-type 2 sensors

Several examples of PtOEP PEBBLES are known in the literature and studies predominately involve steady state spectroscopy. Time resolved spectroscopy has been shown to give a good indication of the kinetic heterogeneity of PtOEP thin film sensors.

Figure 5.3 shows the unquenched time resolved emission of PtOEP ormosil PEBBLES prepared from increasing concentrations of PtOEP [$1 - 100 \times 10^{-5} \text{ mol dm}^{-3}$] immobilized in hydrogel thin film type 2 sensors (all prepared at the same PEBBLE:Polymer ratio and spin coating speed). There is a decrease in lifetime with increasing concentration as seen for type 1 sensors described in chapter 4. At all concentrations kinetic fits were poor for a single exponential as shown for the highest ($25 \times 10^{-5} \text{ mol dm}^{-3}$) and lowest ($1 \times 10^{-5} \text{ mol dm}^{-3}$) concentration doped PEBBLES (figure 5.4), whereas good fits to a double exponential decay were seen for all concentrations, (figure 5.5). There is no significant difference in the amplitudes and rates whether the film is wet or dry, (figure 5.6). Table 5.1 summarizes the rates and amplitudes for a free double exponential fit for the unquenched emission of PtOEP in PtOEP ormosil PEBBLES of increasing concentration in hydrogel polymers in wet and dry

films. The results of fitting the unquenched decays to a double exponential in which the rate constants are fixed, as is appropriate for the monomer-dimer equilibrium model, are summarized in table 5.2. Analysis of the data in Table 5.2 in terms of a monomer-dimer is shown in figure. 5.7, from which K_D for in ormosil PEBBLES is calculated to be 1000 ± 70) $\text{mol}^{-1} \text{dm}^{-3}$

5.6.2.2 Effect of PEBBLE size

For ormosil PEBBLES the size of the PEBBLES is related to the hydrolysis time and concentration of PTMS during the initial synthetic step. As detailed in table 5.2. 100, 300 and 500nm PEBBLES were prepared, When the PEBBLES are immobilised in hydrogel polymer, the unquenched emission shows a decrease in lifetime with decreasing PEBBLE size as shown in figure 5.8. The residuals from a double exponential are shown in figure 5.9 and indicate that the goodness of fit increases with increasing PEBBLE hydrolysis time shown in the literature to be an increase in PEBBLE diameter. The rates and amplitudes from a free double exponential are summarized in table 5.3.

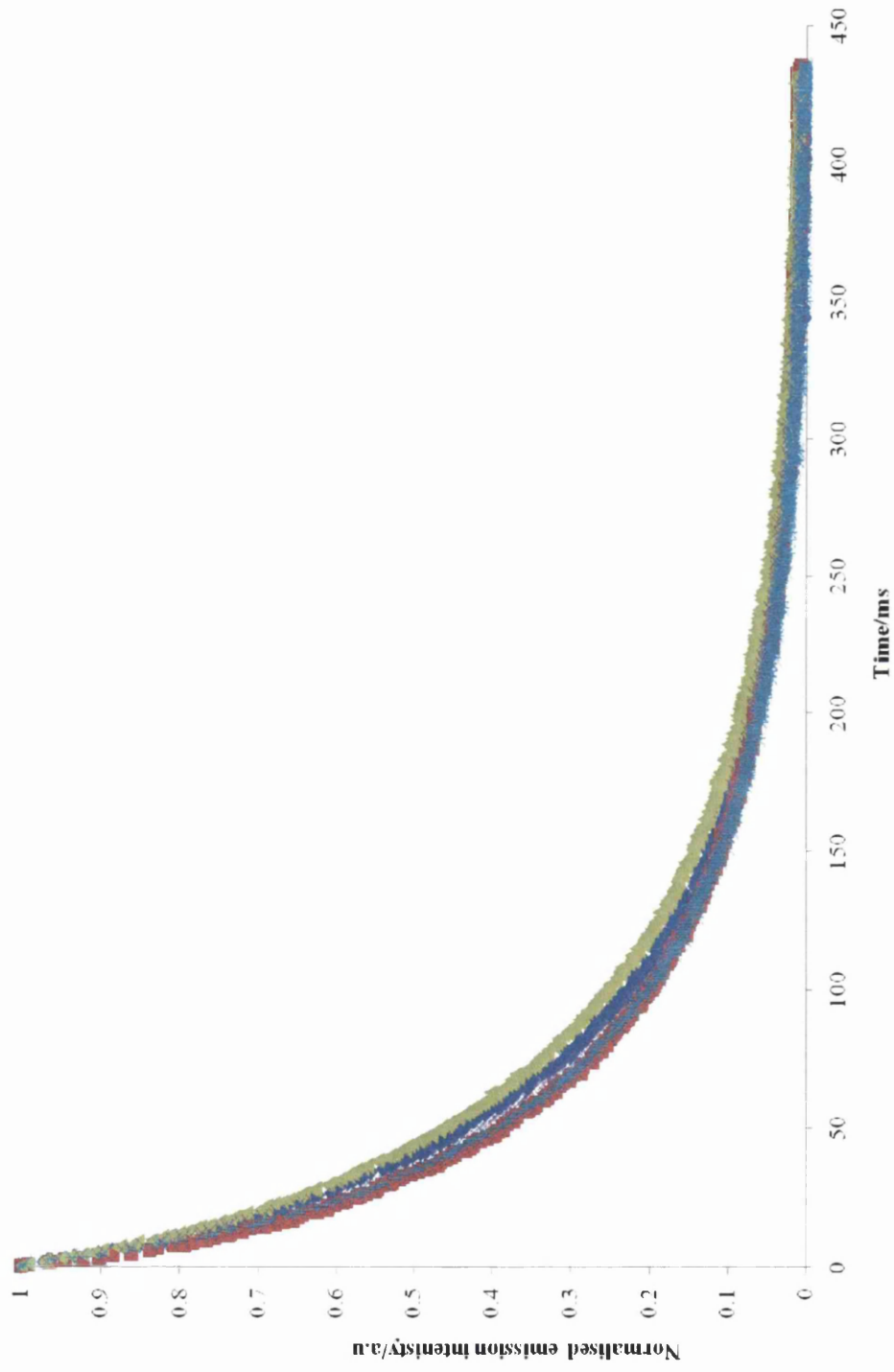


Figure 5.3 Unquenched time resolved emission decay for varying concentrations of PtOEP doped ormosil PEBBLEs immobilised in hydrogel polymer thin film sensors. $[\text{PtOEP}] = 1.5 - 24 \times 10^{-5} \text{ mol dm}^{-3}$ where: $\blacktriangle = 1.53$; $\bullet = 3$; $\times = 6$; $\blacksquare = 12$; $\blacksquare = 24 \times 10^{-5} \text{ mol dm}^{-3}$.

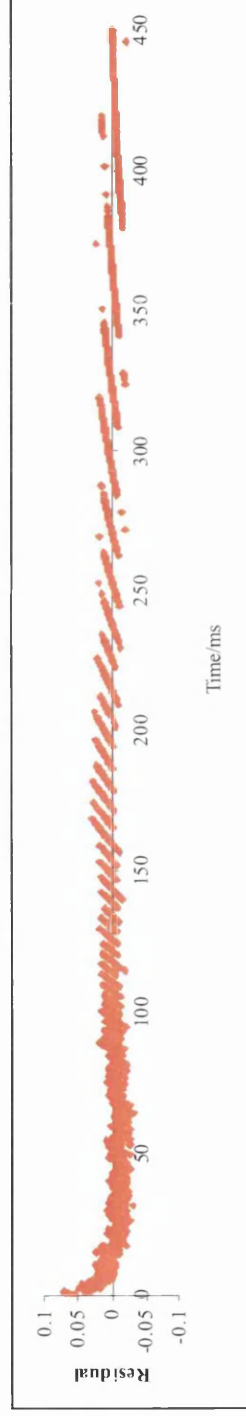
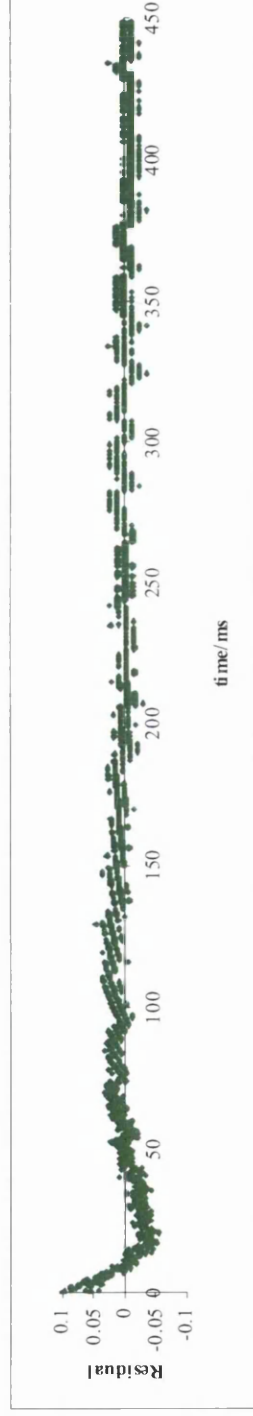
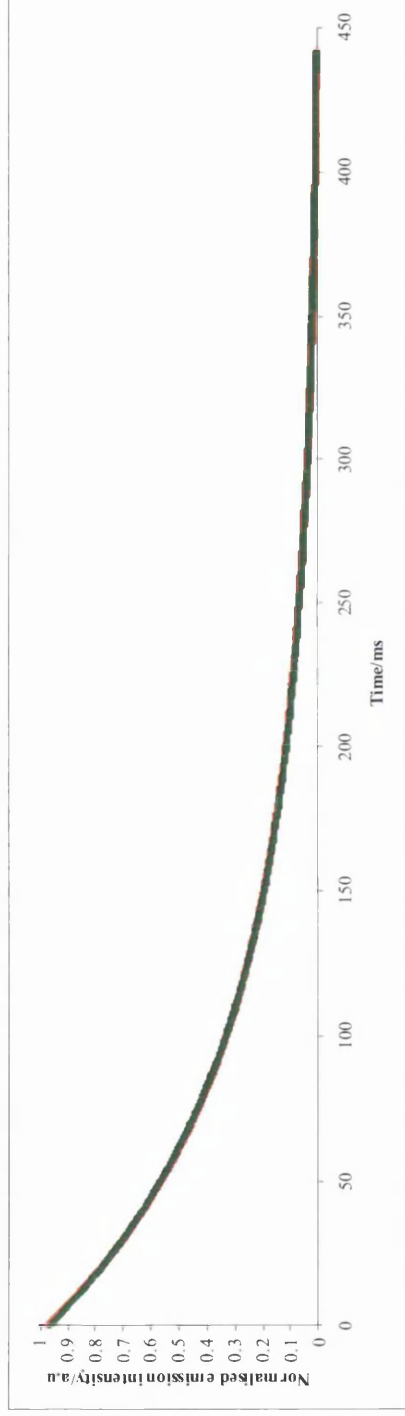


Figure 5.4. Unquenched time resolved emission for PtOEP PEBBLES/Hydrogel thin film sensor $[PtOEP]=1.5 \times 10^{-5}$ and 24×10^{-5} mol dm⁻³ with fits to a single exponential.

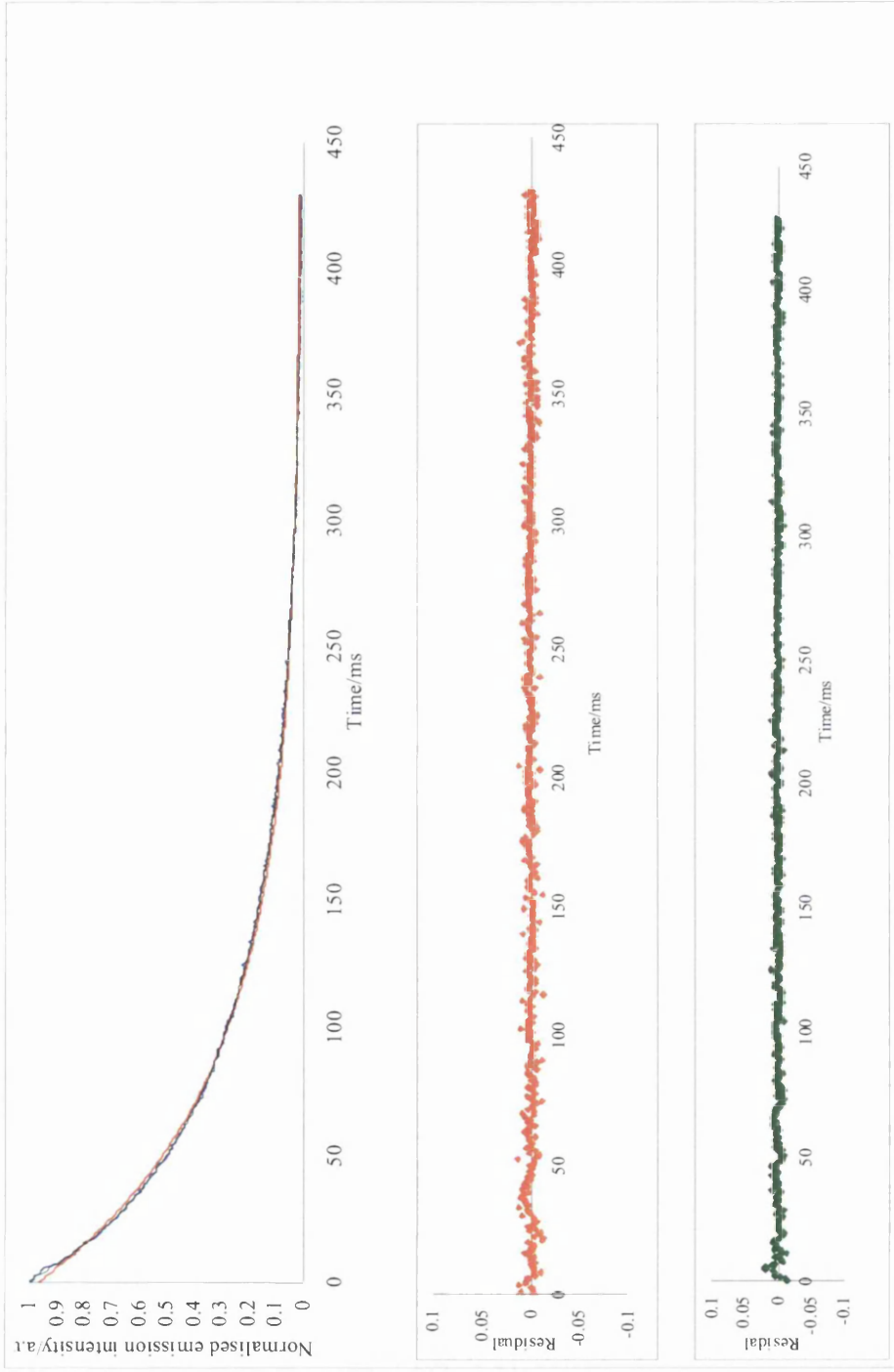


Figure 5.5 Unquenched time resolved emission for PtOEP PEBBLEs/Hydrogel thin film sensor [PtOEP] = 1.5×10^{-5} and 24×10^{-5} mol dm⁻³ with fits to a double exponential.

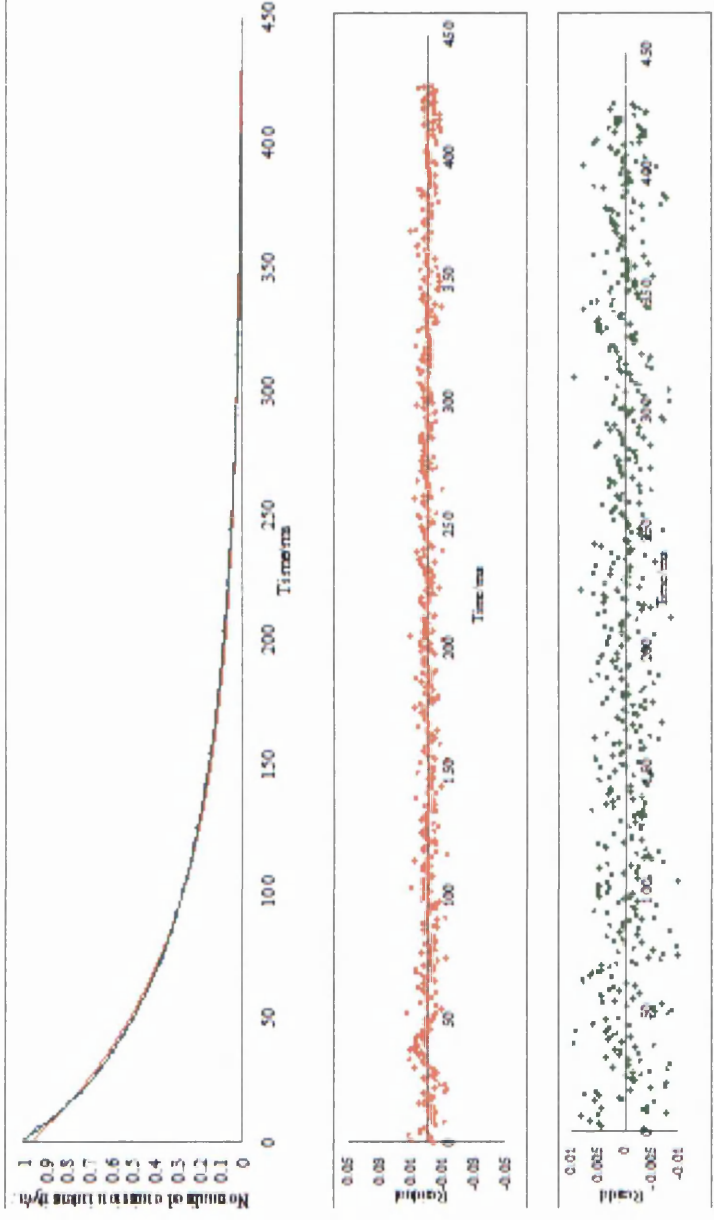


Figure 5.6 A comparison of the unquenched emission from PtOEP PEBBLES/hydrogel sensor when wet and dry and corresponding fits to a double exponential for $[PtOEP]=1.5 \times 10^{-5} \text{ mol dm}^{-3}$

Table 4.12. Comparison of steady state and time resolved emission data for PtOEP/hydrogel with [PtOEP] = 1.1×10^{-5} mol dm⁻³ for measurement of gaseous and dissolved oxygen concentration

[porphyrin]/ 10 ⁻⁵ mol dm ⁻³	α_1 fast	α_2 slow	k_1 fast	k_2 slow
Dry films				
1.5	0.08	0.920	0.014	0.009
3	0.099	0.901	0.012	0.009
6	0.112	0.888	0.026	0.011
12	0.147	0.853	0.030	0.011
24	0.197	0.803	0.059	0.012
Wet films				
1.24	0.078	0.922	0.015	0.010
3.10	0.091	0.909	0.013	0.010
6.20	0.111	0.889	0.027	0.013
12.4	0.145	0.855	0.031	0.012
24.8	0.201	0.799	0.058	0.014

Table 5.2 Contributions from fast and slow components for fixed double exponential fits of the type $Y = A + \alpha_1 e^{-0.0527t} + \alpha_2 e^{-0.0101t}$ for PtOEP in ormosil PEBBLEs immobilized in a hydrogel polymer.

[porphyrin]/ $10^{-5} \text{ mol dm}^{-3}$	Percentage contribution		Percentage contribution	
	Dry film	wet film	Dry film	wet film
	α_1 (fast)	α_2 (slow)	k_1 (fast)	k_2 (Slow)
1.24	8	92	7.8	92.2
3.10	9.9	90.1	9.1	90.9
6.20	11.2	88.8	11.1	88.9
12.4	14.7	85.3	14.5	85.5
24.8	19.7	80.3	20.1	79.9

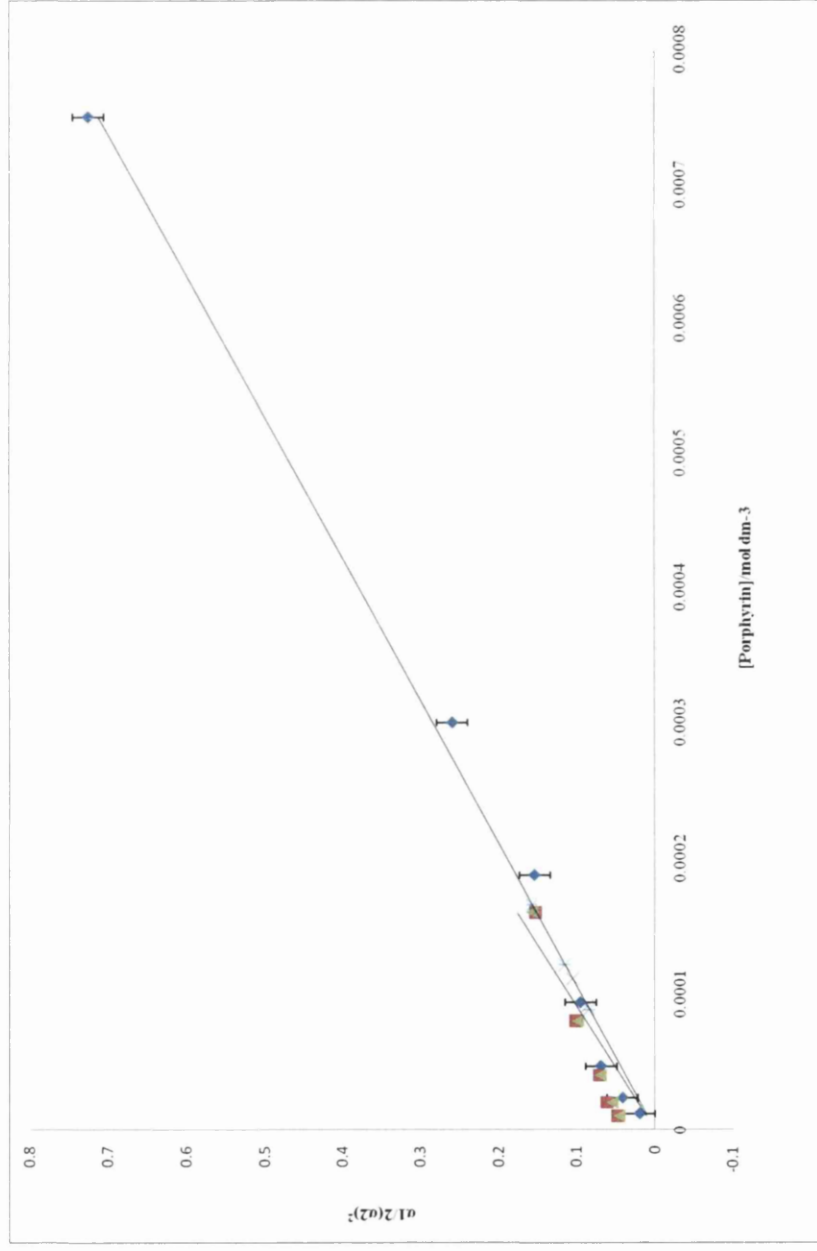


Figure 5.7 A plot of $\alpha_1/2(\alpha_2)^2$ against $[\text{PtOEP}]/\text{hydrogel}$ type 1 sensors where α_1 is the amplitude of the slow species representing a monomer and α_2 is the amplitude of the fast species representing a dimer. \diamond = TYPE 1 sensors; \blacktriangle = type 2 dry PEBBLE; \blacksquare = type 2 in wet PEBBLE; Δ = PEBBLEs size - wet \bullet = PEBBLE size - dry. Solid line is the line of best fit with gradient = $K_D = 990$. Errors calculated from linear regression analysis.

Table 5.3 Summary of published experimental conditions to synthesis PEBBLES, [PTMS] and hydrolysis time used to control Ormosil particle size. *Indicates experimental conditions used to prepare the ormosil PEBBLES used in this study.

Average diameter/nm	[PTMS]/M	Hydrolysis time/min
800	0.06	0.5
570	0.06*	2
300	0.06*	4
280	0.03	20
150	0.02	20
100	0.01*	20

The time resolved emission decays of PtOEP ormosil PEBBLES of increasing diameter immobilized in hydrogel are shown in figure 5.8 All unquenched time resolved emission were all good fits to a double exponential. Analysis using a fixed rate analysis shows an increase in contribution of the dimer with decreasing PEBBLE diameter, (suggested reason is a decrease in concentration). When added to a plot of the porphyrin concentration and $\alpha_1/2(\alpha_2)^2$ where α_1 is the amplitude of the slow species representing a monomer and α_2 is the amplitude of the fast species representing a dimer. Figure 5.9. All of the single lumophore type 2 sensors discussed in this chapter can be described using the monomer dimer relationships. The contribution of dimer increases with increasing PtOEP concentration and with decreasing PEBBLE size.

5.6.1.3 Dual lumophore sensor

5.6.1.3.1 Type 2 sensors

Lee et al. have recently prepared ratiometric PEBBLES for intracellular oxygen sensing, using Rh6g as the reference dye. Figure 5.10 shows the unquenched time-resolved emission for PtOEP/Rh6G PEBBLES incorporated in a hydrogel polymer as a wet and a dry film. Both decays show good free fits to the same double exponential decay with $\alpha_1=0.08 (\pm 0.002)$ and $\alpha_2 0.92 (\pm 0.002)$ and $k_1= 0.010 (\pm 0.0008) \times 10^6 \text{ s}^{-1}$ and $k_2= 0.050 (\pm 0.001) \times 10^6 \text{ s}^{-1}$. This suggests that the presence of a second dye in the PEBBLE does not affect the kinetic heterogeneity.

5.6.1.3.2 Type 3 and type 4 sensor

Figure 5.11 shows the time resolved emission decays for type 3 and 4 sensors, prepared by spin coating PtOEP ormosil PEBBLES on a precast C153 hydrogel layer and spin coating PtOEP and C153 PEBBLES in a single layer respectively. Both show good fits to a double exponential with similar rates of the fast and slow species for gaseous and dissolved oxygen. When the sensor was examined as a dissolved oxygen sensor, both the type 3 and 4 sensors showed good fits to double exponential analysis.

There appeared to be leaching of the C153 layer of the type 3 sensors into the top ormosil layer, and although this did not affect the kinetic heterogeneity of the ormosil sensing material, it was decided that, because of this, type 4 sensors were most suited for further investigation.

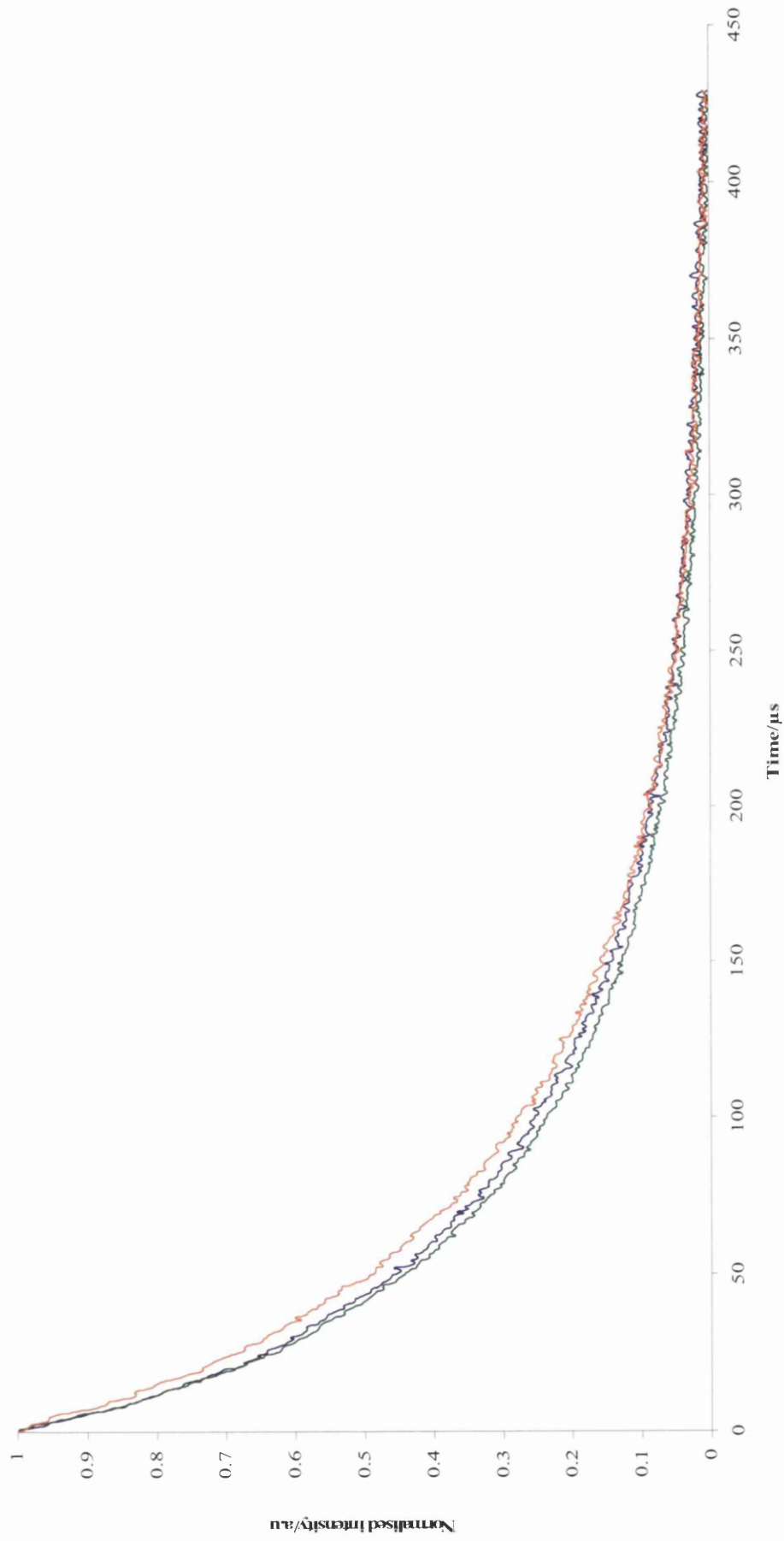


Figure 5.8 Unquenched time resolved emission decay for PtOEP doped ormosil PEBBLEs of varying sizes immobilised in hydrogel polymer thin film sensors with fits to a double exponential, red = 100nm, green= 300nm and blue = 500nm.

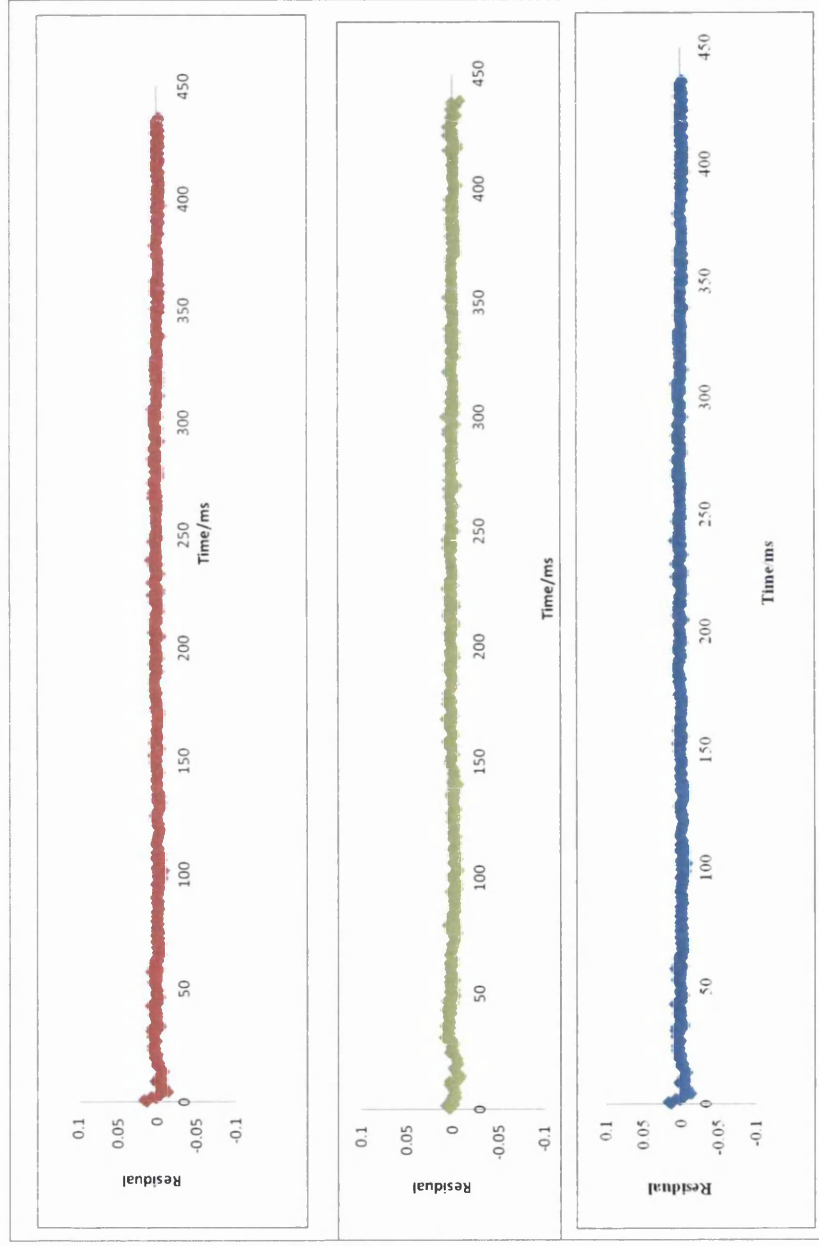


Figure 5.9 Comparison of residuals for fits to a double exponential for PEBBLEs of varying sizes immobilised in hydrogel polymer thin film sensors red= 100nm, green = 300nm and blue = 500nm.

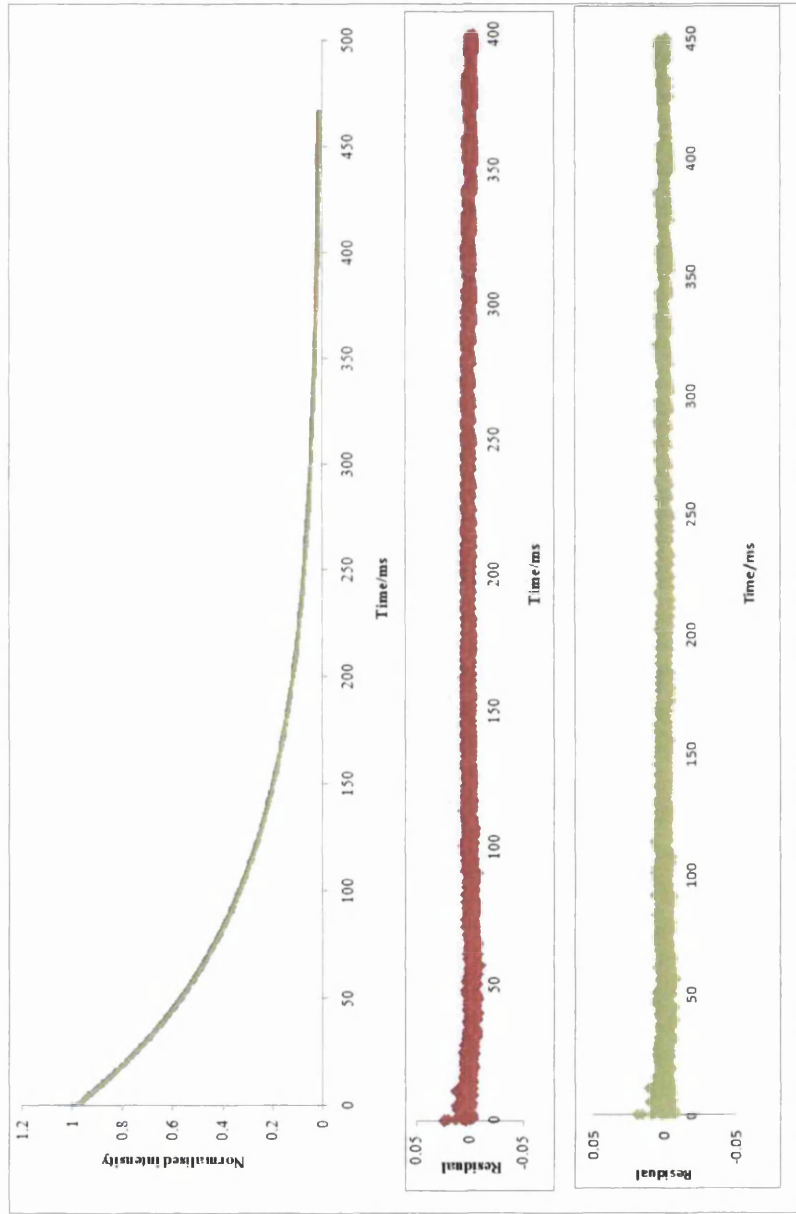


Figure 5.10 Time resolved emission for PtOEP in PtOEP/Rh6G PEBBLES immobilised in hydrogel polymer under nitrogen. \blacktriangle = dry $\hat{\phi}$ = wet. Solid line is the double exponential fit ($Y = a + \alpha_1 e^{-k_1 t} + \alpha_2 e^{-k_2 t}$) where a is a small zero offset correction, $k_1 = 0.010 (\pm 0.0008) \times 10^6 \text{ s}^{-1}$ and $k_2 = 0.050 (\pm 0.001) \times 10^6 \text{ s}^{-1}$ for both the wet and dry film. b: residuals for double exponential fit dry; c: residuals for double exponential fit wet.

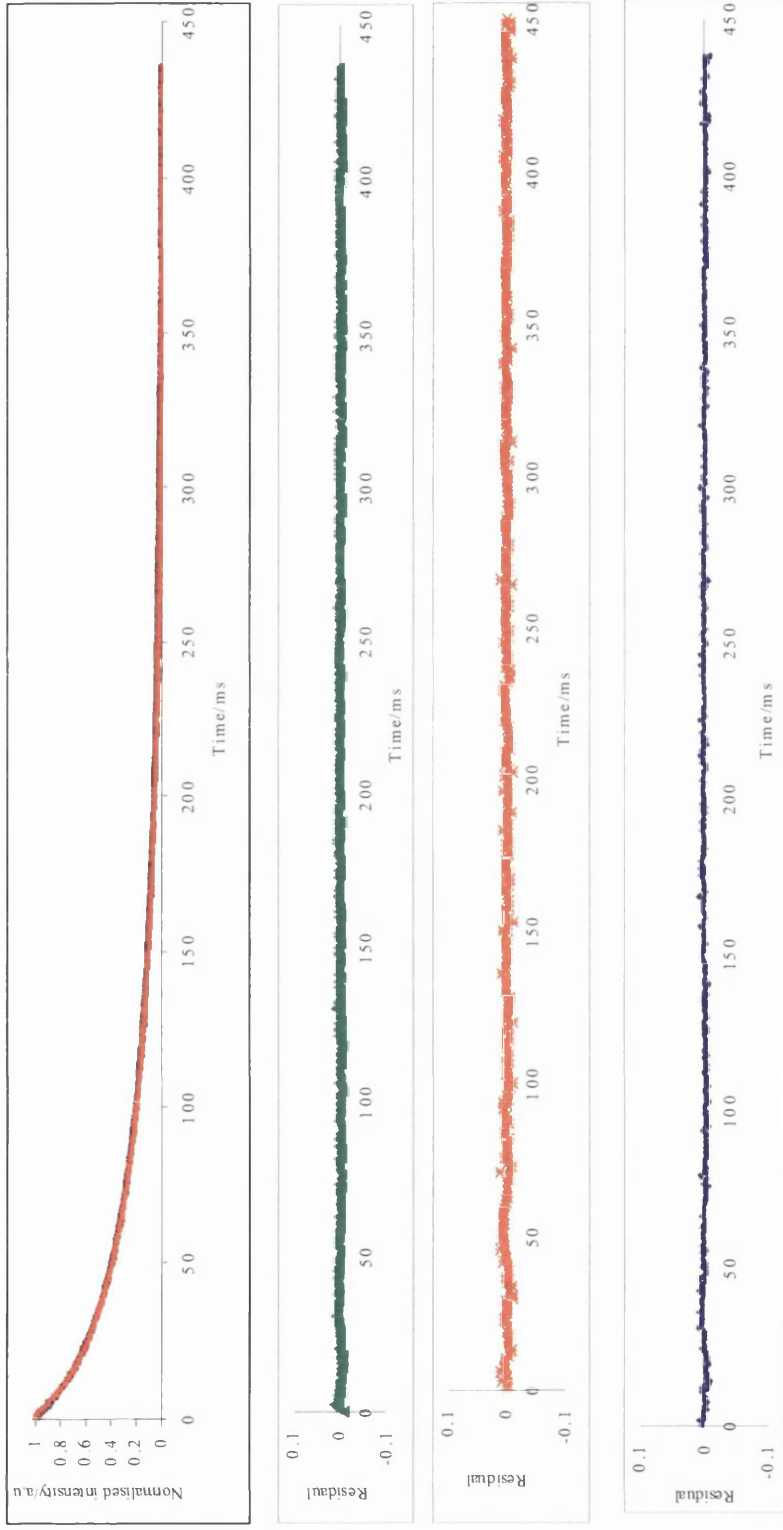


Figure 5.11 Time resolved emission for PtOEP in PtOEP ormosil PEBBLEs immobilised in hydrogel polymer under nitrogen. ▲ = type 3 sensor (dry), * = type 4 sensor (dry) and ◆ = type 4 sensor (wet) solid line is the fit to a double exponential. b-c: residual for double exponential fit ▲ = type 3 sensor (dry), * = type 4 sensor (dry) and ◆ = type 4 sensor (wet) respectively

Table 5.4 Amplitudes of the two contributions from a fixed double exponential analysis of the type $Y = A + \alpha_1 e^{-0.0527t} + \alpha_2 e^{-0.0101t}$ of time resolved emission from 100, 300 and 500nm PtOEP/PEBBLEs hydrogel film in the absence of oxygen.

PEBBLE diameter/nm	Percentage contribution		Percentage contribution	
	Dry film	wet film	Dry film	wet film
	k_1 (Fast)	k_2 (Slow)	k_1 (Fast)	k_2 (Slow)
100	19.7	80.3	20.1	79.9
300	15.2	84.8	16.2	83.8
500	13.1	86.9	12.8	87.2

5.6.2 Response characteristics of ormosil nanoparticles in hydrogel

5.6.2.1 Single lumophore sensor

5.6.2.1.1 Effect of concentration

A series of PEBBLES were prepared with differing concentrations of PtOEP (1.4 to 24.5×10^{-5} mol dm⁻³) The steady state and time resolved emission Stern-Volmer plots of PEBBLES immobilized in hydrogel is shown in figure 5.12 . Both steady state and time resolved Stern Volmers show linear plots for both gaseous and dissolved oxygen.

5.6.2.1.2 Effect of PEBBLE size

The unquenched steady state emission of the PtOEP ormosil PEBBLES immobilized in a hydrogel polymer is shown in figure 5.13, where the insert is the linear relationship between the PEBBLE size and maximum unquenched emission intensity of the PtOEP PEBBLE/hydrogel.

5.6.2.2 Dual lumophore type 2 sensor

Rh6G is a fluorescent dye, insensitive to oxygen and has an excitation band overlapping with the Soret band of PtOEP. An excitation wavelength of 382 nm was chosen to simultaneously excite both PtOEP and Rh6G, which give emission at 656 and 571 nm respectively. This simultaneous excitation reduces the need for complex excitation and detection systems.

There is no shift in emission maximum of PtOEP when immobilised in the ormosil nanosensors. Figure 5.14 shows the emission of the dual lumophore ormosil PEBBLES suspended in water as a function of increasing oxygen concentration. The PtOEP has a linear Stern-Volmer response to oxygen concentration.

5.6.2.2.1 Type 2 Thin film sensors for gaseous and dissolved oxygen sensing

There is a slight red shift in the emission maximum of Rh6G when the ormosil nanosensors are immobilised in the hydrogel matrix which is thought to be a result of the microenvironment of the PEBBLES [38].

Figure 5.15 shows the luminescence emission from the dual lumophore PEBBLE immobilised in a hydrogel thin film sensor as a function of increasing oxygen pressure from 0 to 320 Torr. The phosphorescent intensity from PtOEP decreases as the oxygen concentration increases while there is no change in the fluorescence intensity from Rh6G. Oxygen

quenching of PtOEP over the pO_2 range 0 to 220 Torr gives a reasonably linear Stern-Volmer plot.

5.6.2.2 Ratiometric sensing

The hydrogel sensing was also characterised as a ratiometric sensor for dissolved oxygen and figure 5.16 shows the results from ratiometric analyses for both gaseous and dissolved oxygen. In both cases linear ratiometric plots are obtained with identical Stern-Volmer constants when the solution phase data is expressed in terms of pO_2 for a given $[O_2]$ (K_{sv} for gas and dissolved oxygen are 0.015 ± 0.003).

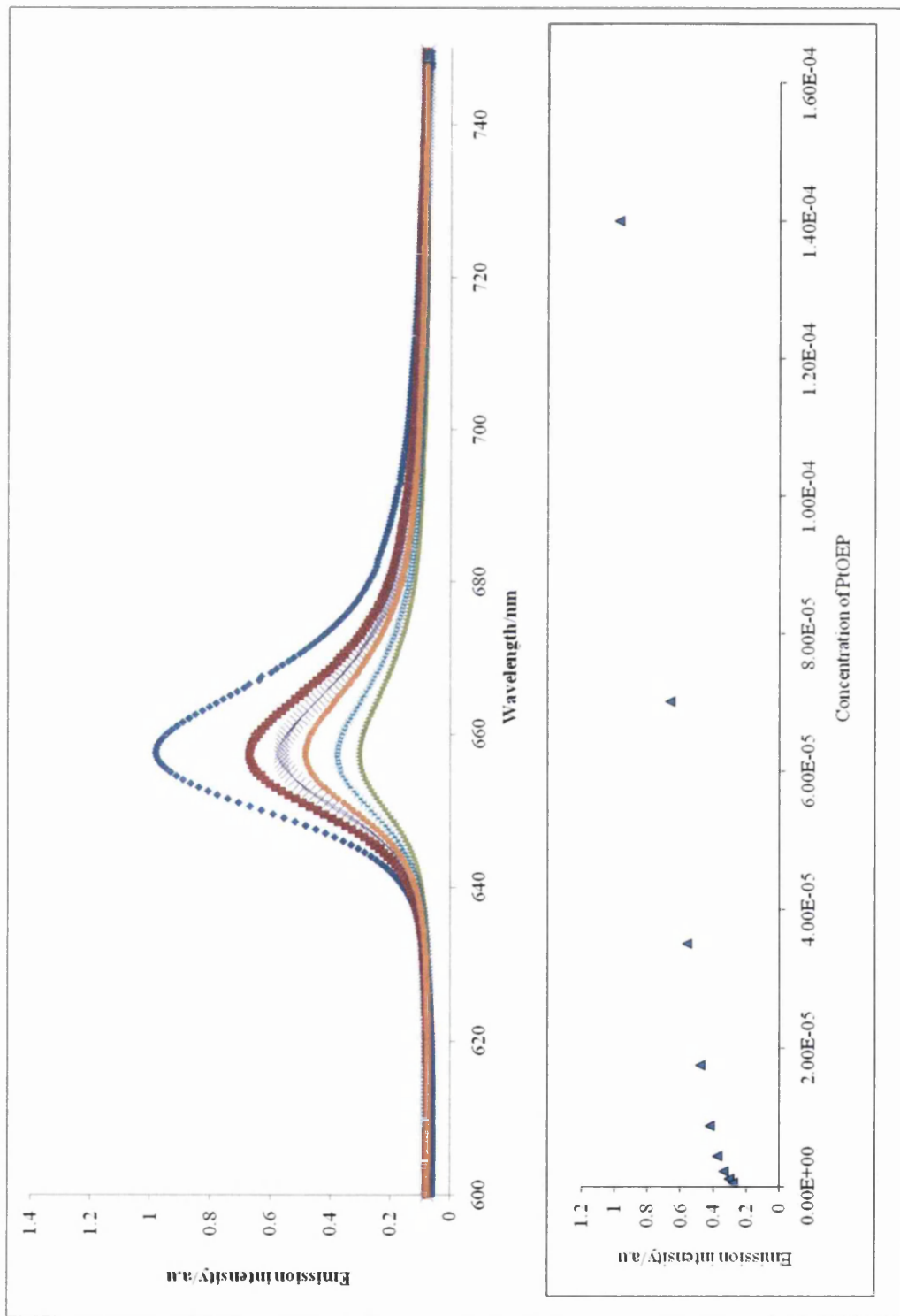


Figure 5.12 Unquenched steady state emission of PtOEP PEBBLEs/hydrogel as function of concentration from $1.5 - 24 \times 10^{-5} \text{ mol dm}^{-3}$.

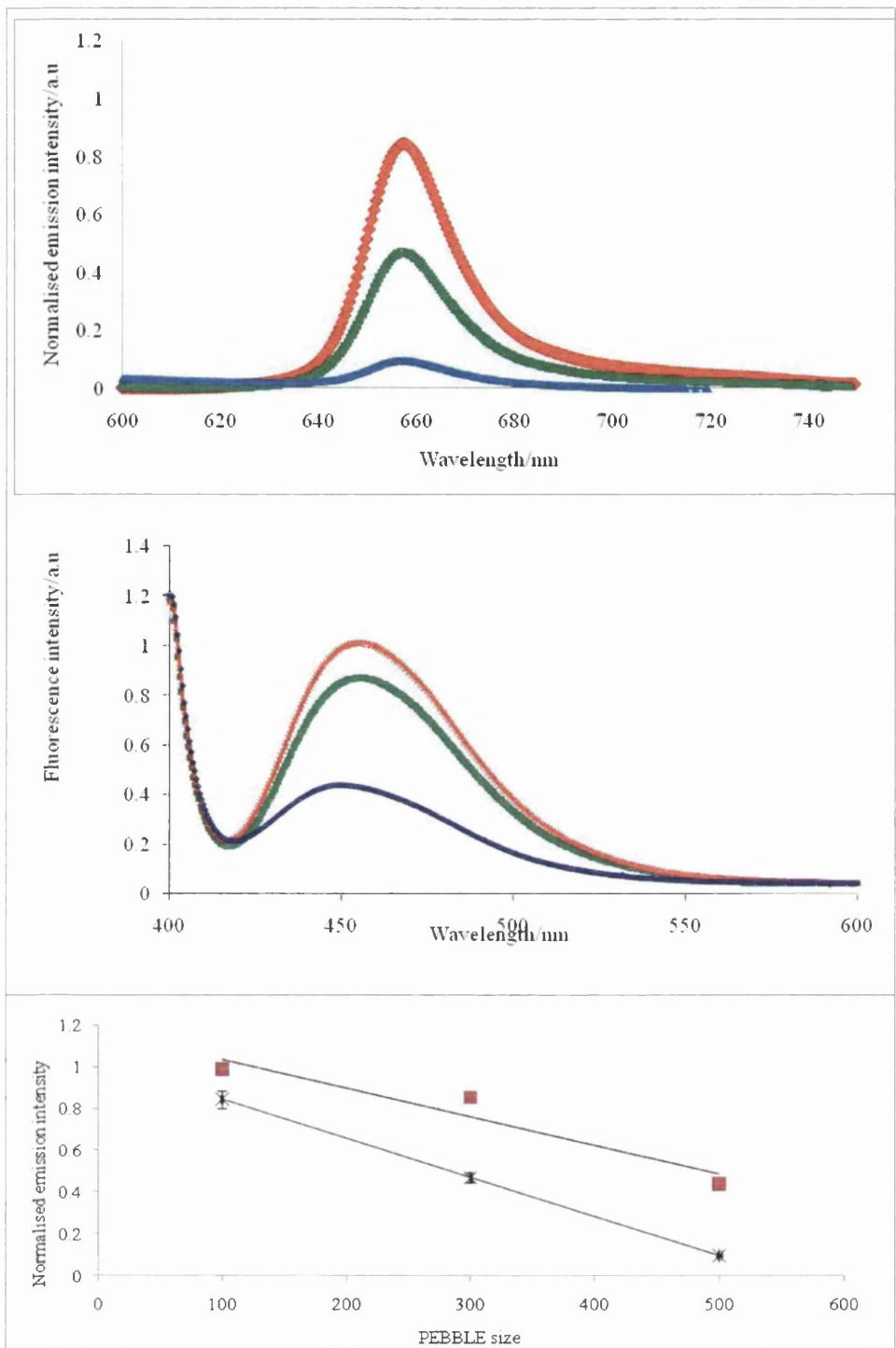


Figure 5.14 Unquenched steady state emission of PtOEP PEBBLES 100, 300 and 500 nm respectively. Insert shows the linear relationship between size and steady state emission. $y = -0.001x + 1.029$. Red = 100nm PEBBLES, green= 300nm PEBBLES and blue = 500nm PEBBLES

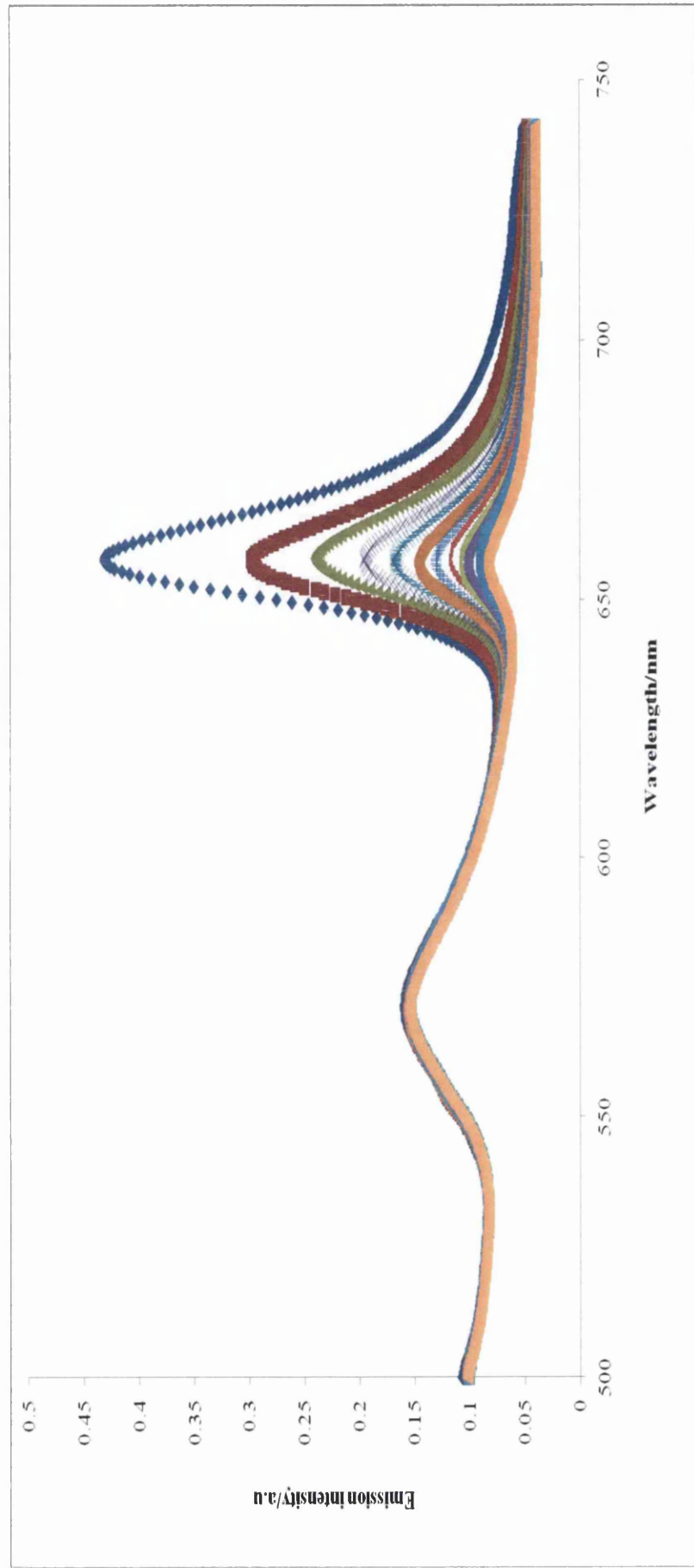


Figure 5.16 Variation in the emission spectrum of the dual lumophore system with increasing pO_2 where: $\blacklozenge=0$, $\blacksquare=33$, $\blacktriangle=53$, $\ast=62$, $\text{+}=75$, $\bullet=91$, $\ast=117$, $\text{-}=132$, $\circ=161$, $\blacklozenge=190$, $\Delta=279$ and $\square=319$ Torr. Excitation wavelength 382 nm.

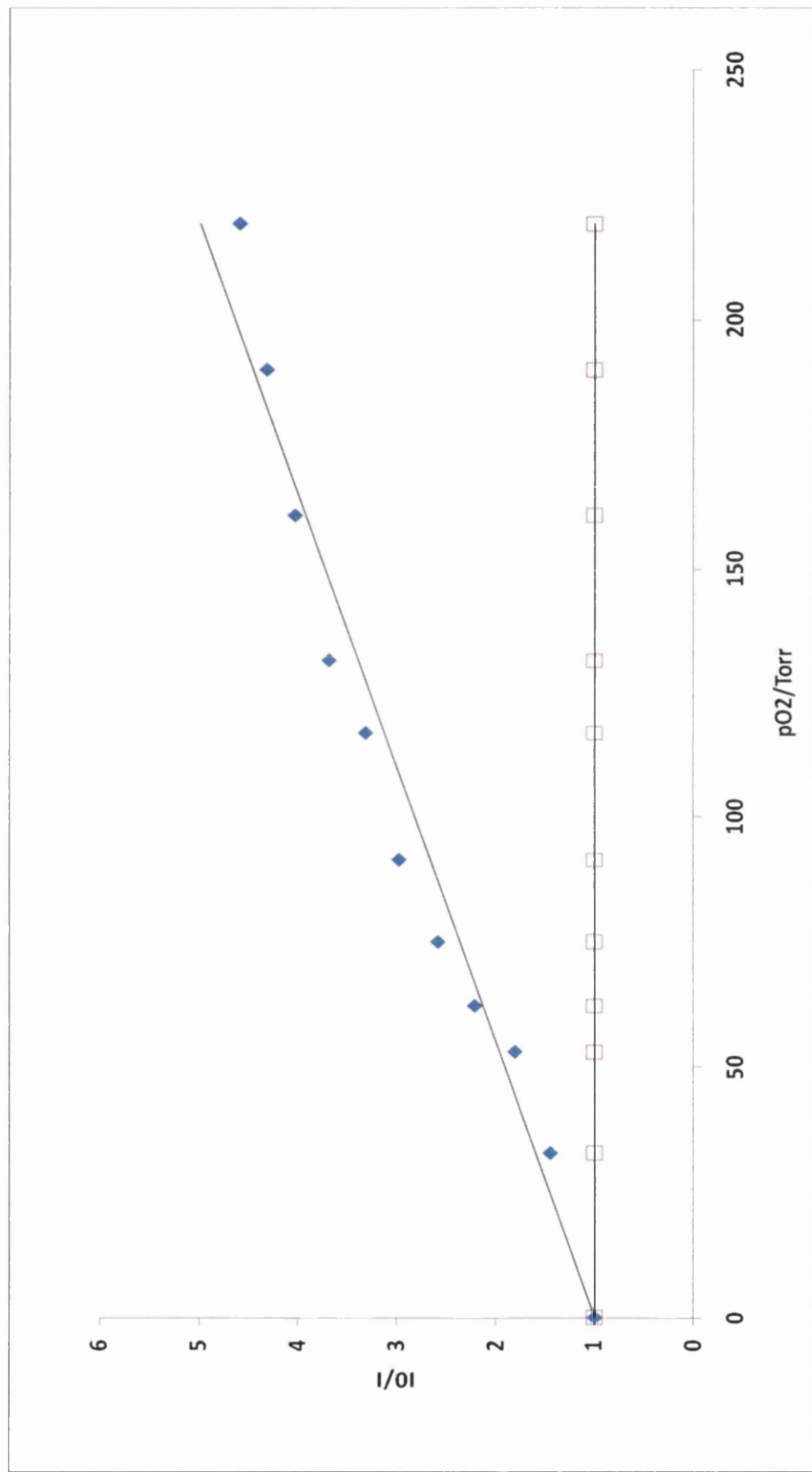


Figure 5.17. Stern-Volmer plots for gaseous oxygen quenching of dual-lumophore sensors. PtOEP (Filled diamonds) Rh6G (open squares).

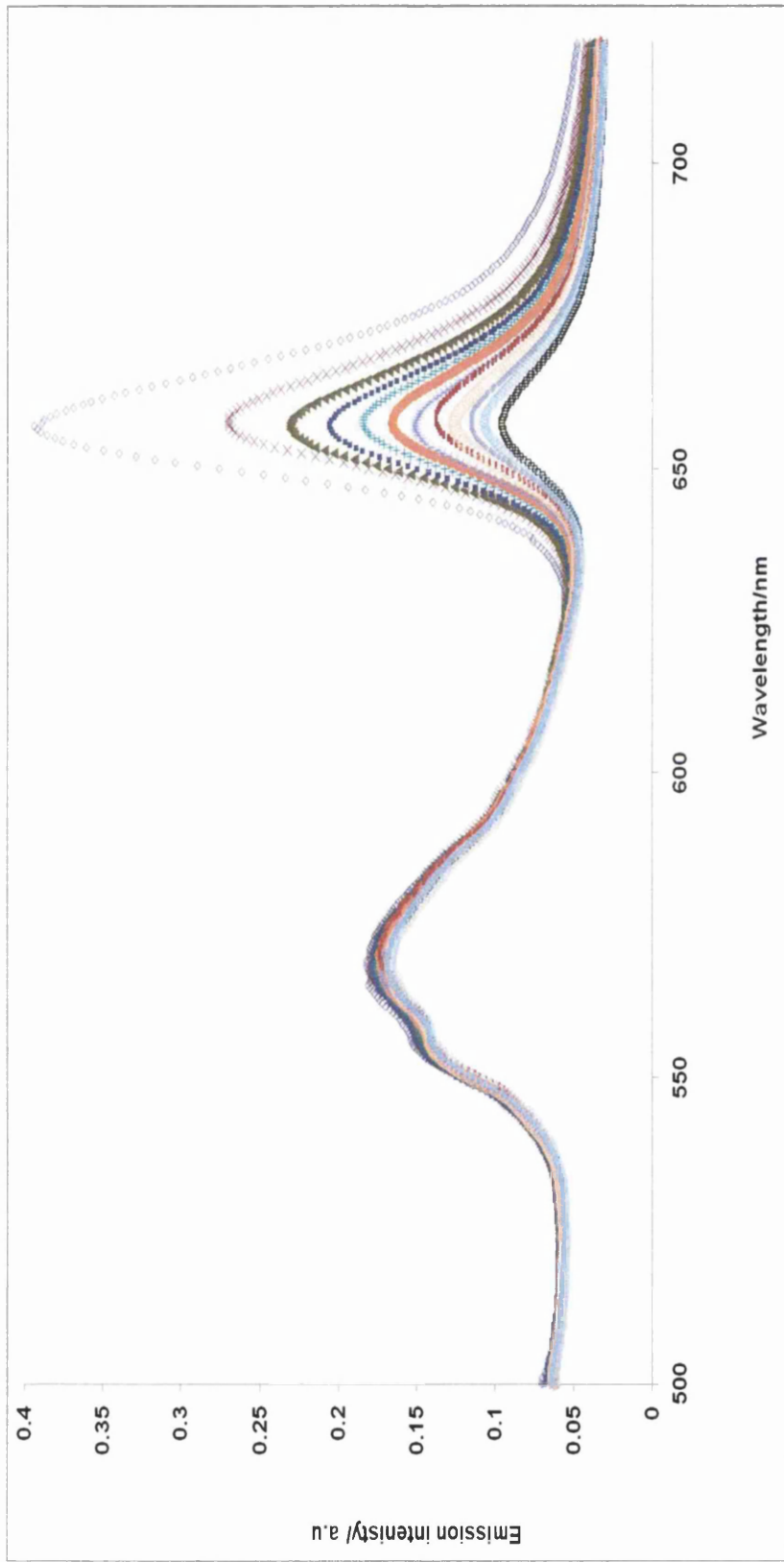


Figure 5.18. Emission spectra of the dual lumophore system with increasing concentration of dissolved oxygen (λ_{exc} 382) where: $\diamond=0$, $x=33$, $\blacktriangle=53$, $\blacksquare=62$, $+ = 75$, $\bullet=91$, $*=117$, $-=132$, $\circ=161$, $\blacklozenge=190$, $\Delta=279$ and $\square=319$ Torr.

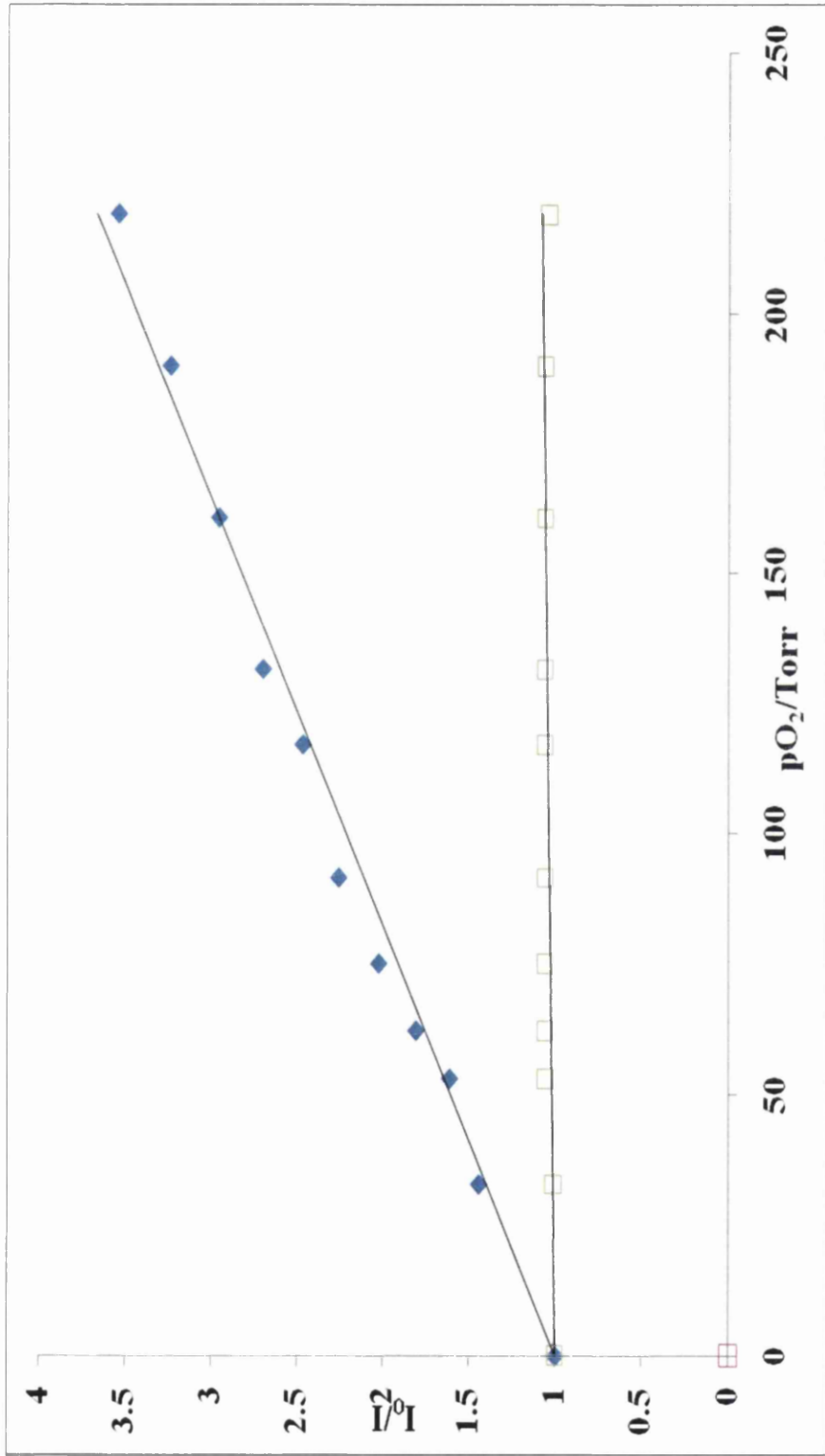


Figure 5.19. Stern-Volmer plots for oxygen quenching of dual-lumiphore sensors (gaseous). PtOEP (filled diamonds), Rh6G (open squares). The solid lines represent a linear fit to the data.

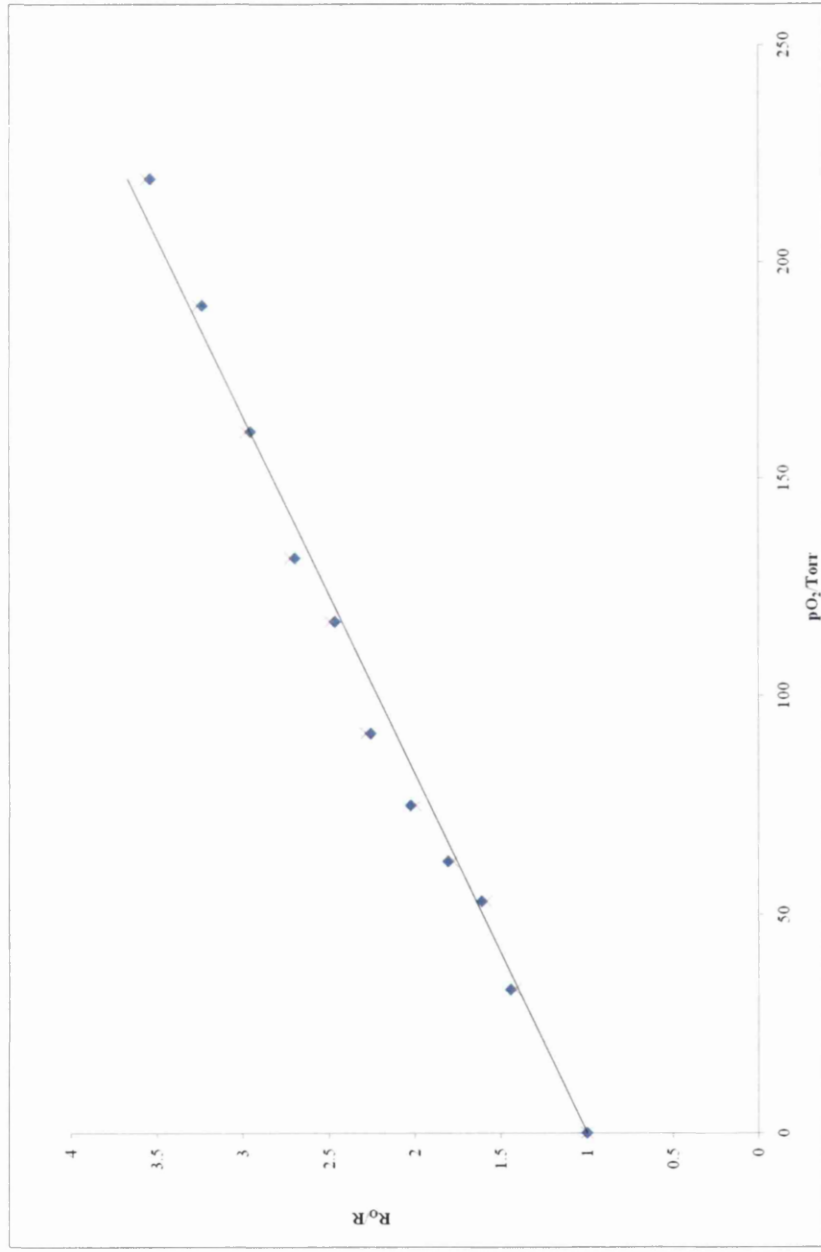


Figure 5.20 Ratiometric Stern-Volmer plot of relative emission intensity ratios for PtOEP/Rh6G ormosil PEBBLEs. R_0 is the ratio between the emission intensities of PtOEP and Rh6G at 0 Torr, R is the ratio at given oxygen pressures. \blacktriangle for gaseous system: x for dissolved oxygen sensing in an atmosphere at the specified partial pressure of oxygen.

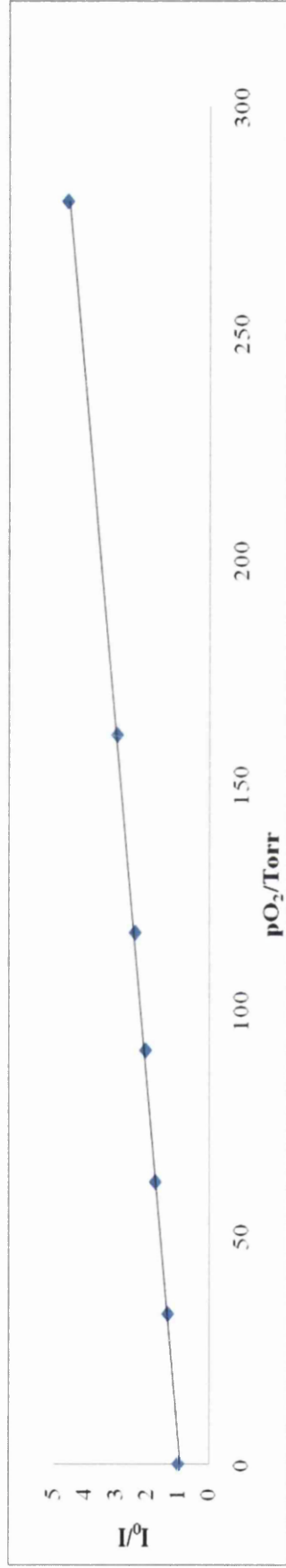
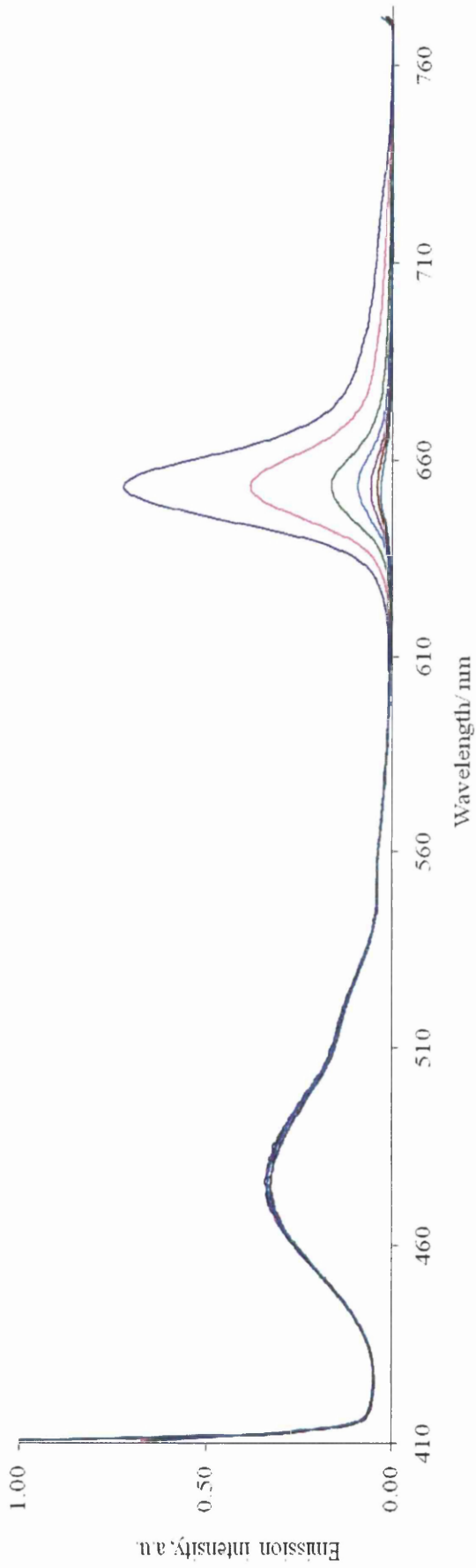


Figure 5.21. Emission spectra of a type 4 sensor composed of 100nm PtOEP and 500nm C153 ormosil PEBBLEs: $\diamond=0$, $\blacktriangle=53$, $\blacksquare=62$, $+ = 75$, $\bullet=91$, $\ast=117$, $\cdot, \circ=161$, and $\square=319$ Torr. . b: Stern-Volmer plots for oxygen quenching of PtOEP in the dual-lumophore sensors (gaseous).

The solid lines represent a linear fit to the data

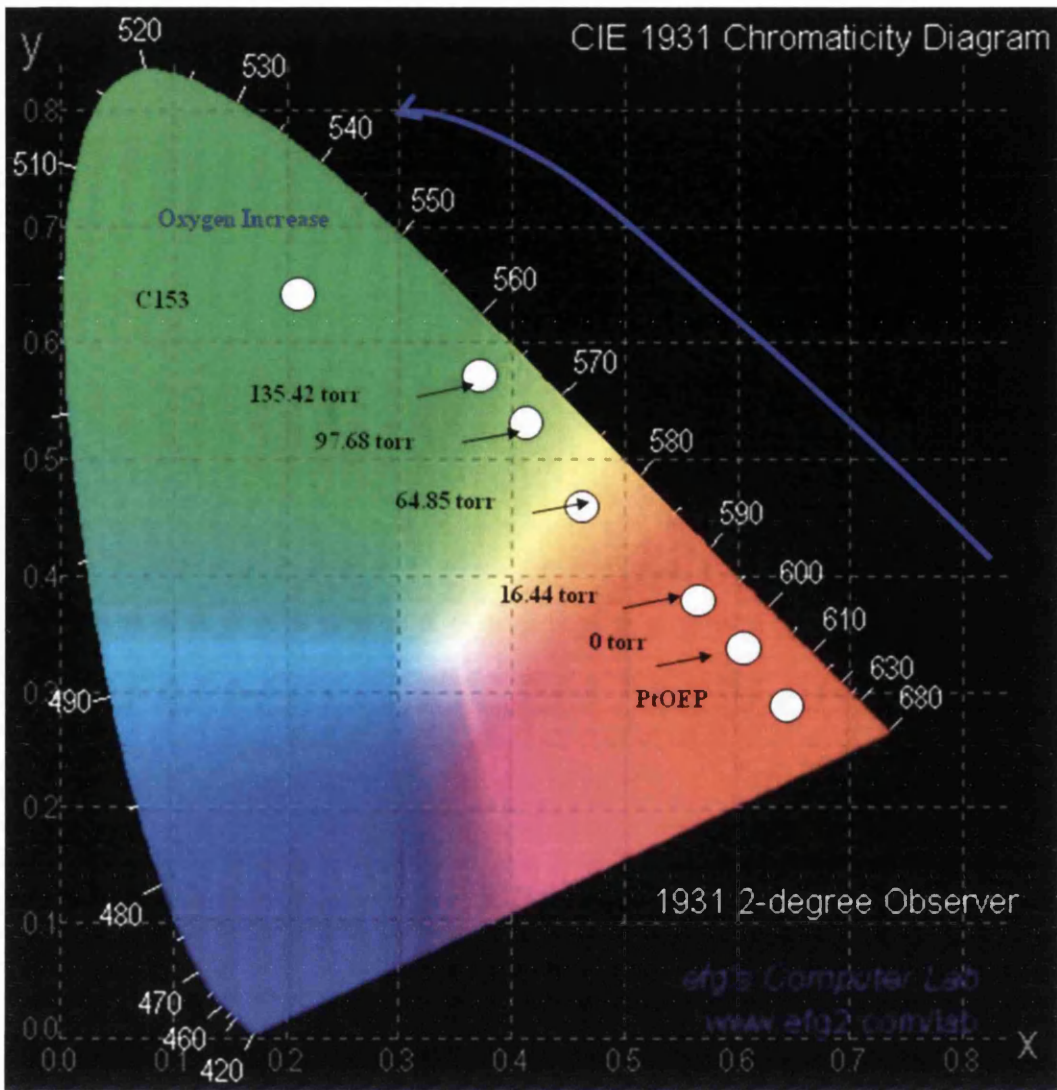


Figure 5.22. CIE Colour chromaticity diagram representing the oxygen quenching (figure 5.21) for a type 4 thin film sensors composed of 100nm PtOEP and 500nm C153 ormsol PEBBLEs. [92]

5.6.2.3 Type 4 dual lumophore sensors

5.6.2.3.1 Colorimetric thin film oxygen sensors

Colorimetric thin film sensors have potential applications in MAP and biotechnology involving gaseous oxygen [89].

The emission colour from lumophore doped ormosil PEBBLEs can be controlled by both the size of the nanoparticle and the concentration of lumophore used to prepare the PEBBLEs. Figure 5.21 shows the emission of a type 4 sensor composed of 100nm PtOEP and 800nm C153 Ormosil PEBBLEs (1:1 w:w ratio) as a function of increasing oxygen concentration; the corresponding Stern Volmer plot is also shown. Figure 5.22 shows the emission of the dual lumophore sensor in terms of CIE colour co-ordinates. The use of PEBBLEs of differing diameter can be used to produce colorimetric sensors with differing responses to oxygen. Table 5.6 summarises the CIE colour co-ordinates for the unquenched emission from 100, 300 and 500 nm PEBBLEs prepared from PtOEP, C153 and C110.

Table 5.6 A summary of the CIE colour co-ordinates for the unquenched emission from 100, 300 and 500 nm PEBBLEs prepared from PtOEP, C153 and C110

Oxygen element	sensing element	Reference element		CIE co-ordinate 100% nitrogen	CIE co-ordinate 100% Oxygen
100nm	PtOEP	100nm	C153	0.69,0.31	0.08,0.75
PEBBLE		PEBBLE			
100nm	PtOEP	300nm	C153	0.69,0.31	0.15,0.60
PEBBLE		PEBBLE			
100nm	PtOEP	500nm	C153	0.69,0.31	0.31, 0.61
PEBBLE		PEBBLE			
100nm	PtOEP	500nm	C110	0.69,0.31	
PEBBLE		PEBBLE			
300nm	PtOEP			0.69,0.35	
PEBBLE					
800nm	PtOEP			0.55,0.45	
PEBBLE					

5.6.3 Optical pH sensing

5.6.3.1 Choice of material

5,6-Carboxyfluorescein was chosen as the pH indicator because it meets certain key criteria, namely: a high quantum yield of emission easily detectable at a single wavelength, compatibility with LED excitation sources, sensitive to pH in the physiological pH range (with pKa 6.5 [7]), and a carboxy group for immobilisation onto alumina to prevent leaching.[13] The hydrogel support matrix was chosen for its excellent mechanical properties, excellent stability across a range of pH [14], excellent water uptake, biocompatibility and low protein adsorption.

5.6.3.2 Optical Response

An indicator pKa of around 7 is required for biotechnological and biomedical measurements at physiological pHs. The measured pKa depends on the intrinsic pKa of the indicator and the indicator environment. Figure 5.25 shows the pH response of aqueous 5,6 – carboxyfluorescein (CF); the pKa is 6.7. Figure 5.26 shows the response of 5,6 – carboxyfluorescein, a) adsorbed onto alumina as a carboxyfluorescein-alumina SAM; and b) when this SAM is suspended in the polyurethane hydrogel. The pH response curves can be described well by equation 4. Table 5.7 collects emission characteristics for the dye in these three environments together with pH response data.

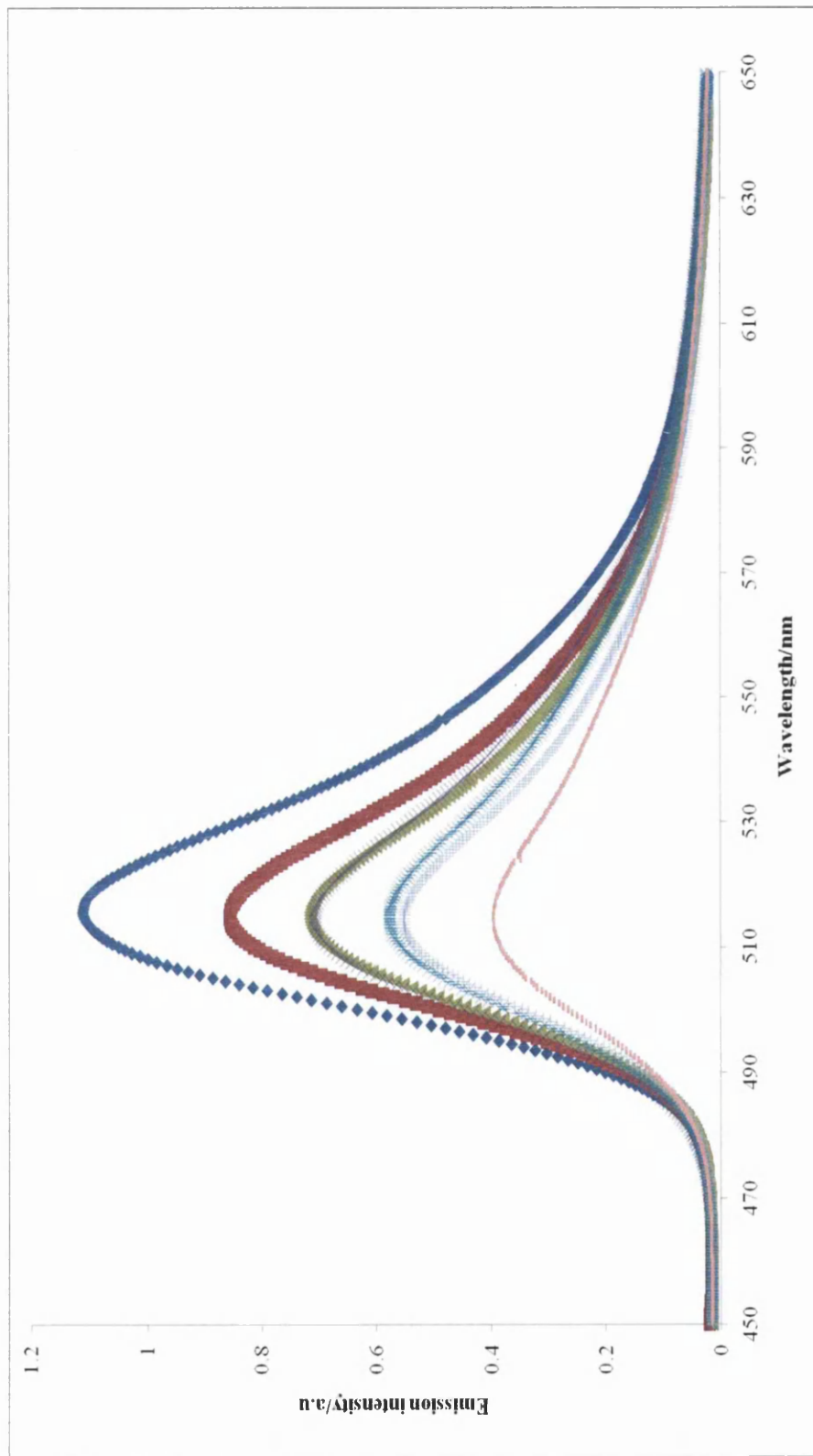


Figure 5.25 the response of aqueous 5,6 –carboxyfluorescein. Where $\diamond=9$, $\blacksquare=8$, $\blacktriangle=7$, $\times=6$, $\ast=5$, $\bullet=4$, $+ =3$ and $\diamond=2$

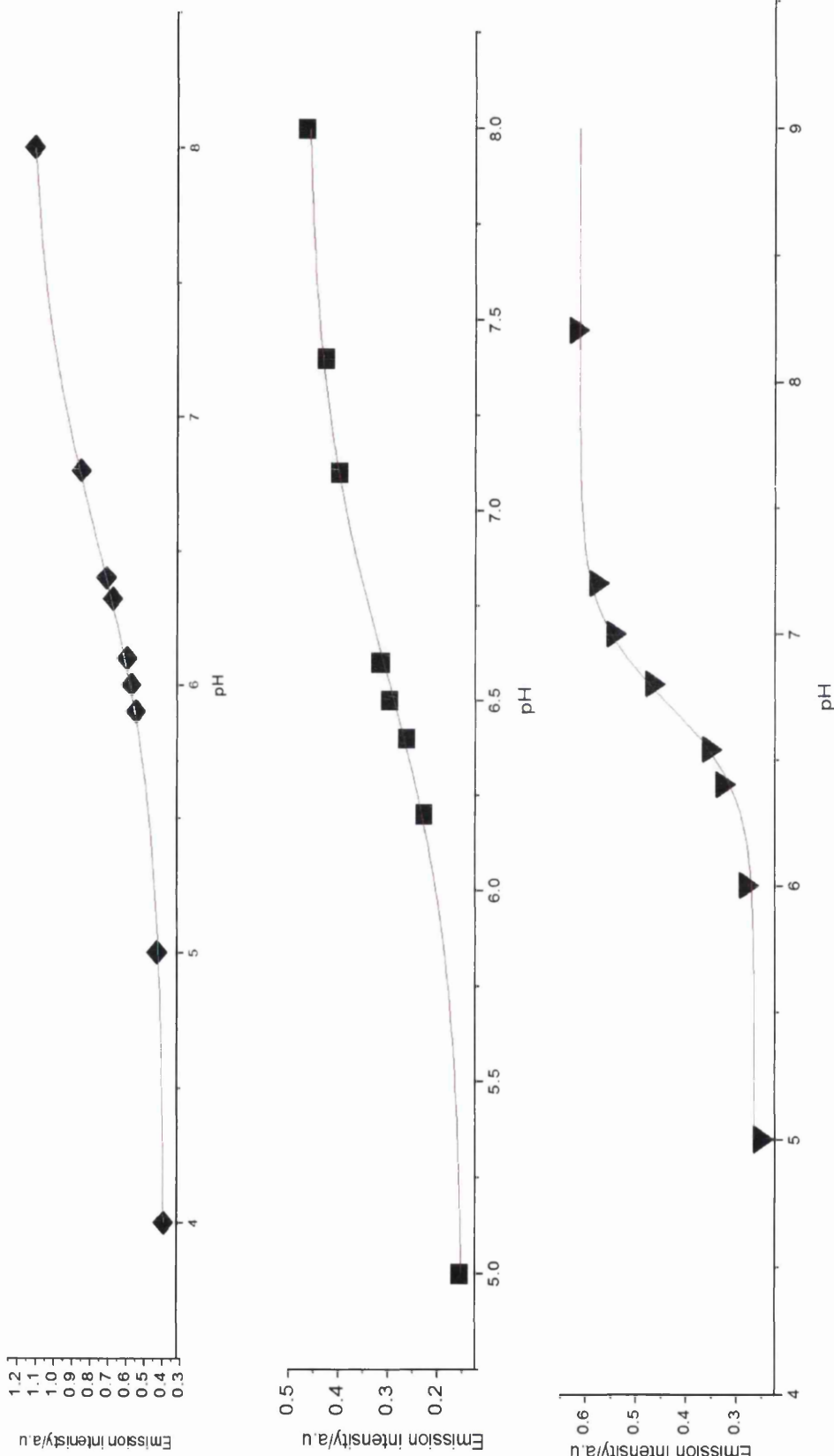


Figure 5.26 the response of 5,6 –carboxyfluorescein, a) adsorbed onto alumina as a carboxyfluorescein-alumina SAM; and b) when this SAM is suspended in the polyurethane hydrogel.

Table 5.7 Compares the emission maxima and Pka values for CF in aqueous solution, CF self assembled film and CF self assembled material in hydrogel film.

Sensing System	(λ_{em} max)/nm at pH 9	pKa $\pm 0.02^*$
Aqueous solution	517 (517 [#])	6.54 (6.5 [#])
CF-SAM	531	6.68
CF-SAM/hydrogel	551	6.72
CF/SAM/TPPormosil/hydrogel	551	6.73

data from [13] * Error estimates from OriginLab fitting program

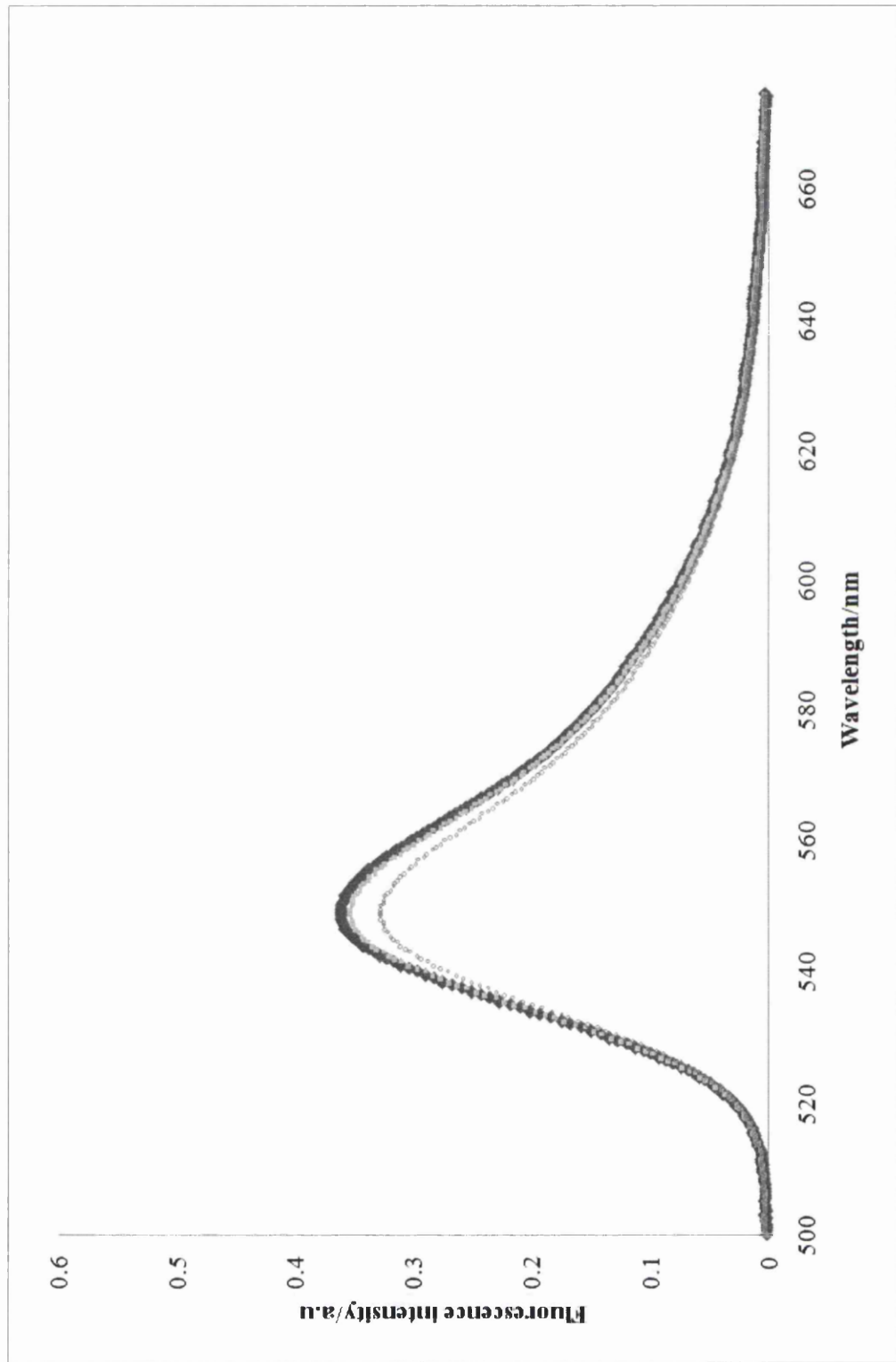


Figure 5.27 Fluorescence emission at pH 6.5 for the CF-SAM sensor as a function of time in solution. X=time 0, \blacktriangle =1 hour and \circ = 5 hours.

The red shifts in emission maxima upon firstly immobilisation on alumina and then suspension in the hydrogel is likely to be a result of varying electrical charges and does not effect the sensor response. [15] Similar behaviour has been seen for carboxyfluorescein when bound in p-HEMA and also polymer bound fluorescein. [4,15]

There is a small shift in pK_a upon adsorption to alumina and a further small shift when these SAMs are suspended in the polyurethane hydrogel. A similar effect was seen when carboxyfluorescein was covalently attached to particles made from amino-modified poly(hydroxyethyl methacrylate) The increase in pK_a in the hydrogel might be attributable to a decrease in the polarity of the microenvironment. [4,15] There is very little evidence of leaching from the self assembled material immobilised in the hydrogel polymer over a prolonged period in solution. Figure shows the fluorescence emission at pH 6.5 for the sensor at times of 0, 1 hour and 5 hours.

5.6.3.3 Ratiometric pH sensor

Tetraphenyl porphyrin has been used as a pH insensitive dye in both pH and carbon dioxide sensors. The emission spectra as a function of pH of: a) TPP; b) TPP ormosil PEBBLES; and c) TPP ormosil PEBBLES immobilized in hydrogel is shown in figure 5.28. There is no significant change in emission properties as a function of pH, although a small red shift in the emission maxima is seen when TPP immobilized in the ormosil nanospheres. Figure 5.29 shows the emission properties of a type 4 ratiometric pH sensor containing TPP/ormosil PEBBLES and 5,6 CF/SAM. Linear and reproducible responses for both sensors were obtained in the pH range 6.8-8.0, which encompasses the clinically relevant range.

5.6.4 Multi-analyte sensors

The previous sections describe the preparation of 2 very different sensing materials, PtOEP ormosil PEBBLEs and CF-SAM, both with excellent photochemical responses to oxygen and pH respectively. A combination of oxygen and pH sensing is extremely important in biotechnology and biomedicine where a sensing system capable of detecting the parameters most influential to cell health (pH, oxygen, glucose, and lactate), that monitors in a non-invasive and non-interactive manner, requiring little human intervention, needs to be developed. Monitoring of blood gases and pH can be critical during hemodialysis. Maintaining a critical oxygen and pH level in fermentation and bioprocessing is vital to maintain productivity and product purity

Simultaneous sensing or more than one analyte has several considerations, to simplify the instrumental aspect of the sensing a single excitation source is wanted, good spectral separation of emission and no cross sensitivity of the analytes. Examples are known in the literature that employ phase modulation technology. Here we describe a sensing system that employs steady state emission from PtOEP ormosil PEBBLEs and CF/SAM material in a type 4 sensor with the potential for ratiometric sensing, which may improve the reliability of measurements without the need for complex lifetime determination.

PtOEP is an example of a hypso porphyrin with both Soret and Q bands. PtOEP and CF show good spectral overlap with 490nm being a suitable wavelength for excitation of both lumophores.

Figure 5.30 shows the emission of a type 4 sensor as a function of increasing oxygen concentration with excitation at 490nm. The corresponding Stern-Volmer plot is linear as shown in the insert of figure 5.30. Changes in pH have little effect on the emission of PtOEP. The emission of the multi analyte sensor as a function of pH in both an oxygen free sample is shown in figure 5.31. The pH response can be describe well using equation 4

There is little evidence of leaching from either sensing material in the film over a 24 hr period.

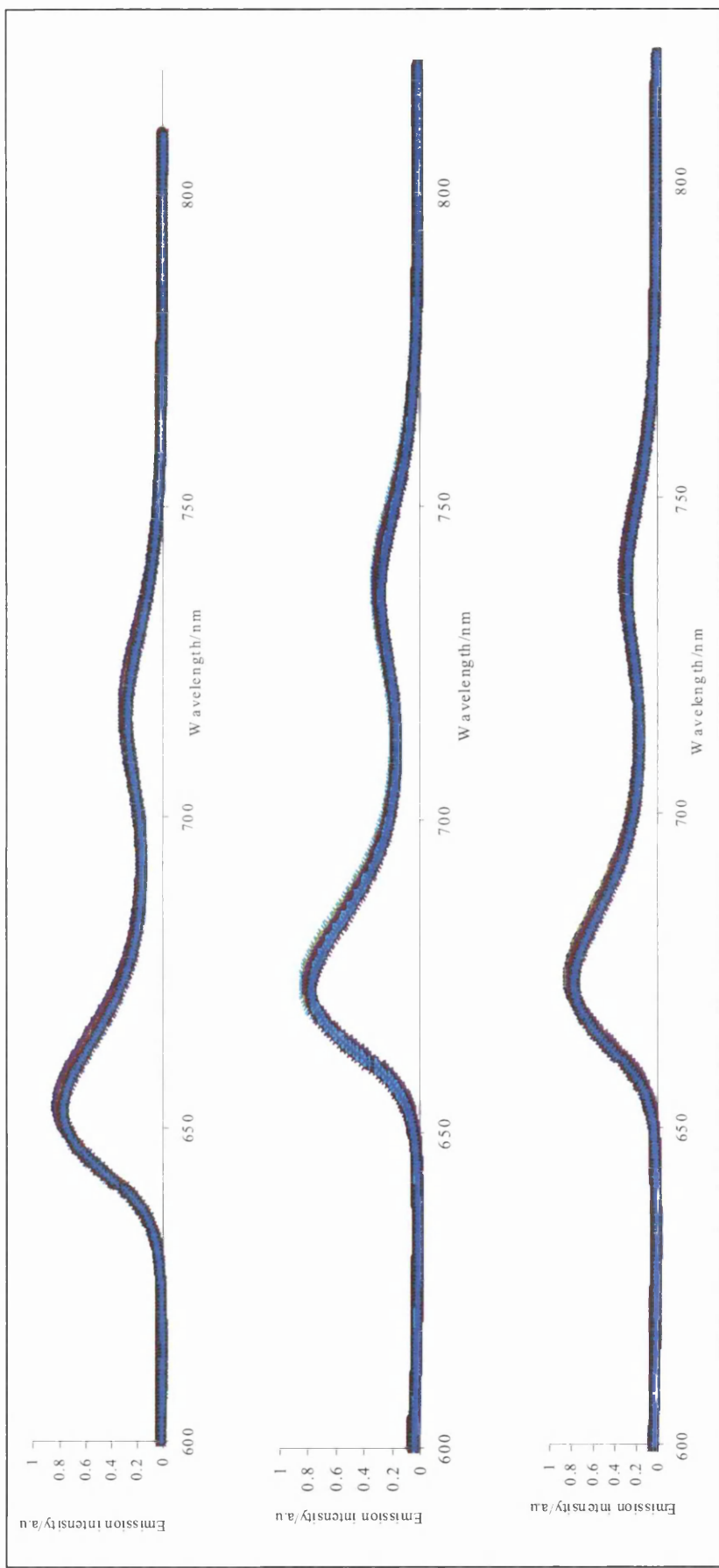


Figure 5.28 The emission spectra as a function of pH of: a) TPP; b) TPP ormosil PEBBLES; and c) TPP ormosil PEBBLES immobilized in hydrogel. Where pH $\circ=9$, $\blacksquare=8$, $\blacktriangle=7$, $\ast=6$, $\ast=5$, $\bullet=4$, $+ =3$ and $\diamond=2$

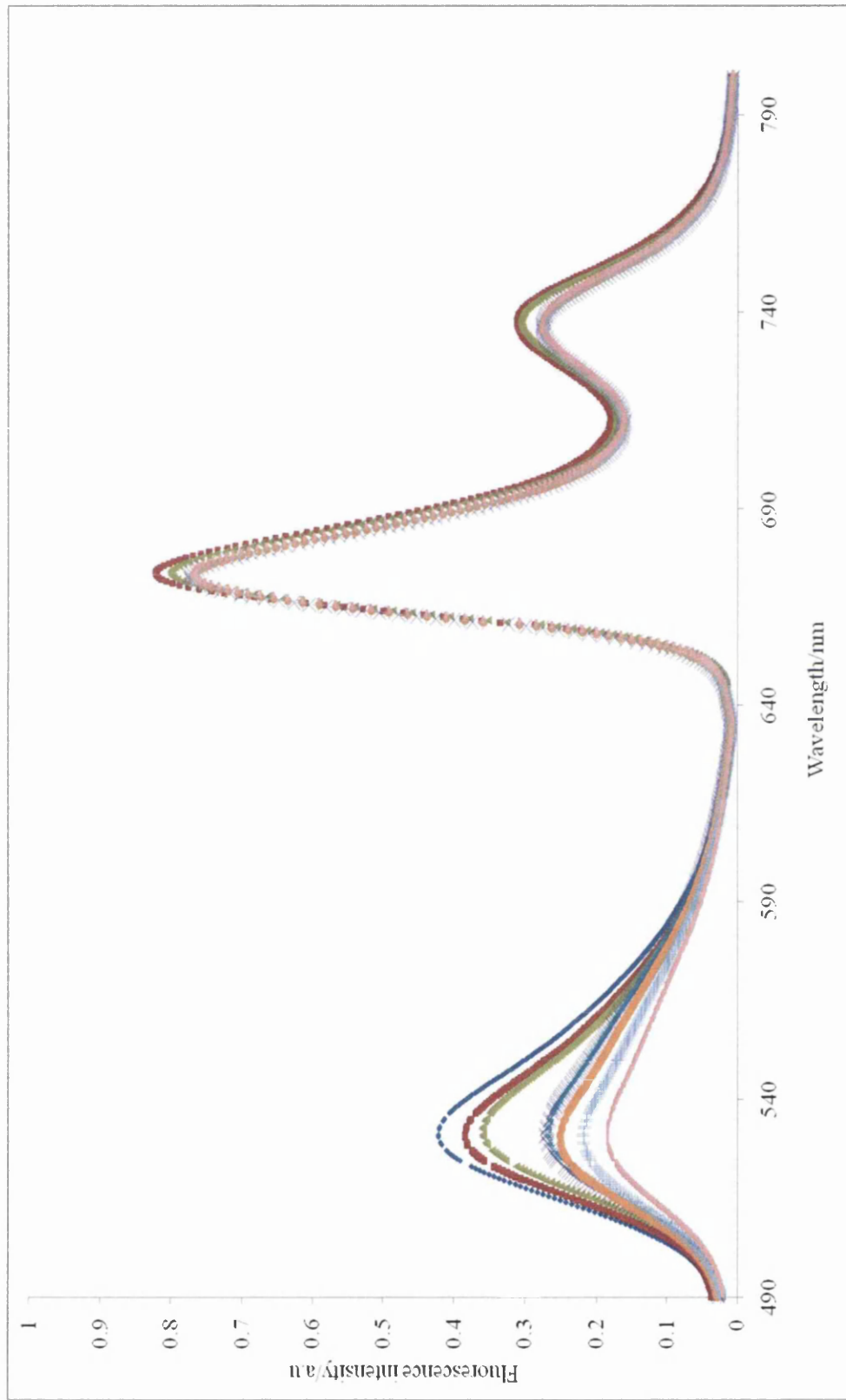


Figure 5.29 Emission from a type 4 thin film sensor for ratiometric pH sensing, with emission from CF-SAM ($\lambda_{em}=551\text{nm}$) and TPP-ormosil PEBBLEs ($\lambda_{em}=690\text{nm}$), where $\circ=9$, $\blacksquare=8$, $\blacktriangle=7$, $\times=6$, $*=5$, $\bullet=4$, $+ =3$ and $\diamond=2$

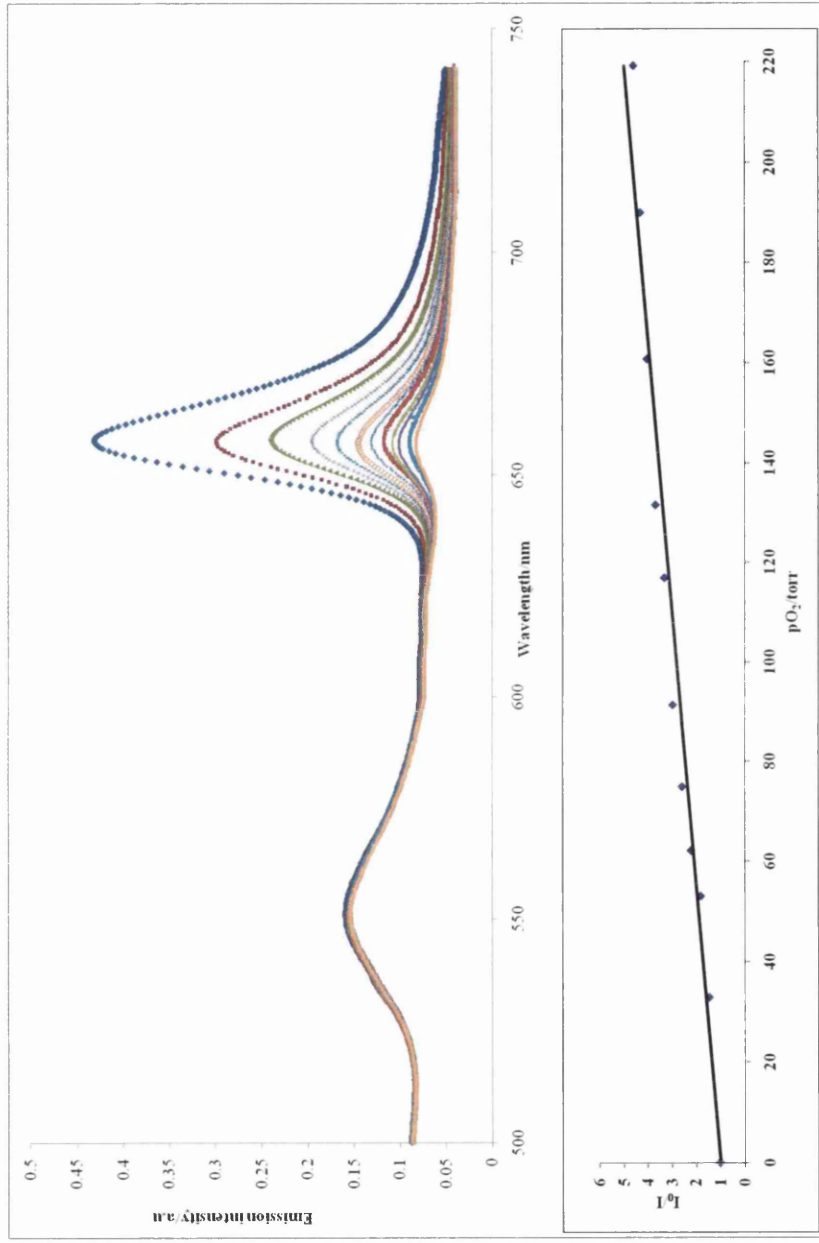


Figure 5.30 Emission of the dual lumophore type 4 sensor as a function of increasing oxygen concentration at pH 7.4 and the corresponding Stern-Volmer plot where: $\diamond=0$, $x=33$, $\blacktriangle=53$, $\blacksquare=62$, $+=75$, $\bullet=91$, $\ast=117$, $-=132$, $\circ=161$, $\blacklozenge=190$, $\Delta=279$ and $\square=319$ Torr.

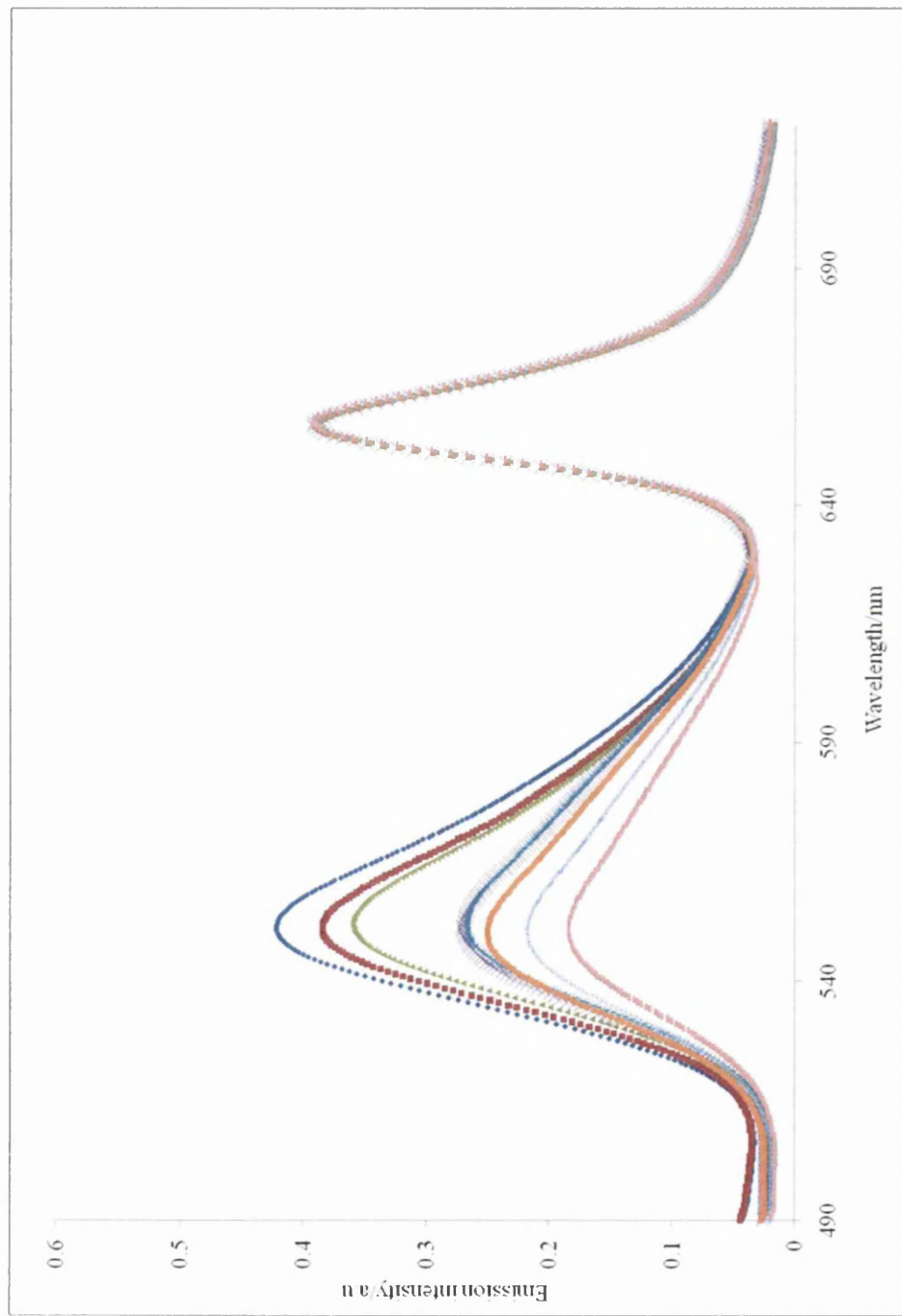


Figure 5.31 Emission from PtOEP/PEBBLEs and CF-SAM immobilised in a hydrogel polymer as a function of pH change in a nitrogen saturated water sample where $\circ=9$, $\blacksquare=8$, $\blacktriangle=7$, $x=6$, $*=5$, $\bullet=4$, $+ =3$ and $\diamond=2$

5.6.5 Conclusions

The use of ormosil PEBBLEs is a convenient way of encapsulating luminescent dyes before immobilization in a thin film sensor. The optical properties and response are unaltered by such a process. Unquenched emission decays can be described well using a double exponential analysis and can be modelled well using equation 5.3, corresponding to a monomer dimer equilibrium. [45] There is no significant change in the equilibrium constant when PtOEP is immobilized in the ormosil PEBBLEs. Although these materials are promising sensing material for both lifetime and steady state experiments, this study has concentrated on steady state methods. The use of analyte insensitive materials such as the fluorescent dyes rhodamine 6G and coumarin 153 allows the design of simple ratiometric and colorimetric sensors for optical oxygen sensing.

We have described an optical oxygen sensing system for both gaseous and dissolved oxygen based on the incorporation of luminescent nanoparticles in a biologically compatible hydrogel. The system shows a linear response to changing oxygen concentration in both gaseous and aqueous systems and the ratiometric sensing provides a simple way of accounting for any fluctuations associated with intensity based sensing without the complicated instrumental set up needed for lifetime based sensors. Both lumophores can be simultaneously excited at 382nm reducing the need for complex excitation systems. The system is also compatible with cheap LED excitation sources. Examination of the unquenched time resolved emission decay under nitrogen for the gaseous and solution studies shows a good fit to a double exponential as seen for previous studies involving PtOEP. [45, 47] This provides two important conclusions i.e. neither immobilising PtOEP in ormosil nanoparticle nor the swelling of the hydrogel polymer with water affect the kinetic heterogeneity of the PtOEP. The sensitivity, quenching constant and lifetimes of PtOEP emission remain unchanged for the gas and dissolved oxygen sensor. The values are comparable to PtOEP immobilised in a polystyrene polymer and as such the hydrogel provides an excellent alternative to polystyrene for optical oxygen sensors. The sensing system has potential in biomedical and industrial applications.

A new easily prepared self assembled material for optically sensing pH in the physiological pH range has been developed and incorporated into a thin hydrogel film The fluorescent

indicator 5,6 carboxyfluorescein has been attached to alumina to produce a sensing material that overcomes the major problem of leaching. When this material is immobilised in a biologically compatible hydrogel polymer the resulting sensor film shows good operational stability and can be calibrated well using equation 4. This method, involving use of a SAM, offers a cheap and simple alternative to immobilization in microspheres or beads.

We suggest that a combinatorial approach to optical oxygen sensing is possible using ormosil PEBBLES and SAMs. An example of a multi-analyte sensor for oxygen and pH showing excellent response to the analyte has been developed which shows good response and no significant leaching from either material.

5.6.6 References

- 1 O.S. Wolfbeis, *Anal. Chem.*, 80, (2008), 4269-4283.
- 2 S.W. Bishnoi, C.J. Rozell, C.S. Levin, M.K. Gheith, B.R. Johnson, D.H. Johnson and N.J. Halas, *Nano Letters*, 6, (2006),1687-1692.
- 3 K.S. Bronk, K.L. Michael, P. Pantano, D.R. Walt, *Anal. Chem.* 67, (1995), 2750-2757.
- 4 J.Shi, Y.Zhu, X.Zhang, W.RG.Baeyens, A.M.Garcia-Campana, *Trends in analytical chemistry*, 23, (2004), 351-360
- 5 J. I. Peterson, R. V. Fitzgerald, and D. K. Buckhold, *Anal. Chem.*, 1984, 56, 62.
- 6 J. L. Gehrich, D. W. Lübbers, N. Opitz, D. R. Hansmann, W. W. Miller, J. K.
- 7 I. Bergman, *Nature*, 218 (1968), 396-400
- 8 T. C. O'Riordan, D. Buckley, V. Ogurtsov, R. O'Connor and D. B. Papkovsky, *Anal. Biochem.*, 278, (2000) , 221-227.
- 9 H.W. Kroneis and H.J. Marsoner, *Sens. Actuators*, (1983), 587-592
- 10 D.B. Papkovsky, *Sens. Actuators B*, 29 (1995), 213-218.
- 11 B.A.DeGraff and J.N. Demas in "Reviews in Fluorescence" Vol. 2, (2005), Springer, New York.
- 12 C. Prininger, I. Klimant and O.S. Wolfbeis, *Anal. Chem.*, 66, (1994), 1841-1847
- 13 B. Papkovsky, N. Papkovskaia, A. Smyth, J.P. Kerry and V.I. Ogurtosov, *Anal. Chem.*, 67 (1995), 4112-4117
- 14 A. Ressel, C. Weiss and T. Feyerabend. *Int. J. Radiat. Oncol. Biol. Phys.*, 49 (2001), 1119 - 1123

- 15 B.D. Ratner, A.S. Hoffman, F.J. Schoen, J.E. Lemons (Eds.), *Biomaterials Science: An Introduction to Materials in Medicine*, Academic Press, New York, Chapter 2, pp. 105-117.
- 16 Y. Amao, *Microchim. Acta*, 143, (2003), 1-8
- 17 K.P. McNamara, T. Nguyen, G. Dumitrascu, J. Ji, N. Rosenzweig and Z. Rosenzweig, *Anal. Chem.*, 73, (2001), 3240-3246.
- 18 S.M. Buck, H. Xu, M. Brasuel, M.A. Philbert and R. Kopelman, *Talanta*, 63, (2004), 41-59.
- 19 L. Lin, L. Xiao, S. Huang, L. Zhao, J. Cui, X. Wang and X. Chen, *Biosensors and Bioelectronics*, 21, (2006), 1703-1709.
- 20 P. Herst and M. Berridge, *Biochimica et Biophysica Acta (BBA) - Bioenergetics*, 1767, (2007), 170-177.
- 21 J.R. Lakowicz, *Principles of Fluorescence Spectroscopy*, 2nd Edition, Kluwer Academic Publishers, Dordrecht, 1999.
- 22 E.R. Carraway, J.N. Demas, B.A. DeGraff and J.R. Bacon, *Anal. Chem.*, 63, (1991), 337-342.
- 23 D.B. Papkovsky, *Methods in optical oxygen sensing: protocols and critical analyses*. In: C.K. Sen and G.L. Semenza, Editors, *Methods in Enzymology* vol. 381, Academic Press, San Diego (2004), 715-735.
- 24 G.T. John, I. Klimant, C. Wittmann and E. Heinzle, *Biotechnol. Bioeng.*, 81, (2003), 829-836.
- 25 R.D. Guarino, L.E. Dike, T.A. Haq, J.A. Rowley, J.B. Pitner and M.R. Timmins, *Biotechnol. Bioeng.*, 86, (2004), 775-787.
- 26 R.N. Gillanders, M.C. Tedford, P.J. Crilly and R.T. Bailey, *Anal. Chim. Acta*, 502, (2004), 1-6.

- 27 R.T.Bailey, F.R.Cruickshank, G.Deans, R.N.Gillanders and M.C.Tedford, *Anal. Chim. Acta*, 487, (2003), 101-108.
- 28 E.R. Carraway, J.N. Demas, B.A. DeGraff and J.R. Bacon, *Anal. Chem.*, 63, (1991), 337-342.
- 29 Y. Xiao, M.F .Mo and C.Choi, *Meas. Sci.Technol.*, 14, (2003), 826-867.
- 30 J.N. Demas, B.A. DeGraff and P.B. Coleman, *Anal. Chem.*, 71, (1999), 793A-800A.
- 31 P. Hartmann, M.J.P. Leiner and M.E. Lippitsch , *Sens. Actuators B*, 29 (1995), 251-257.
- 32 A.Mills and M. Thomas, *Analyst*, 122, (1997), 63-70.
- 33 A.Mills and F.C. Williams, *Thin Solid Films*, 306, (1997), 163-170.
- 34 P. Douglas and K. Eaton, *Sens. Actuators B*, 82, (2002), 48-53.
- 35 P.M. Gewehr and D.T. Delpy, *Med. Biol. Eng. Comput.*, 32 (1994), 659-664.
- 36 Y.Kostov, G.Rao, *Sens Actuators B.*, 90 (2003), 139-142.
- 37 M. Valledor, J.C. Campo, F.J. Ferrero, J.C. Viera, M. Gonzalez, C. Blanco, J.M. Costa, I. Sanchez and A. Sanz-Medel, Instrumentation and Measurement Technology Conference, 2005. IMTC 2005. Proceedings of the IEEE, Volume: 2, 1172-1176.
- 38 S. Lee and I. Okura, *Spectrochim. Acta A*, 54 (1998), 91-100.
- 39 S. Lee and I. Okura, *Analyst*, 122, (1997), 81-84.
- 40 D.B. Papkovsky, G.V. Ponomarev, W. Trettnak and P. O'Leary, *Anal. Chem.*, 67 (1995), 4112-4117.
- 41 H.A. Clark, M. Hoyer, S. Parus, M.A. Philbert and R Kopelman *Mikrochimica Acta*, 131 (1999), 121-128.

- 42 H. Xu, S.M. Buck, R. Kopelman, M.A. Philbert, M. Brasuel, E. Monson, C. Behrend, B. Ross, A. Rehemtulla and Y.L. Koo, (2005) *Topics in Fluorescence Spectroscopy*, 10, 69-125, Springer.
- 43 Y.L. Koo, Y Cao, R Kopelman, S.M. Koo, M. Brasuel and M.A. Philbert (2004) *Anal. Chem.*, 76, 2498-2505.
- 44 D.B. Papkovsky, *Sensors and Actuators B*, 11 (1993), 293-300.
- 45 V.Hughes and P.Douglas, *J.Fluorescence*, 16 (2006), 403-409.
- 46 S.H.Im, GE.Khalil, J. Callis, B.H.Ahn, M.Gouterman, and Y.Xia, *Talanta*, 67 (2005), 492-497.
- 47 K. Eaton and P. Douglas, *Sens. Actuators B*, 82, (2002), 94-104.
- 48 G.S. Vasylevsk, S.M. Borisov, C. Krause and O.S. Wolfbeis, *Chem. Mater.*, 18, (2006), 4609-4616.
- 49 L. Tolosa, Y. Kostov, P. Harms and G. Rao, *Biotechnol. Bioeng.* 80 , (2002), 594-597.
- 50 X.D. Ge, Y. Kostov and G. Rao, *Biotechnol. Bioeng.* 89 , (2005), 329-334.
- 51 O.S. Wolfbeis, Fiber-optic chemical sensors and biosensors, *Anal. Chem.*, 72, (2000), 81R-89R.
- 52 B. Weidgans, C. Krause, I. Klimant and O.S. Wolfbeis, , *Analyst*, 129, (2004), 645-650.
- 53 J.W. Parker, O. Laksin, C. Yu, M.L. Lau, S. Klima, R. Fisher, I. Scott and B.W. Atwater, *Anal. Chem.*, 65, (1993), 2329-2334.
- 54 J.M. Zen, A.S. Kumar and D.M. Tsai,, *Electroanalysis*, 15, (2003),1073-1087.
- 55 P. Richard, *Handbook of Fluorescent Probes and Research Products* (9th ed.), Molecular Probes (2002).

- 56 L.L. Song, E.J. Hennink, I.T. Young and H.J. Tanke, *Biophys. J.* 68, (1995), 2588-2600.
- 57 J.C. Watson, E.M. Doppenberg, M.R. Bullock, A. Zauner, M.R. Rice, D. Abraham, H.F. Young, *Stroke*, 28, (1997), 1624-1630.
- 58 A. Zauner, E. Doppenberg, J.J. Woodward, C. Allen, S. Jebraili, H.F. Young, R. Bullock, *Neurol.Res.* 19 (1997) 265-273.
- 59 B.R. Soller, *IEEE Eng. Med. Biol.* 6/7 (1994) 327-335.
- 60 S A. Grant, K. Bettencourt, P. Krulevitch, J. Hamilton, R. Glass *Sens. Actuators B* 72 (2001) 174-179.
- 61 M.L. Wahl, P.M. Pooler, P. Brand, D.B. Leeper, *J. Cell. Physiol*, 183, (2000), 373-380.
- 62 B.H. Hao, I. Manners, M.A. Winnik, *Anal. Chem.*, 77, (2005), 8075-8085.
- 63 B.H. Hao, I. Manners, M.A. Winnik, *Chem. Mater.*, 17, (2005), 3160-3171,
- 64 M.F. Choi and D. Xiao, *Analyst*, 124, (1999), 695-698.
- 65 T.M. Butler, B.D. McGrath, C.J. McDonagh, *Non-Cryst solids*, 224, (1998), 249.
- 66 N.A. Peppas, Preparation methods and structures of hydrogels, CRC Press, Boca Raton, FL 1986.
- 67 G.S. Vasylevsk, S.M. Borisov, C. Krause and O.S. Wolfbeis, *Chem. Mater.*, 18, (2006), 4609-4616.
- 68 B.S. Rao, J.B. Puschett, K. Matyjaszewski, *J. Appl. Polym. Sci.* 43 (5) (1991) 925.
- 69 G.E. Badini, K.T.V. Grattan, A.C.C. Tseung, *The Analyst* 120, (1995), 1025.
- 70 L.Y. Ma, H.Y. Wang, H. Xie, L.X. Xu, *Spectrochim. Acta Part A: Mol. Biomol. Spectrosc.* 60, (2004), 1865.
- 71 D. Millar, M. Uttamalal, R. Henderson, A. Keeper, *Chem. Commun.*, 4, (1998), 477-490.

- 72 Z. Liu, S. Gao, T. Chen, *J. Polym. Sci. Part A: Polym. Chem.* 43, (2005), 3447-3452.
- 73 J. Goicoechea, C.R. Zamarre, I.R. Matras, F.J. Arregui *Sens. Actuators B.* 132, (2008), 305-311.
- 74 M. Blumentritt, K. Melhorn, J. Flachsbarth, M. Kroener, W. Kowalsky, H. Johannes, *Sens. Actuators B*, 131, (2008), 504-508.
- 75 L. Basabe-Desmonts, D.N. Reinhoudt and M. Crego-Calama, *Chemical Society Reviews*, 36, (2007), 993-1017.
- 76 M. Brasuel, R. Kopelman, T.J. Miller, R. Tjalkens and M.A. Philbert, *Analytical Chemistry*, 73, (2001), 2221-2228.
- 77 Y.F. Cao, Y.E.L. Koo, S.M. Koo and R. Kopelman, *Photochemistry and Photobiology*, 81, (2005), 1489-1498.
- 78 F. Gao, L.J. Tang, L. Dai and L. Wang, *Spectrochimica Acta Part a-Molecular and Biomolecular Spectroscopy*, 67, (2007), 517-521.
- 79 S. Hornig, C. Biskup, A. Grafe, J. Wotschadlo, T. Liebert, G.J. Mohr and T. Heinze, *Soft Matter*, 4, (2008), 1169-1172.
- 80 J.W. Aylott, J.W, *Analyst*, 128, (2003), 309-312.
- 81 H.A. Clark, S.L.R. Barker, M. Brasuel, M.T. Miller, E. Monson, S. Parus, Z.Y. Shi, A. Song, B. Thorsrud, R. Kopelman, A. Ade, W. Meixner, B. Athey, M. Hoyer, D. Hill, R. Lightle and M.A. Philbert, *Sens Actuators B*, 51 (1998), 12-16.
- 82 H. Pang, N.Kwok, *Sens. Actuators B*, 123, (2007), 120-126.
- 83 E. Monson, M. Brasuel, M. A. Philbert and R. Kopelman, *Biomedical Photonics Handbook*. T. Vo-Dinh, editor. CRC Press, Boca Raton, FL (2003).
- 84 Y.E. Koo Y. Cao , R.Kopelman , S.M.Koo, M. Brasuel M, M.A.Philbert, *Anal Chem.*, 76, (2004), 2498-505.

- 85 D. R. Uhlmann, G. Teowee, and J. Boulton, *Journal of Sol-Gel Science and Technology* 8, (1997), 1083- 1091.
- 86 R. Q. Albuquerque, Z. Popovic, L. De Cola, and G. Calzaferri, *Chem. Phys.Chem.*, 7 (2006), 1050-1055.
- 87 B.H. Han, I. Manners, and M. A. Winnik, *Anal. Chem.*, 77, (2005) , 8075-8080.
- 88 Y. Amao, Y. Ishikawa, and I. Okura, *Anal. Chim. Acta*, 445, (2001), 177-180.
- 89 X.X. He, J.Y. Chen, K.M. Wang, D.L. Qin and W.H. Tan, *Talanta*, 72, (2007), 1519-1526.
- 90 R. C. Evans, P. Douglas, J. A. G. Williams and D. L. Rochester, *J. Fluoresc.*, 16, (2006), 201.
- 91 S.Ricketts, P.Douglas, *Sens. Actuator B*. In press, 2008
- 92 R. W. G. Hunt, 'Measuring Colour', Ellis Horwood, 1991.

Chapter 6

Conclusions

6.1 Conclusions

In this work several novel and known luminescent systems have been investigated for use in three different technological applications namely 1: near infrared probes for non-covalent labelling of biomolecules, 2: kinetic heterogeneity of a Pt porphyrin in optical thin film sensors, and 3: nanomaterials for optical analyte sensing. Particular attention has been paid to designing materials with useable characteristics applicable to biomedicine and biotechnology.

6.1.1 A squarylium dye as non-covalent protein probes

The squarylium dye (SQ-1) described in this work, incorporates the squaric acid group for added photostability and sulfobutyl groups for improved water solubility and reduced propensity to aggregate. The moderate photochemical properties improve significantly upon binding to albumins, which can be ascribed to electrostatic interactions. Excitation is compatible with common diode lasers and this increases the useability of the dye. Squarylium dyes are not commonly used in biomedicine, yet the imaging characteristics in paraformaldehyde fixed cells, and the low cytotoxicity, both suggest the possibility of live cell imaging.

6.1.2 Understanding the kinetic heterogeneity of PtOEP based sensing materials

PtOEP is one of the most commonly used metalloporphyrins for optical oxygen sensing. Understanding the kinetic heterogeneity of PtOEP in optical thin film sensors is a step towards the design and implementation of a usable sensor. The unquenched time resolved emission of PtOEP in polymer thin film sensors are all good fits to a double exponential. The concentration dependent time resolved emission of PtOEP in ethyl cellulose and a biomedically compatible polymer can be modelled as a monomer:dimer equilibrium with increasing proportion of dimer at higher PtOEP concentration and in the presence of plasticisers. The hydrogel polymer shows excellent potential as a polymer for both gaseous and dissolved oxygen sensing, with no significant difference in the kinetic heterogeneity when wet or dry. The type 1 PtOEP/hydrogel sensor shows excellent sensing characteristics for an optical oxygen sensor operating in with steady state and lifetime mode.

6.1.3 Nanomaterials for optical sensing

Nanomaterials are key to the development of multianalyte sensing systems. Single and multilumophore ormosil nanoparticles can be prepared for a variety of hydrophobic lumophores sensitive to different analytes. The nanoparticles can easily be immobilised in polymers to prepare thin film optical sensors for lifetime and steady state sensing. Ormosil nanoparticles are ideal for optical oxygen sensing, having the excellent properties associated with sol gel glasses but the added advantage of being able to improve the hydrophilicity of the nanosphere by careful choice of the siloxane precursors.

PtOEP ormosil nanoparticles are efficiently quenched by molecular oxygen and this can be described well by the Stern-Volmer relationship yielding linear plots.

We have described an optical oxygen sensing system for both gaseous and dissolved oxygen based on the incorporation of luminescent nanoparticles in a biologically compatible hydrogel. This sensor has potential application in both industrial and biomedical applications. The system shows a linear response to changing oxygen concentration in both gaseous and aqueous systems and the ratiometric sensing provides a simple way of accounting for any fluctuations associated with intensity based sensing without the complicated instrumental set up needed for lifetime based sensors. The lumophores can be simultaneously excited at 382nm reducing the need for complex excitation systems, and making the sensor compatible with cheap LED excitation sources. Comparison of the sensor response to either gaseous or dissolved oxygen shows no difference in either Stern-Volmer constants or curve fits to unquenched time-resolved emission decays.

A new easily prepared self assembled material for optically sensing pH in the physiological pH range has been developed and incorporated into a thin hydrogel film. The fluorescent indicator 5,6 carboxyfluorescein has been attached to alumina to produce a sensing material that overcomes the major problem of leaching. When this material is immobilised in a biologically compatible hydrogel polymer the resulting sensor film shows good operational stability and can be calibrated well using equation 1. This method, involving use of a SAM, offers a cheap and simple alternative to microspheres and beads.

Once characterised the nanoparticles can be used for a combinatorial approach to designing ratiometric sensors for oxygen, pH and oxygen, and pH. Careful choice of lumophore and nanoparticle preparation condition allows the design of colorimetric sensing systems for the qualitative and semi quantitative determination of oxygen concentration for gaseous and dissolved oxygen

6.2 Final remarks

All the sensing material described in this study are compatible with currently commercially available LED and laser sources. The development of new instrumentation, particularly that which is compatible with NIR dyes, is expected to enhance the development of this area or research significant.

Nanoparticles are key to the development of optical sensing, especially sensing on the microscale; they provide a photostable matrix for lumophore immobilisation and dramatically reduce leaching from the optical sensor. For intracellular analyte sensing, new materials for nanoparticles will be needed to reduce the size of the nanoparticles, while it is expected that developments in surface functionalisation will aid biocompatibility.